Soft-Virtual Computation and Threshold Resummation in QCD for Drell-Yan process in Standard Model and Beyond

A

Thesis Submitted

in Fulfillment of the Requirements

for the Degree of

PHD

By

KAJAL SAMANTA

Under the Supervision of **Dr. M. C. KUMAR**

Department of Physics

Indian Institute of Technology Guwahati

May 3, 2021

Abstract

This thesis arises in the context of precision calculation in QCD in the framework of soft-virtual computation and threshold resummation for the Drell-Yan process in the Standard Model and beyond. Soft-virtual corrections capture significant contributions near partonic threshold region $z \to 1$. In the absence of complete fixed order results at higher orders, the first step to achieve the precise theoretical results is soft-virtual computation. This kind of calculation has been successfully performed in many SM and beyond SM processes. Another way to improve the accuracy of the results for inclusive cross-section over the fixed order is to resum threshold enhanced logarithms to all orders. These logarithms play a crucial role in the threshold region. The threshold resummation is well understood in the Mellin-N space. We follow the conventional procedure to obtain soft-virtual coefficients from the available form factor in the literature. We use these coefficients to get resum results using standard methodology. The Drell-Yan process in hadron collisions is essential because of its clean final state. In the context of QCD calculation, three-loop soft-virtual results are available in the literature for the SM DY process. Here, we use these SV results to give the predictions for inclusive dilepton production as well as on-shell Z, $W^{\pm}$ productions at next-to-next-to-next-to leading logarithmic ($\mathrm{N^3LL}$) accuracy and match these results with three loop soft-virtual results using the minimal prescription procedure. In addition to the standard $\ln N$ exponentiation, we study the numerical impact of exponentiating N-independent part of the universal soft function and the complete form factor that appears in the resummed predictions in N space. We extend this precision phenomenology to other scenarios where dilepton can be produced via spin-2 particle. For this, we consider large extra dimensions (ADD) and warped extra dimension scenarios. In these cases, the dilep-

ton can be produced via both the $q\bar{q}$ and gg initiated subprocesses at the LHC as spin-2 particle couples universally to the SM particles via energy-momentum tensor. Therefore, dilepton production via spin-2 particle at LHC is a combination of Higgs like and DY like process. Consequently, the QCD phenomenology of this process is very interesting to study. Precision studies in QCD have been done for this process and observed a large K-factor at NLO mimicking the large QCD correction for Higgs production at LHC. Here, we present the complete NNLO QCD correction for RS model and extend this analysis by resumming the threshold logarithms up to NNLL accuracy. For the ADD case, we present the results up to N^3LL accuracy and match these with three loop soft-virtual results. Further, we study the dilepton production scenario at the LHC via spin-2 particles with non-universal couplings $i.e$ spin-2 particles couple to SM fermions and gauge bosons with different couplings. The phenomenology of such a graviton is similar, to some extent, to that of the RS model. However, unlike the RS model, the parameter space of this model is much flexible and less constrained because of its non-universal couplings. The complete NNLO QCD corrections are already available in the literature. We extend this precision to NNLO+NNLL accuracy in QCD and study a detailed phenomenology of this model. These precise results will be helpful to extract SM parameters accurately and to provide stringent bound on model parameters in the search of such BSM scenarios at the present LHC and future high energy hadron colliders.

TH-2530_166121003

Declaration

This is to certify that the thesis entitled "**Soft-Virtual Computation and Threshold Resummation in QCD for Drell-Yan process in Standard Model and Beyond**", submitted by me to the *Indian Institute of Technology Guwahati*, for the award of the degree of PhD, is a bonafide work carried out by me under the supervision of Dr. M. C. Kumar. The content of this thesis, in full or in parts, have not been submitted to any other University or Institute for the award of any degree or diploma. I also wish to state that to the best of my knowledge and understanding nothing in this report amounts to plagiarism.

Kajal Samanta

Signed:

Kajal Samanta
Department of Physics,
Indian Institute of Technology Guwahati,
Guwahati-781039, Assam, India.

Date: 03/05/2021

Disclamer

The bibliography included in this thesis is, by no means complete but contains the ones which are consulted thoroughly by me. I apologize for inadvertently missing out some of the research papers, review articles and other scientific documents pertaining to the focus of this thesis which should also have been cited. For illustration purpose some of the figures in this thesis are taken from other sources and properly cited.

Certificate

This is to certify that the thesis entitled "**Soft-Virtual Computation and Threshold Resummation in QCD for Drell-Yan process in Standard Model and Beyond**", submitted by Kajal Samanta (166121003), a research scholar in the *Department of Physics*, *Indian Institute of Technology Guwahati*, for the award of the degree of PhD, is a record of an original research work carried out by him under my supervision and guidance. The thesis has fulfilled all requirements as per the regulations of the institute and in my opinion has reached the standard needed for submission. The results embodied in this thesis have not been submitted to any other University or Institute for the award of any degree or diploma.

Signed:

Supervisor: Dr. M. C. Kumar
Department of Physics,
Indian Institute of Technology Guwahati,
Guwahati-781039, Assam, India.

Date: 03/05/2021

To my family and to all covid warriors...

Acknowledgement

It would have been impossible to write this thesis without the direct and indirect support and the help of the people around me throughout the journey. The list is endless, it is only possible to mention some of them.

I would like to express my sincere gratitude to my supervisor, Dr. M. C. Kumar, for his continuous guidance, support, enthusiasm and giving me freedom and motivation. I also thank him for introducing me to the collaborators and exciting new problems which helped me to learn and gain experience in the field of my research. His dedication, hard work and immense knowledge always inspire me to learn new things.

I wish to show my appreciation to Dr. Goutam Das, one of our collaborators, for his immense and valuable input in my work. I wish to extend my special thanks to Prof. V. Ravindran, Pooja Mukherjee and A. H. Ajjath for collaborating in my projects and making them more effective and rich.

I would also like to show my deep appreciation to my doctoral committee members, Prof. P. Poulose, Dr. Soumitra Nandi and Dr. Subhaditya Bhattacharya, for the useful suggestions and yearly evaluations of my research work. I acknowledge the academic help of HoDs, Prof. Poulose Poulose and Prof. Subhradip Ghosh. I thank technical assistants, academic and non-academic staff of our department for various helps in my research period. I am also thankful to Param Ishan, IIT Guwahati for the supercomputer facility.

I am grateful for having beautiful friendships with Lopamudra, Suman, Dibyendu, Sayandeep and Abhisek. Also, I feel lucky to meet the most joyful per-

sons, Sayan Da, Sovan Da, and Charu sir. I have many precious memories with them. I thank all my batch mates Mousumi, Abhilasha, Apurba, Dangka, Nilamoni, Ritupan, Priyanka, Mahananda, Abdelsalam and Ogaro for their friendship throughout the years. I also thank my school close friends, Souvik, Swarup and Bishnu for supporting me in every possible way.

Last but not least, I want to thank my family for their love, support, sacrifices and patience.

Kajal Samanta

Synopsis

This is an exhilarating time in particle physics; the world's most powerful machine is now exploring high energy physics at a very unprecedented level of accuracy. The Standard Model (SM) describes the physics of fundamental particles and their interactions. Over the decades, the SM predictions are well tested through various experiments; LEP, Tevatron etc. The last and most wanted member of the standard model, the Higgs boson, has been discovered in the last decade at the Large Hadron Collider (LHC) at the centre of mass energies of 7 and 8 TeV, and the properties of these Higgs bosons are very similar to that of SM predicted. With the LHC upgraded to 13 TeV in run II, this Higgs boson's spin and parity properties have been established. With sophisticated detector technology and high luminosity, it has become possible to study the SM's predictions to a very high degree of precision at the hadron colliders like Tevatron and LHC. To match these precise experimental results, one requires a parallel development in theoretical predictions. Improvement of theoretical predictions can be made by including the quantum corrections as they are usually large. LHC collide two protons with very high energies (13 TeV) and high luminosities (139 $\texttt{fb}^{-1}$). Therefore the corresponding partonic centre of mass-energy can scan a sizeable kinematic region hence an ideal candidate for the discovery machine. As proton is a composite state of colour particles called partons, there will be huge radiation of colour particles in each collision. To have a precise theoretical prediction, this radiation has to be taken into account through strong interaction quantum corrections. This interaction has the strongest coupling constant, therefore, contributes the most of quantum corrections.

Although the SM is a very successful theory in explaining the interactions

of fundamental particles and has been tested experimentally to good accuracy, there are some open problems that SM can not address. This is the motivation to look for some beyond Standard Model (BSM) scenarios. Over the many past years, some of the BSM scenarios like supersymmetry (SUSY), extra dimensions (ED) and Dark matter has gained significant attention in particle physics phenomenology.

In this thesis, our primary focus is the precision calculation of the Drell-Yan (DY) process in the Standard Model and beyond in the context of soft-virtual calculation and threshold resummation in QCD. We follow the general formalism available in the literature to compute SV and resum coefficients. The threshold resummation is done in Mellin space where partonic coefficient functions can be factorized into a process dependent and exponent process independent part. To have a physical observable, one needs Mellin inversion. We follow the minimal prescription for Mellin inversion. We convolute the partonic coefficient function with parton distribution function (PDF) using `LHAPDF` subroutine. All the analytical calculations have been done using `FORM` programme.

Standard Model Drell-Yan cross section at N^3LO_{sv}+N^3LL accuracy in QCD at LHC

DY production has been a standard candle at the hadron colliders and is extremely important for luminosity monitoring because of its pristine final state. This is one of the hadronic processes which is well understood theoretically. DY is also an important process experimentally for several BSM searches. Higher-order perturbative QCD corrections to DY provides ample opportunity to explore the structure of the perturbation series. Thus DY serves as an important process in collider experiments. Owing the importance of this process, precision studies have been done for it. The NLO and NNLO QCD results are already available in the literature. The calculation of complete N^3LO cross-section is extremely difficult due to the increasing number of subprocesses involved; however, there has been significant progress in obtaining third-order contribution to this process in QCD. Very recently, the first result at complete N^3LO from virtual photon mediator has been calculated by Duhr et.al. In

the absence of complete N^{3}LO result, the best possible way to improve this process is by incorporating soft-virtual (SV) corrections, threshold resummation and mixed QED⊗QCD computation.

Here we present SM DY cross-section at N^{3}LO$_{sv}$+N^{3}LL accuracy in QCD and on-shell production of massive gauge bosons in the same order. For the resummation, we have extracted the process dependent term up to third order in α_s (g_{03}) and the universal (process independent) exponentiation at the same accuracy (g_4). We explore all the possibilities of doing resummation. First, we study the general resummation prescriptions, namely N and $\overline{N}$. Then we exponentiate complete soft pieces, usually keep in the process dependent part, coming from the universal soft distribution function. Because of the universality of the soft function we exponentiate this function and notice that the perturbative convergence for the `Soft` case is a bit faster than the `Standard` N and $\overline{N}$ case. We also presented our results when the complete process dependent part have been exponentiated and found that the convergence rate of the perturbation series is competing with that of the `Soft` case We also study all kinds of theoretical uncertainties, namely renormalization and factorization scales in our prediction. We note that more and more terms in the exponentiation give a better reduction in the theoretical uncertainties. For the case of massive gauge bosons production, we observe a significant reduction of theoretical uncertainty order by order. However, at N^{3}LO$_{sv}$+N^{3}LL, the uncertainties increase. This is because of the unavailability of N^{3}LO PDF. At this accuracy, this PDF is also essential. We also estimate the uncertainty coming from non-perturbative PDF for five different PDF groups; `ABMP16`, `CT14`, `MMHT2014`, `NNPDF31`, `PDF4LHC15`.

Inclusive cross section in RS model at NNLO+NNLL accuracy in QCD at LHC

This chapter focuses on massive KK production in the RS framework. The SM can not address the Higgs mass hierarchy problem; extra dimension models give a solution to this problem. Out of several extra-dimensional models, RS provides a straightforward solution to the hierarchy problem and its collider signals being looked extensively at the LHC. In the RS model, all the SM particles are confined to

the four-dimensional brane, whereas only gravity can propagate extra-dimensional. This extra dimension is compactified with periodic boundary conditions, which leads to a tower of Kaluza-Klein (KK) modes. These KK modes are well separated can decay to various final states like DY, $\gamma\gamma$ etc. This feature leads to resonant excess in distributions of dilepton pairs. The search for RS resonances is going on at the LHC from time to time. As graviton can couple through energy-momentum tensor, it can couple to quarks and gluons by universal coupling. Therefore, unlike the SM DY process, dilepton can be produced both gluon (Higgs like), and quark (DY like) initiated process. This process is also important phenomenologically to understand the QCD perturbative structure. Precision calculations of this model are available up to NNLO$_{sv}$. The NLO calculation was done long before and was found to be about 50% of LO. This necessitates the computation of higher-order corrections for the convergence of the perturbation series.

Here we provide the complete NNLO result in QCD for invariant mass distribution of dilepton in this model. We note that at resonance with $M_1 = 1.5$ TeV, the NNLO K-factor is about 1.73, i.e. extra 20% contribution is coming from this computation. We have studied details phenomenology along with perturbative and non-perturbative uncertainty. We have also provided 3-loop soft virtual result with theoretical uncertainty. We further extend this precision calculation by resumming the threshold logarithms to NNLL accuracy and matching it with the NNLO result. We observe that the inclusion of NNLL result gives an extra 2% contribution to NNLO. We have also estimated the scale uncertainty in this computation and found a reduction in renormalization scale uncertainty compared to NNLO, where an increment in 7-point scale uncertainty depends on the kinematic region.

QCD phenomenology of exotic spin-2 production at the LHC

In this chapter, we focus on one particular BSM scenario where massive generic spin-2 fields interact with the SM fermions and gauge bosons with different coupling strength. The phenomenology of such a graviton is similar to some extent to that of the RS model where the massive graviton couples with equal strength

to fermions and bosons in the SM. However, unlike the RS model, the parameter space of the non-universal case is much flexible and less constrained at the LHC searches so far. In the context of Higgs characterization, this model has been studied extensively in the diboson channels. It has been observed that the K-factors for different channels give sizeable contribution depending on model parameters as well as phase space region. This necessitates further higher-order QCD corrections for this model. The first complete next-to-next-to-leading order (NNLO) computation has been performed in the dilepton channel. It has been observed that the K-factors at NLO and NNLO are significantly different from those of RS and ADD. In the present model, the graviton production occurs at the LO via Higgs-like and DY-like processes similar to the ADD or RS model, but with different couplings to quarks (k_q) and gluons (k_g). This particular feature of this model controls the higher-order radiative corrections for different channels in different parameter spaces.

Owing to this particular feature, we estimated the resummation effect of this model up to NNLO+NNLL accuracy. First, we study the effect of different coupling parameters (k_q and k_g) and found that the cross-section gets maximum correction near the universal line. We note that the qg channel at NLO plays a crucial role in the higher-order result. Because of this, we define K-factor with respect to NLO and present the results. Inclusion of NNLL result to NNLO result gives extra 2% enhancement in the cross-section and also reduce scale uncertainty. We have also estimated uncertainty coming from non-perturbative source. We note that at this order, non-perturbative uncertainty is about $\pm 4\%$ whereas the perturbative uncertainty is about $\pm 2\%$.

Dilepton production in ADD model at N^{3}LO$_{sv}$+N^{3}LL accuracy in QCD at LHC

In this chapter, we study the precision calculation of inclusive cross-section of the DY process in the ADD model. In chapter 2, we have discussed spin-2 production in the RS framework. In the ADD model, KK graviton couples with universal strength to the SM stress-energy tensor and the analytical perturbative coefficients are the same as the generic universal spin-2 case like RS. Phenomenologically, however,

the ADD KK states provide a different signature from that of the RS model at the LHC. The dilepton invariant mass distribution in the ADD model provides a continuum distribution; in the RS model, one finds well-separated massive KK resonances. Precision calculations of this model have also been done. The NLO and NNLO result in QCD is available in the literature. The NLO corrections in the high Q-region around $Q = 2500$ GeV contribute by about 40% of LO, while NNLO corrections add an additional 25% of LO to the total invariant mass distribution. The NNLO corrections are too large enough to truncate the perturbation theory at this order and necessitates the computation of higher-order corrections for the convergence of the perturbation series.

Here we present this model's result up to $\mathrm{N^3LO}_{sv}$+$\mathrm{N^3LL}$ accuracy in QCD at the LHC. We observe that the three-loop SV corrections that we have computed here are found to contribute an additional 1-2% of LO to the invariant mass distribution at $Q = 2500$ GeV, demonstrating a very good convergence of the perturbation theory. We also note that the three-loop SV corrections are negative in the low Q-region while in the high Q-region, they are positive because of threshold enhancement. We have also computed the resum result up to $\mathrm{N^3LL}$ accuracy in QCD for standard $\overline{N}$ prescription and matched this result with $\mathrm{N^3LO}_{sv}$. We observe an enhancement of cross-section around 2% of LO compared to NNLO at this order. We have estimated all kinds of uncertainties (perturbative and non-perturbative). For perturbative uncertainties, we have estimated the uncertainties coming from the renormalization and factorization scale. Furthermore, for non-perturbative uncertainties, we have calculated the intrinsic PDF uncertainties for five different groups, namely `ABMP16, CT14, MMHT2014, NNPDF31, PDF4LHC15`. We also study the dependence of our results on the ADD model parameters, namely the scale M_s and the number of extra dimensions d.

Publications included in the thesis

1. *Precision QCD phenomenology of exotic spin-2 search at the LHC* : Goutam Das, M.C. Kumar, **Kajal Samanta** [JHEP 04 (2021) 111] [arXiv: 2011.15121]

2. *Resummed inclusive cross-section in Randall-Sundrum model at NNLO+NNLL* : Goutam Das, M.C. Kumar, **Kajal Samanta** [JHEP 07 (2020) 040] [arXiv: 2004.03938]

3. *Resummed Drell-Yan cross-section at* N^3LL : Ajjath A.H, Goutam Das, M.C. Kumar, Pooja Mukherjee, V. Ravindran, **Kajal Samanta** [JHEP 10 (2020) 153] [arXiv: 2001.11377]

4. *Resummed inclusive cross-section in ADD model at* N^3LL*+NNLO* : Goutam Das, M.C. Kumar, **Kajal Samanta** [JHEP 10 (2020) 161] [arXiv: 1912.13039]

Schools/Workshops/Conferences attended

1. Presented talk at *International Workshop on Precision QCD @LHC*
   28*th* - 31*st* January 2020,
   Indian Institute of Technology, Hyderabad, India.

2. Presented talk at *SERB Main Schools in Theoretical High Energy Physics*
   7*th* - 26*th* December 2019,
   S.G.T.B. Khalsa College, University of Delhi , Delhi, India.

3. Attended *Madgraph School 2019*
   18*th* - 22*nd* November 2019,

The Institute of Mathematical Sciences , Chennai, India.

4. Presented poster at *International Meeting on High Energy Physics*
   $17th$ - $22nd$ January 2019,
   Institute of Physics, Bhubaneswar, India.

5. Attended *GIAN course on Infrared Structure of Perturbative Gauge Theories*
   $4th$ - $13th$ December 2017,
   Indian Institute of Technology, Hyderabad, India.

6. Attended *School-cum-workshop on Collider Physics: Events, Analysis and QCD*
   $27th$ - $31st$ March 2017,
   Indian Institute of Technology, Guwahati, India.

Contents

List of Figures

List of Tables

Chapter 1

Introduction

In particle physics, we study the dynamics of elementary particles. By elementary particles, we meant the particles which do not have any structure. From time to time, the number of elementary particles is changing. For examples, before the discovery of the electron, it was considered that the atoms are elemental. After discovering the electron in 1897, it was suggested that atoms are not elementary; they consist of electrons and a positively charged nucleus. Later it was also proved that the nucleus also has a structure; they consist of proton and neutron called nucleons. These nucleons are consists of quarks and gluons, which are elementary. Therefore, it is not straight forward to say which particles are elementary; instead, it is easy to tell which particles are not elementary. The dynamics of these elementary particles can be described by the Standard Model (SM). It is a gauge theory with gauge group $SU(3)_c \otimes SU(2)_L \otimes SU(1)_Y$. In nature, there are four fundamental interactions that the elementary particles experience; electromagnetic force, Weak force, strong force and gravity, and SM can describe three of them. Gravity is not included in the SM. The $SU(3)_c$ gauge group describes the interaction of coloured particles called strong interaction, $SU(2)_L$ describes the dynamics of weakly charged particles called weak interaction and $U(1)_Y$ describes the dynamics of charged particles called electromagnetic interaction. The particle spectrum of SM consists of six quarks flavour (u, d, c, s, t, b) with three different colors; red green and blue, eight gluons, three charged leptons $(e^{\pm}, \mu^{\pm}, \tau^{\pm})$, three neutrinos corresponding to these three

leptons (ν_e, ν_μ, ν_τ), three weak gauge bosons ($W^\pm, Z$) ,one photon (γ) and one Higgs boson (H). Many of these particles were predicted by SM even before their discovery; for example, Z boson was predicted in 1968 when scientists attempted to formulate a theory for weak interaction in the same way of electromagnetic interaction. For this prediction, Sheldon Glashow, Steven Weinberg, and Abdus Salam shared the Nobel prize in 1979 [5–7]. Finally, Z boson was discovered in 1983 in bubble chamber experiments at CERN. The third generation of quarks was predicted in 1973 by Makoto Kobayashi and Toshihide Maskawa to explain the observed CP violation in kaon decay. Later these quarks were named top and bottom by Haim Harari in 1975. The top quark was discovered in 1995 by CDF and D0 experiments at the Fermi lab. On the other hand, bottom quark was discovered in 1977 by the Fermilab. Higgs boson was predicted in 1964 in the context of explaining the origin of mass of gauge bosons [8–10], and Peter Higgs won the Nobel prize in 2013 for this prediction. Higgs boson has been discovered in the last decade at the Large Hadron Collider (LHC) at the centre of mass energies of 7 and 8 TeV [11, 12] and the properties of these Higgs bosons are very similar to that of SM predicted. With the LHC upgraded to 13 TeV in run II, this Higgs boson's spin and parity properties have been established. The discovery of the Higgs boson makes the SM the most decorated theory in particle physics.

Though the SM is a very successful theory because of its significant achievements and predictions, it is still not the fundamental theory. There are some open problems that can not be explained by the SM. This theory is unable to address the unification of gauge interactions, the hierarchy between the electroweak scale and Planck scale, the origin of neutrino masses, cosmological constant problem, the baryon asymmetry in the universe, existence of dark matter, etc. To address these issues, physicists have made various attempts with the concepts beyond the scope of the SM and in new physics scenarios, which we call beyond the standard model physics (BSM). In the next section, we address some of these problems that motivated the study of these BSM scenarios.

1.1 Motivation for the beyond standard model physics

1.1.1 Unification of gauge interaction

After the unification of electromagnetic and weak interactions at the scale of the order of 100 GeV, the unification of the coupling strength of electromagnetic, weak and strong interactions is also expected at some scale called the GUT scale of the order of 10^{16} GeV. At this scale, all these forces can have a common origin. The coupling strength of gravity, which is not included in the SM, is the order of unity at the Planck scale M_{pl} (10^{19} GeV). In the context of the GUT scale, it is also possible to unify gravity with three other interactions.

The electromagnetic and gravitational interaction are long-range forces, and it is possible that they may have a common origin. With this idea, the first attempt was made by Kaluza and Klein in 1920 to unify electromagnetic interaction with gravity, considering one extra spatial dimension [13]. This extra dimension is compactified in a tiny size and hence need very high energy to probe them. They also assumed that the photon field originates from the fifth component $g_{\mu 5}$ of a five-dimensional metric tensor. The extra dimension models provide a solution for the unification of the fundamental forces.

1.1.2 Higgs mass hierarchy

Higgs boson couples to all massive particles with the coupling strength proportional to the mass of the particles. The Higgs self-coupling lead to the mass correction of Higgs. These mass correction diagrams are quadratically divergent like $\int d^4k(k^2 -$

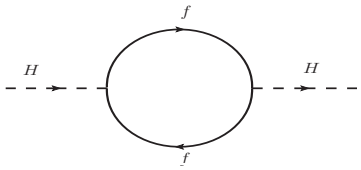

Figure 1.1: Higgs mass correction diagrams with fermion loop

$m^2)^{-1} \propto \Lambda$ for some cutoff scale Λ. More precisely,

$$\Delta M_H^2 = \frac{\Lambda^2}{32\pi^2}\left[6\lambda_f + \cdots\right] \tag{1.1}$$

Where λ_f is the Higgs boson coupling to fermions. If the SM is valid up to the GUT scale or Planck scale, then Λ will be the order of M_{GUT} or M_{pl}. With this choice of Λ, the quantum correction to the Higgs mass can be much larger than the Higgs mass itself. The correction is quadratically sensitive to the choice of the cut-off scale. This problem is known as Higgs mass hierarchy problem.

To address this problem, many BSM scenarios have been proposed, such as supersymmetry (SUSY) [14], large extra dimension model (ADD) [15], warped extra dimension model (RS) [16]. In SUSY, the presence of a supersymmetric partner of fermion can solve this problem. The quadratic divergence of Higgs mass coming from the fermion loops can be cancelled out by those from the superpartner and provide the correct Higgs mass. In the large extra dimension model, the Planck scale can be lowered as much as a few TeV scale depending on the volume of the extra dimensions, which reduces the Planck scale and can solve this hierarchy problem. In the warped extra dimension model, the fundamental masses could be the order of the Planck scale. Still, because of the exponential warped factor of the higher dimensional metric, the physical mass could be of the order of TeV on four dimensions. Thus the hierarchy problem can be addressed in different BSM scenarios.

1.1.3 Cosmological constant problem

The cosmological constant problem is the disagreement between the observed values of vacuum energy density and the large theoretical value of zero-point energy calculated from quantum field theory. The cosmological constant (Λ) was first introduced by Albert Einstein into general relativity in 1917. Einstein field equation reads

$$R_{\mu\nu} - \frac{1}{2}g_{\mu\nu} + \Lambda g_{\mu\nu} = \frac{8\pi G_N}{c^4}T_{\mu\nu} \tag{1.2}$$

The Λ can be interpreted as energy density of the vacuum. Energy momentum tensor of the vacuum can be written as

$$T_{\mu\nu}^{vac} = -\frac{c^4\Lambda}{8\pi G_N} g_{\mu\nu} \tag{1.3}$$

Substituting Eq.(1.3) in Eq.(1.2) and comparing it with perfect fluid energy momentum tensor, one can show

$$c^2\rho_{vac} = \frac{c^4\Lambda}{8\pi G_N} \tag{1.4}$$

where ρ_{vac} is the vacuum energy density. It is observed that measured and calculated value of this vacuum energy density differ a lot.

$$\frac{\rho_{vac}^{obs}}{\rho_{vac}^{mes}} \sim 1.0 \times 10^{-123} \tag{1.5}$$

This the worst prediction from theoretical side. There is no way to describe this discrepancy in the SM.

1.1.4 Dark matter problem

The total mass energy of the universe contains 68% dark energy, 5% ordinary matter and 27% non-visible matter [17]. The effect of this non-visible matter can be seen through various observation. This non-visible matter of the universe is called Dark Matter (DM). The existence of DM was first proposed by dutch physicist Jacobus Kapteyn in 1922 using stellar velocities. Later from other observation like Galaxy rotation curves, Velocity dispersions results, Gravitational lensing etc., confirm that DM exists in the universe. Unlike normal matter, dark matter does not interact with the photon; hence they are electrically neutral. The Dark matter density almost constant for a long time, implying they interact very weakly with matter particles. As 27% of the mass energy of the universe is Dark matter, it means that dark matter particles have to be massive. One possible dark matter candidate in SM are neutrinos, but they are almost massless and do not form structure. Therefore,

neutrino as a dark matter candidate is ruled out. There is no possible way for SM particles to be dark matter. Because of this, physicists are looking for some BSM scenarios. Weakly Interacting Massive Particles (WIMP) is one of the most studied dark matter candidate. However, so far, there is no signature of WIMP in experiments. Physicists are also looking for other possibilities of dark matter like Feebly Interacting Massive Particles (FIMP) and Strongly Interacting Massive Particles (SIMP).

1.2 Beyond standard model scenarios

There are many BSM scenarios proposed to address various problems that the SM does not address. Physicists also proposed many new physics scenarios as a more fundamental theory where SM is the effective theory of these fundamental theories. Some of them are Super Symmetry (SUSY), extra dimension models, techni-colour, unparticles, Z' and Dark matter models. These models are important to answer some unsolved problems in SM and are interesting in their own domain to see how they address these unsolved problems and give their interesting collider signatures. As mentioned before, extra dimension models can solve the unification of the fundamental interactions and Higgs mass hierarchy problem. We will discuss these extra dimension models in a detailed manner.

Kaluza and Klein first introduced the concept of extra dimension in order to unify electromagnetism and gravity [13]. They consider that our space is four dimensions with a fifth dimension being compactified a the circle of radius R. The co-ordinates are denoted as $x^A = (x^\mu, y)$, where $A = 0, 1, 2, 3, 5$, $\mu = 0, 1, 2, 3$ and $y = x^5$. The volume of the extra dimension is $L = 2\pi R$. This extra dimension has physical implication at the energy scale that can probe this length. We first consider the physical implication of this extra dimension for the scalar field. The Lagrangian of the scalar field can be written as,

$$\mathcal{L} = -\frac{1}{2}\partial_A\phi(x^\mu, y)\partial^A\phi(x^\mu, y) \qquad A = 0, 1, 2, 3, 5 \tag{1.6}$$

This $\phi(x^\mu, y)$ will satisfy the periodic boundary condition $y = y + 2\pi R$. One can perform the Fourier decomposition of ϕ along the y direction using this boundary condition and will obtain

$$\phi(x^\mu, y) = \frac{1}{\sqrt{2\pi R}} \sum_{-\infty}^{\infty} \phi^{(n)}(x^\mu) e^{i\frac{n}{R}y} \tag{1.7}$$

Here $\phi^{(-n)} = (\phi^{(n)})^\dagger$. Therefore, after compactification the action can be written as,

$$S = \int d^4x \left\{ \frac{1}{2}\partial_\mu \phi^{(0)} \partial^\mu \phi^{(0)} + \sum_{n=1}^{\infty} \left[\partial_\mu \phi^{(n)\dagger} \partial^\mu \phi^{(n)} - \frac{n^2}{R} \phi^{(n)\dagger} \phi^{(n)} \right] \right\} \tag{1.8}$$

We can see that the action describes the infinite number of particles with masses $m^2_{(n)} = \frac{n^2}{R^2}$. This tower of particles is called the Kaluza-Klein tower. If the field has mass m_0 in 5-dimensions, then the particles will have masses $m^2_{(n)} = m_0^2 + \frac{n^2}{R^2}$ in four dimensions, where the n define the mode of Kaluza-Klein tower.

A similar observation can also be made for electromagnetic field in $(4+1)$ dimensions. After a Fourier decomposition along the compact dimensions, the electromagnetic field can be written as [18, 19],

$$A_A(x^\mu, y) = \frac{1}{\sqrt{2\pi R}} \sum_n A_A^{(n)}(x^\mu) e^{i\frac{n}{R}y} \tag{1.9}$$

Then the action becomes

$$S = \int d^4x \sum_n \left[\frac{1}{4} F^{(-n)}_{\mu\nu} F^{(n)\mu\nu} + \frac{1}{2} \left(\partial_\mu A_5^{(-n)} + i\frac{n}{R} A_\mu^{(-n)} \right) \left(\partial^\mu A_5^{(n)} + i\frac{n}{R} A^{(n)\mu} \right) \right] \tag{1.10}$$

One can choose a gauge transformation to make A_5 constant along the extra dimensions to remove the mixed terms,

$$A_\mu^{(n)} \to A_\mu^{(n)} - i\frac{R}{n} \partial A_5^{(n)}, \tag{1.11}$$

$$A_5^{(n)} \to 0, \qquad \text{for} \quad \text{n} \neq 0 \tag{1.12}$$

In this gauge, the action can be written as

$$S = \int d^4x \Bigg\{ \Bigg(-\frac{1}{4} F^{(0)}_{\mu\nu} F^{(0)\mu\nu} + \frac{1}{2} \partial^\mu A^{(0)}_5 \partial_\mu A^{(0)}_5 \Bigg) + \sum_{n\geq 1} \Bigg(-\frac{1}{4} F^{(n)}_{\mu\nu} F^{(-n)\mu\nu} + \frac{1}{2} \frac{n^2}{R^2} A^{(n)}_\mu A^{(-n)\mu} \Bigg) \Bigg\} \tag{1.13}$$

The covariant derivative becomes

$$D_\mu = \partial_\mu + i g_5 A_\mu = \partial_\mu + i g_5 \frac{1}{\sqrt{2\pi R}} A^{(0)}_\mu + \cdots \tag{1.14}$$

The mass spectrum consists of a massless gauge field $A^{(0)}_\mu$ with $g_4 = g_5 \frac{1}{\sqrt{2\pi R}}$, an infinite tower of massive gauge bosons with mass $m^2_{(n)} = \frac{n^2}{R^2}$ and a massless scalar field $A^{(0)}_5$.

Therefore, a massless field propagating in the extra dimension will give rise to KK modes of massive particles in 4 dimension. So far, we have not seen any such a mode from the experimental side. One reason for that is that our collider energy may not be sufficiently high to probe the extra dimension length.

1.2.1 Large extra dimension model (ADD)

The hierarchy problem is a long-standing problem in particle physics. In particle physics, we have two scales; the electroweak scale at which electroweak symmetry breaking happens and the Planck scale where gravitational interaction strength become unity. The order of the electroweak scale is 10^2 GeV, whereas the Planck scale is the order of 10^{19} GeV. If SM is valid up to the Planck scale, then there should be some mechanism to generate this large gap between these two scales. On the other hand, it can be asked why gravity is so small compared to the other interaction. This problem is called the scale hierarchy problem in particle physics. The gravity itself is not there in the SM. Arkani Hamed, Dimopoulos and Dvali proposed a framework based on KK theory to solve this hierarchy problem, and this framework is called the Large extra dimension model (ADD) [15]. According to this model,

our spacetime has $4+n$-dimensions. Similar to the KK theory, this extra dimension will form a compact manifold. The SM particles are confined to the 4 dimensions, whereas gravity can propagate through these extra dimensions. As gravity can propagate through these extra dimensions, they will form massive KK modes. These KK modes will be accessible in experiments only when the energy scale E will be much much greater than the volume of the extra dimensions. If gravity propagates through them, we can see deviations from the inverse square low. How small R is probed in the experiments, for that, we need to study the gravitational force between two massive particles in the presence of extra dimensions.

According to Newton's law, gravitational force between two massive particles of mass m_1 and m_2 in 4 dimension is

$$F(r) \sim \frac{G_N^{(4)} m_1 m_2}{r^2} = \frac{1}{M_{pl(4)}^2} \frac{m_1 m_2}{r^2} \tag{1.15}$$

In $4+n$ dimension, this equation will be

$$F(r) \sim \frac{G_N^{(4+n)} m_1 m_2}{r^{2+n}} = \frac{1}{M_{pl(4+n)}^{2+n}} \frac{m_1 m_2}{r^{2+n}} \tag{1.16}$$

If L is the size of extra dimension then depending on the distance between the particles the force structure can be written as,

$$F(r) \sim \frac{1}{M_{pl(4+n)}^{2+n}} \frac{m_1 m_2}{r^{2+n}} \qquad \text{for} \quad \mathrm{r} \ll \mathrm{L} \tag{1.17}$$

$$F(r) \sim \frac{1}{M_{pl(4+n)}^{2+n}} \frac{m_1 m_2}{r^2 L^n} \qquad \text{for} \quad \mathrm{r} \gg \mathrm{L} \tag{1.18}$$

One can compare the last expression with 4-dimensional Newton's law to obtain

$$M_{pl(4)}^2 \sim M_{pl(4+n)}^{n+2} L^n = M_{pl(4+n)}^{n+2} V_n \tag{1.19}$$

Where V_n is the volume of compact extra dimension. From the above equation, one can find the allowed size of the extra dimensions. If one chooses $M_{pl(4+n)}$ of the

order 1 TeV and $M_{pl(4)}$ of the order of 10^{19} GeV then

$$L \sim \left\{ \frac{M_{pl(4)}^2}{M_{pl(4+n)}^{n+2}} \right\}^{\frac{1}{n}} \sim 10^{32/n}\text{TeV}^{-1} \sim 10^{32/n}10^{-17}\text{cm} \tag{1.20}$$

- $n = 1 \implies L \sim 10^{15} cm$ This choice is obviously ruled out.
- $n = 2 \implies L \sim 1mm$ This is also not allowed because gravity has been tested up to $L \sim 200\mu m$ [20–23].
- $n = 3 \implies L \sim 10^{-6} cm$ This is allowed because gravity has not been tested yet to such small scale. Therefore, the size of the extra dimensions can be lying in this length scale.

From the particle physics experimental point of view, the SM has been tested upto few TeV and the effect of extra dimensions has not been seen so far. Therefore, the size of the extra dimension has to be less than 1 TeV^{-1}.

1.2.1.1 Gravity in $4+n$ dimension

General Metric tensor in $(4+n)$ dimension considering 4 dimensional flat space and compactified n space can be written as

$$ds^2 = (\eta_{\mu\nu} + h_{\mu\nu})dx^\mu dx^\nu - r^2 d\Omega_{(n)}^2 \tag{1.21}$$

where x^μ is 4-dimensional coordinate, $\eta_{\mu\nu}$ is the 4-dimensional flat Minkowski metric, $h_{\mu\nu}$ is the fluctuation of $\eta_{\mu\nu}$ around its minimum value and $d\Omega_{(n)}^2$ is the line elements of extra dimensions. Now gravity can propagate through all dimensions whereas the SM particles are confined only in the 4 dimensional plane called Brane. In the $4+n$ dimensions bulk, the action can be written as

$$S^{(4+n)} = -M_{pl(4+n)}^{2+n} \int d\Omega_{(n)} r^n \int d^4x \sqrt{g^{(4)}} R^{(4)} \tag{1.22}$$

The gravitational metric tensor is a symmetric tensor $g_{AB} = \eta_{AB} + h_{AB}$. The number of independent components of this metric tensor is $\frac{(4+n)(5+n)}{2} - 2(4+n)$.

The $2(4+n)$ factor is coming from the coordinate transformation condition and gauge fixing condition. The zero modes of the metric contains one 4-dimensional graviton, n massless vectors, and $n(n+1)$ massless scalar particles. For non zero modes, each KK modes contain one massive spin-2 tensor, $(n-1)$ massive vectors and $\frac{n(n-1)}{2}$ massive scalars. For a particular mode $\overrightarrow{k}$, the metric tensor can be written as

$$\left(\begin{array}{c|c} G_{\mu\nu}^{\overrightarrow{k}} & V_{\mu j}^{\overrightarrow{k}} \\ \hline V_{\mu j}^{\overrightarrow{k}} & S_{jk}^{\overrightarrow{k}} \end{array}\right)$$

where, μ and ν run from $0 \to 3$, i and j run from $5 \to (4+n)$. The first block represent 4-dimensional gravity by 4×4 matrix. They satisfy the condition

$$\partial^{\mu} G_{\mu\nu}^{\overrightarrow{k}} = 0, \qquad G_{\mu}^{\mu\,\overrightarrow{k}} = 0 \tag{1.23}$$

The 2nd and 3rd block form 4-dimensional vectors by $(n-1) \times (n-1)$ matrix and they satisfy the condition

$$\partial^{\mu} V_{\mu j}^{\overrightarrow{k}} = 0, \qquad \hat{k}_j V_{\mu}^{j\,\overrightarrow{k}} = 0 \tag{1.24}$$

and results $n-1$ independent vectors. The 4th block represents the scalar with $n \times n$ matrix, which satisfy the condition

$$\hat{k}^j S_{jk}^{\overrightarrow{k}} = 0, \qquad S_{j}^{j\,\overrightarrow{k}} = 0. \tag{1.25}$$

But there is one scalar that does not satisfy the 2nd condition of the above equation. This special scalar is called radion. The expression of all these fields in unitary gauge are given below;

$$H^{\overrightarrow{k}} = \frac{1}{\alpha} h_j^{\overrightarrow{k}\,j} \qquad \text{Radion} \tag{1.26}$$

$$S_{ij}^{\vec{k}} = h_{ij}^{\vec{k}} - \frac{\alpha}{n-1}\left(\eta_{ij} + \frac{\hat{k}_i\hat{k}_j}{\hat{k}^2}\right)H^{\vec{k}} \qquad \text{Scalars} \tag{1.27}$$

$$V_{\mu j}^{\vec{k}} = \frac{i}{\sqrt{2}}h_{\mu j}^{\vec{k}} \qquad \text{Vectors} \tag{1.28}$$

$$G_{\mu\nu}^{\vec{k}} = h_{\mu\nu}^{\vec{k}} + \frac{\alpha}{3}\left(\eta_{\mu\nu} + \frac{\partial_\mu\partial_\nu}{\hat{k}^2}\right)H^{\vec{k}} \qquad \text{Gravitons} \tag{1.29}$$

The equation of motion of these fields are

$$(\Box + \hat{k}^2)G_{\mu\nu}^{\vec{k}} = \frac{1}{M_{pl(4+n)}}\left\{ -T_{\mu\nu} + \frac{T_\mu^\mu}{3}\left(\eta_{\mu\nu} + \frac{\partial_\mu\partial_\nu}{\hat{k}^2}\right)\right\} \tag{1.30}$$

$$(\Box + \hat{k}^2)V_{\mu j}^{\vec{k}} = 0, \qquad (\Box + \hat{k}^2)S_{ij}^{\vec{k}} = 0 \tag{1.31}$$

$$(\Box + \hat{k}^2)H^{\vec{k}} = \frac{\alpha}{3M_{pl(4+n)}}T_\mu^\mu \tag{1.32}$$

1.2.1.2 Phenomenology of ADD model

In the large extra dimension model, gravity can propagate through all $(4+n)$ dimensions called bulk, whereas SM fields are confined to the brane. To describe the interactions of the gravitons with SM particles, we need to develop an effective field theory for brane. In this effective theory, the interaction action can be written as

$$S_{\text{int}} = -\frac{\kappa}{2}\sum_{\vec{k}=0}^{\infty}\left\{h_{\mu\nu}^{\vec{k}}(x)T^{\mu\nu}(x)\right\}. \tag{1.33}$$

This action implies that graviton can couple to energy-momentum tensor with coupling strength κ, where $\kappa = \frac{\sqrt{16\pi}}{M_{pl}}$. The zeroth mode corresponds to the massless

graviton. Though the coupling strength is suppressed by the Planck scale, in the effective theory approach, this scale is equal to the scale of effective theory M_s, which corresponds to the $M_{pl(4+n)}$. Therefore, graviton can couple to SM gauge bosons and fermions with equal coupling strength irrespective of their charges, colours and masses. The effect of these gravitons can be seen in any scattering process; the final states of the scattering process can be produced through virtual graviton exchange. The real emission of the KK modes would lead to the information of missing energy in the collider experiments.

In the case of the virtual graviton exchange processes, one needs to consider a graviton propagator with a sum over all KK modes. This graviton propagator can be written as

$$\kappa^2\mathcal{D}(Q^2) = \kappa^2 \sum_{\overrightarrow{k}} \frac{1}{Q^2 - m^2_{\overrightarrow{k}} + i\epsilon}, \qquad \text{where} \quad q^2 = Q^2. \tag{1.34}$$

In large extra dimension model, the mass difference between the KK modes are small and hence it can be approximated that the mass distribution is continuous. The number of the KK modes in the small mass interval $dm_{\overrightarrow{k}}$ can be written as

$$\Delta\,\overrightarrow{k}^{\,2} = \rho(m^2_{\overrightarrow{k}})dm^2_{\overrightarrow{k}}, \tag{1.35}$$

where $\rho(m^2_{\overrightarrow{k}})$ is density of KK modes in continuum limit. In this limit, Eq.(1.34) can be written as

$$\kappa^2\mathcal{D}(Q^2) = \frac{8\pi}{M_s^4}\left(\frac{Q}{M_s}\right)^{(n-2)}\Big\{ -i\pi + 2I(M_s/Q)\Big\}. \tag{1.36}$$

The integral $2I(M_s/Q)$ corresponds to the non resonant production of KK modes and π corresponds to the resonant production of a single time-like KK mode [2]. Here, we consider the explicit cutoff scale on KK sum is equal to the scale of extra dimension [2, 24] The integral takes the form

$$I(\omega) \sim \int_0^{\omega} dx \frac{x^{n-1}}{1-x^2}, \tag{1.37}$$

$$I(\omega) = -\sum_{\vec{k}=1}^{n/2-1} \frac{1}{2\,\vec{k}} \omega^{2\vec{k}} - \frac{1}{2}\log(\omega^2 - 1)\,, \qquad n = \text{even}\,, \tag{1.38}$$

$$I(\omega) = -\sum_{\vec{k}=1}^{(n-1)/2} \frac{1}{2\,\vec{k} - 1} \omega^{2\vec{k}-1} + \frac{1}{2}\log\left(\frac{\omega+1}{\omega-1}\right)\,, \qquad n = \text{odd}\,. \tag{1.39}$$

1.2.1.3 Experimental searches for ADD model

In an extra dimension model, the KK modes of graviton can couple to SM gauge bosons and fermions with universal coupling and the KK modes are continuous. Therefore the signature of this kind of model can be probe in the collider only through the deviation from the SM observables values. Presently the world's most sophisticated collider, the LHC, is looking for this signature over time to time. Several experimental data are available regarding the lower bound of the model parameters M_s and n. The lower limits on the scale M_s obtained from both ATLAS and CMS collaborations using 7 TeV data [25, 26] are $M_s = 2.4$ TeV corresponding to $n = 3$ in HLZ formalism [2]. With the availability of 8 TeV data, this lower bound further pushed to 3.3 TeV. Now 13 TeV data are also available from ATLAS and CMS [27, 28]. From di-photon channel data ATLAS results [1] are presented in Tab.(1.1). Similar results are also provided by CMS collaboration using dilepton

No. of extra dimensions (n)	Without K-factor	With K-factor
3	8.1	8.6
4	6.8	7.2
5	6.1	6.5
6	5.7	6.1

Table 1.1: M_s observed limit (TeV) for di-photon channel from ATLAS collaboration [1] in HLZ formalism

channel data [3] and is presented in Tab.(1.2).

No. of extra dimensions (n)	Observed limit (TeV)
3	8.6
4	7.2
5	6.5
6	6.1

Table 1.2: M_s observed limit (TeV) for dilepton channel from CMS collaboration [3] in HLZ formalism

1.2.2 Warped extra dimension model (RS)

In the last section, we discussed ADD model. ADD model is the first simplest extra dimension model to address the hierarchy problem. The hierarchy between the electroweak scale and Planck scale can be solved by considering the large volume of the extra dimension, and the scale of this effective theory (M_s) could be as small as a few TeV, which become new cutoff scale for the SM. However, the hierarchy between the electroweak scale and Planck scale has not been solved because this model leads to another hierarchy between the fundamental length $M_s^{-1} \sim 10^{-16} mm$ and the size of the extra dimensions $R \sim 10^{32/n} M_s^{-1}$. This model assumed that the extra dimensions are flat. Therefore, the *backreaction* of gravity to the presence of the branes themselves has been ignored. This assumption is good only when the tension of the branes are small.

A good motivation to solve the remaining hierarchy problem in the ADD model comes from the Randall-Sundrum model (RS) [16]. According to this model, our space-time is 5 dimensional, *i.e* it considered only one extra dimension. This extra dimension has length r and compactified in a circle with a circumference of $2\pi r$. Similar to the ADD, gravity can propagate through this extra dimension and SM fields are confined in the 4- dimensional brane. The higher dimensional metric of this model is

$$ds^2 = e^{-A(y)} \eta_{\mu\nu} dx^\mu dx^\nu + dy^2, \tag{1.40}$$

where $y = r\phi$ is the coordinate of the extra dimension, x^μ is the usual 4-dimension coordinate, and $A(y)$ is the warped factor, determine the curvature of the extra dimension. The value of this warped factor is $2ky$, where k is the scale of the Planck

scale's order. This model's important feature is this warped factor that can solve the hierarchy problem between the electroweak scale and Planck scale without requiring a large volume of extra dimension. This extra dimension has S^1/Z_2 symmetry, which means $0 \leq y \leq \pi r$ will specify the whole metric. Another feature of this model is that it has two branes, the SM brane on which SM fields are located and the Planck brane. The SM brane is located at $y = \pi r$ in order to account for the weakness of gravity on it. The Planck brane is located at $y = 0$, where its gravitational interaction is expected to be large.

Now we will discuss how this warped factor solves the Higgs mass hierarchy problem. Consider H as a complex scalar field Higgs doublet. The action can be written as

$$S_H = -\int d^4x \left[e^{-2\pi kr} \eta_{\mu\nu} \partial_\mu H^\dagger \partial_\nu H - M_5^2 e^{-4\pi kr} |H|^2 + \lambda e^{-4\pi kr} |H|^4 \right]. \tag{1.41}$$

The M_5 represent the Higgs mass near the 5 dimensional cutoff scale. If we re-scale the Higgs fields by $H \to e^{\pi kr}$, the action will be

$$S_H = -\int d^4x \left[\eta_{\mu\nu} \partial_\mu H^\dagger \partial_\nu H - (M_5 e^{-\pi kr})^2 |H|^2 + \lambda |H|^4 \right]. \tag{1.42}$$

Now compare the the above equation with usual 4-dimensional Higgs field action.

$$S_H = -\int d^4x \left[\eta_{\mu\nu} \partial_\mu H^\dagger \partial_\nu H - m_{Higgs} |H|^2 + \lambda |H|^4 \right]. \tag{1.43}$$

Higgs mass is identified $m_{Higgs} = M_5 e^{-\pi kr}$. The mass is scaled down by a factor $e^{-\pi kr}$ because of the fact that Higgs bosons are located on SM brane at $y = \pi r$. If Higgs bosons were located at Planck brane at $y = 0$, there would not be any shift of the Higgs mass.

Now one can ask what should be the scale of this effective RS theory, or more precisely, what should the value of the warped factor to get correct Higgs physical mass. For this, we consider 4-dimensional gravity is embedded in 5-dimensional metric

$$ds^2 = e^{-2ky} \Big\{ \eta_{\mu\nu} + h_{\mu\nu} \Big\} dx^\mu dx^\nu - dy^2. \tag{1.44}$$

Therefore, 5-dimensional Einstein-Hilbert action containing 4-dimensional metric can be written as

$$S = -M_5^3 \int_{-r}^{r} e^{-4ky} \sqrt{g^{(4)}} e^{2ky} R^{(4)} dy. \tag{1.45}$$

From this equation one can find the 4-dimensional effective Planck scale

$$M_{pl}^2 = \frac{M_5^3}{k}(1 - e^{-2kr}). \tag{1.46}$$

We can see that for $M_{pl} \sim M_5$, 4-dimensional Planck scale does not get significant modification because of the extra dimension.

1.2.2.1 Gravity in RS model

In Eq.(1.44) we present the metric of the RS model and Eq.(1.45) represents the action of this model. Using these two equation, the KK decomposition of this model can be written as

$$h_{\mu\nu}(x^\mu, y) = \sum_{n=0}^{\infty} h_{\mu\nu}^{(n)}(x^\mu) f^{(n)}(y). \tag{1.47}$$

This $h_{\mu\nu}^{(n)}$ will satisfy the the equation

$$\Box h_{\mu\nu}^{(n)} = m_n^2 h_{\mu\nu}^{(n)}. \tag{1.48}$$

The function $f^{(n)}(y)$ is chosen in such a way that they will satisfy the orthogonal condition

$$\int_0^{\pi r} dy e^{-2ky} f^{(n)}(y) f^{(m)}(y) = \delta_{nm}, \tag{1.49}$$

with the equation of motion

$$-\partial_5(e^{-4ky}\partial_5 f^{(n)}(y)) = m_n^2 e^{-2ky} f^{(n)}(y). \tag{1.50}$$

The solution of the above differential equation is

$$f^{(n)}(y) = \frac{e^{2ky}}{C_n}\Big(J_2(\alpha_n) + a_n Y_2(\alpha_n)\Big), \tag{1.51}$$

where J_2 and Y_2 are the 2nd order bessel functions of the first kind and 2nd kind, $\alpha_n = m_n e^{ky}/k$, C_n and a_n are two arbitrary constant. If we define $x_n = \alpha_n(\pi)$, then the continuity of $f^{(n)}$ leads $a_n = x_n^2 e^{2\pi kr}$ and $J_1(x_n) = 0$. Therefore, the mass of the RS KK modes are given by

$$m_n = k x_n e^{-\pi kr}, \tag{1.52}$$

where the x_n are the zeros of the first order Bessel function, $x_1 = 3.8317$, $x_2 = 7.0156$, $x_3 = 10.1735$. The other constant C_n can be obtained from the orthogonal condition given in Eq.(1.49) and the result is

$$C_n = \frac{e^{\pi kr}}{\sqrt{kr}} J_2(x_n). \tag{1.53}$$

We can see that the masses of the RS KK modes depends on the zeros of the Bessel function and unlike ADD, these masses are not continuous.

1.2.2.2 Phenomenology of RS model

The interaction Lagrangian of the massive RS KK modes with the SM fields is given by

$$\mathcal{L}_{int} \sim -\frac{1}{M_{pl}} T^{\mu\nu} h^{(0)}_{\mu\nu} - \frac{1}{M_{pl} e^{-\pi kr}} \sum_{n=1}^{\infty} T^{\mu\nu} h^{(n)}_{\mu\nu}, \tag{1.54}$$

where $T^{\mu\nu}$ is the energy-momentum tensor of the SM. The above equation implies that the Planck scale suppresses coupling to the zeroth mode and the SM. However, for the higher modes, this suppression has been rescaled by the warped factor. The SM fields couple to the higher-order RS KK modes with effective coupling c_0, where $c_0 = k/M_{pl}$. Therefore, this model has two parameters: the effective coupling c_0 and the mass of the first KK mode m_1. Like the ADD model, RS graviton also couples to the SM particles universally irrespective of their charges, colours and masses. Therefore, these massive KK modes can be produced at high energy collider experiments and then decay to the SM particles with decay width Γ_n. The

propagator of the graviton can be written as

$$\mathcal{D}(Q^2) = \sum_n \frac{1}{Q^2 - m_n^2 + i m_n \Gamma_n} = \frac{1}{m_0^2} \sum_n \frac{x^2 - x_n^2 - i\frac{\Gamma_n}{m_0} x_n}{(x^2 - x_n^2)^2 + \frac{\Gamma_n^2}{m_0^2} x_n^2}, \tag{1.55}$$

where $x = Q/m_0$ and $x_n = m_n/m_0$. The presence of the massive KK modes will give a heavy resonance in the invariant mass distribution for the Drell-Yan or Diphoton kind of channel. This resonance pattern is a distinct feature of the RS model from the ADD signal.

1.2.2.3 Experimental searches for RS model

There have been several experimental searches at the LHC for warped extra dimensions in the past, yielding stringent bounds on the RS model parameters, the mass of the first resonance mode m_1 and the coupling strength c_0. In the dilepton channel using the combined 8 and 13 TeV data at the LHC, the observed 95% CL lower limit on the RS resonance is 1.38(2.98) TeV for $c_0 = 0.01(0.1)$ [4]. The detailed results are presented in Tab.(1.3). Similar kind of analysis has also been done by ATLAS

Channel Name	$c_0 = 0.01$		$c_0 = 0.1$	
	Obs. (TeV)	Exp. (TeV)	Obs. (TeV)	Exp. (TeV)
$e^{\pm}$	1.46	1.48	2.78	2.93
$\mu^{\pm}$	1.26	1.41	3.03	3.03
$e^{\pm} + \mu^{\pm}$	1.46	1.61	3.11	3.23
$e^{\pm} + \mu^{\pm}$13 TeV only	1.38	1.45	2.98	3.15

Table 1.3: The observed and expected 95% CL lower limits of the graviton mass m_1 in RS model for the combined 8 and 13 TeV data in CMS collaboration [4].

collaboration in di-photon channel using 13 TeV data. The lower limit at 95% CL on the RS first resonance mass is found to be 4.1 TeV for $c_0 = 0.1$ [1].

There is another scenario of graviton production where the massive KK modes of gravitons couple to the SM fields non-universally *i.e* gravitons couple to SM fermions and gauge bosons fields with different couplings. The phenomenology of this kind of model is somewhat similar to the warped extra dimension model,

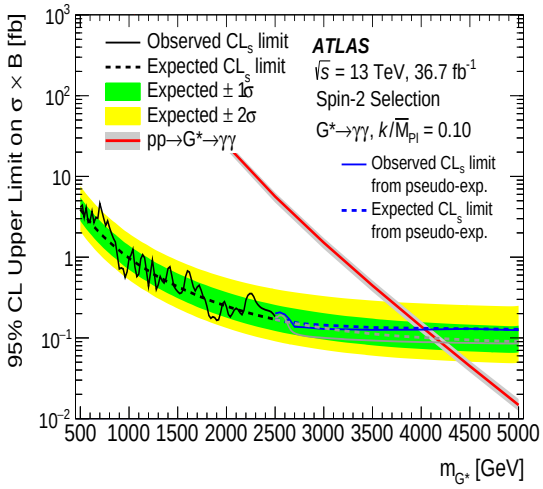

Figure 1.2: Upper limits on the production cross section times branching ratio to two photons at 13 TeV of the lightest KK graviton as a function of its mass M_{G*} for $c_0 = 0.1$ [1]

but the parameters space of this model is less constrained. In Ch.(6) we study this scenario in details.

1.3 Need for precise theoretical results

To understand the dynamics of fundamental particles, one requires precise results both from theoretical and experimental sides. Any deviation in the experimental results from the known theory (the SM) would lead to the BSM signatures. The Standard Model predictions have been tested very well through different collider experiments since the early 20th century. In collider experiments, one accelerates particles to very high energy to achieve the insight of these particles and let them produce a new final state through various interaction. The centre of mass-energy ($E_{\rm CM}$) for head-to-head collision of two particles with mass m_1 and m_2 and energy E_1 and E_2 can be written as

$$E_{\rm CM} = \left[2E_1E_2 + (m_1^2 + m_2^2) + 2\sqrt{E_1^2 - m_1^2}\sqrt{E_2^2 - m_2^2}\right]^{1/2}. \tag{1.56}$$

Here we consider natural unit where $\hbar = 1$ and $c = 1$.

Almost three dozen of colliders had been made between the late '50s and now. The most powerful and sophisticated collider available now to explore fundamental physics is the Large Hadron Collider (LHC). It was built by CERN between 1998 to 2008 with the collaboration of more than 10000 scientists, many universities and laboratories as well as more than 100 countries. It is a circular collider with a circumference of 26.7 kilometres and kept at a depth ranging from 50 to 175 metres. It collides with two protons with very high energy. Therefore, its centre of mass-

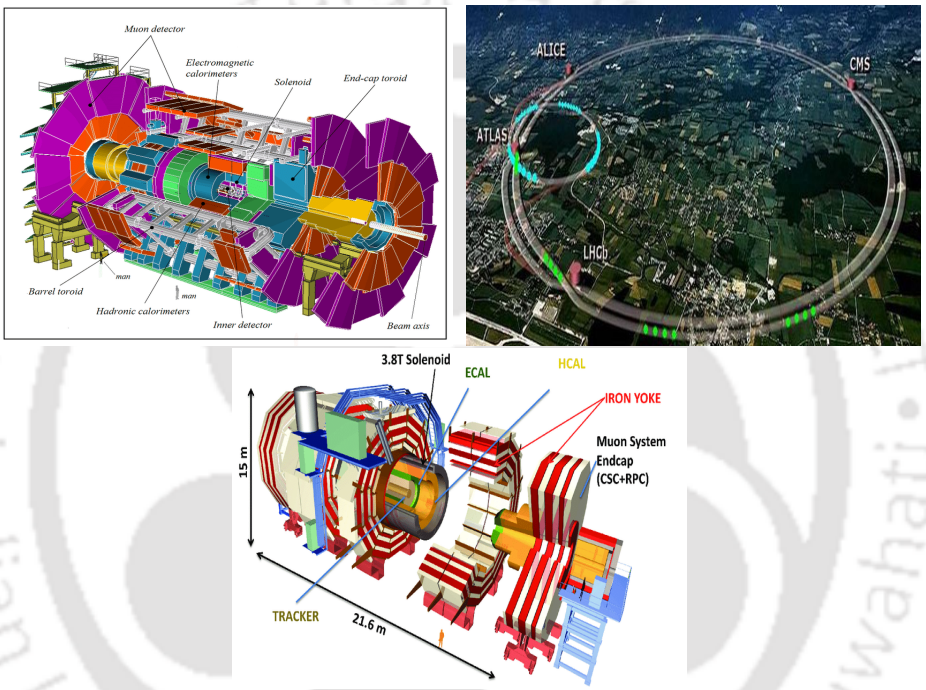

Figure 1.3: Large Hadron Collider (middle) and it's two detectors ATLAS and CMS

energy can scan a large kinematical region hence it is a perfect discovery machine. The last and most wanted member of the standard model, the Higgs boson, has been discovered in the last decade at the LHC at the centre of mass energies of 7 and 8 TeV, and the properties of these Higgs bosons are very similar to that of SM predicted. With the LHC upgraded to 13 TeV in run II, this Higgs boson's spin and parity properties have been established. With sophisticated detector technology and high luminosity, it has become possible to study the SM's predictions to a very high degree of precision at this collider. To match these experimental results, we need precise theoretical results. This can be achieved by considering the quantum correction of the theory.

Hadrons are not fundamental; they are made of quarks and gluons, generally known as partons. Therefore, to understand the outcome of a high energy collision involving hadrons, it is important to understand the dynamics of these partons inside hadrons. Parton Model describes how hadrons interact in the high energy collision via its parton. The original parton model was proposed by Richard Feynman in the "infinite momentum frame". In this frame, the proton is considered ultra-relativistic and therefore, one can neglect the mass of hadrons as well as partons. According to this model, a parton coming from a hadron is parallel to this hadron and carries a momentum fraction z_i of the hadron momentum p.

$$\hat{p}_i = z_i p, \qquad 0 \leq z_i \leq 1, \tag{1.57}$$

where $\hat{p}_i$ is the parton momentum (We will use $\hat{}$ to define partonic quantities). The parton momentum is not fixed, and the distribution function of the parton inside the proton is $f_i(z_i)$, known as the parton distribution function (PDF). This PDF gives information about the probability of finding a parton inside a proton with fractional momentum z_i.

Another assumption of the parton model is that the interaction between proton and elementary particles can be written as the interaction between partons and elementary particles and then can be weighted by PDF to have hadronic quantities. Therefore, if $\hat{\sigma}$ is the parton level cross-section, then the hadron level cross-section can be written as

$$\sigma(p) = \sum_i \int_0^1 dz f(z) \hat{\sigma}_i(zp), \tag{1.58}$$

p is the momentum of the proton. These PDF are constructed in such a way that they fulfil certain criteria:

- The difference between quark and anti-quark PDF integrated over momentum fraction z, will give the number of constituents quarks inside proton.

$$\int_0^1 [f_u(z) - f_{\bar{u}}(z)] = 2; \quad \int_0^1 [f_d(z) - f_{\bar{d}}(z)] = 1 \tag{1.59}$$

For rest of the partons it is zero.

- The sum of all partons momentum must be equal to proton momentum.

$$\sum_i \int_0^1 z f_i(z) dz = 1 \tag{1.60}$$

The precise theoretical results can be achieved by calculating the partonic coefficient function ($\hat{\sigma}(z_i p)$) accurately. This can be done by considering the quantum correction of the theory, and therefore, the partonic coefficient function can be written in a perturbative series of the coupling constant of the theory. The strong interaction has the strongest coupling constant and will dominate over other quantum corrections. Therefore, the higher-order perturbative QCD corrections are significant to obtain a precise theoretical prediction. In the next chapter, we will discuss the methodology of QCD perturbation theory.

Chapter 2

Precision Calculation in QCD

To achieve the precise theoretical results, quantum corrections of strong interaction are very important because of its largest coupling constant. The theory which describes the dynamics of strong interaction is called quantum chromodynamics (QCD). It is a $SU(3)$ gauge theory which contains 8 gauge bosons called gluons. These gauge bosons interact only with the coloured particles like quarks and to themselves. The self-interaction among these gauge bosons makes QCD different from QED. The interaction Lagrangian of the QCD can be written as

$$\mathcal{L} = -\frac{1}{4}F^a_{\mu\nu}F^{a\mu\nu} + \overline{\psi}_i(i\gamma^\mu\mathcal{D}^{ij}_\mu - m\delta^{ij})\psi_j - \frac{1}{2\zeta_0}(\partial_\mu A^{a\mu})^2 - \overline{c}^a(-\partial^\mu\mathcal{D}^{ac}_\mu)c^c \tag{2.1}$$

where $F^a_{\mu\nu}$ is the field strength tensor

$$F^a_{\mu\nu} = \partial_\mu A^a_\nu - \partial_\nu A^a_\mu + \hat{g}_s f^{abc} A^b_\mu A^c_\nu \tag{2.2}$$

$\mathcal{D}^{ij}_\mu$ and $\mathcal{D}^{ab}_\mu$ are the covariant derivative for quarks and gluons fields

$$\mathcal{D}^{ij}_\mu = \delta^{ij}\partial_\mu - i\hat{g}_s T^{ij}_a A_{a\mu} \tag{2.3}$$

$$\mathcal{D}^{ab}_\mu = \delta^{ab}\partial_\mu - \hat{g}_s f^{abc} A^c_\mu \tag{2.4}$$

The last term of the equation Eq.(2.2) is responsible for gluon self-coupling, which is not present for QED. This makes QCD different from QED. The other terms of the above equations are

ψ : quarks field $\quad$ A^a_μ : gluons field

c^a : Ghost fields $\quad$ T^a_{ij} : Generators of $SU(3)$ group

f^{abc} : Structure constant of $SU(3)$ group

i, j: colours indices in the fundamental representation

a, b, c : colours indices in adjoint representation

m: mass of quarks field

ζ_0 : gauge parameters $\quad$ $\hat{g}_s$: bare strong coupling constant

The first and second term in Eq.(2.1) represent the kinetic term for quarks and gluons fields, the third term represents the gauge fixing term, and the last term is coming to remove the unphysical polarization of the gluons fields.

2.1 Fixed Order Computation

As mention in the last chapter, the precise theoretical results can be obtained by taking into account the quantum correction of the theory. Therefore, any physical quantity can be written as a perturbation series where the expansion parameter is the coupling strength of the theory. In QCD, the partonic observables can be written as

$$\hat{C}(Q^2) = C_0(Q^2) + \hat{\alpha}_s C_1(Q^2) + \hat{\alpha}_s^2 C_2(Q^2) + \cdots \tag{2.5}$$

The first term on R.H.S is called leading order partonic quantity, second term is called next-to-leading order (NLO) partonic quantity, third term is called next-to-next-leading order (NNLO) partonic quantity and so on. At The LHC, the hadronic

cross section can be written as

$$C(Q^2) = f_a(x_1) \otimes f_b(x_2) \otimes \hat{C}(Q^2) \tag{2.6}$$

where x_1, x_2 are the momentum fraction carried by partons coming from hadrons, $f_a(x_1)$ and $f_b(x_2)$ are the parton distribution function. The LO computation is straightforward. However, higher order computation will lead several singularities. There are many regularization schemes to regularize these singularities, for example; massive gluon scheme, ultra violet cutoff method, dimensional regularization etc. Here, we will work with dimensional regularization scheme *i.e* our space time has $4 + \epsilon$ dimensions where ϵ is the regulator. Therefore singularities will appear as power of $\frac{1}{\epsilon}$.

Depending on the origin, there are two kind of singularities, UV singularities, and IR singularities. To understand the origin of these singularities, let us consider the typical diagrams at NLO computation in QCD for quark anti-quark annihilation as shown in Fig.(2.1) The first diagram is called virtual diagram and the second one is called real emission diagram. For virtual correction, the matrix

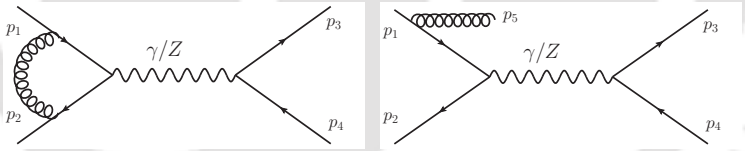

Figure 2.1: Example diagrams for quark anti-quark annihilation process at NLO in QCD

amplitude will contain $\int_0^\infty \frac{d^4k}{(k^4)}$ where k is the loop momenta. This integration is logarithmically divergent in 4 dimension when $k \to \infty$. In $4 + \epsilon$ dimension these infinities will appear as pole in ϵ. This kind of singularity is called UV singularity. To absorb these singularities, one needs to redefine the bare quantities in the QCD Lagrangian. The redefinition of bare quantities is called renormalization. Therefore, after renormalization the bare quantities in the Lagrangian can be written as

$$\hat{\psi} = Z_\psi(\mu_r)\psi(\mu_r); \qquad \hat{g}_s = Z_g(\mu_r)g_s(\mu_r) \tag{2.7}$$

where Z_ψ is the wave function renormalization coefficient, ψ could be quark, gluon

or ghost fields, Z_g is the coupling strength renormalization coefficient. We use ' $\hat{}$ ' for bare quantities and with out ' $\hat{}$ ' for renormalized quantities. The factorization between bare quantities and renormalized quantities will introduce a new unphysical scale μ_r, called the renormalization scale.

Running strong coupling constant :

The renormalized strong coupling constant is not constant but depend on unphysical renormalization scale μ_r. We define $\hat{a}_s = \hat{g}_s^2/16\pi^2$ and $a_s = g_s^2/16\pi^2$ then,

$$S_\epsilon \frac{\hat{a}_s}{\mu_0^\epsilon} = Z(\mu_r^2)\frac{a_s(\mu_r^2)}{\mu_r^\epsilon} \tag{2.8}$$

where μ_0 is introduced to make strong coupling constant dimensionless in $4+\epsilon$ dimension. The L.H.S of Eq.(2.8) is independent on μ_r whereas, R.H.S is a function of μ_r. Therefore,

$$\mu_r^2 \frac{d\hat{a}_s}{d\mu_r^2} = 0 \tag{2.9}$$

This equation leads to the renormalized group equation (RGE) of a_s and it reads as

$$\frac{d\log a_s(\mu_r^2)}{d\log \mu_r^2} = \frac{\epsilon}{2} - \frac{d\log Z(\mu_r^2)}{d\log \mu_r^2} \tag{2.10}$$

Now we define a new function called β-function as

$$\frac{da_s(\mu_r^2)}{d\log \mu_r^2} = \frac{\epsilon}{2} + \frac{1}{a_s(\mu_r^2)}\beta(a_s(\mu_r^2)) \tag{2.11}$$

This β-function can be written as a series of a_s as

$$\beta(a_s(\mu_r^2)) = -\sum_{n=0}^{\infty} \beta_n \left(a_s(\mu_r^2)\right)^{n+2} \tag{2.12}$$

Using Eq.(2.11) and Eq.(2.12) one can find the solution for $Z(\mu_r^2)$ and the solution is

$$Z(\mu_r^2) =1 + a_s(\mu_r^2)\frac{2\beta_0}{\epsilon} + a_s^2(\mu_r^2)\left(\frac{4\beta_0^2}{\epsilon^2} + \frac{\beta_1}{\epsilon}\right) + a_s^3(\mu_r^2)\left(\frac{8\beta_0^3}{\epsilon^3} + \frac{14\beta_0\beta_1}{3\epsilon^2} + \frac{2\beta_2}{3\epsilon}\right)+ a_s^4(\mu_r^2)\left(\frac{16\beta_0^4}{\epsilon^4} + \frac{46\beta_0^2\beta_1}{3\epsilon^3} + \frac{9\beta_1^2+20\beta_0\beta_2}{6\epsilon^2} + \frac{\beta_3}{2\epsilon}\right) + \mathcal{O}(a_s^5(\mu_r^2)) \tag{2.13}$$

where the β's are given below [29–37].

$$\begin{aligned}
\beta_0 &= \frac{11}{3}C_A - \frac{2}{3}n_f \\
\beta_1 &= \frac{34}{3}C_A^2 - 4n_fT_FC_F - \frac{20}{3}n_fT_FC_A \\
\beta_2 &= \frac{2857}{54}C_A^3 - \frac{1415}{27}C_A^2T_Fn_f + \frac{158}{27}C_AT_F^2n_f^2 + \\
&\quad \frac{44}{9}C_FT_F^2n_f^2 - \frac{205}{9}C_FC_AT_Fn_f + 2C_F^2T_Fn_f \\
\beta_3 &= \left(\frac{17152}{243} + \frac{448}{9}\zeta_3\right)C_AC_FT_F^2n_f^2 + \left(-\frac{4204}{27} + \frac{352}{9}\zeta_3\right)C_AC_F^2T_Fn_f + \\
&\quad \frac{424}{243}C_AT_F^3n_f^3 + \left(\frac{7073}{243} - \frac{656}{9}\zeta_3\right)C_A^2C_FT_Fn_f + \left(\frac{7930}{81} + \frac{224}{9}\zeta_3\right)C_A^2T_F^2n_f^2 + \\
&\quad \frac{1232}{243}C_FT_F^3n_f^3 + \left(-\frac{39143}{81} + \frac{136}{3}\zeta_3\right)C_A^2C_FT_Fn_f + \left(\frac{150653}{486} - \frac{44}{9}\zeta_3\right)C_A^4 + \\
&\quad \left(\frac{1352}{27} - \frac{704}{9}\zeta_3\right)C_F^2T_F^2n_f^2 + 46C_F^3T_Fn_f + \left(\frac{512}{9} - \frac{1664}{3}\zeta_3\right)n_f\frac{N(N^2+6)}{48} + \\
&\quad \left(-\frac{704}{9} + \frac{512}{3}\zeta_3\right)n_f^2\frac{(N^4-6N^2+18)}{96N^2} + \left(\frac{80}{9} + \frac{704}{3}\zeta_3\right)\frac{N^2(N^2+36)}{24}
\end{aligned} \tag{2.14}$$

where $C_A = N$, $C_F = \frac{N^2-1}{2N}$, n_f is the number of active quark flavour and is equal to 5, $T_F = \frac{1}{2}$ and $N = 3$ for $SU(3)$ gauge theory. The solution for a_s can be written as

$$\begin{aligned}
a_s(\mu_r) =& \frac{2\pi}{\beta_0\ln(\mu_r^2/\Lambda^2)}\left[1 - \frac{2\beta_1}{\beta_0^2}\frac{\ln\{\ln(\mu_r^2/\Lambda^2)\}}{\ln(\mu_r^2/\Lambda^2)}\right. \\
&\left. + \frac{4\beta_1^2}{\beta_0^4\ln^2(\mu_r^2/\Lambda^2)}\left\{\left(\ln\{\ln(\mu_r^2/\Lambda^2)\} - \frac{1}{2}\right)^2 + \frac{\beta_2\beta_0}{\beta_1^2} - \frac{5}{4}\right\}\right]
\end{aligned} \tag{2.15}$$

Here we include first three terms in the β-function. Now for $n_f < 17$, β_0 is positive. Therefore, a_s will decrease with increasing μ_r implying that a_s is asymptotically

free. In Eq.(2.15), the expansion parameter is $\frac{\ln\{\ln(\mu_r^2/\Lambda^2)\}}{\ln(\mu_r^2/\Lambda^2)}$. This is small only when $\mu_r \gg \Lambda$ and become singular at $\mu_r = \Lambda$. This singularity is called the Landau pole. Below Λ, the strong coupling constant is large and perturbative QCD (pQCD) is not applicable here. Above Λ, one can safely apply pQCD. The value of Λ depends on the number of active quark flavors (n_f), the renormalization scheme and the value of strong coupling constant. For example, in the $\overline{MS}$ scheme and for four loop α_s, the value of Λ is 210 ± 14 MeV for $n_f = 5$ and 292 ± 16 MeV for $n_f = 4$. These values of Λ correspond to the same value of world average $\alpha_s(M_Z) = 0.1181 \pm 0.0011$ [200].

Real emission and infrared singularities

After removing the UV singularities by renormalizing the bare parameters in the Lagrangian, the leftover singularities are the infrared singularities. For the diagram in the right panel of Fig.(2.1), the amplitude is proportional to $1/(p_1 - p_5)^2$. In the massless limit *i.e* when both quarks and gluons are massless, the denominator can be written as

$$2p_1.p_5 = 2E_1E_5(1 - \cos\theta_{15}) \tag{2.16}$$

where E_1 is the energy of incoming parton, E_5 is the energy of the emitted gluon and θ_{15} is the angle between incoming parton and emitted gluon. During phase space integration, the cross section will diverge if $E_5 \to 0$ or $\theta_{15} \to 0$ or both $E_5 \to 0$, implies that the emitted gluons are soft and collinear to the parent partons. First kind of singularity is called `soft` singularity. This singularity can be removed by taking into account the virtual diagrams along with the real emission diagrams according to KLN theorem. The second kind of singularity ($\theta_{15} \to 0$) is called `collinear` singularity. This singularity will appear only when a massless particle couples to another massless particle. Therefore, sometimes this singularity is called a mass singularity. Collinear singularities can be absorbed into PDFs by redefining them. Together the soft singularity and collinear singularity are called the infrared singularity.

In this QCD improved parton model picture, the PDFs depend on a scale μ_f called factorization scale. The evolution equation for the quark distribution function is

$$\frac{\partial f(x,\mu_f^2)}{\partial \ln \mu_f^2} = \frac{a_s}{4\pi}\int_x^1 \frac{dy}{y} f(y,\mu_f^2) P_{qq}(x/y) + \mathcal{O}(a_s^2) \tag{2.17}$$

This equation describes the evolution of quark distribution function due to gluon radiation and is known as **DGLAP** equation. This equation can be solved numerically once $f(x,\mu_0^2)$ is known where, μ_0 is the starting scale usually taken as the mass of Z boson m_Z. In a more compact form this **DGLAP** equation can be written as

$$\frac{\partial}{\partial \ln \mu_r^2}\begin{bmatrix} q_i \\ g \end{bmatrix} = \frac{a_s}{4\pi}\begin{bmatrix} P_{qq} & 2n_f P_{qg} \\ P_{qg} & P_{gg} \end{bmatrix} \otimes \begin{bmatrix} q_i \\ g \end{bmatrix} \tag{2.18}$$

where P_{qq}, P_{qg}, P_{gg} are the Altarelli splitting functions known up to four loop [38–43]. $P_{ab}(z)$ implies that a parton b with momentum p_b splits into parton a with momentum p_a where $p_a = zp_b$. The LO splitting functions are given below

$$\begin{aligned}
P_{qq}^{(0)}(z) &= \frac{4}{2}\left(\frac{1+z^2}{(1-z)_+} + \frac{3}{2}\delta(1-z)\right) \\
P_{qg}^{(0)}(z) &= \frac{1}{2}\left(z^2 + (1-z)^2\right) \\
P_{gq}^{(0)}(z) &= \frac{4}{3}\left(\frac{1+(1-z)^2}{z}\right) \\
P_{gg}^{(0)}(z) &= 6\left(\frac{z}{(1-z)_+} + \frac{1-z}{z} + z(1-z) + (\frac{11}{12} - \frac{n_f}{18})\delta(1-z)\right)
\end{aligned} \tag{2.19}$$

where the **plus** functions are defined as

$$\int_0^1 f(z)[g(z)]_+ dz = \int_0^1 [f(z) - f(1)]g(z)dz \tag{2.20}$$

The singularities appearing in P_{qq} and P_{gg} when $z \to 1$ are regularized by so-called **plus** distribution functions which guarantees that the integrations of the splitting functions are finite when convoluted by PDF provided PDF $\to 0$ when $z \to 1$.

After removing and absorbing all singularities by renormalization and fac-

torization, the finite hadronic cross section at LHC can be written as

$$\sigma(\tau) = \sigma^{(0)} \sum_{ab=q,\bar{q},g} \int_0^1 dx_1 \int_0^1 dx_2 \; f_a(x_1,\mu_f^2) \; f_b(x_2,\mu_f^2) \\ \int_0^1 dz \; \Delta_{ab}(z,Q^2,\mu_f^2)\delta(\tau - z x_1 x_2)\,, \tag{2.21}$$

where $\sigma^{(0)}$ is born level cross section, $f_a(x_1,\mu_f^2)$ and $f_b(x_2,\mu_f^2)$ are the parton distribution functions, S is the hadronic centre of mass energy, $\hat{s}$ is the partonic centre of mass energy, $\tau = Q^2/S$, $z = Q^2/\hat{s}$ and $\Delta_{ab}(z,Q^2,\mu_f^2)$ is parton coefficient function. The partonic coefficients are obtained from the partonic cross section using perturbation theory.

$$\Delta_{ab}(z,Q^2,\mu_f^2) = \sum_{n=0}^{\infty} \alpha_s^{(n)}(\mu_r^2)\Delta_{ab}^{(n)}(z,Q^2,\mu_f^2,\mu_r^2) \tag{2.22}$$

The L.H.S of Eq.(2.21) is independent on unphysical scales μ_r and μ_f whereas, R.H.S is function of μ_r and μ_f. If one convolutes all order partonic coefficient functions with all order PDF then these scale dependency will vanish. So far we don't have any technology to compute all order partonic coefficients. Therefore, truncation of the series in Eq.(2.22) at any order will give scale dependent results. However inclusion of more and more higher order terms in the series will reduce this scale dependency.

2.1.1 Soft-Virtual Computation

The partonic coefficient function to any order n, can be written as

$$\Delta_{ab}^{(n)}(z,Q^2,\mu_f^2,\mu_r^2) = C_{ab,1}(Q^2,\mu_f^2,\mu_r^2)\delta(1-z) + \sum_{i=0}^{2n-1} C_{ab,2}^{(i)}(Q^2,\mu_f^2,\mu_r^2) f(\mathcal{D}_i(z)) \\ + C_{ab,3}(Q^2,\mu_f^2,\mu_r^2) f_{reg}(z) \tag{2.23}$$

where the distribution function $\mathcal{D}_i(z)$ has the form

$$\mathcal{D}_i(z) = \left(\frac{\ln^i(1-z)}{1-z}\right)_+ \tag{2.24}$$

The first term in Eq.(2.23) is coming from virtual correction and soft gluon radiation, the second term is the effect of soft and collinear gluon radiation and together these two terms is called soft-virtual (SV) partonic coefficient function. The third term is called regular part which is process dependent and also finite when $z \to 1$. The SV cross section constitutes a significant contribution to the partonic cross section in the limit $z \to 1$ and can be computed order by order in the strong coupling.

In $d = 4 + \epsilon$ space time dimensions, the threshold enhanced partonic soft-virtual cross-section to all orders in perturbation theory in z space can be written [44, 45] as

$$\Delta^{(\mathrm{sv})}(z, Q^2, \mu_r^2, \mu_f^2) = \mathcal{C} \exp\left(\Psi^I\left(z, Q^2, \mu_r^2, \mu_f^2, \epsilon\right)\right)\Big|_{\epsilon=0} \qquad I = q, g \tag{2.25}$$

Here Ψ is a distribution function which is finite in the limit $\epsilon \to 0$. The symbol $\mathcal{C}$ denotes the Mellin convolution (denoted below as $\otimes$) which in the above expression should be treated as

$$\mathcal{C} \exp\Big(f(z)\Big) = \delta(1-z) + \frac{1}{1!} f(z) + \frac{1}{2!} f(z) \otimes f(z) + \cdots, \tag{2.26}$$

with $f(z)$ being a function containing only $\delta(1-z)$ and plus distributions. The finite exponent in the above is re-factorized in the threshold limit and gets contribution from the form factor $\left(\hat{\mathcal{F}}^I(\hat{a}_s, q^2, \mu^2, \epsilon)\right)$ with $q^2 = -Q^2$, soft-collinear function $\left(\Phi^I(\hat{a}_s, z, Q^2, \mu^2, \epsilon)\right)$ (later called as soft function) as well as mass factorization kernels $\left(\Gamma^I(\hat{a}_s, z, \mu_f^2, \mu^2, \epsilon)\right)$ and takes the following form in dimensional regularization:

$$\begin{aligned}\Psi^I\Big(z, Q^2, \mu_r^2, \mu_f^2, \epsilon\Big) =& \left(\ln\left[\mathcal{Z}^I(\hat{a}_s, \mu_r^2, \mu^2, \epsilon)\right]^2 + \ln\left|\hat{\mathcal{F}}^I(\hat{a}_s, q^2, \mu^2, \epsilon)\right|^2\right)\delta(1-z) \\ &+ 2\Phi^I(\hat{a}_s, z, Q^2, \mu^2, \epsilon) - 2\mathcal{C}\ln\Gamma^I(\hat{a}_s, z, \mu_f^2, \mu^2, \epsilon)\,.\end{aligned} \tag{2.27}$$

μ keeps the strong coupling $(\hat{a}_s)$ dimensionless in the $d = 4+\epsilon$ dimensions. $\mathcal{Z}^I(\hat{a}_s, \mu_r^2, \mu^2, \epsilon)$

denotes the overall UV renormalization constant. This overall renormalization constant is 1 for vector current and for gluon operator, it has the following form [46].

$$\begin{aligned}\mathcal{Z}^g(\hat{a}_s,\mu_r^2,\mu^2,\epsilon) =& 1+\hat{a}_s\left(\frac{\mu_r^2}{\mu^2}\right)^{\epsilon/2} S_\epsilon\left\{\frac{2\beta_0}{\epsilon}\right\}+\hat{a}_s^2\left(\frac{\mu_r^2}{\mu^2}\right)^{\epsilon} S_\epsilon^2\left\{\frac{2\beta_1}{\epsilon}\right\}+\\ &\hat{a}_s^3\left(\frac{\mu_r^2}{\mu^2}\right)^{3\epsilon/2} S_\epsilon^3\left\{\frac{1}{\epsilon^2}(-2\beta_0\beta_1)+\frac{2\beta_2}{\epsilon}\right\}+\mathcal{O}(\hat{a}_s^4)\end{aligned} \tag{2.28}$$

The bare quark form factor satisfies the Sudakov K+G equation [44, 45, 47–53] which follows as a consequence of the gauge invariance as well as renormalization group invariance,

$$\frac{d\ln\hat{\mathcal{F}}^I}{d\ln q^2}=\frac{1}{2}\left[\mathcal{K}^I(\hat{a}_s,\frac{\mu_r^2}{\mu^2},\epsilon)+\mathcal{G}^I(\hat{a}_s,\frac{q^2}{\mu_r^2},\frac{\mu_r^2}{\mu^2},\epsilon)\right]. \tag{2.29}$$

The function $\mathcal{K}^I$ contains all the infrared poles in ϵ whereas the function $\mathcal{G}^I$ is finite in the limit $\epsilon\to 0$. The renormalisation group invariance leads to the following solutions of these functions in terms of cusp anomalous dimensions (A):

$$\frac{d\mathcal{K}^I}{d\ln\mu_r^2}=-\frac{d\mathcal{G}^I}{d\ln\mu_r^2}=A^I(a_s(\mu_r))=\sum_{i=1}^{\infty}a_s^i(\mu_r)A_i^I\,. \tag{2.30}$$

The cusp anomalous dimensions A_i^I are maximally non-abelian and satisfy the following relation

$$A^q=\frac{C_F}{C_A}A^g \tag{2.31}$$

A_i^I are known to fourth order [40, 54, 55, 55–57, 57–65, 65] and some of them are collected in App.(A.1). The solution of $\mathcal{K}^I$ can be written as a power series of bare coupling constant as

$$\mathcal{K}^I\left(\hat{a}_s,\frac{\mu_r^2}{\mu^2},\epsilon\right)=\sum_{i=1}^{\infty}\hat{a}_s^i\left(\frac{\mu_r^2}{\mu^2}\right)^{i\epsilon/2}S_\epsilon^i\mathcal{K}^{I,(i)}(\epsilon) \tag{2.32}$$

where

$$\begin{aligned}
\mathcal{K}^{I,(1)}(\epsilon) &= \frac{1}{\epsilon}\Big\{ -2A_1^I \Big\} \\
\mathcal{K}^{I,(2)}(\epsilon) &= \frac{1}{\epsilon^2}\Big\{ -2\beta_0 A_1^I \Big\} + \frac{1}{\epsilon}\Big\{ -A_2^I \Big\} \\
\mathcal{K}^{I,(3)}(\epsilon) &= \frac{1}{\epsilon^3}\Big\{ -\frac{8}{3}\beta_0^2 A_1^I \Big\} + \frac{1}{\epsilon^2}\Big\{ \frac{2}{3}\beta_1 A_1^I + \frac{8}{3}\beta_0 A_2^I \Big\} + \frac{1}{\epsilon}\Big\{ -\frac{2}{3}A_3^I \Big\}
\end{aligned} \tag{2.33}$$

The μ_r independent piece of the $\mathcal{G}^I$ can be written in perturbative series as

$$\mathcal{G}^I(a_s(q),\epsilon) = \sum_{j=1}^{\infty} a_s^j(q)\mathcal{G}_j^I(\epsilon)\,, \tag{2.34}$$

where the coefficients $\mathcal{G}_j^I(\epsilon)$ can be decomposed as

$$\mathcal{G}_i^I(\epsilon) = 2B_i^I + f_i^I + C_i^I + \sum_{k=1}^{\infty} \epsilon^k G_{ik}^I\,, \tag{2.35}$$

where

$$\begin{aligned}
C_1^I &= 0\,, \\
C_2^I &= -2\beta_0 G_{11}^I\,, \\
C_3^I &= -2\beta_1 G_{11}^I - 2\beta_0\Big(G_{21}^I + 2\beta_0 G_{12}^I\Big)\,.
\end{aligned} \tag{2.36}$$

The coefficients G_{ik}^I are the finite coefficients found in terms of QCD color factors and can be extracted from explicit calculation of quark form factor. Note that up to the third order one also needs coefficients G_{22}^I, G_{31}^I and thereby needs the three-loop calculation of the form factor. Similar to the cusp anomalous dimension, the coefficients f_i^I have been found to be maximally non-abelian to third order in strong coupling *i.e.* they satisfy

$$f_i^g = \frac{C_F}{C_A} f_i^q\,. \tag{2.37}$$

The initial state collinear singularities are removed using the Altarelli-Parisi (AP) splitting kernels $\Gamma^I(\hat{a}_s, \mu_f^2, \mu^2, z, \epsilon)$. They satisfy the well-known DGLAP

evolution given as,

$$\frac{d\Gamma^I(z,\mu_f^2,\epsilon)}{d\ln\mu_f^2} = \frac{1}{2}P_{II}(z,\mu_f^2)\otimes\Gamma^I(z,\mu_f^2,\epsilon)\,, \tag{2.38}$$

where $P_{II}(z,\mu_f^2)$ is the AP splitting functions. The perturbative expansion for these splitting functions has the following form:

$$P_{II}(z,\mu_f^2) = \sum_{i=0}^{\infty} a_s^{i+1}(\mu_f)P_{II}^{(i)}(z)\,. \tag{2.39}$$

As discussed before, only the diagonal terms of the splitting functions contribute to the SV cross-section. The diagonal part of the splitting functions is known to contain the $\delta(1-z)$ and distributions, and can be written as

$$P_{II}^{(i)} = 2\Big[B_{i+1}\delta(1-z) + A_{i+1}\mathcal{D}_0\Big] + P_{II}^{(reg,i)}(z)\,. \tag{2.40}$$

The finiteness of the soft-virtual cross-section demands that the soft-collinear function Φ^I will also satisfy similar Sudakov type equation like the form factor *i.e.* one can write

$$\frac{d\Phi^I}{d\ln Q^2} = \frac{1}{2}\left[\overline{\mathcal{K}}^I(\hat{a}_s,z,\frac{\mu_r^2}{\mu^2},\epsilon) + \overline{\mathcal{G}}^I(\hat{a}_s,z,\frac{Q^2}{\mu_r^2},\frac{\mu_r^2}{\mu^2},\epsilon)\right], \tag{2.41}$$

where $\overline{\mathcal{K}}^I(\hat{a}_s,z,\frac{\mu_r^2}{\mu^2},\epsilon)$ contains all the poles and $\overline{\mathcal{G}}^I(\hat{a}_s,z,\frac{Q^2}{\mu_r^2},\frac{\mu_r^2}{\mu^2},\epsilon)$ is finite in the dimensional regularization such that Ψ^I becomes finite as $\epsilon\to 0$. The solution to the above equation has been found [44, 45] to be

$$\Phi^I = \sum_{j=1}^{\infty}\hat{a}_s^j\frac{j\epsilon}{1-z}\left(\frac{Q^2(1-z)^2}{\mu^2}\right)^{j\epsilon/2}\mathcal{S}_\epsilon^j\;\hat{\Phi}^I{}_{(j)}(\epsilon)\,. \tag{2.42}$$

$\hat{\Phi}^I{}_{(j)}$ can be found from the solution of the form factor by the replacement as $A^I\to -A^I, \mathcal{G}^I(\epsilon)\to\overline{\mathcal{G}}^I(\epsilon)$. Notice that $\overline{\mathcal{G}}^I(\epsilon)$ are now new finite z-independent coefficients coming from the soft function whereas the z dependence has been taken out in Eq.(2.42). This can be found by comparing the singular and non-singular terms in $\hat{\Phi}^I{}_{(j)}$ with those coming from the form factors, overall renormalisation constants,

splitting kernel and the lower order SV terms. The coefficient $\overline{\mathcal{G}}^I$ has same structure as the form factor in Eq.(2.35) after setting $f_i^I \to -f_i^I, B_i^I \to 0, \gamma_i^I \to 0$,

$$\overline{\mathcal{G}}_i^I = -f_i^I + \tilde{C}_i^I + \sum_{k=1}^{\infty} \epsilon^k \tilde{G}_{ik}^I \,, \tag{2.43}$$

where

$$\begin{aligned} \tilde{C}_1^I &= 0, \\ \tilde{C}_2^I &= -2\beta_0 \tilde{G}_{11}^I, \\ \tilde{C}_3^I &= -2\beta_1 \tilde{G}_{11}^I - 2\beta_0 \Big(\tilde{G}_{21}^I + 2\beta_0 \tilde{G}_{12}^I \Big) . \end{aligned} \tag{2.44}$$

The coefficients f_i^I are same as those that appear in the quark form factor in Eq.(2.35). The coefficients $\tilde{G}_{ij}^I$ requires the form factor up to three loops. Note that one has to perform the following expansion in Eq.(2.42) in order to get all the distributions and delta function coming from the soft function,

$$\frac{1}{(1-z)} \Big[(1-z)^2 \Big]^{j\epsilon/2} = \frac{1}{j\epsilon} \delta(1-z) + \sum_{k=0}^{\infty} \frac{(j\epsilon)^k}{k!} \mathcal{D}_k \,. \tag{2.45}$$

It is worth noting that $\overline{\mathcal{G}}^I$ as well as the complete soft function Φ_I satisfy the maximally non-abelian property up to three loops. Moreover Φ_I is also universal in the sense that it only depends on the initial legs and is completely unaware of the color neutral final state. Expanding $\Delta^{(\mathrm{sv})}$ in powers of a_s as

$$\Delta_{ab}^{(\mathrm{sv})} = \delta_{ab} \sum_{i=0}^{\infty} a_s^i \Delta^{(i)} \,, \tag{2.46}$$

with the born contribution being $\Delta^{(0)} = \delta(1-z)$. Therefore, Ψ which is finite while the individual contributions to it contain UV and IR singularities. Decomposing the later ones as sum of singular and finite parts as

$$\begin{aligned} \ln \left| \hat{\mathcal{F}} \right|^2 (Q^2) &= \mathcal{L}_{\mathcal{F}}^{\mathrm{sing}}(Q^2, \mu_r^2) + \mathcal{L}_{\mathcal{F}}^{\mathrm{fin}}(Q^2, \mu_r^2) \\ \Phi(z, Q^2) &= \Phi^{\mathrm{sing}}(z, Q^2, \mu_f^2, \mu_r^2) + \Phi_{\mathcal{D}}^{\mathrm{fin}}(z, Q^2, \mu_f^2, \mu_r^2) + \Phi_{\delta}^{\mathrm{fin}}(Q^2, \mu_f^2, \mu_r^2)\delta(1-z) \\ \mathcal{C} \ln \Gamma(z, \mu_f^2) &= \mathcal{L}_{\Gamma}^{\mathrm{sing}}(z, \mu_f^2, \mu_r^2) + \mathcal{L}_{\Gamma\mathcal{D}_0}^{\mathrm{fin}}(\mu_f^2, \mu_r^2)\mathcal{D}_0 + \mathcal{L}_{\Gamma\delta}^{\mathrm{fin}}(\mu_f^2, \mu_r^2)\delta(1-z) \end{aligned} \tag{2.47}$$

Substituting the above equations in Eq.(2.27), we can easily show that all the singular terms in the limit $\epsilon \to 0$ cancel among themselves. In addition, $\mathcal{D}_0$ terms in finite part of $\mathcal{C} \ln \Gamma$ go away when added to $\Phi_{\mathcal{D}}^{\text{fin}}$ resulting in a finite distribution.

2.2 Resummation

In Eq.(2.23), we have seen that partonic coefficient function contains $\mathcal{D}_i$ contribution for higher order.

$$\begin{aligned} f(\mathcal{D}_i) \quad &\text{at} \quad NLO \sim a_1\mathcal{D}_1 + a_2\mathcal{D}_0 \\ f(\mathcal{D}_i) \quad &\text{at} \quad NNLO \sim b_1\mathcal{D}_3 + b_2\mathcal{D}_2 + b_3\mathcal{D}_1 + b_4\mathcal{D}_0 \\ f(\mathcal{D}_i) \quad &\text{at} \quad N^3LO \sim c_1\mathcal{D}_5 + c_2\mathcal{D}_4 + c_3\mathcal{D}_3 + c_4\mathcal{D}_2 + c_5\mathcal{D}_1 + c_6\mathcal{D}_0 \end{aligned} \tag{2.48}$$

In certain kinematic regions ($z \to 1$), these contributions can be enhanced when convoluted with the parton distribution functions spoiling the reliability of the perturbation theory. Hence we need to include these potentially large terms to all orders in perturbation theory for any sensible predictions. This procedure is known as resummation. The formalism to resum these lagre logarithms was studied to a great extent in the past [66–71]. There is another approch to resum these logarithms based on Soft-Collinear Effective Theory (SCET) and also studied extensively in the literature [72–75]. In this thesis, we have considered the former approch. Resumming these logarithms in the z space is technically challenging due to the complexity involved in computing the convolutions . However, in the Mellin N space, the convolutions become simple products allowing us to study the impact of these large logarithms to all orders in a systematic fashion. In the following, we will describe how this can be done in Mellin N space.

2.2.1 Mellin Transformation

The general expression of Mellin transformation of a function $f(z)$ is given by

$$f(N) = \int_0^1 z^{N-1} f(z) dz \tag{2.49}$$

Now consider the Mellin transformation of singular distribution $\mathcal{D}_i(z)$

$$I_n(N) = \int_0^1 z^{N-1} \mathcal{D}_n(z) dz = \int_0^1 \frac{z^{N-1} - 1}{1 - z} \ln^n(1 - z) dz \tag{2.50}$$

This integration can be solved using harmonic polylogarithms [70, 76]

$$I_n(N) = (-1)^{n+1} n! S_{\overrightarrow{1,\cdots,1}}(N) \tag{2.51}$$

and

$$\begin{aligned} n! S_{\overrightarrow{1,\cdots,1}}(N) \simeq & \theta_{(n,1)} \ln^n \overline{N} + \frac{1}{2}\theta_{(n,3)} n(n-1)\zeta_2 \ln^{n-2} \overline{N} + \frac{1}{3}\theta_{(n,4)} n(n-1)(n-2)\zeta_3 \ln^{n-3} \overline{N} + \\ & \frac{1}{4}\theta_{(n,5)} n(n-1)(n-2)(n-3)\left(\zeta_4 + \frac{1}{2}\zeta_2^2\right) \ln^{n-4} \overline{N} + \cdots \end{aligned} \tag{2.52}$$

where $\theta_{(i,j)} = 1$ for $i \geq j$ and $\theta_{(i,j)} = 0$ else, $\overline{N} = Ne^{\gamma_e}$ where γ_e is the Euler's constant. Using Eq.(2.51) and Eq.(2.52) one can find the following solutions

$$\begin{aligned} I_0(N) &= -\ln \overline{N} \\ I_1(N) &= \frac{1}{2}\ln^2 \overline{N} + \frac{1}{2}\zeta_2 \\ I_2(N) &= -\frac{1}{3}\ln^3 \overline{N} - \zeta_2 \ln \overline{N} - \frac{2}{3}\zeta_3 \\ I_3(N) &= \frac{1}{4}\ln^4 \overline{N} + \frac{3}{2}\zeta_2 \ln^2 \overline{N} + 2\zeta_3 \ln \overline{N} + \frac{27}{20}\zeta_2^2 \end{aligned} \tag{2.53}$$

Mellin transformation of some other functions are given below [77]

$$
\begin{aligned}
&M\Big[\delta(1-z)\Big] = 1 \\
&M\Big[\big((1-z)^{n-1}\big)_+\Big] = \Gamma(n)\Big[\frac{\Gamma(N)}{\Gamma(N+n)} - \frac{1}{\Gamma(1+n)}\Big] \\
&M\Big[z^{-n/2}\big((1-z)^{n-1}\big)_+\Big] = \Gamma(n)\Big[\frac{\Gamma(N-n/2)}{\Gamma(N+n/2)} - \frac{1}{\Gamma(1+n)}\Big] \\
&M\Big[\big(z^{-n/2}(1-z)^{n-1}\big)_+\Big] = \Gamma(n)\Big[\frac{\Gamma(N-n/2)}{\Gamma(N+n/2)} - \frac{\Gamma(1-n/2)}{\Gamma(1+n/2)}\Big] \\
&M\Big[\big(\log^{n-1}\frac{1}{z}\big)_+\Big] = \Gamma(n)\Big[N^{-n} - 1\Big]
\end{aligned}
\tag{2.54}
$$

Convolution of two functions in Mellin space can be written as

$$
\begin{aligned}
M\Big[f \otimes g\Big](N) &= \int_0^1 dx x^{N-1} \int_0^1 dy \int_0^1 dz f(y) g(z) \delta(x - yz) \\
&= \int_0^1 dy y^{N-1} f(y) \int_0^1 dz z^{N-1} g(z) = f(N) g(N)
\end{aligned}
\tag{2.55}
$$

where $f(n), g(N)$ are the Mellin transformation of $f(z), g(z)$ respectively. This equation can be generalized to any number of functions in general.

2.2.2 Partonic Co-efficients in Mellin Space

In Mellin space, the hadronic cross section given in Eq.(2.21), can be written as

$$
\sigma_N(Q^2) = \sigma^{(0)} \sum_{a,b} f_{a/h_1,N}(\mu_f^2) f_{b/h_2,N}(\mu_f^2) \Delta_{ab,N}(a_s, \mu_f^2, \mu_r^2) \tag{2.56}
$$

where $f_{a/h,N}(\mu_f^2)$ is the parton distribution function and $\Delta_{ab,N}(a_s, \mu_f^2, \mu_r^2)$ is the partonic coefficient function in N-space respectively. Here our main focus is to calculate all order perturbative threshold enhanced partonic coefficient function. The threshold region $z \to 1$ corresponds to the limit $N \to \infty$ in the Mellin space.

In this region the partonic coefficient function can be written as

$$\Delta_{ab,N}(a_s,\mu_f^2,\mu_r^2) = \mathcal{O}\left(\frac{1}{N}\right) \qquad \text{for} \quad a \neq b \tag{2.57}$$

Therefore, in the threshold region only $q\bar{q}$ and gg subprocesses will not be suppressed. The threshold enhanced partonic coefficient function of these subprocesses can be organized [66, 68, 70] as,

$$\Delta_N(a_s,\mu_f^2,\mu_r^2) = g_0^I \exp\left(G_N^I\right), \tag{2.58}$$

The exponent G_N^I resums large-N terms at all orders and is given in terms of the universal cusp anomalous dimensions A and D as given below ,

$$G_N^I = \int_0^1 dz \frac{z^{N-1}-1}{1-z}\left[\int_{\mu_f^2}^{Q^2(1-z)^2} \frac{d\omega^2}{\omega^2} 2\ A(a_s(\omega^2)) + D(a_s(Q^2(1-z)^2))\right]. \tag{2.59}$$

The G_N^I only contains the `plus` distributions and can also be written in a perturbative series. The first term above equation represents the soft collinear radiation of gluon whereas the second term is coming from the wide angle soft radiation of gluons. Recalling that in the context of resummation $a_s \ln N \sim \mathcal{O}(1)$, one can write,

$$G_N^I = \ln N\ g_1^I + g_2^I + a_s\ g_3^I + a_s^2\ g_4^I\,, \tag{2.60}$$

Successive terms in the above expression determines the logarithmic accuracy. For example, the first coefficient (g_1^I) resums all leading logarithms (LL) to all orders, whereas the first two coefficients ($g_1^I + g_2^I$) also resums next to leading logarithms (NLL) and so on. Note that the universality of the resummed exponent is a direct consequence of the soft-gluon emission near the partonic threshold. The exponent is thus universal in the sense that it will only depend on the initial legs being gluons or quarks. The expressions for the resummed exponents g_i^I can be found in [70, 78] up to N^{3}LL order, also see [79] for N^{4}LL order in DIS. For consistency, we have also derived the same and collected in the App.(A.1).

The process dependent coefficient g_0^I on the other hand depends on the

specific process under consideration. It gets contribution from the entire form factor as well as from the $\delta(1-z)$ part coming from the soft function. It can be also written as a perturbative series as,

$$g_0^I = 1 + a_s g_{01}^I + a_s^2 g_{02}^I + a_s^3 g_{03}^I + \dots . \tag{2.61}$$

The successive terms in the resummed exponent Eq.(2.60) along with the corresponding terms in Eq.(2.61) define the accuracies leading logarithmic (LL), next to LL (NLL), NNLL and N^{3}LL etc.

The resummed results, will differ depending on how we treat the N-independent constants. We define various schemes that differentiate how these constants are treated in our numerical implementation for the phenomenological studies. This allows us to investigate numerical impact of the various resummed results in detail.

- `Standard` N `exponentiation:` The Mellin transformation of $\mathcal{D}_i$ can be decomposed as

$$\lim_{N\to\infty} \int_0^1 dz z^{N-1} G_+(z, Q^2) = G_0(Q^2) + G_N(Q^2) \tag{2.62}$$

with $G_N(Q^2)\big|_{N=1} = 0$. Here $G_0(Q^2)$ contains all N independent part and $G_N(Q^2)$ contains all N dependent part. One can keep this $G_0(Q^2)$ in the g_0 and define g_0 as

$$g_0(Q^2) = \exp\left(\mathcal{L}_{\mathcal{F}}^{\text{fin}} + 2\Phi_\delta^{\text{fin}} - 2\mathcal{L}_{\Gamma\delta}^{\text{fin}} + G_0(Q^2)\right) \tag{2.63}$$

and the above result can be expanded in powers of a_s:

$$g_0(Q^2) = 1 + \sum_{n=1}^{\infty} a_s^i g_{0i}(Q^2)\,. \tag{2.64}$$

This prescription is called `Standard` N `exponentiation`.

- `Standard` $\overline{N}$ `exponentiation:` This approach differs from the previous one in the definition of large-N variable. In this case, the large logarithm is simply

$\ln \overline{N}$ and these terms are exponentiated to all orders through the resummed exponent. It is evident that this only accounts for reshuffling of γ_E between g_0 and G_N in Eq.(2.58) which now takes the following form:

$$\Delta_{\overline{N}}(Q^2) = \bar{g}_0(Q^2) \exp\left(G_{\overline{N}}(Q^2)\right). \tag{2.65}$$

The resummed exponent $G_{\overline{N}}$ also takes a different form compared to the standard N exponent,

$$G_{\overline{N}}(Q^2) = \ln \overline{N}\ \bar{g}_1(\overline{N}, Q^2) + \bar{g}_2(\overline{N}, Q^2) + a_s\ \bar{g}_3(\overline{N}, Q^2) + a_s^2\ \bar{g}_4(\overline{N}, Q^2) + \cdots . \tag{2.66}$$

The resummed coefficients $\bar{g}_i$ in the above equation which defines the resummed accuracy, differs from g_i in Eq.(2.60). The present scheme is defined by demanding $G_{\overline{N}} = 0$ when $\overline{N} = 1$.

$$\lim_{N\to\infty} \int_0^1 dz z^{N-1} G_+(z, Q^2) = G_0'(Q^2) + G_{\overline{N}}(Q^2) \tag{2.67}$$

where $G_{\overline{N}}(Q^2)\big|_{\overline{N}=1} = 0$. With this definition, the rest of the N independent terms from the Mellin moment of G_+ is combined with finite parts of form factor, soft distribution function and the AP kernels. The N independent constant $\bar{g}_0$ is given by

$$\bar{g}_0(Q^2) = \exp\left(\mathcal{L}_{\mathcal{F}}^{\text{fin}} + 2\Phi_{\delta}^{\text{fin}} - 2\mathcal{L}_{\Gamma\delta}^{\text{fin}} + G_0'(Q^2)\right) \tag{2.68}$$

and the above result is expanded in powers of a_s:

$$\bar{g}_0(Q^2) = 1 + \sum_{n=1}^{\infty} a_s^i \bar{g}_{0i}(Q^2). \tag{2.69}$$

- `Soft exponentiation:` In the standard $\overline{N}$ (N) exponentiation, one exponentiates $\ln \overline{N}$ ($\ln N$) and certain $\overline{N}$ (N) independent terms which arise from G_+, subjected to the condition $G_{\overline{N}} = 0$ ($G_N = 0$) when $\overline{N} = 1$ ($N = 1$). The remaining $\overline{N}$ (N) independent terms in the Mellin space of G_+ along with

$\delta(1-z)$ coefficients give the coefficient $\overline{g}_0$ (g_0). In principle, we can define a scheme wherein the entire $\overline{N}$ (N) independent terms of G_+ can be kept in the exponent. More specifically, we define the scheme (relaxing $G_{\overline{N}}=1$ ($G_N=0$) for $\overline{N}=1$ ($N=1$)) wherein we exponentiate all the terms coming from the finite part of soft distribution function and those from the AP kernels. That is, the exponential contains

$$G_{\overline{N}}^{\text{Soft}} = G_{\overline{N}} + 2\Psi_{\delta}^{\text{fin}} - 2\mathcal{L}_{\Gamma\delta}^{\text{fin}} \tag{2.70}$$

that is,

$$\Delta_N(Q^2) = g_0^{\text{Soft}}(Q^2)\exp\left(G_{\overline{N}}^{\text{Soft}}(Q^2)\right). \tag{2.71}$$

with

$$\begin{aligned} G_{\overline{N}}^{\text{Soft}}(Q^2) =& \ln\overline{N}\; g_1^{\text{Soft}}(\overline{N},Q^2) + g_2^{\text{Soft}}(\overline{N},Q^2) + a_s\; g_3^{\text{Soft}}(\overline{N},Q^2) \\ &+ a_s^2\; g_4^{\text{Soft}}(\overline{N},Q^2) + \cdots . \end{aligned} \tag{2.72}$$

The remaining N independent terms define g_0^{Soft} that is obtained by expanding $\exp(\mathcal{L}_{\mathcal{F}\delta}^{\text{fin}})$ in power series expansion in a_s:

$$g_0^{\text{Soft}}(Q^2) = 1 + \sum_{n=1}^{\infty} a_s^i g_{0i}^{\text{Soft}}(Q^2). \tag{2.73}$$

- `All exponentiation:` The soft function and the form factor satisfy K+G type Sudakov integro-differential equations given in Eq.(2.29) and Eq.(2.41) and the AP kernels satisfy renormalisation group equation Eq.(2.38) governed by AP splitting functions. Hence, their solutions given the boundary conditions demonstrate exponential. The z space solutions that we obtained carry all order information on the distribution $\mathcal{D}_j$ in terms of universal cusp A, soft f and collinear B anomalous dimensions and certain process dependent constants resulting from the form factor. Hence it is natural to study the numerical impact of the entire contribution in the Mellin space without imposing any condition on the N dependent terms. This can be easily achieved and the

result for $\hat{\sigma}_N$ can be written as

$$\Delta_N = \exp\left(G_{\overline{N}}^{\rm All}\right), \tag{2.74}$$

where

$$G_{\overline{N}}^{\rm All}(Q^2) = \mathcal{L}_{\mathcal{F}}^{\rm fin}(Q^2) + 2\Phi_{\delta}^{\rm fin}(Q^2) - 2\mathcal{L}_{\Gamma\delta}^{\rm fin} + G_0'(Q^2) + G_{\overline{N}}(Q^2) \tag{2.75}$$

where $G_{\overline{N}}^{\rm All}$ is expanded as

$$G_{\overline{N}}^{\rm All}(Q^2) = \ln \overline{N}\; g_1^{\rm All}(Q^2) + g_2^{\rm All}(Q^2) + a_s\; g_3^{\rm All}(Q^2) + a_s^2\; g_4^{\rm All}(Q^2)\,. \tag{2.76}$$

The present scheme was already explored in [80, 81] for studying inclusive cross section for the production of Higgs boson at the LHC. For similar studies for DY and DIS in $\overline{\rm MS}$ schemes, see [82].

2.2.3 Inverse Mellin Transformation

After achieving all order resummed partonic cross-section in Mellin space, one needs Mellin inversion to obtain the results in the physical z space. Here, we discuss the related issues for the Mellin inversion of the partonic cross-section. The Mellin inversion, the resummed partonic cross-section is given by

$$\sigma(\tau) = \frac{1}{2\pi i}\sum_{n=0}^{\infty} a_s^n \int_{c-i\infty}^{c+\infty} \Delta_N \tau^N dN \tag{2.77}$$

where c is real number and has to be chosen in such a way that $\int_0^1 d\tau \tau^{c-1}\sigma(\tau)$ is convergent. The contour of the integral Eq.(2.77) is shown in Fig.(2.2). The contour of the integration is displaced to C_0. The deformed contour C_1 (as shown in Fig.(2.2)) will also give the same results as by C_0 as long as there is no pole in between them. One can rewrite the Eq.(2.77) in terms of real variables ϕ and c

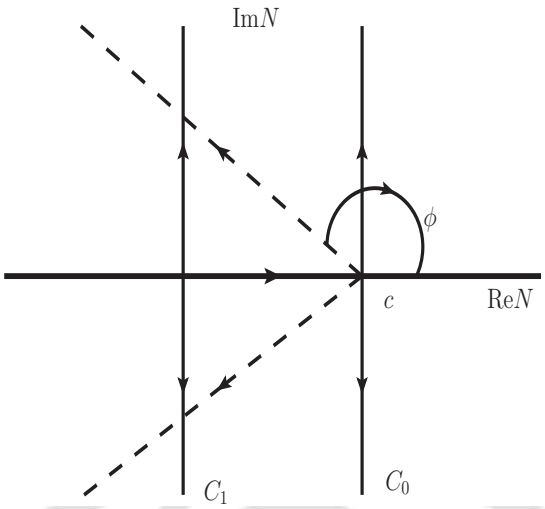

Figure 2.2: Integration contour of Mellin inversion of Eq.(2.77)

[83],as shown in the above figure.

$$\sigma(\tau) = \frac{1}{\pi}\sum_{n=0}^{\infty} a_s^n \int_0^{\infty} dz \mathrm{Im}\big[\exp(i\phi)\tau^{-c-z\exp(i\phi)}\Delta_{N=c+z\exp(i\phi)}\big] \tag{2.78}$$

Now the contour is characterized by c and ϕ. Obviously, the integration does not depend on the choice of the c and ϕ values, but for numerical stability one needs to choose $\phi > \pi/2$ [84].

The integration in Eq.(2.77), hits the singularity when $N = N_L$. The N_L is the solution of $\omega = 1$ where, $\omega = 2\beta_0 a_s \ln \overline{N}$. This is called Landau pole. To avoid this pole, various schemes are available in literature, for example Borel prescriptions [85–87], Minimal prescriptions (MP) [68] etc. In constant c in the Mellin inversion, is chosen in such a way that all singularities in the integrand are to the left of the integration contour and the Landau pole at $N = N_L$ and $N = N_L^2$ lie far to the right of the contour.

2.2.4 Matching Procedure

To incorporate the resummed results with the fixed order results, one need to add them systematically. The simple addition will lead to the double-counting of the

SV cross-section in the result. To understand this, let discuss the properties of the series in Eq.(2.57). If one keeps the exponent up to the second term and g_0 also up to the second term and truncate the series at a_s, then the result will be NLO soft-virtual coefficients plus NLL resummation for all higher order. Similarly up to third term in the exponent and in g_0 will give NNLO soft-virtual coefficients plus NNLL resummation for all higher order. Therefore, the addition in Eq.(2.57) with fixed order result will give double counting of SV results which are present in both cases. To obtain the correct result, one has to subtract this SV part and this procedure is known as Matching. The Matched cross section has following form,

$$\begin{aligned}\left[\frac{d\sigma}{dQ}\right]_{N^nLL+N^mLO} &= \frac{Q}{S}\sum_{ab\in\{q,\bar{q},g\}}\frac{d\hat{\sigma}_{LO}}{dQ}\int_{c-i\infty}^{c+i\infty}\frac{dN}{2\pi i}(\tau)^{-N}\delta_{ab}f_{a,N}(\mu_f^2)f_{b,N}(\mu_f^2)\\ &\times\left(\left[\frac{d\hat{\sigma}_N}{dQ}\right]_{N^nLL}-\left[\frac{d\hat{\sigma}_N}{dQ}\right]_{tr}\right)+\left[\frac{d\sigma}{dQ}\right]_{N^mLO}. \end{aligned} \tag{2.79}$$

The second term inside the bracket has been introduced to remove double counting of singular terms, which are already present in the FO result, i.e. in the last term of the above expression. In particular, for N^{3}LL matching with N^{3}LO$_{\rm sv}$, we need the resummed expression keeping up to $\mathcal{O}(a_s^2)$ terms in the resummed exponent Eq. (2.60) and subtracting all the leading singular terms that are already present in the N^{3}LO cross-section. This is done by subtracting the expanded resummed cross-section up to the same order as FO. The matched formula in Eq.(2.79) also gives the opportunity to match different orders in FO and resum series.

In this thesis, I study the precision calculation of the Drell-Yan process in the Standard Model and beyond in the context of soft-virtual correction and threshold resummation in QCD. We will discuss them in detail in the next chapters.

Chapter 3

Standard Model Drell-Yan cross section at N^{3}LL accuracy in QCD at LHC

In this chapter, we discuss the precise theoretical result for inclusive cross-section for Drell-Yan (DY) production as well as on-shell $Z, W^{\pm}$ productions at next-to-next-to-next-to leading logarithmic (N^{3}LL) accuracy. Apart from the standard $\ln N$ exponentiation, we study the numerical impact of exponentiating N-independent part of the soft function and the complete $\overline{g}_0$ that appears in the resummed predictions in N space. All the analytical pieces needed in these different approaches are extracted from the soft-virtual part of the inclusive cross section known to next-to-next-to-next-to leading order (N^{3}LO). We perform a detailed analysis on the scale and PDF variations and present predictions for 13 TeV LHC for the neutral Drell-Yan process as well as on-shell charged and neutral vector boson productions.

3.1 Introduction

Drell-Yan production has been a standard candle at the hadron colliders and is extremely important for luminosity monitoring. This is one of the hadronic processes

which is well understood theoretically. For example, NNLO correction in QCD [88–90] to this process was computed three decades ago. DY is also an important process experimentally for several BSM searches. Experimentally, one has a clean environment for precise measurements in terms of the kinematics of the final state lepton pairs. The higher-order perturbative QCD corrections to DY provide an ample opportunity to explore the structure of the perturbation series. Thus DY serves as an important process in collider experiments. At the LHC, the strong interaction dynamics dominate over others. Hence, there have been attempts to go beyond NNLO accuracy to improve the theoretical side's precision. The calculation of complete N^{3}LO cross-section is extremely difficult due to the increasing number of subprocesses involved. However, there has been significant progress in obtaining the third-order contribution to this process in QCD. Very recently, the first result at complete N^{3}LO from only virtual photon mediator has been calculated in [91]. From the theory side, DY is seen to be extremely stable with respect to factorization and renormalization scales already at NNLO. The scale uncertainty has been seen to be reduced to 2% for a canonical variation of factorization and renormalisation scales compared to NLO where uncertainty is about 9.2%, whereas the K-factor seems to improve marginally from 1.25 at NLO to 1.28 at NNLO. However, keeping in mind the importance of this process, it is worth studying these results from the next orders and devising methods to incorporate higher-order corrections. Since a complete calculation beyond the NNLO level is difficult and challenging, the soft-virtual (SV) contributions are often computed as the first step. In addition, this constitutes a significant part of the cross-section in the region where the partonic scaling variable approaches the limit $z \to 1$ (threshold region). The SV cross-sections are known for many SM processes *e.g.* Higgs production [44, 45, 92–96], Higgs associated production [97], top pair production [98–101], bottom quark annihilation [102], pseudo-scalar Higgs production [103]. For DY production, using the three loop quark form factor [104], exploiting the universal structure of the soft part [105] of SV cross section to Higgs production [92], the dominant soft-virtual (SV) corrections for DY at third order were obtained [106] and later these results were independently reproduced in [107]. It is also worth noting that the same result was independently obtained in [108] using soft-gluon resummation.

The SV contributions dominate at every order in the perturbation theory through large logarithms spoiling the reliability of the fixed order predictions. The resolution to this is to resum these large logarithms to all orders as was discussed in Sec.(2.2). Resummation of these large logarithms is thus very important to correctly describe the cross- section in the threshold region. Moreover, it has been very well established that the resummed results give sizable contributions to the cross-section in threshold region. In fact many SM fixed order calculations have been improved with the corresponding resummed results, for example, the inclusive Higgs production in gluon fusion [78, 80, 81, 93, 108] (see also [109] for renormalization group improved prediction) as well as in bottom quark annihilation [110], top quark production [100], deep inelastic scattering [70, 79], DY production [93, 108, 111], pseudo-scalar Higgs production [112–114], spin-2 production [115, 116] etc. Threshold resummation improves not only the inclusive fixed order results but also differential observables like rapidity [66, 117–120], transverse momentum [121, 122] and in the context of LHC precision measurements, it is important to include these corrections, and they are shown to improve the fixed order results.

As discussed in Sec.(2.2), there is an intrinsic ambiguity on what is exponentiated and what is not. Based on this, there are various resummation prescriptions, and they have a different numerical impact. It has been already seen in [79] that the perturbative convergence is improved if one exponentiates the large-$\overline{N}$ terms instead of N. Apart from the standard threshold exponentiation, one can also do '`Soft exponentiation`' and '`All exponentiation`'. The '`All exponentiation`' was studied in the context of the SM Higgs production [80, 81] and was shown to improve the scale uncertainty better than the standard threshold approach. The form factor is process dependent and therefore is non-universal, unlike the soft function. However, the form factor as well as the soft function both satisfy the similar Sudakov K+G type equation [44, 45, 50–53]. Therefore, they can be treated in the same way as soft function, and the solution to the K+G equation for the form factor becomes N independent constant in the exponent. The numerical impact of this has already been studied in the past for the DY production in [82] where the authors show that both in DIS scheme and in $\overline{\text{MS}}$ scheme, the complete form factor

exponentiates to the orders are currently known.

The goal of the present chapter is to study the effect of threshold logarithms at N^{3}LL accuracy and match it to the known N^{3}LO$_{sv}$ results. We perform this study for the neutral DY production as well as for on-shell Z and $W^{\pm}$ productions.

3.2 Theoretical Formalism

The parton model picture of the DY process is illustrated in Fig.(3.1) and the

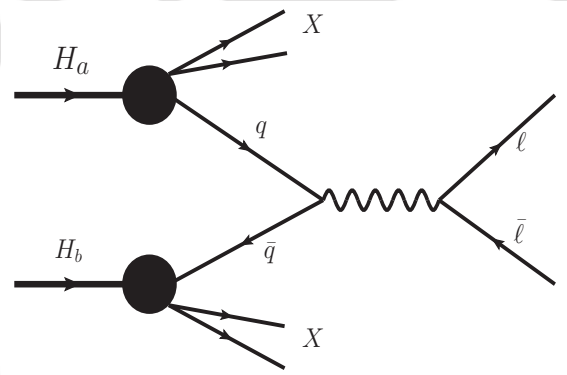

Figure 3.1: Parton model picture of Drell-Yan process at the LHC

hadronic cross-section for this or on-shell $Z, W^{\pm}$ production at the LHC can be written as

$$\sigma = \sigma^{(0)} \sum_{ab=q,\bar{q},g} \int_0^1 dx_1 \int_0^1 dx_2 \; f_a(x_1,\mu_f^2) \; f_b(x_2,\mu_f^2) \int_0^1 dz \; \Delta_{ab}(z,Q^2,\mu_f^2)\delta(\tau - z x_1 x_2)\,, \tag{3.1}$$

where $\sigma = \frac{d\sigma}{dQ}(\tau, Q^2)$ for DY production, Q is the invariant mass of the dilepton pair and $\tau = Q^2/S$ where S is the hadronic centre of mass energy. Here $f_a(x_1,\mu_f^2)$ and $f_b(x_2,\mu_f^2)$ are the non-perturbative PDFs of the partons a, b carrying momentum fractions x_1, x_2 of the incoming protons at the factorization scale μ_f. These PDFs are appropriately convoluted with perturbatively calculable partonic coefficients $\Delta_{ab}(z,Q^2,\mu_f^2)$. For the on-shell $Z, W^{\pm}$ production, $\sigma = \sigma_V, V = Z/W^{\pm}$ and $Q^2 = M_V^2$, where M_V is the mass of the vector boson. The partonic coefficients

are obtained from the partonic cross-section using perturbation theory. For the DY production, we include contributions from γ and Z as well as their interference. The prefactors for DY and $Z, W^{\pm}$ production are given as below:

$$\begin{aligned}\sigma_{DY}^{(0)} &= \frac{2\pi}{n_c}\left[\frac{Q}{S}\mathcal{F}^{(0)}\right],\\ \sigma_{Z}^{(0)} &= \frac{2\pi}{n_c}\left[\frac{\pi\alpha}{8s_w^2c_w^2S}\right],\\ \sigma_{W^{\pm}}^{(0)} &= \frac{2\pi}{n_c}\left[\frac{\pi\alpha}{4s_w^2S}\right],\end{aligned} \tag{3.2}$$

where S is the hadronic centre-of-mass energy and $n_c = 3$ in QCD. For DY production, the factor $\mathcal{F}^{(0)}$ is found to be,

$$\begin{aligned}\mathcal{F}^{(0)} = \frac{4\alpha^2}{3Q^2}\Bigg[Q_q^2 - \frac{2Q^2(Q^2-M_Z^2)}{((Q^2-M_Z^2)^2+M_Z^2\Gamma_Z^2)\,c_w^2s_w^2}Q_q g_e^V g_q^V \\ + \frac{Q^4}{((Q^2-M_Z^2)^2+M_Z^2\Gamma_Z^2)\,c_w^4s_w^4}\Big((g_e^V)^2+(g_e^A)^2\Big)\Big((g_q^V)^2+(g_q^A)^2\Big)\Bigg].\end{aligned} \tag{3.3}$$

Here α is the fine structure constant, c_w, s_w are sine and cosine of Weinberg angle respectively. M_Z and Γ_Z are the mass and the decay width of the Z-boson.

$$g_a^A = -\frac{1}{2}T_a^3\,, \qquad g_a^V = \frac{1}{2}T_a^3 - s_w^2Q_a\,, \tag{3.4}$$

Q_a being electric charge and T_a^3 is the weak isospin of the electron or quarks.

The partonic cross-section can be in a power series of strong coupling constant as Eq.(2.22) and can be decomposed as

$$\Delta_{ab}(z,Q^2,\mu_f^2) = \Delta_{ab}^{(\mathrm{sv})}(z,Q^2,\mu_f^2) + \Delta_{ab}^{(\mathrm{reg})}(z,Q^2,\mu_f^2)\,. \tag{3.5}$$

The first term $\Delta^{(\mathrm{sv})}$ is called the SV partonic coefficient its expression is given in Eq.(2.46). It contains distributions such as $\delta(1-z)$ coming from form factor and soft radiation and $\mathcal{D}_+$, whereas the second term $\Delta^{(\mathrm{reg})}$ contains those terms that are regular in the scaling variable z. Using the universality of the soft function, one can obtain the SV coefficients from the form factor. The three-loop the quark form

factor is already available in literature [104]. In [106], the three-loop SV results are presented using these form factor and for completeness, we collect them here in Mellin space.

The typical diagrams for three loop quark form factor are shown below,

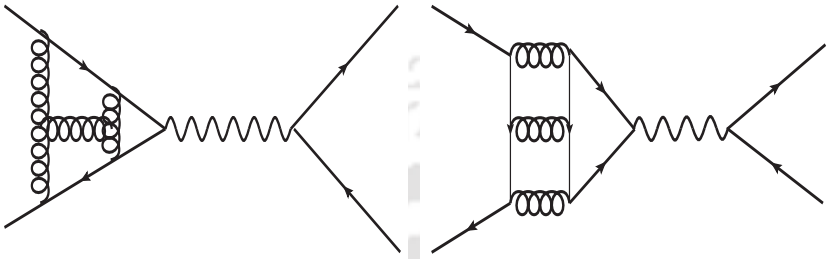

Figure 3.2: Diagrams related to three loop quark form factor.

$$\Delta_N^{\mathrm{sv},(1)} = \overline{\mathbf{L}}^2\left(2A_1\right) + \overline{\mathbf{L}}\left(2A_1 L_{fr} - 2A_1 L_{qr} + 2f_1\right) + \overline{g}_{01}, \tag{3.6}$$

$$\begin{aligned}
\Delta_N^{\mathrm{sv},(2)} = {} & \overline{\mathbf{L}}^4\left(2{A_1}^2\right) + \overline{\mathbf{L}}^3\left(4{A_1}^2 L_{fr} - 4{A_1}^2 L_{qr} + \frac{4}{3}A_1\beta_0 + 4A_1 f_1\right) + \overline{\mathbf{L}}^2\Big(10{A_1}^2\zeta_2 \\
& + 2{A_1}^2 L_{fr}^2 - 4{A_1}^2 L_{fr}L_{qr} + 2{A_1}^2 L_{qr}^2 - 2A_1\beta_0 L_{qr} - 4A_1 B_1 L_{fr} + 4A_1 B_1 L_{qr} \\
& + 4A_1 f_1 L_{fr} - 4A_1 f_1 L_{qr} + 4A_1 G_{11} + 4A_1\tilde{G}_{11} + 2A_2 + 2\beta_0 f_1 + 2f_1^2\Big) \\
& + \overline{\mathbf{L}}\Big(10{A_1}^2\zeta_2 L_{fr} - 10{A_1}^2\zeta_2 L_{qr} + 4A_1\beta_0\zeta_2 - A_1\beta_0 L_{fr}^2 + A_1\beta_0 L_{qr}^2 \\
& + 10A_1\zeta_2 f_1 - 4A_1 B_1 L_{fr}^2 + 8A_1 B_1 L_{fr}L_{qr} - 4A_1 B_1 L_{qr}^2 + 4A_1 G_{11} L_{fr} \\
& - 4A_1 G_{11} L_{qr} + 4A_1\tilde{G}_{11} L_{fr} - 4A_1\tilde{G}_{11} L_{qr} + 2A_2 L_{fr} - 2A_2 L_{qr} - 2\beta_0 f_1 L_{qr} \\
& + 4\beta_0\tilde{G}_{11} - 4B_1 f_1 L_{fr} + 4B_1 f_1 L_{qr} + 4f_1 G_{11} + 4f_1\tilde{G}_{11} + 2f_2\Big) + \overline{g}_{02},
\end{aligned} \tag{3.7}$$

$$\begin{aligned}
\Delta_N^{\mathrm{sv},(3)} = {} & \overline{\mathbf{L}}^6\left(\frac{4}{3}{A_1}^3\right) + \overline{\mathbf{L}}^5\left(4{A_1}^3 L_{fr} - 4{A_1}^3 L_{qr} + \frac{8}{3}{A_1}^2\beta_0 + 4{A_1}^2 f_1\right) + \overline{\mathbf{L}}^4\Big(10{A_1}^3\zeta_2 \\
& + 4{A_1}^3 L_{fr}^2 - 8{A_1}^3 L_{fr}L_{qr} + 4{A_1}^3 L_{qr}^2 + \frac{8}{3}{A_1}^2\beta_0 L_{fr} - \frac{20}{3}{A_1}^2\beta_0 L_{qr} \\
& - 4{A_1}^2 B_1 L_{fr} + 4{A_1}^2 B_1 L_{qr} + 8{A_1}^2 f_1 L_{fr} - 8{A_1}^2 f_1 L_{qr} + 4{A_1}^2 G_{11} \\
& + 4{A_1}^2\tilde{G}_{11} + 4A_1 A_2 + \frac{4}{3}A_1\beta_0^2 + \frac{20}{3}A_1\beta_0 f_1 + 4A_1 f_1^2\Big) + \overline{\mathbf{L}}^3\Big(20{A_1}^3\zeta_2 L_{fr} \\
& - 20{A_1}^3\zeta_2 L_{qr} + \frac{4}{3}{A_1}^3 L_{fr}^3 - 4{A_1}^3 L_{fr}^2 L_{qr} + 4{A_1}^3 L_{fr}L_{qr}^2 - \frac{4}{3}{A_1}^3 L_{qr}^3
\end{aligned}$$

$$
\begin{aligned}
&+\frac{44}{3}{A_1}^2\beta_0\zeta_2-2{A_1}^2\beta_0L_{fr}^2-4{A_1}^2\beta_0L_{fr}L_{qr}+6{A_1}^2\beta_0L_{qr}^2+20{A_1}^2\zeta_2f_1\\
&-8{A_1}^2B_1L_{fr}^2+16{A_1}^2B_1L_{fr}L_{qr}-8{A_1}^2B_1L_{qr}^2+4{A_1}^2f_1L_{fr}^2\\
&-8{A_1}^2f_1L_{fr}L_{qr}+4{A_1}^2f_1L_{qr}^2+8{A_1}^2G_{11}L_{fr}-8{A_1}^2G_{11}L_{qr}+8{A_1}^2\tilde{G}_{11}L_{fr}\\
&-8{A_1}^2\tilde{G}_{11}L_{qr}+8A_1A_2L_{fr}-8A_1A_2L_{qr}-\frac{8}{3}A_1\beta_0^2L_{qr}-\frac{8}{3}A_1\beta_0B_1L_{fr}\\
&+\frac{8}{3}A_1\beta_0B_1L_{qr}+4A_1\beta_0f_1L_{fr}-12A_1\beta_0f_1L_{qr}+\frac{8}{3}A_1\beta_0G_{11}+\frac{32}{3}A_1\beta_0\tilde{G}_{11}\\
&+\frac{4}{3}A_1\beta_1-8A_1B_1f_1L_{fr}+8A_1B_1f_1L_{qr}+4A_1f_1^2L_{fr}-4A_1f_1^2L_{qr}\\
&+8A_1f_1G_{11}+8A_1f_1\tilde{G}_{11}+4A_1f_2+\frac{8}{3}A_2\beta_0+4A_2f_1+\frac{8}{3}\beta_0^2f_1+4\beta_0f_1^2\\
&+\frac{4}{3}f_1^3\Big)+\overline{\mathbf{L}}^2\Big(25{A_1}^3\zeta_2^2+10{A_1}^3\zeta_2L_{fr}^2-20{A_1}^3\zeta_2L_{fr}L_{qr}+10{A_1}^3\zeta_2L_{qr}^2\\
&+8{A_1}^2\beta_0\zeta_2L_{fr}-28{A_1}^2\beta_0\zeta_2L_{qr}+\frac{16}{3}{A_1}^2\beta_0\zeta_3-2{A_1}^2\beta_0L_{fr}^3\\
&+2{A_1}^2\beta_0L_{fr}^2L_{qr}+2{A_1}^2\beta_0L_{fr}L_{qr}^2-2{A_1}^2\beta_0L_{qr}^3-20{A_1}^2\zeta_2B_1L_{fr}\\
&+20{A_1}^2\zeta_2B_1L_{qr}+20{A_1}^2\zeta_2f_1L_{fr}-20{A_1}^2\zeta_2f_1L_{qr}+20{A_1}^2\zeta_2G_{11}\\
&+20{A_1}^2\zeta_2\tilde{G}_{11}-4{A_1}^2B_1L_{fr}^3+12{A_1}^2B_1L_{fr}^2L_{qr}-12{A_1}^2B_1L_{fr}L_{qr}^2\\
&+4{A_1}^2B_1L_{qr}^3+4{A_1}^2G_{11}L_{fr}^2-8{A_1}^2G_{11}L_{fr}L_{qr}+4{A_1}^2G_{11}L_{qr}^2\\
&+4{A_1}^2\tilde{G}_{11}L_{fr}^2-8{A_1}^2\tilde{G}_{11}L_{fr}L_{qr}+4{A_1}^2\tilde{G}_{11}L_{qr}^2+20A_1A_2\zeta_2+4A_1A_2L_{fr}^2\\
&-8A_1A_2L_{fr}L_{qr}+4A_1A_2L_{qr}^2+8A_1\beta_0^2\zeta_2+2A_1\beta_0^2L_{qr}^2+12A_1\beta_0\zeta_2B_1\\
&+28A_1\beta_0\zeta_2f_1+2A_1\beta_0B_1L_{fr}^2+4A_1\beta_0B_1L_{fr}L_{qr}-6A_1\beta_0B_1L_{qr}^2\\
&-2A_1\beta_0f_1L_{fr}^2-4A_1\beta_0f_1L_{fr}L_{qr}+6A_1\beta_0f_1L_{qr}^2-8A_1\beta_0G_{11}L_{qr}\\
&+4A_1\beta_0G_{12}+8A_1\beta_0\tilde{G}_{11}L_{fr}-16A_1\beta_0\tilde{G}_{11}L_{qr}+4A_1\beta_0\tilde{G}_{12}-2A_1\beta_1L_{qr}\\
&+10A_1\zeta_2f_1^2+4A_1B_1^2L_{fr}^2-8A_1B_1^2L_{fr}L_{qr}+4A_1B_1^2L_{qr}^2-8A_1B_1f_1L_{fr}^2\\
&+16A_1B_1f_1L_{fr}L_{qr}-8A_1B_1f_1L_{qr}^2-8A_1B_1G_{11}L_{fr}+8A_1B_1G_{11}L_{qr}\\
&-8A_1B_1\tilde{G}_{11}L_{fr}+8A_1B_1\tilde{G}_{11}L_{qr}-4A_1B_2L_{fr}+4A_1B_2L_{qr}+8A_1f_1G_{11}L_{fr}\\
&-8A_1f_1G_{11}L_{qr}+8A_1f_1\tilde{G}_{11}L_{fr}-8A_1f_1\tilde{G}_{11}L_{qr}+4A_1f_2L_{fr}-4A_1f_2L_{qr}\\
&+4A_1G_{11}^2+8A_1G_{11}\tilde{G}_{11}+2A_1G_{21}+4A_1\tilde{G}_{11}^2+2A_1\tilde{G}_{21}-4A_2\beta_0L_{qr}\\
&-4A_2B_1L_{fr}+4A_2B_1L_{qr}+4A_2f_1L_{fr}-4A_2f_1L_{qr}+4A_2G_{11}+4A_2\tilde{G}_{11}\\
&+2A_3-4\beta_0^2f_1L_{qr}+8\beta_0^2\tilde{G}_{11}-4\beta_0B_1f_1L_{fr}+4\beta_0B_1f_1L_{qr}-4\beta_0f_1^2L_{qr}\\
&+4\beta_0f_1G_{11}+12\beta_0f_1\tilde{G}_{11}+4\beta_0f_2+2\beta_1f_1-4B_1f_1^2L_{fr}+4B_1f_1^2L_{qr}
\end{aligned}
$$

$$
\begin{aligned}
&+ 4f_1^2 G_{11} + 4f_1^2 \tilde{G}_{11} + 4f_1 f_2 \Big) + \overline{\mathbf{L}} \Big(25 {A_1}^3 \zeta_2^2 L_{fr} - 25 {A_1}^3 \zeta_2^2 L_{qr} \\
&+ 20 {A_1}^2 \beta_0 \zeta_2^2 - 5 {A_1}^2 \beta_0 \zeta_2 L_{fr}^2 - 10 {A_1}^2 \beta_0 \zeta_2 L_{fr} L_{qr} + 15 {A_1}^2 \beta_0 \zeta_2 L_{qr}^2 \\
&+ \frac{16}{3} {A_1}^2 \beta_0 \zeta_3 L_{fr} - \frac{16}{3} {A_1}^2 \beta_0 \zeta_3 L_{qr} + 25 {A_1}^2 \zeta_2^2 f_1 - 20 {A_1}^2 \zeta_2 B_1 L_{fr}^2 \\
&+ 40 {A_1}^2 \zeta_2 B_1 L_{fr} L_{qr} - 20 {A_1}^2 \zeta_2 B_1 L_{qr}^2 + 20 {A_1}^2 \zeta_2 G_{11} L_{fr} - 20 {A_1}^2 \zeta_2 G_{11} L_{qr} \\
&+ 20 {A_1}^2 \zeta_2 \tilde{G}_{11} L_{fr} - 20 {A_1}^2 \zeta_2 \tilde{G}_{11} L_{qr} + 20 A_1 A_2 \zeta_2 L_{fr} - 20 A_1 A_2 \zeta_2 L_{qr} \\
&- 8 A_1 \beta_0^2 \zeta_2 L_{qr} + \frac{32}{3} A_1 \beta_0^2 \zeta_3 + \frac{2}{3} A_1 \beta_0^2 L_{fr}^3 - \frac{2}{3} A_1 \beta_0^2 L_{qr}^3 + 4 A_1 \beta_0 \zeta_2 B_1 L_{fr} \\
&- 4 A_1 \beta_0 \zeta_2 B_1 L_{qr} + 10 A_1 \beta_0 \zeta_2 f_1 L_{fr} - 30 A_1 \beta_0 \zeta_2 f_1 L_{qr} + 8 A_1 \beta_0 \zeta_2 G_{11} \\
&+ 28 A_1 \beta_0 \zeta_2 \tilde{G}_{11} + \frac{16}{3} A_1 \beta_0 \zeta_3 f_1 + 4 A_1 \beta_0 B_1 L_{fr}^3 - 4 A_1 \beta_0 B_1 L_{fr}^2 L_{qr} \\
&- 4 A_1 \beta_0 B_1 L_{fr} L_{qr}^2 + 4 A_1 \beta_0 B_1 L_{qr}^3 - 2 A_1 \beta_0 G_{11} L_{fr}^2 - 4 A_1 \beta_0 G_{11} L_{fr} L_{qr} \\
&+ 6 A_1 \beta_0 G_{11} L_{qr}^2 + 4 A_1 \beta_0 G_{12} L_{fr} - 4 A_1 \beta_0 G_{12} L_{qr} - 2 A_1 \beta_0 \tilde{G}_{11} L_{fr}^2 \\
&- 4 A_1 \beta_0 \tilde{G}_{11} L_{fr} L_{qr} + 6 A_1 \beta_0 \tilde{G}_{11} L_{qr}^2 + 4 A_1 \beta_0 \tilde{G}_{12} L_{fr} - 4 A_1 \beta_0 \tilde{G}_{12} L_{qr} \\
&+ 4 A_1 \beta_1 \zeta_2 - A_1 \beta_1 L_{fr}^2 + A_1 \beta_1 L_{qr}^2 - 20 A_1 \zeta_2 B_1 f_1 L_{fr} + 20 A_1 \zeta_2 B_1 f_1 L_{qr} \\
&+ 20 A_1 \zeta_2 f_1 G_{11} + 20 A_1 \zeta_2 f_1 \tilde{G}_{11} + 10 A_1 \zeta_2 f_2 + 4 A_1 B_1^2 L_{fr}^3 - 12 A_1 B_1^2 L_{fr}^2 L_{qr} \\
&+ 12 A_1 B_1^2 L_{fr} L_{qr}^2 - 4 A_1 B_1^2 L_{qr}^3 - 8 A_1 B_1 G_{11} L_{fr}^2 + 16 A_1 B_1 G_{11} L_{fr} L_{qr} \\
&- 8 A_1 B_1 G_{11} L_{qr}^2 - 8 A_1 B_1 \tilde{G}_{11} L_{fr}^2 + 16 A_1 B_1 \tilde{G}_{11} L_{fr} L_{qr} - 8 A_1 B_1 \tilde{G}_{11} L_{qr}^2 \\
&- 4 A_1 B_2 L_{fr}^2 + 8 A_1 B_2 L_{fr} L_{qr} - 4 A_1 B_2 L_{qr}^2 + 4 A_1 G_{11}^2 L_{fr} - 4 A_1 G_{11}^2 L_{qr} \\
&+ 8 A_1 G_{11} \tilde{G}_{11} L_{fr} - 8 A_1 G_{11} \tilde{G}_{11} L_{qr} + 2 A_1 G_{21} L_{fr} - 2 A_1 G_{21} L_{qr} \\
&+ 4 A_1 \tilde{G}_{11}^2 L_{fr} - 4 A_1 \tilde{G}_{11}^2 L_{qr} + 2 A_1 \tilde{G}_{21} L_{fr} - 2 A_1 \tilde{G}_{21} L_{qr} + 8 A_2 \beta_0 \zeta_2 \\
&- 2 A_2 \beta_0 L_{fr}^2 + 2 A_2 \beta_0 L_{qr}^2 + 10 A_2 \zeta_2 f_1 - 4 A_2 B_1 L_{fr}^2 + 8 A_2 B_1 L_{fr} L_{qr} \\
&- 4 A_2 B_1 L_{qr}^2 + 4 A_2 G_{11} L_{fr} - 4 A_2 G_{11} L_{qr} + 4 A_2 \tilde{G}_{11} L_{fr} - 4 A_2 \tilde{G}_{11} L_{qr} \\
&+ 2 A_3 L_{fr} - 2 A_3 L_{qr} + 8 \beta_0^2 \zeta_2 f_1 + 2 \beta_0^2 f_1 L_{qr}^2 - 8 \beta_0^2 \tilde{G}_{11} L_{qr} + 8 \beta_0^2 \tilde{G}_{12} \\
&+ 12 \beta_0 \zeta_2 B_1 f_1 + 10 \beta_0 \zeta_2 f_1^2 + 2 \beta_0 B_1 f_1 L_{fr}^2 + 4 \beta_0 B_1 f_1 L_{fr} L_{qr} - 6 \beta_0 B_1 f_1 L_{qr}^2 \\
&- 8 \beta_0 B_1 \tilde{G}_{11} L_{fr} + 8 \beta_0 B_1 \tilde{G}_{11} L_{qr} - 8 \beta_0 f_1 G_{11} L_{qr} + 4 \beta_0 f_1 G_{12} - 8 \beta_0 f_1 \tilde{G}_{11} L_{qr} \\
&+ 4 \beta_0 f_1 \tilde{G}_{12} - 4 \beta_0 f_2 L_{qr} + 8 \beta_0 G_{11} \tilde{G}_{11} + 8 \beta_0 \tilde{G}_{11}^2 + 4 \beta_0 \tilde{G}_{21} - 2 \beta_1 f_1 L_{qr} \\
&+ 4 \beta_1 \tilde{G}_{11} + 4 B_1^2 f_1 L_{fr}^2 - 8 B_1^2 f_1 L_{fr} L_{qr} + 4 B_1^2 f_1 L_{qr}^2 - 8 B_1 f_1 G_{11} L_{fr} \\
&+ 8 B_1 f_1 G_{11} L_{qr} - 8 B_1 f_1 \tilde{G}_{11} L_{fr} + 8 B_1 f_1 \tilde{G}_{11} L_{qr} - 4 B_1 f_2 L_{fr} + 4 B_1 f_2 L_{qr} \\
&- 4 B_2 f_1 L_{fr} + 4 B_2 f_1 L_{qr} + 4 f_1 G_{11}^2 + 8 f_1 G_{11} \tilde{G}_{11} + 2 f_1 G_{21} + 4 f_1 \tilde{G}_{11}^2
\end{aligned}
$$

$$+ 2f_1\tilde{G}_{21} + 4f_2G_{11} + 4f_2\tilde{G}_{11} + 2f_3\Big) + \overline{g}_{03}\,. \tag{3.8}$$

Here $\overline{\mathbf{L}} = \ln\overline{N}$, $L_{fr} = \ln\left(\frac{\mu_f^2}{\mu_r^2}\right), L_{qr} = \ln\left(\frac{Q^2}{\mu_r^2}\right)$. The coefficients $\overline{g}_{0i}$ are given in App.(A.1).

These SV coefficients in Mellin space can be used to extract all the process dependent and independent resum ingredients for different resum prescriptions. We collect all these ingredients in App. (A) up to N^{3}LL accuracy in QCD.

3.3 Numerical Results

In this section, we present the numerical impact of resummed threshold corrections for neutral DY production as well as on-shell $Z/W^{\pm}$ production at the LHC. For neutral DY production we consider all the partonic channels at the FO case up to NNLO with off-shell γ^*, Z intermediate states. Detailed analysis is done for 13 TeV LHC, however it can be extended to other centre of mass energies.

3.3.1 Soft-virtual corrections for neutral DY

We start our discussion by examining the SV corrections at N^{3}LO. For our numerical study, we use the following electro-weak parameters for the vector boson masses and widths, Weinberg angle (θ_w) and the fine structure constant (α):

$$\begin{aligned} m_Z &= 91.1876 \text{ GeV}, \quad \Gamma_Z = 2.4952 \text{ GeV}\,, \\ m_W &= 80.379 \text{ GeV}, \quad \sin^2\theta_w = 0.2311 \quad \alpha = 1/128\,. \end{aligned} \tag{3.9}$$

We present our results for the default choice of hadronic center of mass energy 13 TeV at the LHC. The parton distribution functions (PDFs) are directly taken from the `lhapdf` [123] routine. The coefficient functions are convoluted with the respective order by order PDFs, however for N^{3}LO$_{sv}$ results we used NNLO PDFs. Except for studying the PDF uncertainties, we use `MMHT2014` [124] parton densities through-

out. The $(n+1)$-loop strong coupling constant is used for computing N^{n}LO order cross sections with $\alpha_s(m_Z) = 0.120(0.118)$ at NLO(NNLO and N^{3}LO) respectively. Except for the study of scale uncertainties, the unphysical scale are set equal to the invariant mass of the dilepton, $\mu_r = \mu_f = Q$.

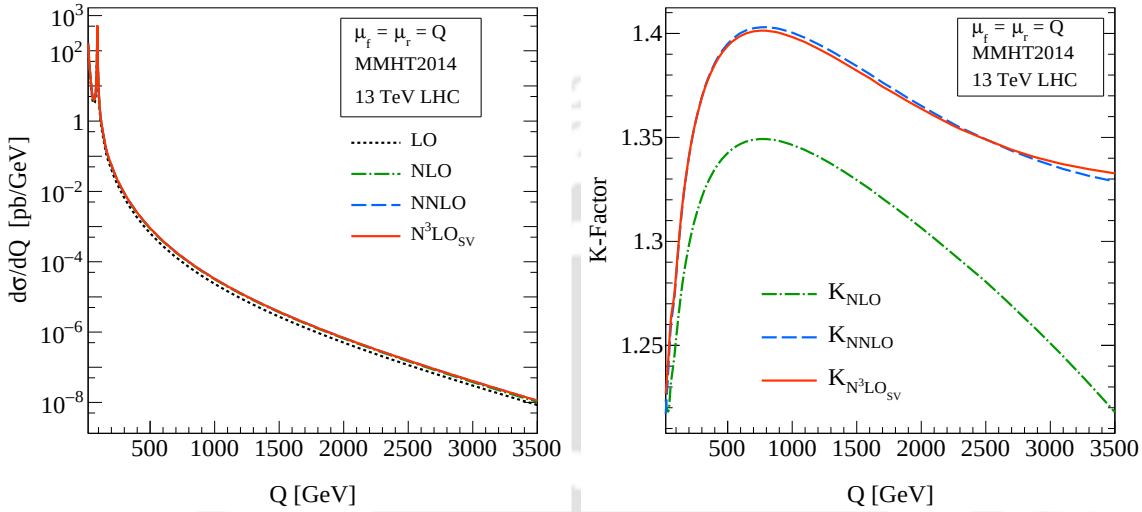

Figure 3.3: The dilepton invariant mass distribution (left panel) and the corresponding K-factors (right panel) are presented to N^{3}LO$_{sv}$ in QCD for 13 TeV LHC.

In Fig.(3.3), we present the invariant mass distribution (left panel) of the dilepton production for the neutral case to N^{3}LO$_{sv}$ in QCD for 13 TeV LHC as well as the corresponding K-factors (right panel). It is worth noting here that at $\mathcal{O}(\alpha_s^3)$ level the $\delta(1-z)$ contribution is comparable but opposite in sign to the sum of logarithmic contributions as is mentioned in [106]. The 3-loop SV corrections are found to be positive up to around $Q = 400$ GeV and remain negative for 400 GeV $< Q <$ 2200 GeV and become positive thereafter as threshold logarithms dominate in the high Q region. At around 3500 GeV, the 3-loop SV corrections contribute by about 2%. The observed values of Q where this change in the sign happens are not fixed but can change with the center of mass energy of incoming protons.

While the perturbation series is asymptotic and the higher orders terms are very small, the reliability of the theory predictions depends somewhat on the uncertainties due to the unphysical factorization (μ_f) and renormalization (μ_r) scales as well as those due to choice of PDFs. To this end, we estimate the 7-point scale uncertainties in the invariant mass distribution at various orders in the perturbation

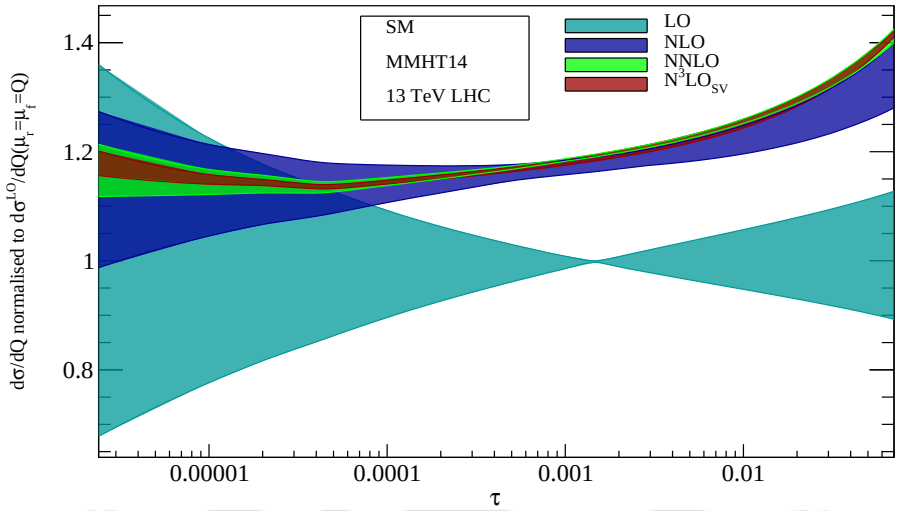

Figure 3.4: 7-point scale variation is plotted against the hadronic τ variable up to $\mathrm{N^3LO}_{sv}$ order. All the figures are normalized to LO contribution evaluated at the central scale $\mu_r = \mu_f = Q$.

theory by varying the scales $\mu = \{\mu_f, \mu_r\}$ in the range $\frac{1}{2} \leq \frac{\mu}{Q} \leq 2$. The scale uncertainties are conveniently presented in terms of the invariant mass distribution at higher orders normalized with respect to LO ones. In Fig.(3.4) we present these normalized distributions up to $\mathrm{N^3LO}_{sv}$ as a function of $\tau = Q^2/S$. At LO, there is no dependence on μ_r, hence the observation that these scale uncertainties are minimum around $\tau = 0.001$ (corresponding to about $Q = 400$ GeV) can be directly related to the behavior of the corresponding quark fluxes. At higher orders, the dependence on μ_r and μ_f is known and the scale uncertainties are found to increase with Q in the region $Q > 400$ GeV. For $Q = 1500$ GeV, they are found to be 6.61%, 2.40%, 0.44% and 0.91% respectively at LO, NLO, NNLO and $\mathrm{N^3LO}_{sv}$. For the 3-loop SV case, the scale uncertainties are expected to get further reduced only after including the regular terms that are not included in the fixed order perturbation theory. However, as we increase Q value, even $\mathrm{N^3LO}_{sv}$ show reasonable reduction in scale uncertainty as threshold logarithms dominate over the regular terms for larger Q values. For completeness, we note that the scale uncertainties for $Q = 3500$ GeV are found to be 12.90%, 4.64%, 1.21% and 0.68% at LO, NLO, NNLO and $\mathrm{N^3LO}_{sv}$ respectively.

Apart from the 7-points scale variation, we also study renormalization scale uncertainty separately. For this, we choose two Q regions; one moderate Q value

(1500 GeV) and one high Q value (3000 GeV) and vary μ_r from $Q/10 \to 10Q$. The results are presented in Fig.(3.5). We notice that in both region N^{3}LO$_{sv}$ provide a better stabilized result with respect to μ_r compare to NNLO results.

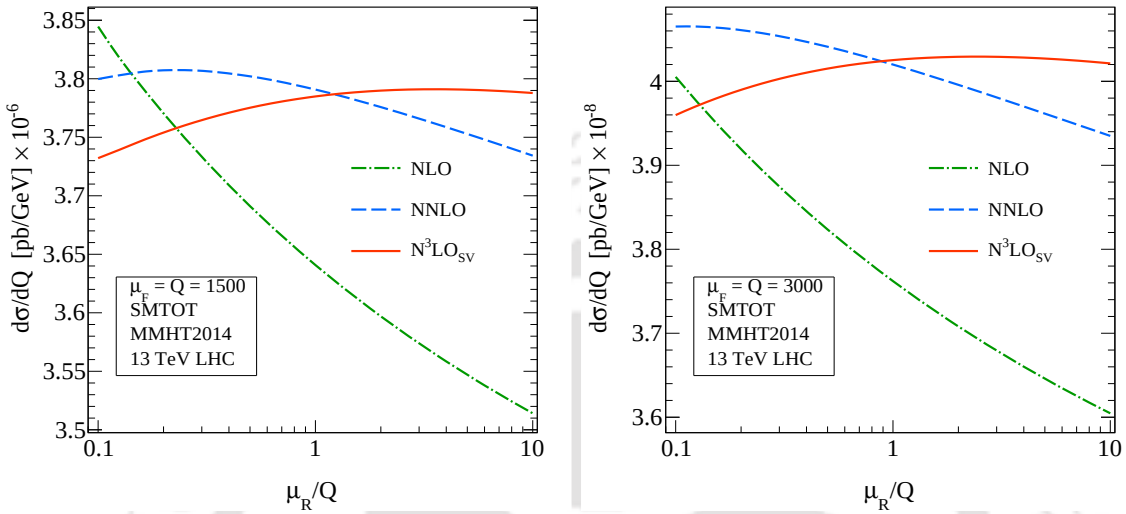

Figure 3.5: Renormalization scale uncertainty at N^{3}LO$_{sv}$ at two different regions (Q = 1500 and Q = 3000 GeV) varying μ_r from $Q/10 \to 10Q$ and keeping $\mu_f = Q$ fixed.

It is interesting to compare the SV results obtained in this article with the full N^{3}LO result recently calculated in [91]. For this comparison we chose the same parameters as in [91]. In particular at N^{3}LO level, we use `PDF4LHC15_nnlo_mc` pdf and strong coupling through four-loop evolution. In order to see how much the SV terms are comparable to the full correction at the third order, we have adapted to DY production through only γ^* as in [91]. The full N^{3}LO correction is negative up to Q = 1 TeV after that it becomes positive up to Q = 2 TeV (see Fig.(2) of [91]). On the contrary, the SV result is positive at lower invariant mass region and becomes negative at Q as low as 100 GeV. This indicates that the contributions from the other subprocesses are really important in the low invariant mass region $Q < 100$ GeV. In fact in the low-Q region, the qg channel really dominates over all other channels including the $q\bar{q}$ (see Fig.(4) of [91]) and thus completely controls the behavior. The $q\bar{q}$ channel on the other hand really becomes important in the higher Q region. Note that SV corrections are intrinsically ambiguous due to the choice of the function $g(z)$ in Eq.(3.10). This essentially does not change the complete cross-section, however when expanded in the limit $z \to 1$, this basically includes a

part of the subleading terms in the $q\bar{q}$ channel. It is thus interesting to study the subleading behavior of the $q\bar{q}$ channel itself by using the treatment performed in [125–127]. At N^{3}LO we have modified the SV result by a proper weight function $g(z)$ which minimizes the subleading regular effects,

$$\sigma = \sigma^{(0)} \sum_{ab=q,\bar{q},g} \int_0^1 dx_1 \int_0^1 dx_2 \int_0^1 dz \; f_a(x_1,\mu_f^2) \; f_b(x_2,\mu_f^2)/g(z) \times \left[\Delta_{ab}(z,Q^2,\mu_f^2) g(z)\right] \delta(\tau - z x_1 x_2) \,. \quad (3.10)$$

With the different choices of the weight function $g(z)$, we observe that $g(z) = z$ gives a result which is very close to the complete result from the $q\bar{q}$ channel at the lower orders. Notice that this choice correctly reproduces the leading collinear logarithm as well as a part of other subleading terms at each order. We present this SVM results in Fig.(3.6). With this modified SV cross-section (denoted as SVM)

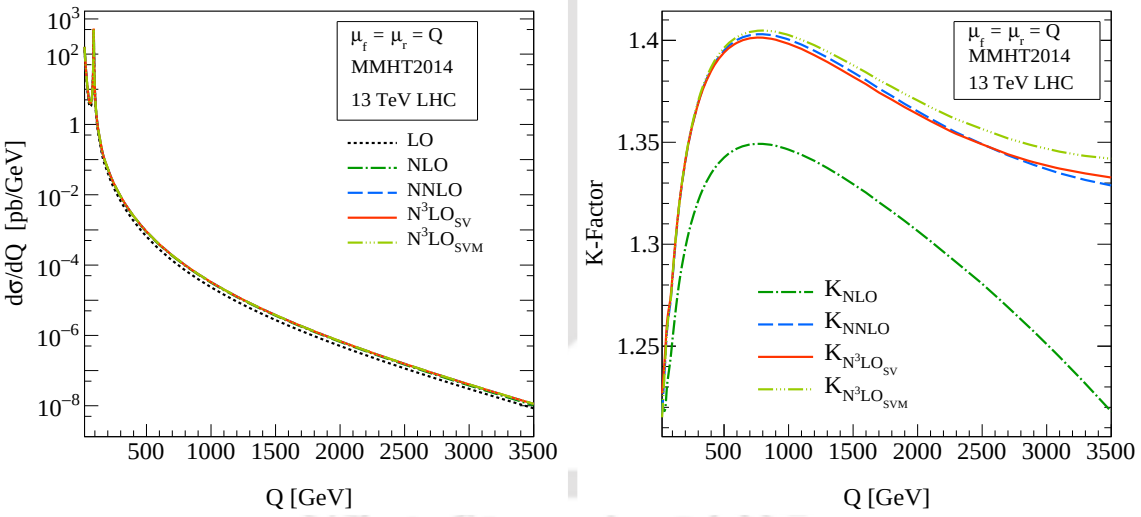

Figure 3.6: The dilepton invariant mass distribution (left panel) and the corresponding K-factors (right panel) are presented to N^{3}LO$_{\rm SVM}$ in QCD for 13 TeV LHC.

we observe that the N^{3}LO corrections are negative below $Q = 1$ TeV and becomes positive afterwards. This shows that the subleading pieces from the $q\bar{q}$ channels are also important in the region below 1 TeV. At $Q = 30$ GeV, the SV(SVM) corrections differ by as large as 5.2%(4.8%) from the complete N^{3}LO. This is direct consequence of the large negative qg contribution in this region. As we approach the threshold region, the SV (SVM) terms dominate and around $Q = 1800$ GeV

they differ only by 0.7% (0.2%) from the exact result, confirming the reliability of the threshold result in this region. For demonstration purpose, we have taken the full N^{3}LO results from the Fig.[2] of [91] and compared them against ours as shown in the Fig.[3.7]. We observe that, the N^{3}LO$_{\rm SV}$ and N^{3}LO$_{\rm SVM}$ follow the same trend whereas complete N^{3}LO follow different trend at low Q value. This is because of the presence of other subprocesses contribution (mainly the qg) at complete N^{3}LO results (see the Fig.[4] of [91]). As we go near the threshold, the $q\bar{q}$ subprocess will dominate over other subprocesses and all these three results converge. This kind of behaviour is also expected for other centre of mass energies but the value of Q will be different depending on the τ value. We note that the modified soft-virtual contributions are in good comparison with the full N^{3}LO results for about $Q \geq 800$ GeV.

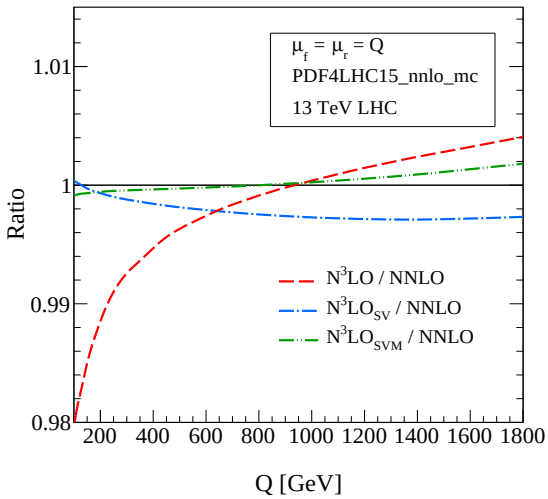

Figure 3.7: Comparison of N^{3}LO$_{\rm SV}$, N^{3}LO$_{\rm SVM}$ and complete N^{3}LO in QCD for 13 TeV LHC.

3.3.2 Resummed results for neutral DY invariant mass

In this section, we study the impact of different resummation schemes as described in the previous section. First we compare the resummed results between two approaches: the `Standard` $\overline{N}$ and `Standard` N prescriptions. We find that the perturbative convergence is better in the case of $\overline{N}$ exponentiation for the scale

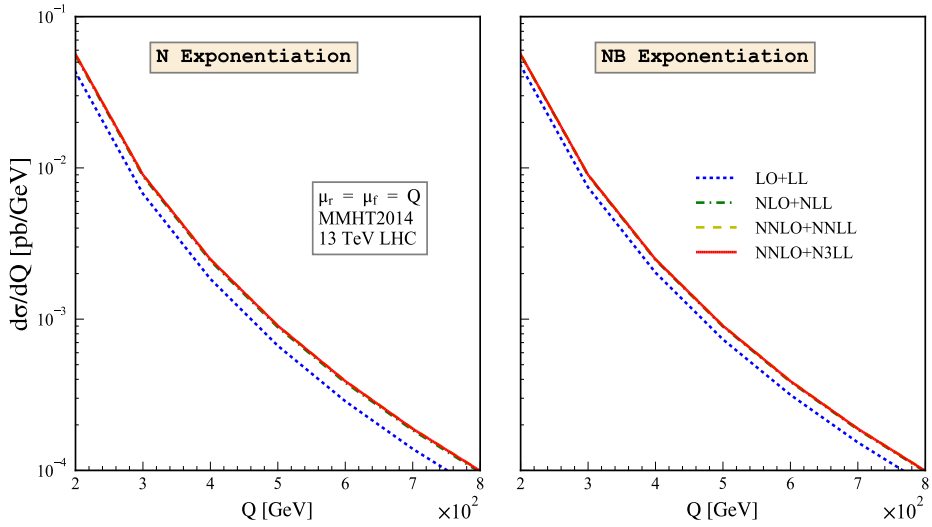

Figure 3.8: The comparison between `Standard` N and $\overline{N}$ resummation approaches for dilepton invariant mass distribution is presented up to N^{3}LL accuracy for 13 TeV LHC.

choice $\mu_r = \mu_f = Q$. This can be clearly seen from Fig.(3.8) where the convergence is already achieved at NLO+NLL whereas in N exponentiation it happens only after NLO+NLL order. At $Q = 2500$ GeV, we see the corrections received in `Standard` N exponentiation is 21.6% at NLO+NLL, 2.2% at NNLO+NNLL whereas in the `Standard` $\overline{N}$ exponentiation these are 6.7% and 2.3% respectively. This observation is also true for different scale choices. This is expected since naively one can expect that as we exponentiate more and more terms the convergence becomes better. In the rest of the discussion we will mention '`Standard`' only in the context of $\overline{N}$ exponentiation unless otherwise stated.

We now investigate the differences resulting from remaining two approaches *viz.* the `Soft exponentiation` and `All exponentiation` to study their perturbative behavior. To illustrate this, we show Fig.(3.9) where we took the ratio with respect to the `Standard` $\overline{N}$ results at each order. Notice that LO+LL results are same for all these three approaches by construction. To this end one sees that at lower orders the resummed cross-sections deviate more from those of $\overline{N}$ exponentiations. At NNLL the `Soft exponentiation` gets additional 0.12% corrections compared to the `Standard` $\overline{N}$ approach at $Q = 100$ GeV. However at N^{3}LL level the `Soft exponentiation` does not improve over the `Standard` $\overline{N}$ results and both

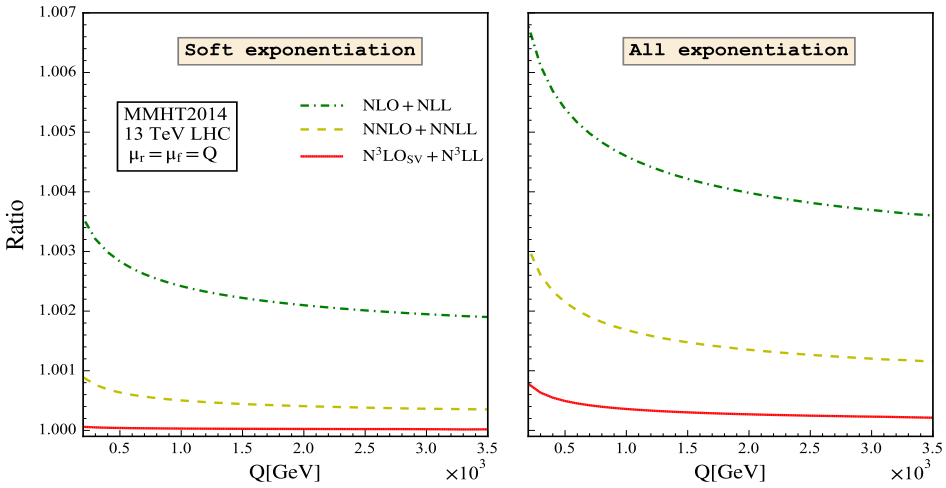

Figure 3.9: Comparison between the `Soft` (left panel) and `All exponentiation` (right panel) with `Standard` $\overline{N}$ approach. Here, the ratio is taken over the `Standard` $\overline{N}$ results.

approaches provide almost same results. On the other hand, `All exponentiation` still gets some contribution from higher orders through the exponentiation of complete $\overline{g}_0$ even at N^{3}LL order. The increment is however very small giving only 0.12% corrections over the `Standard` $\overline{N}$ scenario.

We have quantified the impact of resummed results through K-factor. In Fig.(3.10) we present the resummed K-factors ($\mathrm{K}_{NLO+NLL}$, $\mathrm{K}_{NNLO+NNLL}$, $\mathrm{K}_{N^3LO_{sv}+N^3LL}$) up to order N^{3}LL. We define the resum K-factor as

$$K_{N^iLO+N^iLL} = \frac{\frac{d\sigma^{N^iLO+N^iLL}}{dQ}}{\frac{d\sigma^{LO}}{dQ}} \tag{3.11}$$

One observes that the perturbative convergence is improved in the case of `All exponentiation` compared to others although marginally. The K factor defined this way will be useful to directly compare against the experimental results. For `All exponentiation` case, we find that the K-factor is 1.294 at $Q = 100$ at NNLL which changes to 1.286 at N^{3}LL. The K-factor increases with Q at any order. At higher $Q = 2500$ GeV the K-factors become 1.362 at NNLL and 1.350 at N^{3}LL.

Next we study the uncertainties resulting from unphysical scale in these approaches. We follow the canonical variation of μ_f and μ_r around the final state

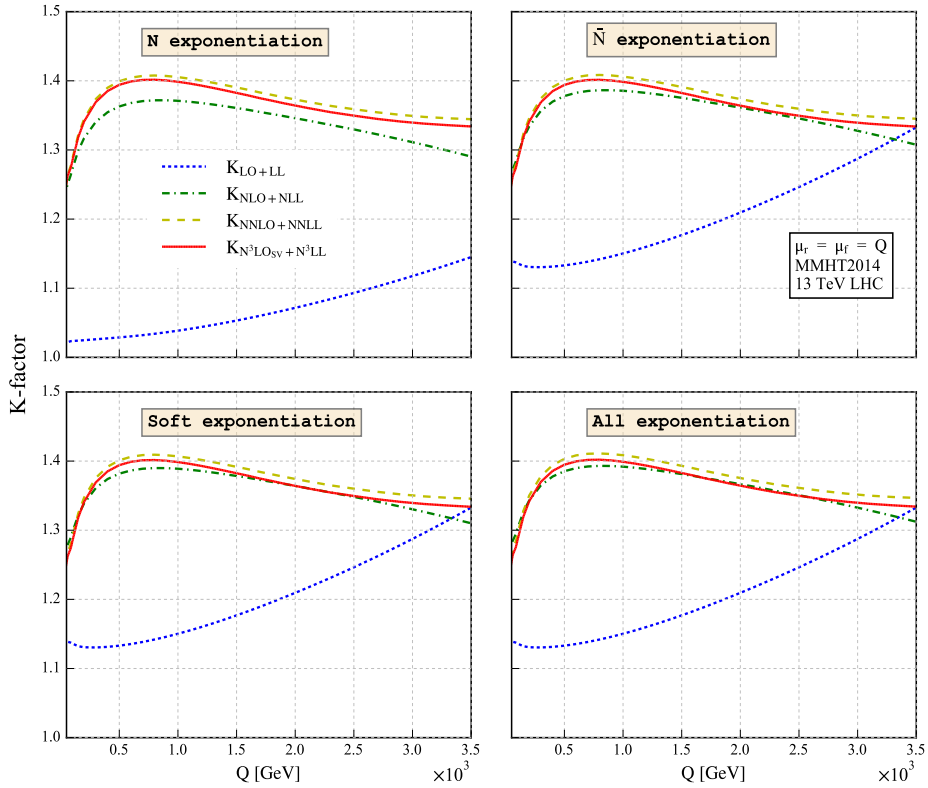

Figure 3.10: The K-factors are shown for resummed results up to N^3LL level for different threshold resummation approaches (discussed in the text).

invariant mass Q within $[1/2, 2]Q$ imposing additional constraint $1/2 \leq \mu_r/\mu_f \leq 2$ as was done in the third order SV prediction in the previous section. We notice that different approaches for resummation provide a systematic reduction in the scale uncertainties. For example, in the `Standard` $\overline{N}$ case, the scale uncertainty reduces from 13.37% at LO+LL to 6.91% at NLO+NLL to 1.99% at NNLO+NNLL. For a higher invariant mass $Q = 1500$ GeV that we have considered in our analysis as we approach towards the threshold region, we notice that scale uncertainties got reduced significantly to 7.61% at LO+LL, 0.90% at NLO+NLL, 0.52% at NNLO+NNLL. In Fig.(3.11), a similar pattern of reduction in the scale uncertainties is seen for the `Soft` and `All exponentiations` as we go to higher logarithmic accuracy for invariant mass up to $Q = 1500$ GeV. However, when we compare among themselves, the scale uncertainties at LO+LL remain the same for all the approaches by construction. For higher logarithmic accuracy, we see that `All` has the smallest uncertainty

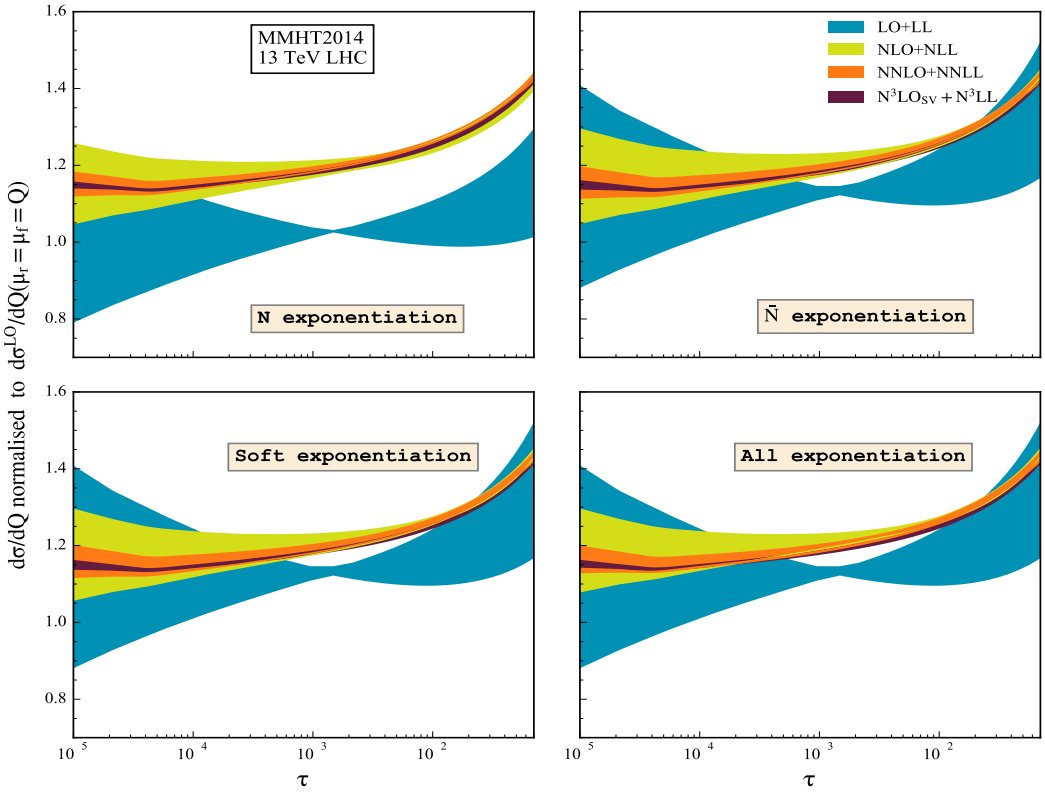

Figure 3.11: 7-point scale variations around the central scale choice ($\mu_r = Q, \mu_f = Q$) are presented as in Fig.(3.4) but for resummed predictions up to N^{3}LL accuracy.

up to NNLO+NNLL through $Q = 1500$ GeV. However, for the `Soft` case that we have considered here the NLO+NLL has larger uncertainty than that of `All` and at NNLO+NNLL the `Soft` is the largest. At N^{3}LO$_{sv}$+N^{3}LL, the scale uncertainties for all the different approaches are found to be less than 1% for the entire Q region we have considered. However, these scale uncertainties at N^{3}LL level are largest for `All` case while $\overline{N}$ and `Soft` have comparable numbers. Though the behaviour of the scale uncertainties in all these three schemes are competing with each other, it can be seen that `All exponentiation` has the largest scale uncertainties at N^{3}LO$_{sv}$+ N^{3}LL and smallest at lower orders for a wide range of Q values. This shows that the sub-leading regular pieces are also important to capture the scale dependence properly. We will again come back on this discussion at the end of this section.

We have also estimated in our resummed predictions the uncertainties from

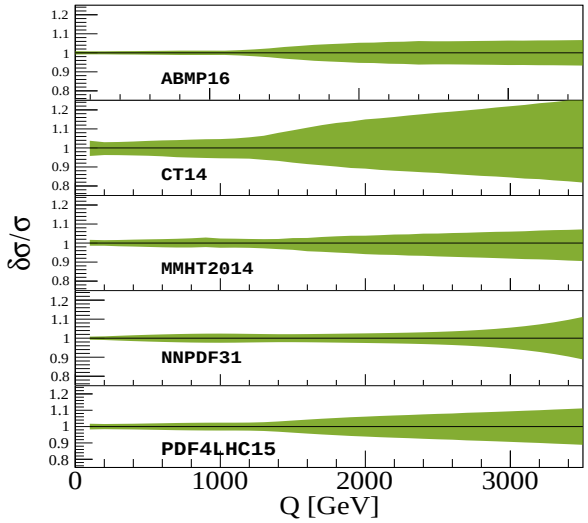

Figure 3.12: Intrinsic PDF uncertainties in dilepton invariant mass distribution have been estimated at NNLO+NNLL level taking $\mu_r = \mu_f = Q$. Here σ is obtained from the central set $n = 0$ provided by the respective PDF group.

the non-perturbative PDFs. We convolute the resummed coefficient at N^{3}LL level with n different sets of a given PDF group and estimate the uncertainty from the `lhapdf` routines. We use the PDFs provided by `ABMP16` (n= 30) [128] , `CT14` (n=57) [129], `MMHT2014` (n=51) [124], `NNPDF31` (n=101) [130] and `PDF4LHC15` (n=31) [131] groups. These results are shown in Fig.(3.12) in terms of $\delta\sigma/\sigma$ where $\delta\sigma$ is the difference between the extrema obtained from n different sets and σ is the one obtained from central set $n = 0$. These PDF uncertainties in general are found to increase with the invariant mass of the dilepton pair and, for the range of Q considered here, we find that they are smallest in the low Q-region for `AMP16` and are largest for `CT14` case. These uncertainties for $Q = 1500$ GeV are found to be 6.14% (`AMBP16`), 16.99% (`CT14`), 6.17% (`MMHT2014`), 4.21% (`NNPDF31`) and 7.43% (`PDF4LHC15`).

Finally, we discuss the matching relation presented in Eq.(2.79). One can match the N^{3}LO$_{sv}$ fixed order results (with $n = 3$) with the resummed results subtracted up to $\mathcal{O}(a_s^3)$ (with $n = 3$) in order to avoid any double counting from the fixed order. So far, we have followed this approach. Instead we can match the complete NNLO fixed order result with the resummed result subtracted up to $\mathcal{O}(a_s^2)$, which also avoids double counting and retains the threshold terms at higher orders

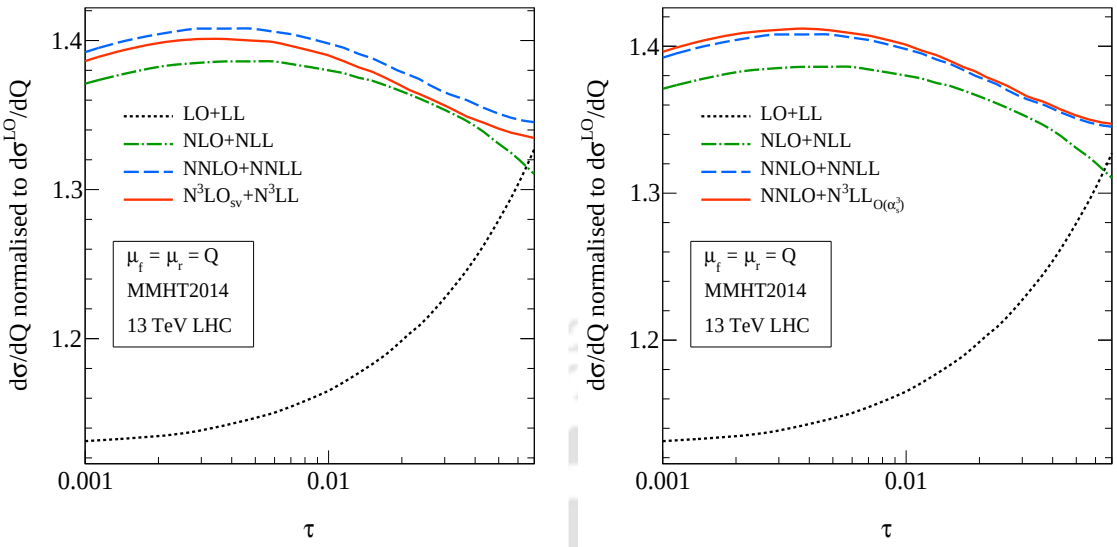

Figure 3.13: Comparison between two different ways of matching with the fixed order. In one case, the matching is done with threshold logarithms kept in the distribution (z) space (left) and in the other case the matching is done with threshold logarithms in the Mellin-N space (right).

in N-space in the threshold limit $N \to \infty$. The difference in these two approaches is sub-leading and has to be related with the fact that N-space threshold results when transformed back into distribution space produces sub-leading logarithms in addition to the plus distributions. In Fig.(3.13) we compare these two approaches setting all the scales same to Q in the `Standard` $\overline{N}$ approach. We see that the threshold terms defined in Mellin-N space provide much better perturbative convergence compared to the z-space definition. This is a well-known observation which shows that the sub-leading pieces are also important at this order. As far as scale uncertainty is concerned, this approach gives better estimate of scale uncertainty at N^{3}LL level reducing in some cases by a factor of two, however the general behavior does not change much.

3.3.3 Resummed prediction for $Z/W^{\pm}$ productions

In this section we present the resummed results for on-shell Z and $W^{\pm}$ productions to N^{3}LO$_{sv}$+N^{3}LL accuracy. We set all the parameters same as the previous section. For pdf, we chose the central value from `MMHT2014` set at the corresponding order.

$\sqrt{S}$ (TeV)	LO	NLO	NNLO	N^3LO_{sv}	LO+LL	NLO+NLL	NNLO+NNLL	N^3LO_{sv}+N^3LL
7	22.286 (±9.99%)	29.041 (±3.47%)	29.994 (±0.87%)	30.246 (±2.28%)	25.466 (±10.51%)	29.996 (±5.99%)	30.148 (±2.04%)	30.242 (±2.27%)
8	26.202 (±10.85%)	33.846 (±3.78%)	34.905 (±0.92%)	35.197 (±2.22%)	29.904 (±11.36%)	34.946 (±6.28%)	35.083 (±2.10%)	35.192 (±2.20%)
13	46.465 (±13.84%)	57.957 (±4.91%)	59.379 (±1.17%)	59.840 (±2.04%)	52.829 (±14.31%)	59.774 (±7.35%)	59.666 (±2.29%)	59.834 (±2.02%)
14	50.610 (±14.27%)	62.770 (±5.08%)	64.231 (±1.12%)	64.723 (±2.02%)	57.512 (±14.73%)	64.627 (±7.51%)	64.540 (±2.32%)	64.717 (±1.99%)

Table 3.1: Fixed order (up to N^3LO_{sv}) and resummed (up to N^3LO_{sv} + N^3LL) cross section (in nb) for on-shell Z-boson production at different center of mass energy of LHC. The scale uncertainty has been estimated using seven-point scale variation around the central scale $(\mu_r, \mu_f) = (1, 1)M_Z$.

$\sqrt{S}$ (TeV)	LO	NLO	NNLO	N^3LO_{sv}	LO+LL	NLO+NLL	NNLO+NNLL	N^3LO_{sv}+N^3LL
7	30.757 (±11.17%)	39.324 (±2.99%)	40.401 (±1.36%)	40.837 (±4.09%)	35.291 (±11.68%)	40.706 (±5.69%)	40.628 (±1.05%)	40.829 (±4.07%)
8	36.238 (±12.00%)	45.937 (±3.23%)	47.100 (±1.53%)	47.615 (±4.19%)	41.519 (±12.51%)	47.531 (±5.91%)	47.359 (±1.08%)	47.606 (±4.18%)
13	64.571 (±14.89%)	79.089 (±4.1%)	80.441 (±2.22%)	81.358 (±4.66%)	73.646 (±15.36%)	81.719 (±6.7%)	80.862 (±1.56%)	81.347 (±4.63%)
14	70.360 (±15.31%)	85.696 (±4.23%)	87.043 (±2.33%)	88.042 (±4.74%)	80.199 (±15.77%)	88.530 (±6.83%)	87.496 (±1.67%)	88.029 (±4.72%)

Table 3.2: Same as Tab.(3.1) but for W^- production at the LHC.

At the LHC, the underlying parton fluxes for W^+ production are larger than for W^- case, consequently the production cross sections for the former case are larger than the latter one. This is true also for higher centre of mass energies. In Tab.(3.1), Tab.(3.3), Tab.(3.2), we present for different center of mass energies at the LHC, the central predictions for on-shell Z, W^+ and W^- respectively along with the corresponding percentage of scale uncertainties. Note that the scale uncertainties are calculated again using the same procedure i.e. the 7-point scale variation around the central scale which is now the vector boson mass i.e. the central scale has been chosen as $(\mu_r, \mu_f) = (1, 1)M_V$, with $V = Z$ for Z production and $V = W^\pm$ for W-boson production. In all the cases we observed that the fixed order scale uncertainties are systematically reduced while going to higher orders, however at N^3LO_{sv}, it again increases which is due to the fact that, at this order there are still missing regular pieces as well as missing N^3LO PDF which are essential to the scale uncertainty. Similar observation is also seen for the matched resummed prediction. We see that compared to the fixed order, the resummed results provide better perturbative convergence.

$\sqrt{S}$ (TeV)	LO	NLO	NNLO	N^{3}LO$_{sv}$	LO+LL	NLO+NLL	NNLO+NNLL	N^{3}LO$_{sv}$+N^{3}LL
7	43.758 (±10.68%)	56.962 (±3.25%)	58.717 (±0.74%)	59.354 (±3.41%)	49.761 (±11.19%)	58.761 (±5.76%)	59.006 (±1.00%)	59.347 (±3.38%)
8	50.820 (±11.50%)	65.525 (±3.50%)	67.400 (±0.88%)	68.140 (±3.48%)	57.742 (±12.00%)	67.578 (±6.00%)	67.728 (±0.95%)	68.131 (±3.46%)
13	86.542 (±14.34%)	107.427 (±4.41%)	109.454 (±1.43%)	110.700 (±3.86%)	98.044 (±14.8%)	110.700 (±6.86%)	109.967 (±0.94%)	110.688 (±3.83%)
14	93.726 (±14.75%)	115.635 (±4.55%)	117.616 (±1.52%)	118.961 (±3.93%)	106.139 (±15.21%)	119.145 (±6.99%)	118.163 (±0.95%)	118.948 (±3.91%)

Table 3.3: Same as Tab.(3.1) but for W^+ production at the LHC.

To further investigate the source of this huge 7-point scale uncertainty at the N^{3}LO$_{sv}$ level, we have calculated the independent μ_r and μ_f uncertainties symmetrized around the central scale. We find that the μ_r scale uncertainty is indeed decreased. For 14 TeV centre-of-mass energies we find the μ_r uncertainty at N^{3}LO$_{sv}$ reduces to $\pm 0.32\%$ for Z case, $\pm 0.49\%$ for W^+ and $\pm 0.51\%$ for W^- production. On the other hand the μ_f uncertainty deteriorates at the N^{3}LO order and could lead to uncertainty as large as about $\pm 5\%$. This is expected since at N^{3}LO level we are missing the correct PDF to cancel the residual μ_f part in the coefficient function. In case of resummed prediction we observe further reduction of μ_r scale uncertainties to $\pm 0.2\%$, $\pm 0.37\%$ and $\pm 0.38\%$ for Z, W^+ and W^- productions respectively. The resummed K-factors as defined before, increases from NNLO+NNLL to N^{3}LO$_{sv}$+N^{3}LL for all the cases. The absolute size of the perturbative corrections however decreases at N^{3}LO$_{sv}$+N^{3}LL compared to the previous orders confirming the reliability of perturbation theory.

Note that one can perform a similar study as we did at the end of Sec.(3.3.1) to estimate the effect of subleading logarithms at the N^{3}LO level. The subleading effects at this region are expected to be comparable to the SV corrections. We find that for on-shell Z production, the SVM cross-section decreases the SV corrections presented above at the third order by 0.1%, while for W case the respective contribution is about 0.2%. We have compared the N^{3}LO$_{SVM}$ result for W-production with the recently obtained exact result at N^{3}LO [132], and we find that including the other subprocesses further bring down the cross-section additionally by 2% of LO.

3.4 Conclusion

We have studied the Drell-Yan production of dilepton as well as on-shell Z and $W^{\pm}$ productions in the context of threshold resummation and presented our results to N^{3}LL accuracy for different resummation prescriptions. The threshold corrections are important in the large invariant mass region (above $Q = 1800$ GeV) for LHC13. However in the moderate invariant mass region also we find substantial contribution from the threshold terms. We have used all the necessary ingredients available to perform resummation, in particular the threshold enhanced large-N as well as the N-independent constants. The standard threshold resummation uses results of the SV cross-section at any given order. In particular we have obtained the N-independent constants at N^{3}LL level using the existing SV results. We have matched our resummed N^{3}LL results with the existing NNLO(N^{3}LO$_{sv}$) cross-section and presented results for 13 TeV LHC. First, we observed that the resummed results obtained by exponentiating the $\ln \bar{N}$ terms give faster convergence of the perturbation series compared to the conventional case where $\ln N$ terms have been exponentiated. Further, we explored other possibilities of doing resummation where we exponentiate complete soft pieces coming from the universal soft distribution function and notice that the perturbative convergence for the `Soft` case is bit faster than the `Standard` $\overline{N}$ case. We also presented our results when the complete g_0 coefficients including the form factor have been exponentiated and found that the convergence rate of the perturbation series is competing with that of the `Soft` case. Over all, we observe that these different approaches show a systematic behavior of the resummed predictions where the convergence of the perturbation series gets better when more and more N-independent terms are exponentiated. For scale uncertainties up to NNLO+NNLL, `All` has the lowest scale uncertainties for a wide range of Q values. We also note that at N^{3}LL accuracy, however, the missing regular pieces are also important and so is N^{3}LO PDFs to tame the overall scale uncertainty.

Chapter 4

Inclusive cross section in RS model at NNLO+NNLL accuracy in QCD at LHC

This chapter is devoted for the precision calculation of DY process within the Randall-Sundrum (RS) framework. The complete next-to-next-to leading order (NNLO) QCD correction has been studied to the dilepton invariant mass distribution. In addition, the soft-virtual (SV) cross-section at next-to-next-to-next-to leading order (N^3LO) as well as threshold resummation to next-to-next-to leading logarithms (NNLL) level have been presented. The analytical coefficient for SV production has been obtained up to three loops very recently along with the process-dependent coefficients needed to perform resummation up to NNLL. We use these coefficients in predicting N^3LO_{SV} results as well as matched NNLO+NNLL results for invariant mass distribution for Drell-Yan (DY) production in RS model. We performed a detailed phenomenological analysis and present our results in terms of mass dependent K-factors for the 13 TeV LHC for the search of such RS Kaluza-Klein (KK) resonances. We performed a detailed analysis including scale variation and parton distribution function (PDF) variations. These new results provide an opportunity to stringently constrain the parameters of the model in particular in the search of heavy spin-2 resonances at the LHC.

4.1 Introduction

A large class of the BSM scenarios are motivated by the large hierarchy between the electroweak symmetry breaking scale and the Planck scale. A wide class of theories have been proposed to address this problem through the introduction of large extra dimensions in the TeV scale brane world scenarios. In particular the models with warped extra dimension as proposed by Randall and Sundrum (RS) [16] are attractive candidates to solve this gauge hierarchy problem as discussed in Sec.(1.2.2) . In its simplest version, it predicts spin-2 Kaluza-Klein (KK) excitations in the TeV mass range which could be accessible at current hadron collider LHC or in any future hadron colliders or electron-positron colliders.

The Precise theoretical results are already available for the processes like Higgs and pseudo-scalar Higgs boson [90, 133–137], DY [88, 90] productions at NNLO accuracy in QCD. The large perturbative corrections for Higgs at NNLO even pushes the accuracy to be calculated to even N^3LO order [138–140]. Recently the DY production has also been calculated to third order in strong coupling [91]. The exclusive observables like rapidity are also being calculated to the same accuracy (see for example [141–150]).

In the context of large extra dimension, the NLO corrections were known for many important processes at the LHC [151–161] within Arkani-Hamed-Dimopoulos-Dvali (ADD) [15] and RS [16] model. It is observed in the NLO QCD computation [151] that the K-factors in the dilepton production case are potentially large and range up to 60%. The matched NLO results with parton shower is also known for di-final processes in ADD [162, 163] and in RS [164] model. The associated production [165] as well as triple gauge boson production processes [166] are also known. In RS model, the triple neutral gauge boson productions are available [167] in ME+PS accuracy in the MadGraph framework. Moreover generic universal and non-universal spin-2 production processes are automatized [168] in Feynrules [169] - MadGraph5_aMC@NLO [170] framework providing NLO accuracy for inclusive and exclusive cross-sections for all relevant channels at the LHC.

The first attempt to go beyond the NLO accuracy has been seen in [171] calculating the SV corrections at NNLO. This has been possible due to the calculation of spin-2 form factor [172] at the same order. Shortly after, the complete NNLO corrections were computed in [173] using the method of reverse unitarity [134] and phenomenological study has been performed in the context of ADD model. There it has been found that the NNLO correction changes the cross-section by 21% over NLO results and constrains the scale uncertainty to 1.6%. Similar accuracy is also available for non-universal spin-2 production [174] where spin-2 couples with different coupling to the SM fields. The first attempt in calculating the SV corrections beyond NNLO can be seen [115] in the context of ADD model in DY invariant mass distribution after the completion of three-loop quark and gluon form factor [175]. The perturbative coefficients are same for any spin-2 production with universal coupling to the SM. There it has been noticed that the N^3LO SV cross-section changes the NNLO by -0.7% at $Q = 1500$ GeV (Q being the invariant mass of the lepton pair). Moreover the authors also performed threshold resummation up to N^3LL accuracy and the corrections are found to be around 1% over NNLO with scale uncertainty reduces to 1.5%.

In this chapter, we present the complete NNLO QCD corrections on massive KK production in the RS framework. We note that the search for the spin-2 resonances at hadron collider experiments has been of significant interest over the last many years. The production of spin-2 particles in hadron collisions proceeds via both quark antiquark annihilation (SM DY-like) as well as the gluon fusion (Higgs-like) channels. In the case of Higgs production via gluon fusion channel, it is well known in the literature that the QCD corrections at NNLO and even beyond contribute substantially to the cross section. In the gluon fusion channel, particularly at the LHC energies, these higher order corrections are absolutely necessary for the convergence of the perturbation theory as well as for the minimization of the factorization and renormalization scale uncertainties. It is in the same spirit such a precise QCD calculations are required for the spin-2 production cross sections as their production rates receive dominant contributions from the gluon fusion channel.

Since the spin-2 RS KK excitations also couples universally to the SM

stress-energy tensor, the analytical perturbative coefficients are same as the generic universal spin-2 case like ADD. Phenomenologically however the RS KK states provide very distinctive signature from that of ADD model at the LHC. While the dilepton invariant mass distribution in the ADD model provides a continuum distribution, in the RS model one finds well-separated massive KK resonances. Using the coefficients already obtained in ADD scenario, we first study the invariant mass distribution for DY production at NNLO accuracy in the RS model.

Next, we extend this precision study to three loop SV correction as well as the NNLL resummation of the threshold logarithms in this model. The SV corrections constitute a significant part of the full cross-section and have been successfully computed for many processes in the SM and BSM scenarios as mentioned in Ch.(3). In the threshold region where partonic $z \to 1$, the truncated fixed order cross-section however becomes unreliable due to the presence of large logarithms. These large logarithms arise due to constrained phase space available for the soft gluons. In order to get a reliable prediction also in these corners of the phase-space, it is thus essential to resum these large logarithms to all orders. Threshold resummation has been performed successfully to inclusive Higgs production [78, 80, 81, 93, 108–110], DY production [93, 108], DIS [70] as well as for pseudo-scalar production [112–114] up to N^3LL accuracy. The first results towards N^4LL corrections are also available recently for DIS in [79]. Moreover for differential observables like rapidity, it is known to NNLL accuracy for many important processes (see for example [66, 117–120, 176]). These higher order corrections of the RS model, presented in the later sections are expected to improve by more than a few percent the bounds on the RS model parameters that are presently obtained from the LHC data using the known NLO K-factors.

4.2 Theoretical Formalism

The interaction Lagrangian of RS model is described in Eq.(1.54). The massive KK modes of graviton can couple to SM fields via energy-momentum tensor. Therefore,

the new vertices that will come into the picture for DY production at LHC are shown below, where B,C,D,E are defined in App.(D)

Fermion-Fermion-Graviton Vertex:	$-i(\kappa/8)(\gamma_\mu(k_{1\nu}+k_{2\nu})+\gamma_\nu(k_{1\mu}+k_{2\mu}))-2\eta_{\mu\nu}(\not{k}_1+\not{k}_2)$	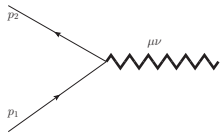
Gluon-Gluon-Graviton Vertex:	$-i(\kappa/2)[(k_1.k_2)C_{\mu\nu,\rho\sigma}+D_{\mu\nu,\rho\sigma}(k_1,k_2)+\zeta^{-1}E_{\mu\nu,\rho\sigma}(k_1,k_2)]$	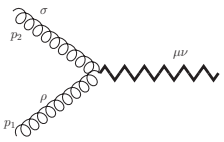
Fermion-Fermion-Gluon-Graviton Vertex:	$ig(\kappa/4)T^a(C_{\mu\nu,\rho\sigma}-\eta_{\mu\nu,\rho\sigma})\gamma_\sigma$	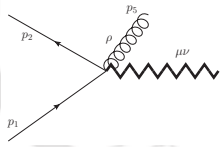
Triple-Gluon-Graviton Vertex:	$g(\kappa/2)f^{abc}(C_{\mu\nu,\rho\sigma}(k_{1\lambda}-k_{2\lambda})+C_{\mu\nu,\rho\lambda}(k_{3\sigma}-k_{1\sigma})+C_{\mu\nu,\sigma\lambda}(k_{2\rho}-k_{3\rho})F_{\mu\nu,\rho\sigma\lambda}(k_1,k_2,k_3))$	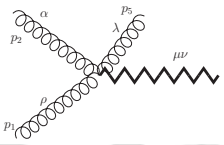

Figure 4.1: Feynman rules for extra vertices due to gravity [2]

Diagrams that will contribute NNLO QCD correction to the DY production in RS model are given below

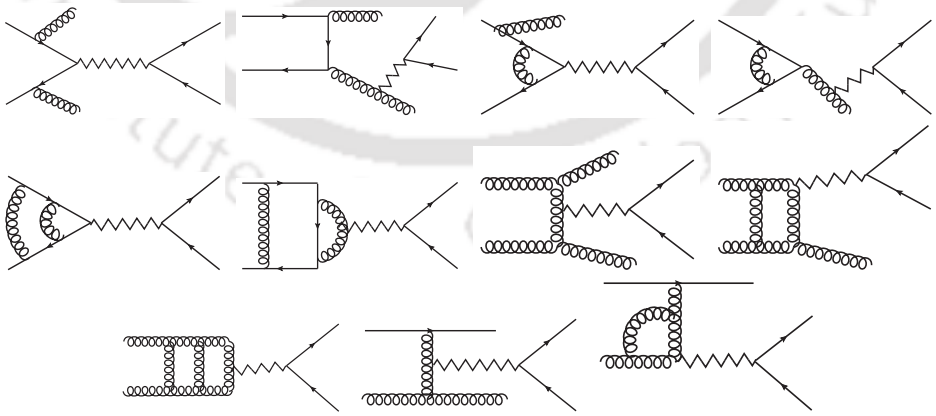

Figure 4.2: Related diagrams for NNLO QCD corrections of DY process in RS model

The invariant mass distribution for DY production at the hadron collider

is given by,

$$2S\,\frac{d\sigma}{dQ^2}\left(\tau,Q^2\right)=\sum_{ab=q,\bar{q},g}\int_0^1 dx_1\int_0^1 dx_2\int_0^1 dz\;\delta(\tau-zx_1x_2)$$
$$\times\,\mathcal{L}_{ab}(x_1,x_2,\mu_f^2)\sum_I\Delta_{ab}^I(z,Q^2,\mu_f^2)\,. \tag{4.1}$$

The summation over I takes care the contributions coming from SM and the RS model. Here Q is the invariant mass of the dilepton, S and $\hat{s}$ denote the center-of-mass energy in the hadronic and partonic frame respectively. The hadronic and partonic threshold variables τ and z are defined as

$$\tau=\frac{Q^2}{S},\qquad z=\frac{Q^2}{\hat{s}}\,. \tag{4.2}$$

They are thus related by $\tau=x_1x_2z$. The partonic cross-section gets contribution from virtual photon and Z boson as in the standard DY process in SM as discussed in the Ch.(3.2), in addition, it also gets contribution from spin-2 propagator decaying to leptons. Here, the SM is treated as background for the signal defined by total SM contributions plus spin-2 contributions. Notice that the signal and background completely get separated from each other in the cross-section after performing the phase-space integration for invariant mass distribution. This gives opportunity to calculate the SM and ADD contributions completely separately and there is no interference term between them. Whereas in the SM case, there is only quark annihilation channel at the born level, in the RS case, both quark annihilation as well as gluon fusion channels are present already at the born level. Up to two loops the contribution from RS spin-2 can be written as,

$$2S\frac{d\sigma_{RS}}{dQ^2}(\tau,Q^2)=\sum_{q,\bar{q},g}\mathcal{F}_{RS}^{(0)}\int_0^1 dx_1\int_0^1 dx_2\int_0^1 dz\;\delta(\tau-zx_1x_2)$$
$$\times\Bigg[\mathcal{L}_{q\bar{q}}\sum_{n=0}^{2}a_s^n\Delta_{q\bar{q}}^{RS,(n)}+\mathcal{L}_{gg}\sum_{n=0}^{2}a_s^n\Delta_{gg}^{RS,(n)}$$
$$+\Big(\mathcal{L}_{gq}+\mathcal{L}_{qg}\Big)\sum_{n=1}^{2}a_s^n\Delta_{gq}^{RS,(n)}$$

$$+\mathcal{L}_{qq}\sum_{n=2}^{2}a_s^n\Delta_{qq}^{RS,(n)}+\mathcal{L}_{q_1q_2}\sum_{n=2}^{2}a_s^n\Delta_{q_1q_2}^{RS,(n)}\Bigg], \tag{4.3}$$

with

$$\begin{aligned}
\mathcal{L}_{q\bar{q}}(x_1,x_2,\mu_f^2) &= f_q^{P_1}(x_1,\mu_f^2)f_{\bar{q}}^{P_2}(x_2,\mu_f^2)+f_{\bar{q}}^{P_1}(x_1,\mu_f^2)\ f_q^{P_2}(x_2,\mu_f^2)\,,\\
\mathcal{L}_{qq}(x_1,x_2,\mu_f^2) &= f_q^{P_1}(x_1,\mu_f^2)f_q^{P_2}(x_2,\mu_f^2)+f_{\bar{q}}^{P_1}(x_1,\mu_f^2)\ f_{\bar{q}}^{P_2}(x_2,\mu_f^2)\,,\\
\mathcal{L}_{q_1q_2}(x_1,x_2,\mu_f^2) &= f_{q_1}^{P_1}(x_1,\mu_f^2)\Big(f_{q_2}^{P_2}(x_2,\mu_f^2)+f_{\bar{q}_2}^{P_2}(x_2,\mu_f^2)\Big)\\
&\quad+f_{\bar{q}_1}^{P_1}(x_1,\mu_f^2)\ \Big(f_{q_2}^{P_2}(x_2,\mu_f^2)+f_{\bar{q}_2}^{P_2}(x_2,\mu_f^2)\Big)\,,\\
\mathcal{L}_{gq}(x_1,x_2,\mu_f^2) &= f_g^{P_1}(x_1,\mu_f^2)\Big(f_q^{P_2}(x_2,\mu_f^2)+f_{\bar{q}}^{P_2}(x_2,\mu_f^2)\Big)\,,\\
\mathcal{L}_{qg}(x_1,x_2,\mu_f^2) &= \mathcal{L}_{gq}(x_2,x_1,\mu_f^2)\,,\\
\mathcal{L}_{gg}(x_1,x_2,\mu_f^2) &= f_g^{P_1}(x_1,\mu_f^2)\ f_g^{P_2}(x_2,\mu_f^2)\,.
\end{aligned} \tag{4.4}$$

Notice that computation of the partonic coefficients at the second order requires evaluation of matrix element as well as the proper phase space for the dilepton pair. Using the method of reverse unitarity [134], where the phase space integrals were converted to loop integrals, the latter has been performed very recently in the case of generic spin-2 production [173]. The advantage is that, one then can re-use all the techniques developed for the multi-loop computation. The analytical result obtained in this way is useful for any spin-2 production with universal coupling to the SM. We use these coefficients to predict complete NNLO cross-section for the RS model.

We further extend this precision calculation by incorporating three loop SV correction. This can be achieved by calculating the spin-2 form factor at three loops [175] as well as the soft function at the same order. The soft function being maximally non-abelian up to three loops, can be extracted from the known Higgs [92, 96] and DY [106, 108] results. Using these informations, the third order coefficients for the SV corrections have been obtained [115] for generic spin-2 coupling and have been applied to ADD model to predict the DY distribution to N^3LO. The analytical coefficients can be also used to predict the SV cross-section in the RS graviton production at the same perturbative order. One can write the SV coefficient in

terms of perturbative expansion in strong coupling,

$$\Delta_{ab}^{(\mathrm{sv},I)} = \sum_{n=0}^{\infty} a_s^n \Delta_{ab}^{(n),I} \,. \tag{4.5}$$

In the SM, only $q\bar{q}$ contributes wheres for the RS scenario both $q\bar{q}$ and gg channels contribute to the SV coefficient. Here we present only the leading order term (*i.e.* $n = 0$) in this series to follow the overall normalization to the coefficient,

$$\begin{aligned}
\Delta_{\mathrm{q\bar{q}}}^{(0),SM} &= \frac{2\pi}{n_c}\delta(1-z)\,, \\
\Delta_{\mathrm{q\bar{q}}}^{(0),RS} &= \frac{\pi}{8n_c}\delta(1-z)\,, \\
\Delta_{\mathrm{gg}}^{(0),RS} &= \frac{\pi}{2(n_c^2-1)}\delta(1-z)
\end{aligned} \tag{4.6}$$

The NNLO cross-section can be improved with the contribution from threshold logarithms at all orders. In particular when partonic $z \to 1$ the contribution from these singular terms becomes large and unreliable and thus needs to be resummed to all orders. We follow the `Standard` $\overline{N}$ prescriptions here. It has been seen that the $\overline{N}$ exponentiation shows better perturbative convergence for DIS [79] as well as in DY [177]. This is because in the second case, the γ_E terms are also exponentiated along with the Mellin-N. It is already shown in the case of DIS [79], that the $\overline{N}$ exponentiation differs as large as 15% at LL compared to N exponentiation, however at the higher logarithmic accuracy these differences get minimized. In the Ch.(3), it has been observed that the resummed K-factors (at $Q = 500$ GeV) in the $\overline{N}$-space are $\mathrm{K}_{LL} = 1.133$, $\mathrm{K}_{NLL} = 1.378$ and $\mathrm{K}_{NNLL} = 1.400$ while in the N-space they are 1.029, 1.363 and 1.399 respectively. This clearly shows a faster convergence for the $\overline{N}$ scenario.

In $\overline{N}$ prescription, all order resum partonic cross section can be organized as

$$(d\hat{\sigma}_N/dQ)/(d\hat{\sigma}_{\mathrm{LO}}/dQ) = g_0^I \exp\left(G_{\overline{N}}^I\right). \tag{4.7}$$

The normalization $(d\hat{\sigma}_{\rm LO}/dQ)$ is given as,

$$\begin{aligned}(d\hat{\sigma}_{\rm LO}/dQ) &= \mathcal{F}^{(0)}_{\rm SM}\frac{Q}{S}\left\{\frac{2\pi}{n_c}\right\} && \text{for SM,}\\ &= \mathcal{F}^{(0)}_{\rm RS}\frac{Q}{S}\left\{\frac{\pi}{8n_c},\frac{\pi}{2(n_c^2-1)}\right\} && \text{for } \{q\bar{q},gg\} \text{ in RS.}\end{aligned} \tag{4.8}$$

All the required process dependent and independent coefficients for $\overline{N}$ exponentiation are collected in App.(B.2) and Eq.(A.4) respectively.

4.3 Numerical Results

In this section we present our numerical results for the dilepton production cross section in the RS model at the LHC. The LO, NLO and NNLO parton level cross sections are convoluted with the respective order by order parton distribution functions (PDF) taken from `lhapdf` [123]. The corresponding strong coupling constant $a_s(\mu_r^2) = \alpha_s(\mu_r^2)/(4\pi)$ is also provided by `lhapdf`. The fine structure constant and the weak mixing angles are chosen to be $\alpha_{\rm em} = 1/128$ and $\sin^2\theta_w = 0.227$ respectively. Here the results are presented for $n_f = 5$ flavors in the massless limit of quarks. The default choice for the centre-of-mass energy of protons is 13 TeV and the choice for the PDF set is `MMHT2014` [124]. Except for the scale variations, we have used the factorization (μ_f) and renormalization (μ_r) scales to be the invariant mass of the dilepton, *i.e.* $\mu_f = \mu_r = Q$. We also note that there have been several experimental searches at the LHC for warped extra dimensions in the past, yielding stringent bounds on the RS model parameters, the mass of the first resonance mode (M_1) and the coupling strength $(\bar{c}_0)$ [1, 4]. Such analyses have already used the K-factors that have been computed in the extra dimension models. In the dilepton channel using the combined 8 and 13 TeV data at the LHC, the observed 95% CL lower limit on the RS resonance is 1.38 (2.98) TeV for $\bar{c}_0 = 0.01$ (0.1)[4]. On the other side, in the di-photon channel using 13 TeV LHC data, the lower limit at 95% CL on the RS first resonance mass is found to be 4.1 TeV for $\bar{c}_0$=0.1 [1].

Here in this work, for our phenomenological study to assess the impact of

QCD corrections, we choose $M_1 = 1.5$ TeV and $\bar{c}_0 = 0.05$. The computational details of the QCD corrections presented here are model independent, and a numerical estimate of the theory predictions for any other choice of the model parameters is straight-forward. For completeness, we also study the dependence of the invariant mass distributions on the model parameters considering the recent bounds on M_1 for different $\bar{c}_0$ values.

4.3.1 Fixed Order Results

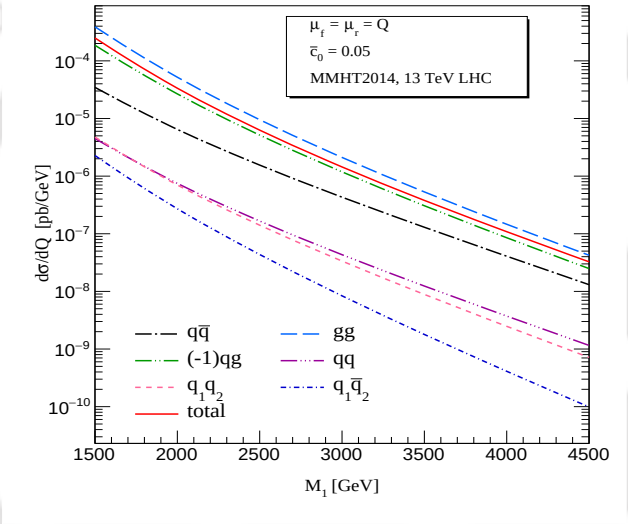

Figure 4.3: Different subprocess contributions for the RS model at NNLO QCD right at the resonance for different M_1 values keeping $\bar{c}_0$ fixed at 0.05.

First we present in Fig.(4.3) the contribution from different subprocesses for the pure RS graviton (GR) at NNLO level right at the resonance region by varying the first resonant mass M_1 and keeping $\bar{c}_0 = 0.05$. At this order in QCD there are six different subprocesses that contribute for GR case, *viz.* $q\bar{q}$, gg, qg, qq, q_1q_2 and $q_1\bar{q}_2$. Here, the dominant contribution comes from the gg-subprocess and it remains dominant for resonance values as large as 4.5 TeV. The next dominant contribution comes from qg-subprocess but it is negative for this entire mass range. This is followed by quark initiated processes with $q\bar{q}$ being the largest in this category. For a typical choice of first resonance $M_1 = 2500$, we find that the total cross-section is 0.63×10^{-5} pb in which the dominant gg subprocess overshoots by 151%. The $q\bar{q}$, qq,

q_1q_2 and $q_1\bar{q}_2$ channels contribute in addition 24.7%, 2.7%, 2.2%, 0.7% respectively of the total cross-section. As stated earlier only the qg channel contributes negatively by about -82% of the total cross-section.

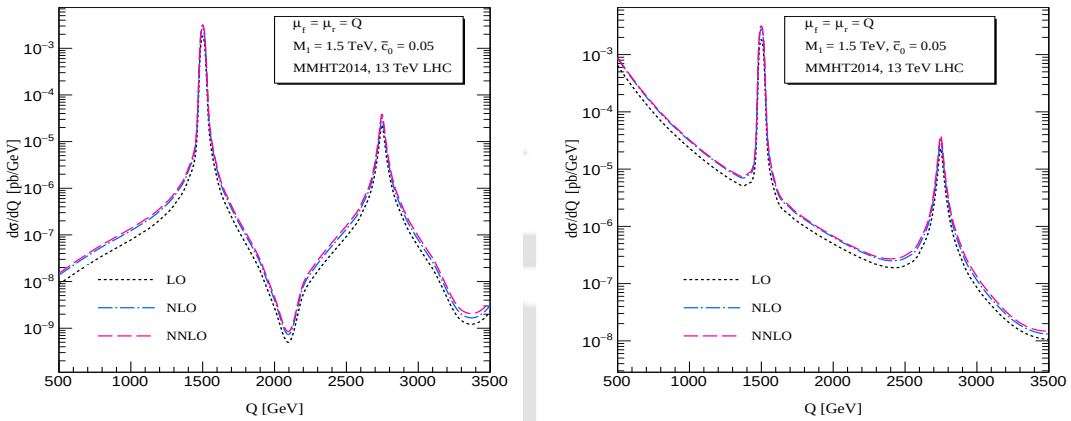

Figure 4.4: Di-lepton invariant mass distribution up to NNLO QCD for pure RS model (left panel) and for the signal (right panel).

Next, we present in Fig.(4.4) the dilepton invariant mass distribution $(d\sigma/dQ)$ as a function of the invariant mass of the dilepton Q for GR and for the signal (SM+GR). The width of the resonance depends on $\bar{c}_0$ and near the resonance region the signal receives most of the contribution from the pure RS graviton. Far away from this resonance region, the RS contribution is found to be comparable to that of the SM background for $Q > 3500$ GeV.

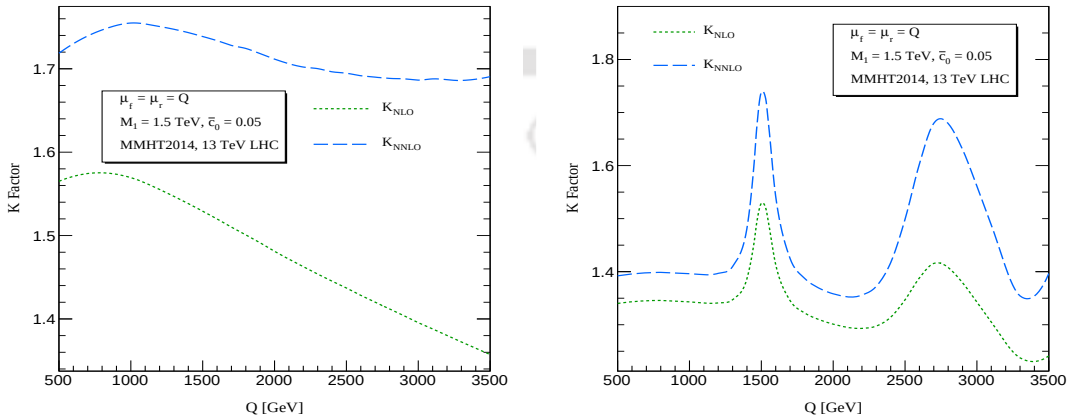

Figure 4.5: The K-factors up to NNLO in QCD for RS model (left panel) and for the signal (right panel).

Q (GeV)	K_{NLO}	K_{NNLO}
500	1.340	1.392
1000	1.343	1.396
1500	1.529	1.738
2000	1.301	1.358
2500	1.347	1.499

Table 4.1: The fixed order K-factors for the signal up to NNLO in QCD for $M_1 = 1.5$ TeV, $\bar{c}_0 = 0.05$ at 13 TeV LHC.

$$K_{NLO} = \frac{d\sigma^{NLO}/dQ}{d\sigma^{LO}/dQ}, \quad K_{NNLO} = \frac{d\sigma^{NNLO}/dQ}{d\sigma^{LO}/dQ}. \tag{4.9}$$

In Fig.(4.5) we present the K-factor, defined in Eq.(5.5), for both GR and the signal cases. We note that it is the same virtual graviton exchange process that contributes both in ADD and RS model. The leading order processes are similar and the QCD corrections are model independent. However, the difference between these two models arise because of the difference in the summation over the tower of KK gravitons and also in the overall wrapped factor. Consequently the relative weight of the contribution from the gravitons in these two models will be different for different invariant mass region. This results in different mass-dependent K-factors in the ADD and RS model. The NLO corrections for pure RS case at $Q = 1000$ GeV are found to contribute by about 57% of LO, while NNLO corrections add an additional 18% of LO to the total invariant mass distribution. In Tab.(4.1) we present the signal K-factors up to NNLO QCD for different Q values. For signal case, the NLO corrections at $Q = 1000$ GeV contribute by about 34% of LO and NNLO corrections add an additional 6% of LO to the total invariant mass distribution. However, right at the resonance region, these NNLO corrections are found to enhance the production cross section by an additional 20% of LO results. This shows that NNLO corrections are indeed essential for this process in order to make any reliable predictions.

In Fig.(4.6) we present the dilepton invariant mass distribution for SM, GR and signal cases. The behavior of the signal K-factor is governed by the respective

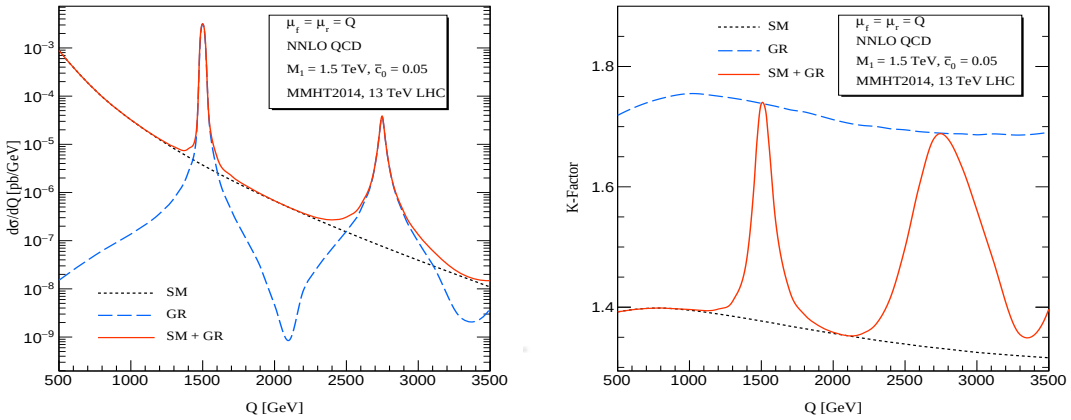

Figure 4.6: Invariant mass distribution of dilepton for the SM, RS model and for the signal (left) and their corresponding K-factors (right).

coupling constants in SM and RS as well as the parton fluxes. As discussed earlier, in the RS case gravity contribution is significant near resonance region and therefore the whole signal K-factor is controlled by RS. In the off resonance region at high Q, both RS and SM contributions are comparable and hence the signal K-factor receives contributions from both RS and SM. Hence, the behavior of the mass dependent K-factor for the signal in the RS model is very distinct from that in the ADD model [115].

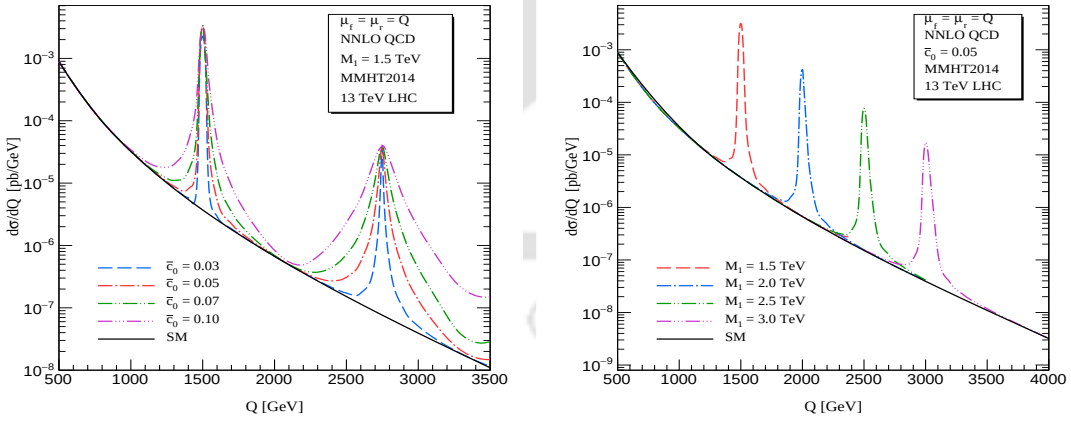

Figure 4.7: Dependence of the dilepton invariant mass distribution for the signal on the RS model parameters $\bar{c}_0$ (left) and the first resonance mass M_1 (right).

We also study the dependence of our results on the RS model parameters, M_1 and $\bar{c}_0$. In Fig.(4.7) we present the dilepton invariant mass distribution by varying $\bar{c}_0$ from 0.03 to 0.1 keeping M_1 fixed at 1.5 TeV in the left panel. We also

M_1 (GeV)	K_{NLO}	K_{NNLO}
1500	1.529	1.738
2000	1.481	1.713
2500	1.436	1.694
3000	1.395	1.686
3500	1.357	1.694
4000	1.320	1.718
4500	1.283	1.760

Table 4.2: The fixed order K-factors for the signal to NNLO in QCD right at the resonance region for different M_1 values and fixed $\bar{c}_0(0.05)$ are presented for 13 TeV LHC.

present the results in the right panel by varying M_1 from 1.5 TeV to 3.0 TeV for a fixed $\bar{c}_0$ (0.05). The width of the resonance depends on $\bar{c}_0$, however, right at the resonance this dependence of the production cross section on this coupling $\bar{c}_0$ cancels with that from decay width (Γ_G) and the height of peak for any given M_1 will be independent of $\bar{c}_0$. Consequently, the respective NNLO K-factors near the resonance region depend on $\bar{c}_0$ but right at the resonance they do not. These signal K-factors are presented in Tab.(4.2) right at the resonance region for different M_1 values. The NNLO corrections increases the K-factors substantially compared to NLO implying the importance of the higher order correction for this process.

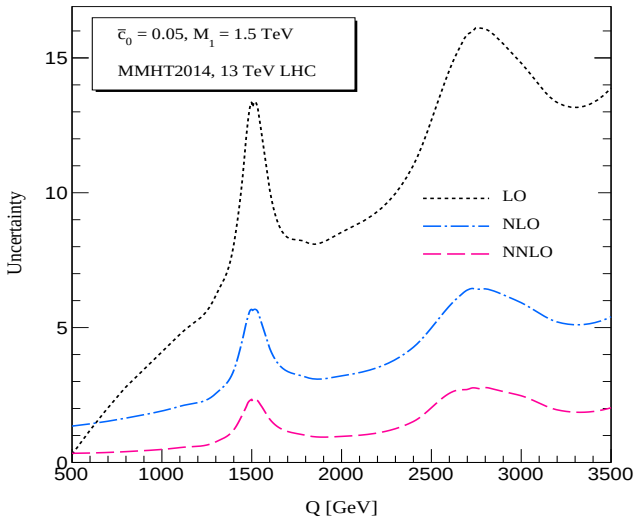

Figure 4.8: 7-point scale variation in the signal is shown up to NNLO for the dilepton invariant mass distribution.

We have considered different sources of theoretical uncertainties in our analysis. First, we considered the uncertainties due to the presence of two unphysical scales μ_r and μ_f in the theory and then those coming from the non-perturbative parton distribution function in the calculation. For the scale uncertainties we follow 7-point scale uncertainty and the results up to NNLO are depicted in Fig.(4.8). The scale uncertainties are found to get reduced significantly from LO to NNLO over the full invariant mass region. For $Q = 1500$ GeV *i.e.* right at the first resonance, the scale uncertainties at LO are $\pm 13.3\%$, at NLO they are $\pm 5.7\%$, at NNLO it further reduces to $\pm 2.3\%$. Away from resonance, the uncertainty also decreases order by order. For example at $Q = 3000$ GeV, the scale uncertainties get reduced from $\pm 14.8\%$ at LO to about $\pm 2.5\%$ at NNLO. In the off-resonance region the uncertainty in general increases with increasing Q which can be tamed with inclusion of further higher order terms in the perturbation theory.

M_1 (GeV)	ABMP16	CT14	MMHT2014	NNPDF31	PDF4LHC15
1500	$2.66 \times 10^{-3}(\pm 4.7\%)$	$3.13 \times 10^{-3}(\pm 9.6\%)$	$3.17 \times 10^{-3}(\pm 4.0\%)$	$2.91 \times 10^{-3}(\pm 2.1\%)$	$3.11 \times 10^{-3}(\pm 5.0\%)$
2000	$3.35 \times 10^{-4}(\pm 5.7\%)$	$4.06 \times 10^{-4}(\pm 12.0\%)$	$4.20 \times 10^{-4}(\pm 5.0\%)$	$3.72 \times 10^{-4}(\pm 2.6\%)$	$4.07 \times 10^{-4}(\pm 6.5\%)$
2500	$5.84 \times 10^{-5}(\pm 6.0\%)$	$7.25 \times 10^{-5}(\pm 14.4\%)$	$7.70 \times 10^{-5}(\pm 5.9\%)$	$6.53 \times 10^{-5}(\pm 3.4\%)$	$7.35 \times 10^{-5}(\pm 7.9\%)$
3000	$1.23 \times 10^{-5}(\pm 6.3\%)$	$1.56 \times 10^{-5}(\pm 17.0\%)$	$1.71 \times 10^{-5}(\pm 6.9\%)$	$1.38 \times 10^{-5}(\pm 5.8\%)$	$1.61 \times 10^{-5}(\pm 9.5\%)$
3500	$2.91 \times 10^{-6}(\pm 6.5\%)$	$3.78 \times 10^{-6}(\pm 20.0\%)$	$4.26 \times 10^{-6}(\pm 8.0\%)$	$3.20 \times 10^{-6}(\pm 11.9\%)$	$3.96 \times 10^{-6}(\pm 11.2\%)$

Table 4.3: Intrinsic PDF uncertainties in the signal at NNLO QCD for different PDF choices are given right at the resonance for different M_1 values. All the results are presented for 13 TeV LHC. The cross sections are given for the central set ($n = 0$) for each PDF group along with the corresponding intrinsic uncertainties in terms of the percentage.

We also estimate the uncertainties coming from the non-perturbative PDFs. For this we calculate the uncertainty due to the intrinsic errors in the PDFs that result from various experimental errors from the global fits. In this case we use the PDF sets `ABMP16` [178], `CT14` [129], `MMHT2014` [124], `NNPDF31` [130], and `PDF4LHC15` [131] provided from the `lhapdf`. The central predictions for these different PDF groups also differ due to different underlying assumptions in global fits for different groups. We calculate the intrinsic PDF uncertainties using 51 sets for `MMHT2014`, 57 sets for `CT14`, 101 sets for `NNPDF31`, 30 sets for `ABMP16` and 31 sets for `PDF4LHC15`. To this end we use all PDF sets extracted at NNLO level. In Tab.(4.3) we present these uncertainties for the dilepton invariant mass distribution to NNLO. We find that around the resonance $M_1 = 1500$ GeV the PDF uncertainty is well within 5% ex-

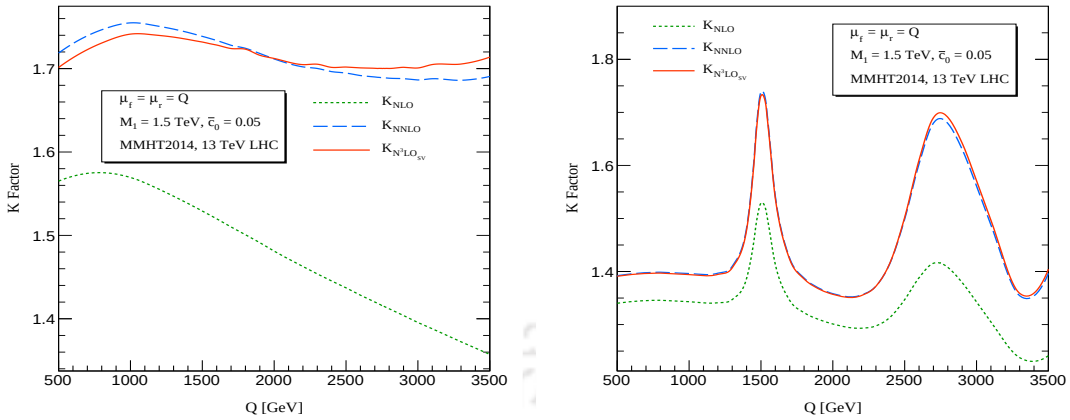

Figure 4.9: K-factors are presented up to N^3LO_{sv} for the RS model (left) and for the signal (right).

cept for the `CT14` which shows relatively increased uncertainty. In the high invariant mass region $Q > 2000$ GeV the uncertainty however increases due to unavailability of sufficient data in those region.

From the above observation we notice that the NNLO corrections for RS production are large enough to truncate the perturbation theory at this order and necessitates the computation of higher order corrections for the convergence of the perturbation series. As a first step beyond, NNLO we studied the three-loop SV correction for dilepton production channel using the universal property of the SV coefficients for generic spin-2 couplings. In Fig.(4.9) we present these three loop SV corrections in terms of the corresponding K-factors up to N^3LO_{sv} as a function of the dilepton invariant mass for pure RS case (left panel) as well as for the signal (right panel). We use `MMHT2014nnlo` set for this analysis. These three-loop SV corrections are found to contribute an additional -0.7% of LO to the NNLO result at first resonance $M_1 = 1500$ GeV for pure RS case, demonstrating a very good convergence of the perturbation theory at this order. In the high invariant mass region away from the RS resonance however we see correction due to third order SV terms is about 1% of LO cross-section. We also note that the three-loop SV corrections are negative in the low Q-region while in the high Q-region they are positive because of threshold enhancement. Therefore, The missing regular piece at third order is important at low invariant mass region. The 7-point scale uncertainty

is seen to increase at the lower invariant mass region while in the higher invariant mass region decreases. To further constraint the scale uncertainty the N^{3}LO PDFs are essential at this order. Also the missing sub-leading pieces are important in particular in the low-Q region (see *eg.* [179, 180]). The μ_r uncertainty however is seen to improve in the whole invariant mass region. Keeping $\mu_f = Q = M_1$ we observe an uncertainty of $\pm 0.9\%$ around the resonance $M_1 = 1500$ GeV for the μ_r variation in the range $(M_1/2, 2M_1)$.

4.3.2 Resum Results

We now move to study the effect of threshold logarithms by resumming them to NNLL accuracy and match to the computed NNLO cross-section in the Sec.(4.3.1). For this, the same choice of SM and RS model parameters has been used as in the fixed order computation. For the inverse Mellin transformation Eq.(2.78), we use $c = 1.9$. In Fig.(4.10) we present the dilepton invariant mass distribution for RS and for the signal at different logarithmic accuracy.

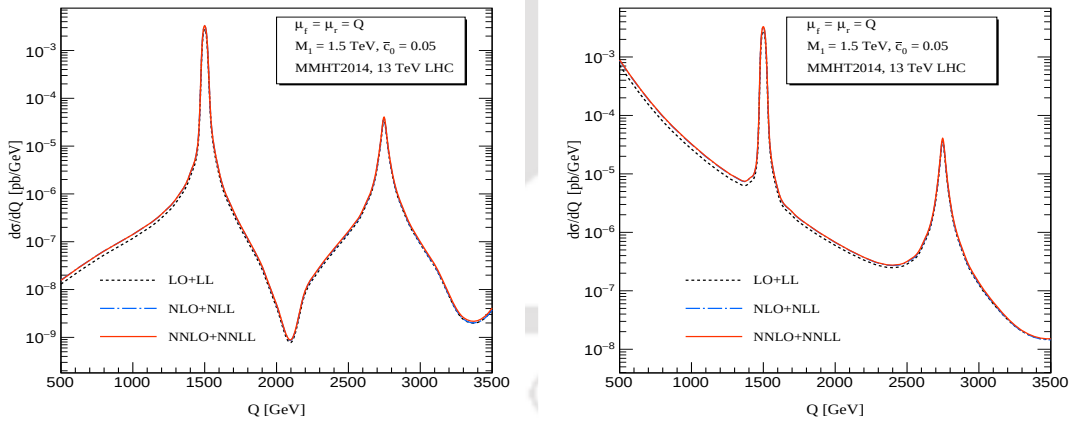

Figure 4.10: Di-lepton invariant mass distribution up to NNLO+NNLL for RS model (left) and for the signal (right).

$$\mathrm{K_{LL}} = \frac{d\sigma^{\mathrm{LO+LL}}/dQ}{d\sigma^{\mathrm{LO}}/dQ}\,,\quad \mathrm{K_{NLL}} = \frac{d\sigma^{\mathrm{NLO+NLL}}/dQ}{d\sigma^{\mathrm{LO}}/dQ}\,,\quad \mathrm{K_{NNLL}} = \frac{d\sigma^{\mathrm{N^2LO+N^2LL}}/dQ}{d\sigma^{\mathrm{LO}}/dQ}\,. \tag{4.10}$$

Q (GeV)	K_{LL}	K_{NLL}	K_{NNLL}	R_2	R_3
500	1.131	1.375	1.397	1.026	1.004
1000	1.148	1.381	1.401	1.029	1.004
1500	1.530	1.786	1.811	1.168	1.042
2000	1.206	1.354	1.367	1.041	1.006
2500	1.390	1.501	1.541	1.114	1.028

Table 4.4: Resum K-factors and the ratios as defined in Eq.(4.10) and Eq.(4.11) as a function of the dilepton invariant mass for the default choice of RS model parameters.

To quantify these resummation effects, we define the resum K-factors in Eq.(4.10) and present the same in Tab.(4.4) for different Q values. The enhancement due to threshold logarithms for the signal is significant for all Q values, however it is more significant at the resonance region. This is because of the underlying born processes for the graviton production in the RS model. At the born level, the RS graviton can be produced via quark-antiquark annihilation process (DY-like) as well as gluon fusion channel (Higgs-like). It is well known that the QCD corrections, particularly, the threshold enhancement in these two channels are different and are more pronounced for gluon fusion channel. Here, the signal receives contribution from RS (DY-like as well as Higgs-like) and the SM background (DY-like). However, at the resonance region GR dominates over the SM background by several orders of magnitude and hence the threshold enhancement due to the gluon fusion channel becomes prominent. Far off the resonance region, the signal is essentially dominated by the SM background and assumes DY-like threshold enhancement. For completeness, we present these resummed K-factors for RS case in Fig.(4.11).

$$R_2 = \frac{d\sigma^{\rm NLO+NLL}/dQ}{d\sigma^{\rm NLO}/dQ}\,, \quad R_3 = \frac{d\sigma^{\rm N^2LO+N^2LL}/dQ}{d\sigma^{\rm NNLO}/dQ}\,. \tag{4.11}$$

In order to further study the enhancement due to threshold resummation for the signal, we consider the ratios of the resummed results to the fixed order results defined in Eq.(4.11). We observe that at resonance ($Q = M_1 = 1500$ GeV), NNLO+NNLL contributes additional 4% enhancement over NNLO. These ratios are presented in Fig.(4.11). Moreover, in Tab.(4.5), we present these resum K-factors right at the resonance for different values of resonance mass M_1.

M_1 (GeV)	K_{LL}	K_{NLL}	K_{NNLL}
1500	1.530	1.786	1.811
2000	1.550	1.743	1.790
2500	1.574	1.703	1.776
3000	1.603	1.670	1.777
3500	1.639	1.644	1.793
4000	1.681	1.623	1.832
4500	1.730	1.607	1.891

Table 4.5: Resum K-factors for signal right at the resonance for different M_1 values are presented up to NNLO+NNLL in QCD for 13 TeV LHC.

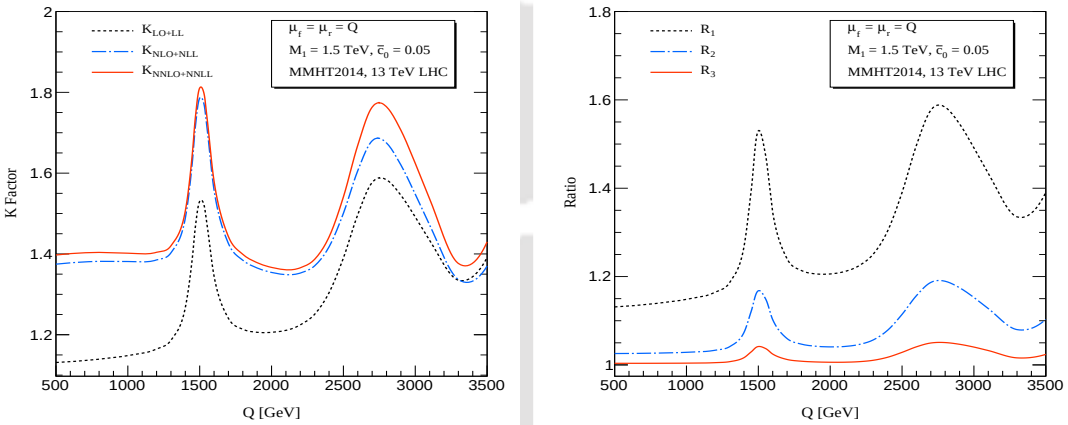

Figure 4.11: Resummed K-factors for the dilepton invariant mass distribution as defined in Eq.(4.10) and the corresponding ratios as defined in Eq.(4.11) (right).

Next, we estimate the theoretical uncertainties in resummed predictions due to the unphysical scales μ_r and μ_f as well as due to the non-perturbative PDFs. The conventional 7-point scale uncertainties for the signal are presented in Fig.(4.12) for different logarithmic accuracy. At the resonance region, these scale uncertainties are estimated to be about $\pm 17.5\%$, $\pm 8.1\%$ and $\pm 3.4\%$ at LO+LL, NLO+NLL and NNLO+NNLL respectively. Moreover, these uncertainties are bit larger than the corresponding ones for the fixed order results presented in Fig.(4.8).

To estimate these uncertainties at the NNLO level and beyond, we contrast these scale uncertainties in the resummed results against those in the fixed order results in Fig.(4.13) (left panel). For the resummed case, the scale uncertainty at NNLO+NNLL for $Q = M_1$ is about 3.4% and is larger than the one 2.3% at NNLO

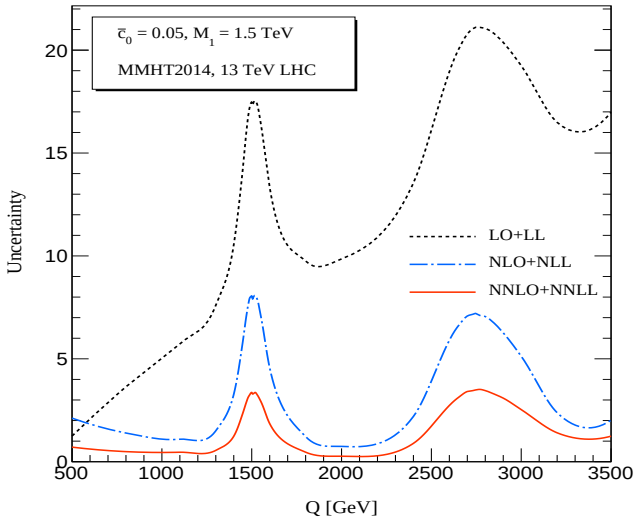

Figure 4.12: 7-point scale uncertainties in the signal are shown up to NNLO+NNLL for dilepton invariant mass distribution.

level. This increase in scale uncertainty can be understood from the fact that in the resummation formalism only threshold logarithms that are significant in the limit $z \to 1$ have been resummed to all orders in QCD but not the logarithms of unphysical scales. Moreover, it is observed that for Higgs-like processes the resummation does not improve the scale uncertainties over the fixed order ones [80] for any choice of central scales. In the present context, the graviton production at the resonance receives significant contribution from this Higgs-like gluon fusion process and hence the associated large scale uncertainty. However, the scale uncertainties only due to the renormalization scale μ_r are found to get reduced from fixed order NNLO level $\pm 1.2\%$ at $Q = 1500$ to the resummed NNLO+NNLL level $\pm 0.5\%$ (see right panel of Fig.(4.13). On the contrary, the factorization scale uncertainty for $Q = 1500$ GeV is found to increase $\pm 0.88\%$ at NNLO to ± 2.58 at NNLO+NNLL level. The overall seven-point scale uncertainties are thus dominated by the factorization scale at this order.

Further, we estimate in our predictions the uncertainty due to the non-perturbative PDF inputs. These uncertainties are obtained for each PDF group by systematically calculating the cross section for each of the available sets. These PDF uncertainties are presented for different resonance mass M_1 values in Tab.(4.6).

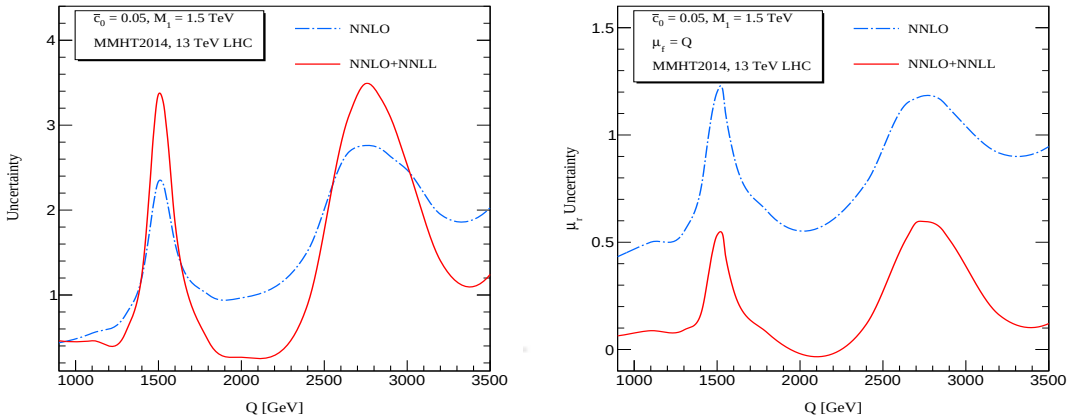

Figure 4.13: Comparison of 7-point scale uncertainties at the signal for NNLO and NNLO+NNLL (left). The uncertainty only due to μ_r scale variation around the central scale Q at NNLO and NNLO+NNLL (right) for fixed $\mu_f = Q$.

This uncertainty for the kinematic range considered and the PDF groups studied, is smallest at $M_1 = 1500$ GeV for `NNPDF31` and largest for `CT14` at $M_1 = 3500$ GeV.

M_1 (GeV)	`ABMP16`	`CT14`	`MMHT2014`	`NNPDF31`	`PDF4LHC15`
1500	$2.77 \times 10^{-3}(\pm 4.7\%)$	$3.26 \times 10^{-3}(\pm 9.4\%)$	$3.30 \times 10^{-3}(\pm 3.8\%)$	$3.04 \times 10^{-3}(\pm 2.1\%)$	$3.25 \times 10^{-3}(\pm 4.9\%)$
2000	$3.50 \times 10^{-4}(\pm 5.7\%)$	$4.25 \times 10^{-4}(\pm 11.9\%)$	$4.39 \times 10^{-4}(\pm 4.7\%)$	$3.90 \times 10^{-4}(\pm 2.6\%)$	$4.26 \times 10^{-4}(\pm 6.4\%)$
2500	$6.12 \times 10^{-5}(\pm 6.1\%)$	$7.62 \times 10^{-5}(\pm 14.3\%)$	$8.06 \times 10^{-5}(\pm 5.6\%)$	$6.87 \times 10^{-5}(\pm 3.3\%)$	$7.72 \times 10^{-5}(\pm 7.8\%)$
3000	$1.30 \times 10^{-5}(\pm 6.4\%)$	$1.65 \times 10^{-5}(\pm 16.9\%)$	$1.79 \times 10^{-5}(\pm 6.5\%)$	$1.45 \times 10^{-5}(\pm 5.6\%)$	$1.69 \times 10^{-5}(\pm 9.4\%)$
3500	$3.08 \times 10^{-6}(\pm 6.7\%)$	$4.02 \times 10^{-6}(\pm 19.8\%)$	$4.49 \times 10^{-6}(\pm 7.5\%)$	$3.41 \times 10^{-6}(\pm 11.2\%)$	$4.20 \times 10^{-6}(\pm 11.1\%)$

Table 4.6: Intrinsic PDF uncertainties in the signal at NNLO+NNLL QCD for different PDF choices are given right at the resonance for different M_1 values. All the results are presented for 13 TeV LHC. The cross sections are given in terms of pb for the central set ($n = 0$) for each PDF group along with the corresponding intrinsic uncertainties in terms of the percentage.

4.4 Conclusion

In the absence of any signature of new physics at the LHC, it is high time to explore possible scenarios where we could make potential discovery of new physics beyond the SM. In particular the RS model provides to be a very good candidate in the search of massive spin-2 resonances. In the literature, it is found that the NLO QCD corrections for the dilepton production process in this model are quite

substantial, implying the need for higher order corrections that augment the search for RS gravitons at collider experiments. In this work, we have studied the NNLO QCD corrections for the dilepton production process through graviton propagator and have presented the results for the dilepton invariant mass distribution up to Q values as high as 3.5 TeV. The underlying born contributions for this process receive both DY-like as well as Higgs-like contributions and hence the corresponding QCD corrections for the signal at the resonance region are very significant, while the QCD corrections off the resonance are mostly SM DY-like. This results in K-factors that are strongly dependent on the invariant mass of the dilepton. We have presented these mass dependent K-factors at NNLO and beyond for 13 TeV LHC. We find that while NLO correction is about 53% of LO, the NNLO correction increases the cross section by additional 21% of LO. The scale uncertainty in the NNLO result at the resonance region also got significantly reduced to as small as 2% for $Q = M_1 = 1500$ GeV.

Further, we have extended our work to include the important SV corrections at the N^3LO level. We find that the SV contribution at this order for $Q = 1500$ GeV is about 0.7% of LO in magnitude but negative in sign, thus demonstrating a very good convergence of the perturbation series. In addition we also studied the threshold resummation by resumming the threshold logarithms to NNLL accuracy and then matching to the fixed order NNLO ones. We find that these resummed results contribute an additional 7% of LO to the NNLO ones. We also note that at this precision level both the electroweak corrections as well as the finite quark mass effects need to be included. They are expected to contribute an additional few percent to the signal cross section. To conclude, we note that our results are most precise theoretical predictions available to date and that these mass dependent K-factors will be useful in the search for RS graviton resonances in the experimental data analysis using dilepton events at the LHC.

Chapter 5

Dilepton production in ADD model at N^{3}LO$_{sv}$+N^{3}LL accuracy in QCD at LHC

In this chapter, we present three loop soft-plus-virtual (SV) corrections to the spin-2 production in ADD model at the Large Hadron Collider (LHC). For this calculation, we make use of the recently computed quark and gluon three loop form factors for the spin-2 production, the universal soft-collinear coefficients as well as the mass factorization kernels. The SV coefficients are presented up to next-to-next-to-next-to leading order (N^{3}LO$_{\rm sv}$). We also use these coefficients at three loops to compute the resummed prediction for inclusive cross-section to next-to-next-to-next-to leading logarithmic accuracy (N^{3}LL) matched to N^{3}LO$_{\rm sv}$. We use the standard technique to derive the Mellin N-dependent coefficients and also the N-independent coefficients to achieve the resummation using the minimal prescription matching procedure. Considering the spin-2 propagator in the large extra dimensional (ADD) model, we also study the numerical impact of these three-loop SV corrections as well as the resummed predictions on the dilepton invariant mass distribution at the 13 TeV LHC. We study details phenomenology of this predictions that will be useful in the experimental searches for large extra dimensions.

5.1 Introduction

The scale hierarchy problem in particle physics is long standing problem and can not be address in SM. As mentioned before, extra dimension scenarios like the ADD and RS models were proposed in this context. In the Ch.(4), we have discussed a details phenomenology of DY production in RS model. Here, we will study DY production in ADD model. Out of several extra dimensional models, ADD model provides a very simple solution to the hierarchy problem and has been looked for extensively at the LHC. In the ADD model all the SM particles are confined to the four dimensional brane whereas only gravity can propagate through the $4+n$ dimensional bulk. These extra dimensions are compactified with periodic boundary conditions which leads to a tower of Kaluza-Klein (KK) modes. These KK modes lead to non-resonant excess in high invariant mass of dilepton pairs which results from the decay of virtual gravitons. The search for non-resonant enhancement from models like ADD has been searched at the LHC from time to time. This kind of signal can only be probed from the deviation of SM background. Therefore, to probe this signal both theoretical and experimental precise results are required. Precise theoretical calculation for this model are already available to NNLO QCD [173]. It is observed in the NLO QCD computation [151] that the K-factors in the dilepton production case are potentially large and range up to 60%. This is because the graviton couples to quarks like the gauge bosons do in the SM, but also to gluons and hence mimic large K-factors of the Higgs boson production case at the LHC. This leads to the computation of the NNLO QCD corrections to the dilepton production process in extra dimension models [173]. The NNLO QCD corrections are found to contribute to the total cross sections by another 10% of the LO predictions. The NNLO K-factors are thus quite different from those of the SM.

To minimize the theory uncertainties it is imperative to go beyond the NNLO in QCD. First step towards higher orders beyond NNLO is to get the SV predictions by calculating the most singular terms at the higher order. SV calculation has been successfully performed in many SM processes as mentioned in Ch.(3), Ch.(4) and has been shown that it constitutes a significant contribution to

the cross-section. Another way to improve the accuracy of the inclusive cross-section over NNLO is to resum threshold enhanced logarithms to all order [66, 181, 182]. These logarithms play an important contribution when partonic threshold variable z takes the limit 1. The resummation is well understood in the Mellin-N space thanks to complete factorization of the soft function.

We also note that the resummation is very important for the differential observable. The threshold enhanced resummation has been performed consistently in double Mellin space for rapidity and for x_F distributions [66, 117–119] (see also [120, 176] for SCET based factorization and resummation). Resummation is essential for observable which are very sensitive to infrared physics for example transverse momentum distribution where logarithms of the type $\ln(Q^2/p_T^2)$ can be very large in the infrared region thus spoiling the fixed order (FO) prediction. Resummation is thus very important to correctly describe the low p_T region and results are available up to N^{3}LL accuracy for many important SM processes. The Higgs p_T spectrum is known to NNLO+N^{3}LL accuracy [183–186] and the uncertainty is found to be reduced by 60% compared to NLO+NNLL in the low p_T region. For the pseudo-scalar production, the p_T spectrum is known to NNLO$_A$+NNLL [187] and the scale variation is found to be improved to 20% in the low-p_T region. Drell-Yan p_T spectrum is also known to same accuracy [184, 185, 188, 189].

In this chapter we improve the inclusive cross-section for spin-2 production in dilepton channel within ADD model beyond NNLO accuracy. First, we calculate the complete SV results at N^{3}LO using the form-factor at three loops and the universal soft function at the same accuracy. Second, we apply the standard threshold resummation technique and extract the process-dependent constant pieces g_{0i} required up to N^{3}LL level.

5.2 Theoretical Formalism

The hadronic cross-section for standard DY production at the hadron collider is given by,

$$\frac{d\sigma^{P_1P_2}}{dQ}(\tau, Q^2) = \frac{Q}{S}\sum_{ab=q,\bar{q},g}\int_0^1 dx_1 \int_0^1 dx_2\; f_a^{P_1}(x_1,\mu_f^2)\; f_b^{P_2}(x_2,\mu_f^2)$$
$$\times \sum_{I\in\{\gamma,Z,G\}}\int_0^1 dz\; \Delta^I(z,Q^2,\mu_f^2)\delta(\tau - z x_1 x_2)\,. \tag{5.1}$$

Here Q is the invariant mass of the dilepton, S and $\hat{s}$ denote the center-of-mass energy in the hadronic and partonic frame respectively. The hadronic and partonic threshold variables τ and z are defined as

$$\tau = \frac{Q^2}{S}, \qquad z = \frac{Q^2}{\hat{s}}\,. \tag{5.2}$$

Similar to the RS case, here also partonic cross-section gets contributions from the SM as well as from spin-2 propagator decaying to leptons. The interference between spin-2 propagator and SM propagators (γ^* and Z) are equal to zero. Here also, the SM is treated as background for the signal defined by total SM contributions plus spin-2 contributions. In the ADD case, both quark annihilation as well as gluon fusion channels are present already at the born level.

The partonic cross-section in the above Eq.(5.1) can have two separate kind of contributions, one which is more singular when $z \to 1$ known as the soft-virtual contribution ($\Delta_{ab}^{(\mathrm{sv}),I}$) and the other is regular contribution ($\Delta_{ab}^{(\mathrm{reg}),I}$) which is finite in the limit $z \to 1$. Thus the decomposition of the partonic cross-section has the following form,

$$\Delta^I(z,Q^2,\mu_f^2) = \mathcal{F}_I^{(0)}\Big(\delta_{ab}\Delta_{ab}^{(\mathrm{sv}),I} + \Delta_{ab}^{(\mathrm{reg}),I}\Big), \tag{5.3}$$

where $\mathcal{F}_I^{(0)}$ is the prefactor which depends on the specific model in consideration.

In case of ADD model, the pre-factor has the following form,

$$\mathcal{F}^{(0)}_{\rm ADD} = \frac{\kappa^4 Q^6}{320\pi^2}|\mathcal{D}(Q^2)|^2\,, \tag{5.4}$$

where $\mathcal{D}(Q^2)$ is defined in Eq.(1.36). The prefactor for SM DY, $\mathcal{F}^{(0)}_{DY}$ is defined in Eq.(3.3). The SV cross-section for spin-2 production is known to two loops in [171] after the subsequent calculation of the two loop form factors [172]. Recently the complete NNLO correction has been performed after calculating the regular piece at second order in strong coupling [173] with reverse unitarity method [134]. We improve this accuracy by first calculating the SV cross-section at the three loops using the method described in Sec.(2.1.1) and the results are presented in the App.(B.1)

The three loop SV results can be improved further by the inclusion of threshold enhanced logarithms to all orders. These threshold logarithms arise from soft and collinear emissions from virtual and real diagrams. Here, we compute the resum results up to N^{3}LL accuracy and match these results with N^{3}LO$_{\rm sv}$ results. We follow the `Standard` $\overline{N}$ prescription for resummation as discussed in Sec.(2.2.2). All the required process dependent and independent coefficients for $\overline{N}$ exponentiation to N^{3}LL accuracy are collected in App.(B.2) and Eq.(A.4) respectively.

5.3 Numerical Results

In this section we present our numerical results for three loop soft-virtual QCD correction to the dilepton production in the ADD model at LHC. The LO, NLO and NNLO parton level cross sections are convoluted with the respective order by order parton distribution function (PDF) taken from `lhapdf` [123]. However, for N^{3}LO$_{\rm sv}$ corrections we convoluted the partonic coefficient functions with the NNLO PDFs due to the unavailability of N^{3}LO PDFs. The corresponding strong coupling constant $a_s(\mu_r^2) = \alpha_s(\mu_r^2)/(4\pi)$ is also provided by the `lhapdf`. The fine structure constant is taken to be $\alpha_{\rm em} = 1/128$ and the weak mixing angle is $\sin^2\theta_w = 0.227$. Here the results are presented for $n_f = 5$ flavors in the massless limit of quarks. The

default choice for the center of mass energy of LHC is 13 TeV and the choice for the PDF set is MMHT2014 [124]. Except for the scale variations, we have used the factorization (μ_f) and renormalization (μ_r) scales to be the invariant mass of the dilepton, i.e. $\mu_f = \mu_r = Q$. We also note that there have been several experimental searches at the LHC for extra dimensions in the past, yielding stringent bounds on the ADD model parameters, the cut-off scale M_s and the number of extra dimensions d. Such analyses have already used the K-factors that have been computed in the extra dimension models. The lower limits on the scale M_S obtained from both ATLAS and CMS collaborations using 7 TeV data [25, 26] are $M_S = 2.4$ TeV corresponding to $d = 3$ in HLZ formalism [2]. After the availability of 8 TeV data this lower bound further pushed to $M_S = 3.3$ TeV for $d = 3$ [27, 28]. Now 13 TeV data are also available and the bound in M_S is given by ATLAS is 5.5 TeV for $d = 3$ using di-photon channel [1]. CMS collaboration also studied the same and the lower bounds are found to be 5.6 TeV for dilepton channel [3] and 5.7 TeV for di-photon channel [190]. Here in our work, for our phenomenological study to assess the impact of QCD corrections, we choose $M_S = 4$ TeV and $d = 3$. The computational details of the QCD corrections presented here are model independent, a numerical estimate of the theory predictions for any other choice of the model parameters is straight-forward. For completeness, we also study the dependence of the invariant mass distributions on the model parameters considering the recent bounds on M_S for different extra dimensions d.

5.3.1 Fixed Order Results

Q (GeV)	$(+)\mathcal{D}_5$ (pb/GeV)	$(+)\frac{\mathcal{D}_0}{\mathcal{D}_5}$	$(-)\frac{\mathcal{D}_1}{\mathcal{D}_5}$	$(-)\frac{\mathcal{D}_2}{\mathcal{D}_5}$	$(-)\frac{\mathcal{D}_3}{\mathcal{D}_5}$	$(+)\frac{\mathcal{D}_4}{\mathcal{D}_5}$	$(-)\frac{\sum \mathcal{D}_i}{\mathcal{D}_5}$	$(+)\delta/\mathcal{D}_5$	tot $/\mathcal{D}_5$
100	0.3560×10^{-8}	0.0552	0.1635	0.5890	0.6312	0.2143	0.1144	0.1036	−0.0108
1000	0.2002×10^{-5}	0.0398	0.1447	0.5584	0.6159	0.2157	0.0632	0.0466	−0.0166
2000	0.5106×10^{-5}	0.0333	0.1378	0.5445	0.6054	0.2207	0.0334	0.0340	+0.0006
3000	0.6431×10^{-5}	0.0284	0.1328	0.5332	0.5951	0.2273	0.0053	0.0269	+0.0216

Table 5.1: Contribution of large logarithms, the constant term $\delta(1-z)$ and the total SV correction (tot) to the dilepton invariant mass distribution at 3-loop level in the ADD model for 13 TeV LHC.

First, we will present in Tab.(5.1) the relative contributions from different logarithmic terms $\mathcal{D}_i$ as well as the $\delta(1-z)$ term with respect to $\mathcal{D}_5$ (the highest distribution appearing at the three loops) to the invariant mass distribution of the dilepton at a_s^3 level. The $\delta(1-z)$ terms are process dependent and need explicit computation while the $\mathcal{D}_i$ can be predicted from the universal nature of the infrared structures in QCD as well as the lower order process dependent contributions. We note that the sub-leading logarithms $\mathcal{D}_3$ and $\mathcal{D}_2$ are negative and are comparable in magnitude to the leading logarithmic $\mathcal{D}_5$ contribution. As a result, the contribution from the sum of logarithmic terms is negative but comparable in magnitude to that of $\delta(1-z)$ term. Consequently, the sign of total soft-plus-virtual (SV) correction at three-loop level i.e. $a_s^3\Delta_{ab}^{(3),\mathrm{G}}$ crucially depends on the relative weightage of these two kind of terms $\mathcal{D}_i(z)$ and $\delta(1-z)$. It can be seen that SV contribution is negative at lower $Q(\sim 100$ GeV) but becomes positive for $Q(> 2000$ GeV).

Next, in Fig.(5.1) we present the dilepton invariant mass distribution for the pure ADD model (GR) case and the signal (SM+GR), along with the corresponding K-factors to $\mathrm{N^3LO_{sv}}$ in QCD. The NLO corrections in the high Q-region around $Q = 2500$ GeV contribute by about 40% of LO, while NNLO corrections add an additional 25% of LO to the total invariant mass distribution. The NNLO corrections are too large to truncate the perturbation theory at this order and necessitates the computation of higher order corrections for the convergence of the perturbation series. The three-loop SV corrections that we have computed here are found to contribute an additional $(1-2)\%$ of LO to the invariant mass distribution, demonstrating a very good convergence of the perturbation theory. We also note that the three-loop SV corrections are negative in the lower Q-region while in the high Q-region they are positive because of threshold enhancement. In Fig.(5.2) we present invariant mass distributions (left panel) and the corresponding K-factors (right panel) for the SM background, GR and the signal up to $\mathrm{N^3LO_{sv}}$ in QCD. At lower Q values (less than 800 GeV), most of the signal contribution is coming from SM and as we go to high Q value the GR contribution starts to dominate as the number of accessible KK modes will increase with Q. Therefore the signal K-factor at high Q value is completely dominated by ADD model which receives contribu-

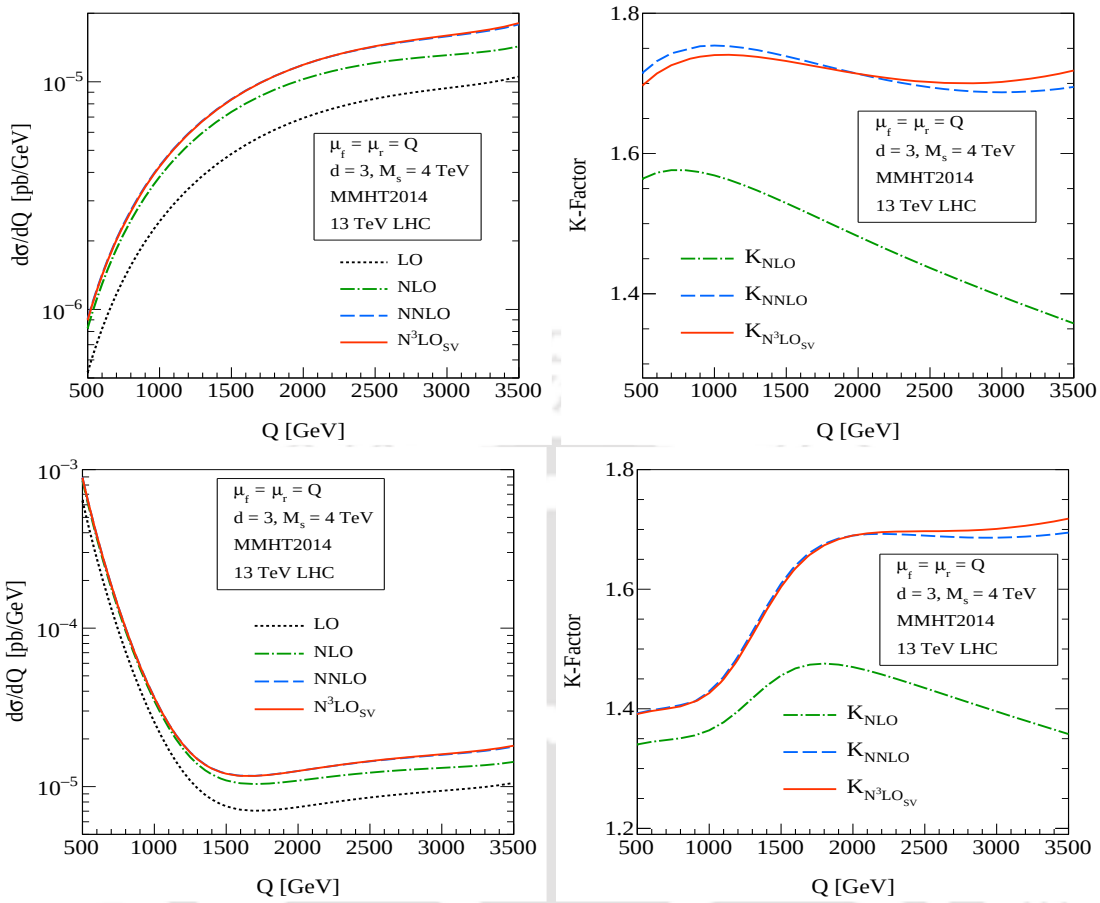

Figure 5.1: Invariant mass distribution of dilepton pair at LHC center of mass energy 13 TeV for ADD model (gravity only) and signal (SM + gravity) (left panel from top to bottom) and their corresponding K factors on the right panel. (from top to bottom)

tions from both quark-anti-quark annihilation as well as gluon fusion channel even at LO in contrast to the SM case where there is only quark-anti-quark annihilation at LO. This results in larger K-factors for the signal compared to those of the SM background,

$$\mathrm{K_{NLO}} = \frac{d\sigma^{\mathrm{NLO}}/dQ}{d\sigma^{\mathrm{LO}}/dQ}\,, \quad \mathrm{K_{NNLO}} = \frac{d\sigma^{\mathrm{NNLO}}/dQ}{d\sigma^{\mathrm{LO}}/dQ}\,, \quad \mathrm{K_{N^3LO_{sv}}} = \frac{d\sigma^{\mathrm{N^3LO_{sv}}}/dQ}{d\sigma^{\mathrm{LO}}/dQ}. \tag{5.5}$$

In Eq.(5.5) we define K-factors for the signal at different orders in QCD. In Tab.(5.2) we present these K-factors as a function of the invariant mass of the dilepton. As the three-loop SV corrections change sign for higher Q values as mentioned above, the signal K-factors at N^{3}LO level ($\mathrm{K_{N^3LO_{sv}}}$) are smaller (larger) than $\mathrm{K_{NNLO}}$ for about $Q < 2000$ ($Q > 2000$) GeV.

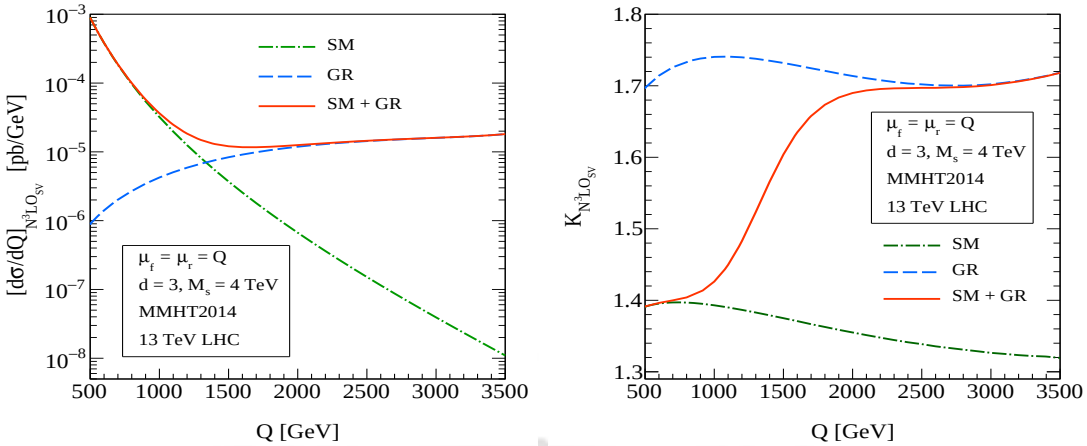

Figure 5.2: The invariant mass distribution (left panel) of dilepton pair at center of mass energy 13 TeV LHC for SM, ADD (GR), signal (SM+GR) and the corresponding K factors (right panel) at N^3LO_{sv} level.

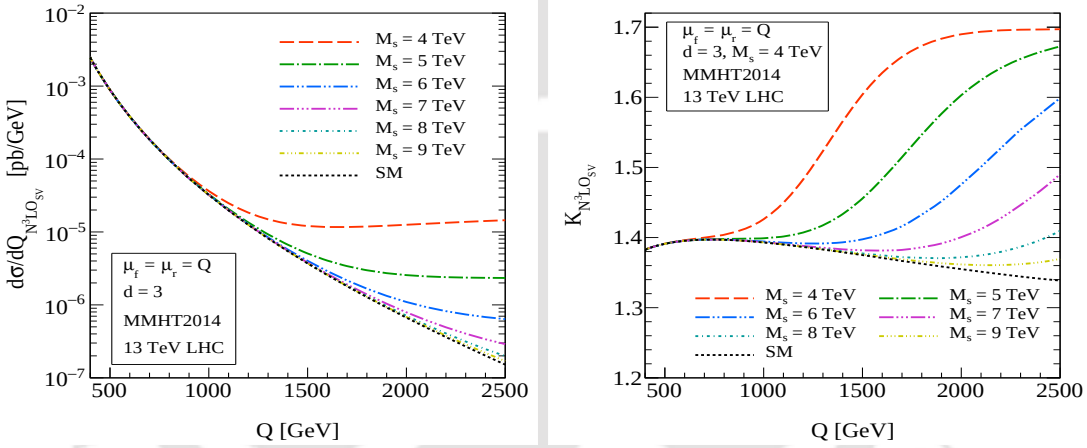

Figure 5.3: Invariant mass distribution of dilepton pair at LHC center of mass energy 13 TeV for signal with $d = 3$ and different M_S values. Corresponding K-factors are shown on the right panel at N^3LO_{sv} level.

We also study the dependence of our results on the ADD model parameters namely the scale M_S and the number of extra dimensions d. In Fig.(5.3) we present the invariant mass distribution (left) and the corresponding K-factors (right) for different values of M_S keeping $d = 3$ fixed. From the figure, we can see that the invariant mass distribution decreases with increase in M_S for any given value of Q and d simply because of the scale M_S suppression in the gravity propagator.

Similarly, we present in Fig.(5.4) the invariant mass distribution (left) and the relevant K-factors (right) for different values of d keeping $M_S = 4$ TeV fixed. From the Fig.(5.4) we can see that the cross section decreases with the number of

Q(GeV)	K_{NLO}	K_{NNLO}	$K_{N^3LO_{sv}}$
200	1.298	1.340	1.341
400	1.333	1.384	1.383
600	1.345	1.398	1.396
800	1.351	1.406	1.404
1000	1.364	1.429	1.426
1200	1.396	1.488	1.483
1400	1.439	1.571	1.566
1600	1.468	1.640	1.635
1800	1.476	1.676	1.674
2000	1.470	1.690	1.690
2200	1.458	1.693	1.696
2400	1.443	1.691	1.697
2600	1.427	1.688	1.697
2800	1.411	1.687	1.698
3000	1.396	1.686	1.701

Table 5.2: The fixed order K-factors for the signal (SM+GR) of dilepton invariant mass distribution at the LHC up to N^3LO_{sv} for select invariant mass values.

extra dimensions d because of the fact that the mass of the graviton mode increases with increasing d resulting in the less number of accessible graviton modes.

We have considered different sources of theoretical uncertainties in our analysis. Firstly, we considered the uncertainties due to the presence of two unphysical scales μ_r and μ_f in the theory and secondly those coming from the non-perturbative parton distribution functions in the calculation. For the scale uncertainties we follow the conventional 7-point scale variation. With this choice, we estimate the 7-point scale uncertainties in our predictions to N^3LO_{sv} and the results are depicted in Fig.(5.5). The upper and lower band of a particular order respectively corresponds to the maximum and minimum values of the invariant mass distributions normalized by LO computed with the default choice of scales. These normalized distributions are obtained by taking the order by order PDFs for both the numerator and the denominator. The scale uncertainties are found to get reduced significantly from LO to N^3LO_{sv}. For example at $Q = 2500$ GeV, the scale uncertainties at LO are 28%, at NLO they are 18%, at NNLO 7% and at N^3LO_{sv} they are 5%. For $Q = 3000$ GeV, the scale uncertainties reduce from 30% at LO to about 4% at N^3LO_{sv}. It is expected that the scale uncertainties get significantly reduced with the inclusion of missing process dependent regular terms at a_s^3 level,

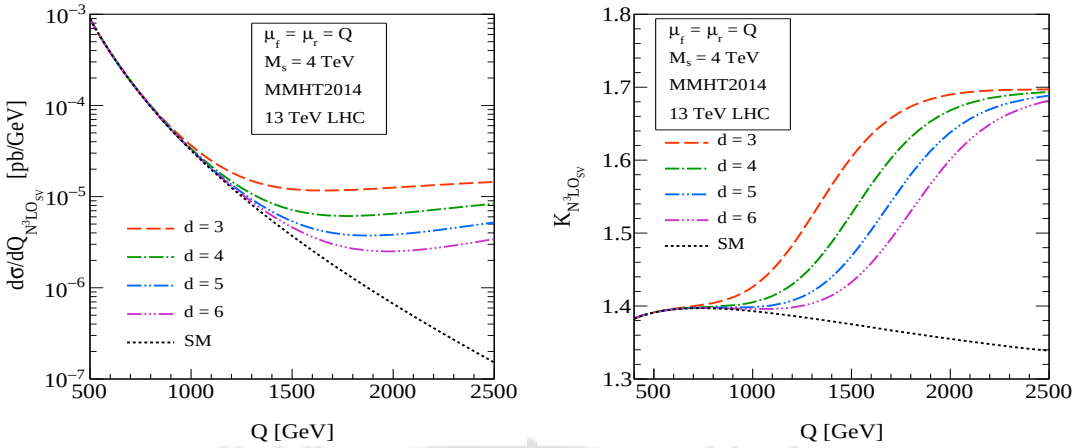

Figure 5.4: Variation of number of extra dimensions d keeping $M_S = 4$ TeV. Invariant mass distribution is shown at the left panel and their corresponding K-factors are on the right panel at N^3LO_{sv} level.

as well as the convolution with the N^3LO level PDFs that are yet to be available.

We also estimate the uncertainties coming from the non-perturbative PDFs. For this we calculate the uncertainty in two different ways, (i) the uncertainty due to the intrinsic error in the PDFs that result from various experimental errors from the global fits, (ii) the uncertainty due to the choice of PDFs provided by different groups. In both the cases we use the PDF sets `MMHT2014`, `CT14` [129], `NNPDF31` [130], `ABMP16` [178] and `PDF4LHC15` [131] provided from the `lhapdf`. For the case-(i) we calculate the intrinsic PDF uncertainties using 51 sets for `MMHT2014`, 57 sets for `CT14`, 101 sets for `NNPDF31`, 30 sets for `ABMP16` and 31 sets for `PDF4LHC15`. To this end we use all PDF sets extracted at NNLO level. In Tab.(5.3) we present these uncertainties for the dilepton invariant mass distribution to NNLO. In Fig.(5.6) we

	% of Uncertainty at $Q = 100$ GeV		% of Uncertainty at $Q = 1000$ GeV		% of Uncertainty at $Q = 2500$ GeV	
PDF Name	NNLO	NNLO+NNLL	NNLO	NNLO+NNLL	NNLO	NNLO+NNLL
MMHT2014	3	3	5	5	12	14
CT14	7	8	10	10	32	31
ABMP16	2	2	3	3	12	12
NNPDF31	2	2	5	5	7	7
PDF4LHC15	4	4	5	5	16	16

Table 5.3: Intrinsic PDF uncertainties (rounded to the nearest integers) for different PDF choices. These uncertainties are given for both fixed order as well as the resummed cross sections for a given value of $Q = 100, 1000, 2500$ GeV.

present intrinsic uncertainty (left panel) plot for different PDFs as a function of Q.

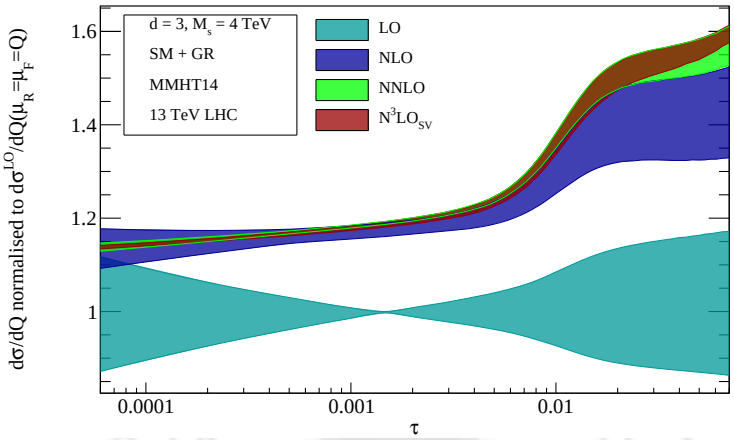

Figure 5.5: Seven point scale variation is shown up to N^{3}LO$_{\rm sv}$ for invariant mass distribution of dilepton pair at 13 TeV LHC. The ADD parameters are chosen as $M_S = 4$ and $d = 3$. All the plots are normalized with LO contribution taken at $\mu_r = \mu_f = Q$ and order-by-order PDF (see text).

At high Q region ($\sim$ 1500 GeV) these uncertainties are high due to the availability of less number of experimental data to constrain the PDF set. In the right panel of Fig.(5.6) we present the relative contribution of different PDFs with respect to our default PDF choice. At lower invariant mass distribution, they are almost equal while in the high invariant mass region, they differ from each other in a significant amount.

At N^{3}LO level we still miss the sub-leading regular pieces in the partonic coefficient. These sub-leading pieces are found to be important in the case of Higgs [179, 180] and $t\bar{t}$ productions [100] in the SM. In the higher invariant mass region, however, the threshold logarithms are expected to dominate over the sub-leading pieces. Since the ADD effects dominate over the SM background in the higher invariant mass region, this threshold correction can capture a significant part of the third order result and can be taken as an approximate estimation of the complete third order correction in its absence.

To further investigate the effect of these missing subleading terms, one can study the ambiguity associated with the definition of SV cross-section. As a first approximation, we multiply a simple polynomial $h(z)$ with the partonic SV coefficient. The function $h(z)$ is such that it becomes unity in the limit $z \to 1$. The

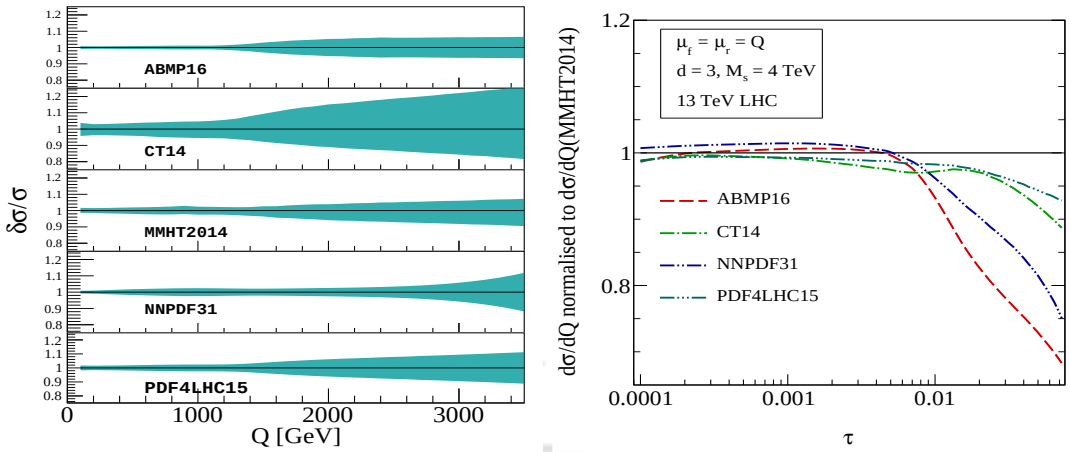

Figure 5.6: PDF uncertainties for different PDFs (left panel) at NNLO and the result for different PDFs (right panel) normalized by the result obtained with the default choice `MMHT2014nnlo` at NNLO.

Eq.(5.1) then takes the form,

$$\frac{d\sigma^{P_1P_2}}{dQ}(\tau,Q^2) = \frac{Q}{S}\sum_{ab=q,\bar{q},g}\int_0^1 dx_1\int_0^1 dx_2\; f_a^{P_1}(x_1,\mu_f^2)\; f_b^{P_2}(x_2,\mu_f^2)/h(\tau/x_1x_2)$$
$$\times\sum_{I\in\{\gamma,Z,G\}}\int_0^1 dz\;\Delta^I(z,Q^2,\mu_f^2)h(z)\;\delta(\tau-zx_1x_2)\,, \tag{5.6}$$

where one can redefine

$$\Delta^I(z,Q^2,\mu_f^2)h(z) = \mathcal{F}_I^{(0)}\left(\delta_{ab}\Delta_{ab}^{(\mathrm{sv}),I}+\tilde{\Delta}_{ab}^{(\mathrm{reg}),I}\right). \tag{5.7}$$

Notice that the SV part is unchanged since $\lim_{z\to1}h(z)\to1$, on the other hand the regular piece is now modified. We denote the SV corrections thus obtained for different choices of $h(z)$ by σ_{SVM} and also note that the choice $h(z)=1$ corresponds to the conventional SV correction. One can exploit this ambiguity of the definition of SV in order to minimize the contributions of regular piece in the absence of it. Similar approaches have been taken previously [125–127] in order to estimate the size of the subleading corrections. We have performed a detailed study with several choices of $h(z)$ and found a sizeable impact which is large in the lower invariant mass region implying the need for subleading corrections in this region. In Fig.(5.7) we present SV coefficients at the first and second orders using different choices of

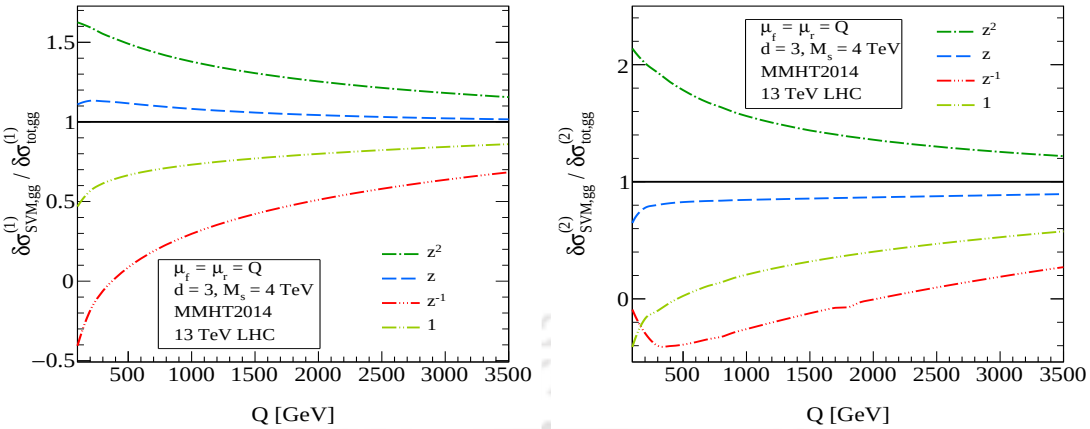

Figure 5.7: The ratio of modified SV coefficient (SVM) for the choices $h(z) = 1, z, z^2, z^{-1}$ and total correction in gg channel at $\mathcal{O}(\alpha_s)$ (left) and $\mathcal{O}(\alpha_s^2)$ (right) for gravity only.

$h(z)$ for the gg subprocess. It can be seen that as we approach the threshold region all the different choices tend to merge indicating that in the threshold region the SV counterpart really dominates. We found that the choice $h(z) = z$ mimics the closest approximation to the full result at NLO and at NNLO. Similar observations are found in case of $q\bar{q}$ subprocess as well. We also note that this choice correctly reproduces the first subleading term ($\ln^{2n-1}(1-z)$) as well as a part of further subleading terms in threshold expansion in both orders. Assuming that this will also hold true for the third order we use a modified SV coefficient with the choice of $h(z) = z$. In Fig.(5.8) we present the K-factors as defined in Eq.(5.5) by including these modified SV corrections at the third order for combined $gg + q\bar{q}$ channels only for the gravity. We found that the modified SV (SVM) result adds up to additional 2% of LO corrections on top of SV corrections for the central choice of the scales in the high invariant mass region. We also emphasize that at this accuracy the other subprocesses will also play an important role. Using the observations made at lower order, we expect that the complete N^{3}LO correction will add up at the most a few percent additional correction to the existing SV result.

5.3.2 Resum Results

In this section we present numerical results for dilepton production through spin-2 propagator at the LHC to N^{3}LO$_{\rm sv}$+N^{3}LL in QCD. In this numerical calculation

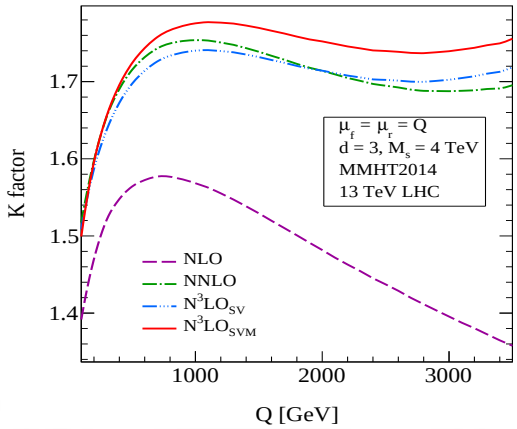

Figure 5.8: The ADD (gravity only) K-factors up to N^{3}LO for combined gg+$q\bar{q}$ channels. At the third order the K-factors are for the conventional SV and for the modified SV (SVM) with $h(z) = z$.

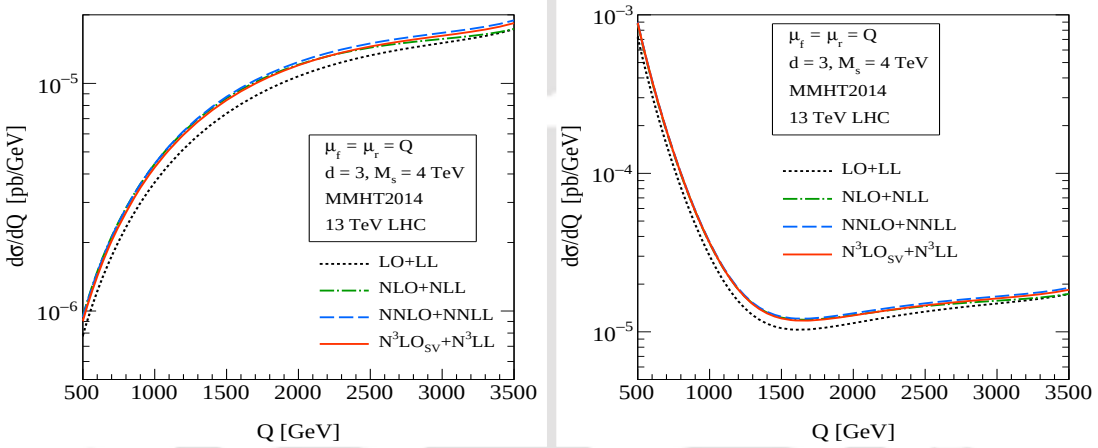

Figure 5.9: Invariant mass distribution of dilepton pair at LHC center of mass energy 13 TeV for pure ADD (left) and signal (right) for different resummed orders.

we use the same choice of SM and ADD model parameters as in the computation of three-loop SV corrections (fixed order). For the inverse Mellin transformation Eq.(2.79), we use $c = 1.9$. In Fig.(5.9) we present the numerical result for invariant mass distribution of dilepton for pure gravity, signal (SM + gravity) at different order. The behavior of these plots is similar to that of the fixed order results presented in Figs.(5.1) & (5.2). We notice significant enhancement of these resummed results over the fixed order ones, for example at $Q = 2400$ GeV, there is 26% enhancement at NLO+NLL over NLO, 8% at NNLO+NNLL over NNLO and 2% at N^{3}LO$_{\rm sv}$+N^{3}LL over N^{3}LO$_{\rm sv}$. In Fig.(5.10), we present the numerical result for invariant mass distribution of dilepton for signal and ADD model with corresponding

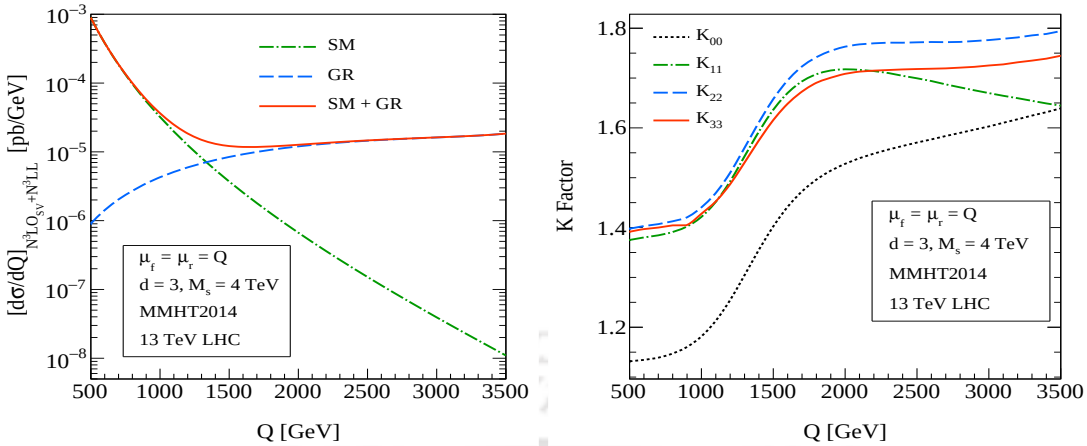

Figure 5.10: Left: Invariant mass distribution of dilepton pair for ADD (GR) and signal (SM+GR) at order N^3LO_{sv}+N^3LL with corresponding background (SM). Right: K-factor of dilepton channel for signal up to order N^3LO_{sv}+N^3LL with $M_s = 4$, $d = 3$.

SM background and the mass dependent K-factors for signal up to N^3LO_{sv}+N^3LL. For phenomenological purpose, we defined the resummed K-factors Eq.(5.8) as

Q(GeV)	K_{00}	K_{11}	K_{22}	K_{33}
200	1.130	1.333	1.346	1.341
400	1.130	1.367	1.389	1.383
600	1.135	1.380	1.403	1.397
800	1.147	1.391	1.413	1.404
1000	1.182	1.421	1.441	1.428
1200	1.255	1.493	1.510	1.487
1400	1.356	1.593	1.611	1.575
1600	1.442	1.670	1.696	1.649
1800	1.496	1.708	1.742	1.691
2000	1.528	1.718	1.763	1.709
2200	1.548	1.714	1.770	1.715
2400	1.564	1.705	1.771	1.717
2600	1.577	1.694	1.772	1.719
2800	1.590	1.681	1.773	1.721
3000	1.603	1.670	1.776	1.725

Table 5.4: Resummed K-factors, defined in Eq.(5.8), for dilepton invariant mass distribution at the LHC to various logarithmic accuracy.

$$\mathrm{K}_{00} = \frac{d\sigma^{\mathrm{LO+LL}}/dQ}{d\sigma^{\mathrm{LO}}/dQ} \qquad \mathrm{K}_{11} = \frac{d\sigma^{\mathrm{NLO+NLL}}/dQ}{d\sigma^{\mathrm{LO}}/dQ}$$
$$\mathrm{K}_{22} = \frac{d\sigma^{\mathrm{N^2LO+N^2LL}}/dQ}{d\sigma^{\mathrm{LO}}/dQ} \qquad \mathrm{K}_{33} = \frac{d\sigma^{\mathrm{N^3LO_{sv}+N^3LL}}/dQ}{d\sigma^{\mathrm{LO}}/dQ}\,. \tag{5.8}$$

As can be seen from the Fig.(5.10), the K-factor K_{22} could be as large as 1.8 for

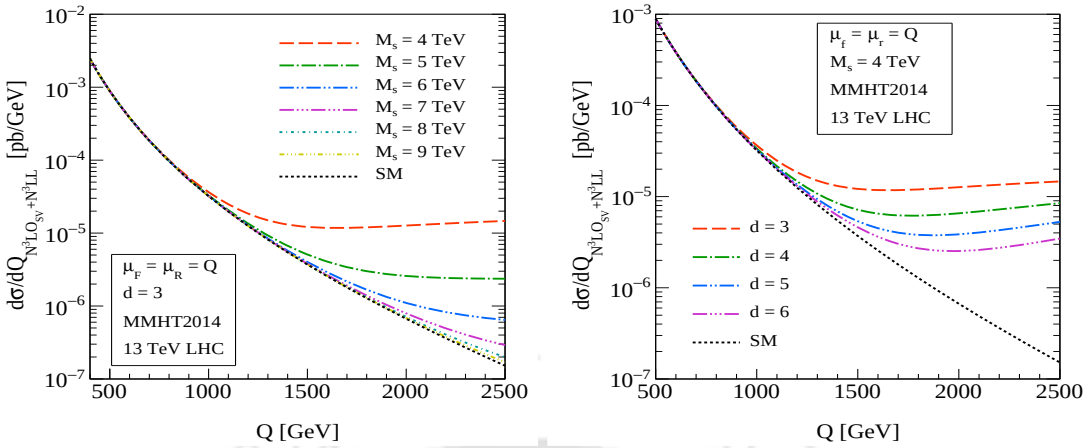

Figure 5.11: Effect of model parameters for invariant mass distribution of dilepton at hadronic center of mass energy 13 TeV for signal at N^3LO_{sv}+N^3LL level. Left panel for M_S variation for $d = 3$ and right panel for d variation for $M_S = 4$.

$Q > 2000$ GeV, while the resummation of the logarithms beyond NNLL decrease the cross sections by about 5% resulting in K_{33} to be around 1.75. These precise QCD predictions are expected to augment experimental searches for large extra dimensions at the LHC. To this end, in Tab.(5.4), we give numerical values for the mass dependent resummed K-factors up to N^3LO_{sv}+N^3LL accuracy. For completeness, we also study the dependence on the ADD model parameters M_S and d, and the corresponding results are depicted in Fig. (5.11).

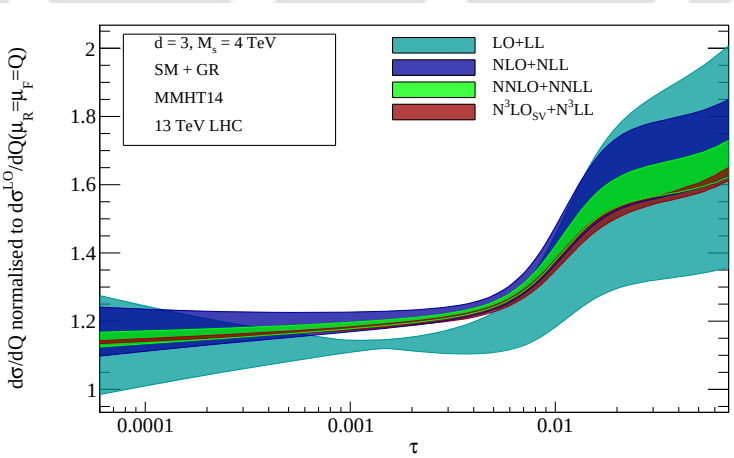

Figure 5.12: Seven point scale variation of invariant mass distribution of dilepton pair at the LHC for the signal with $M_S = 4$ and $d = 3$. All the plots are normalized with LO contribution calculated at $\mu_r = \mu_f = Q$ and corresponding PDF at different order.

Finally we estimate the uncertainties in our resummed results due to the unphysical scales μ_r and μ_f, and those due to the parton densities that are non-

perturbative in nature. For scale uncertainties we follow the same procedure as in fixed order case by taking the 7-point scale variation and the results are shown in Fig.(5.12) as a function of the dilepton invariant mass Q. The scale uncertainties are found to get reduced significantly from LO+LL to N^{3}LO$_{\rm sv}$+N^{3}LL. For example at $Q = 2500$ GeV, the scale uncertainties are 56% at LO+LL, 22% at NLO+NLL, 10% at NNLO+NNLL and are as small as 2% at N^{3}LO$_{\rm sv}$+N^{3}LL. We observe that the scale uncertainty bands at higher orders lie inside the ones at lower orders. The scale uncertainties are conventionally used for estimating the contribution from the missing higher order contributions. In that sense, these resummed results have better theory predictions over the fixed order ones.

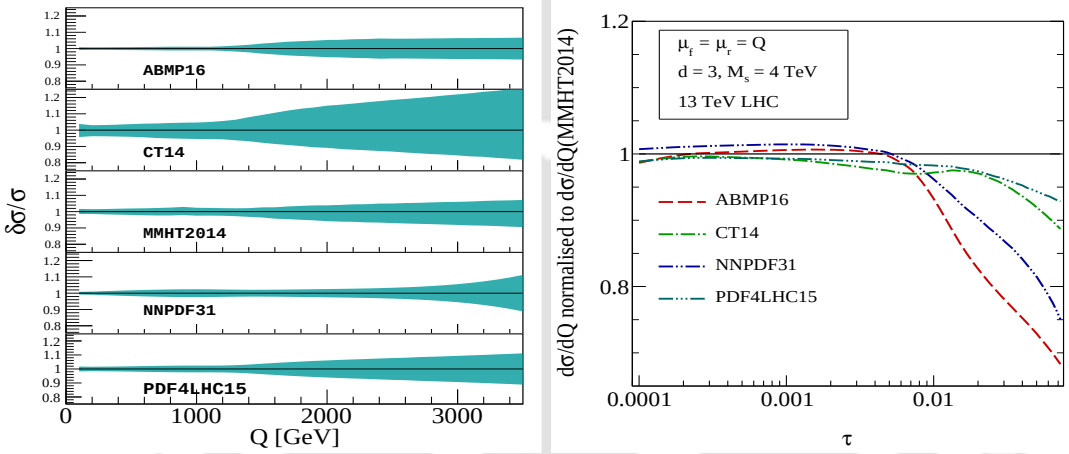

Figure 5.13: The intrinsic PDF uncertainties for different PDF groups at NNLO+NNLL order are shown in the left panel as a function of the dilepton invariant mass Q. In the right panel, the invariant mass distributions for different PDF groups at NNLO+NNLL order (computed with central set) normalized with that obtained from the default choice `MMHT2014nnlo` PDF set.

The intrinsic uncertainties in a given PDF set as well as those from the choice of the PDF group itself are estimated as in the fixed order case. We present these results in Fig.(5.13). We observe that the intrinsic PDF uncertainties are very much similar to those of the fixed order case as can be seen from the Tab.(5.3). This is simply because the results for resummation of the threshold logarithms still use the parton densities extracted at NNLO accuracy. Moreover, we also present the uncertainties due to the choice of the PDFs group in terms of the distributions normalized with respect to those obtained from `MMHT2014` group.

We point out that at this level of accuracy, the electro-weak (EW) corrections as well as finite quark mass effects will be important in the higher invariant mass region. However, it is also important to note that unlike SM case, the spin-2 production is dominated by the gluon fusion process and hence the relative contribution of these EW corrections is expected to be smaller than that in the SM. Overall these corrections can contribute an additional few percent (in magnitude) to the overall signal cross section.

5.4 Conclusion

In this chapter, we have computed the higher order QCD corrections beyond NNLO for the spin-2 production at hadron colliders. Specifically, we have calculated three-loop SV corrections to the spin-2 production, thanks to the recent computation of the quark and gluon form factors at three loop level. We have performed a detailed phenomenological study at N^3LO_{sv} in QCD and presented our numerical results for the dilepton invariant mass distribution in the ADD model for 13TeV LHC. The three-loop SV corrections are about 2% over the existing NNLO result. The conventional 7-point scale uncertainties of about 8% at NNLO in the high invariant mass region get reduced to about 5% at three-loop level. Moreover, we have estimated the possible uncertainty in the approximation used to compute the SV corrections at three-loop level and found that the leading and further partial subleading collinear terms contribute by an additional few percent to the SV results presented here. In addition we have also extracted the process-dependent coefficients coming from the form factor and the soft-collinear function to third order. Using these coefficients we perform resummation of large threshold logarithms up to N^3LL accuracy. We also study the numerical impact of these resummed result after matching it to N^3LO_{sv} fixed order result. While the quantitative enhancement of these resummed results is approximately 2% over the known fixed order NNLO results, the resummed predictions reduce the scale uncertainties significantly to as low as 2%. For completeness, we also estimated the PDF uncertainties in our predictions using the parton densities available at NNLO level from various groups. The uncertainties from these

non-perturbative inputs are estimated to be maximum of about 10% around invariant mass region $Q \sim 1000$ GeV although at higher Q values they increase further. Finally, we conclude that the perturbation theory predictions in QCD for massive spin-2 production are now very precise and are at par comparable to the accuracy that is achieved for the well known weak bosons (Z/W) and the most sought Higgs boson in the SM.

Chapter 6

QCD phenomenology of exotic spin-2 production at the LHC

In this chapter, we have studied the complete next-to-next-to leading order (NNLO) QCD correction matched with next-to-next-to leading logarithm (NNLL) for Drell-Yan production via spin-2 particle at the Large hadron collider (LHC). We consider generic spin-2 particle which couples differently to quarks and gluons (non-universal scenario). The threshold enhanced analytical coefficient has been obtained up to third order using the universal soft function and the process dependent form factors at the same order. We performed a detailed phenomenological analysis and gave a prediction for the 13 TeV LHC for the search of such BSM signature. We also provide ingredients required for the third-order soft-virtual (SV) prediction as well as the N^3LL resummation, and study the impact on LHC searches.

6.1 Introduction

In this work, we focus on one particular BSM scenario where generic massive spin-2 fields interact with the SM ones. Such a model is well motivated in the context of search for spin-2 particles (graviton) that couple to SM bosons and fermions differently. The phenomenology of such a graviton is similar to some extent to

that of the RS model [16] where the massive graviton couples with equal strength (universal) to fermions and bosons in the SM. However unlike the RS model, the parameter space of the non-universal case is much flexible and less constrained at the LHC searches so far. In the context of Higgs characterization, this model has been studied extensively in the diboson channels [191]. Later, a complete automation has been done at NLO [168] in the FeynRules [169]-MadGraph5_aMC@NLO [170] framework. A detailed phenomenology has been performed there for wide range of parameters space including parton shower effects. It has been observed that the K-factors for different channels give sizeable contribution that depend on the choice of model parameters as well as phase space region. This necessitates further higher order QCD corrections for this model. The first complete next-to-next-to leading order (NNLO) computation has been performed [174] in the dilepton channel. A detailed analysis has been presented there along with the comparison to the universal scenario. It has been observed that the K-factors at NLO and NNLO are significantly different from those of the ADD [15, 173] and RS [16] models. In the present model, the graviton production takes place at the LO via Higgs-like and DY-like processes similar to the ADD or RS model, but with different couplings to quarks (k_q) and gluons (k_g). This particular feature of this model controls the size of the contributions from different channels at higher orders for different choices of model parameters.

The observed discrepancy between the K-factors for the graviton production in the universal and the non-universal cases can be explained to some extent with the help of additional parton radiations at higher orders. For example, a DY-like process with small k_q coupling can receive large corrections when the graviton couples with large coupling k_g to gluon emitted from the quark lines at higher orders. Similar is the case for Higgs-like graviton process. The contribution of other parton level subprocesses initiated by qg starting from NLO and $qq\prime$ from NNLO onwards will have further noticeable contributions. For example at NLO, the $q\bar{q}$ subprocess gets corrections a few times larger than the LO subprocess for the choice of parameters where $k_q \ll k_g$ simply due to the fact that high k_g contribution appear at NLO from $q\bar{q}$ subprocess itself. The contribution from the qg channel could be

as large as that one for $q\bar{q}$ channel for different parameter choices. The presence of such model dependent large contributions at higher orders for an inclusive process can not be estimated with a simple scaling of the lower order cross sections with the conventional (NLO/NNLO) K-factors computed either in the SM or in the RS model. This motivates not only a detailed phenomenological study at higher orders in QCD but also questions the convergence of the perturbation theory. This is particularly important in the higher mass region where one would normally expect the BSM effect. This region receives large corrections from threshold logarithms and needs a procedure to resum them to all orders. The resummation procedure has been pioneered [70, 78, 82, 108, 181, 182, 192, 193] over the last few decades to systematically include those large contributions in the threshold region from all orders for better predictions of the perturbative theory.

At the LHC energies where the parton fluxes are large, the threshold logarithms can give sizeable contribution and through resummation these lead to better perturbative convergence as well as theoretical uncertainties. In the last three chapters, we have studied the effect of these large threshold logarithms at $\mathrm{N^3LL(NNLL)}$ accuracies. In view of this, we systematically include the threshold resummation effects in DY production for non-universal spin-2 model and present a detailed phenomenological results up to NNLL accuracy. Moreover we have also computed the necessary ingredients to perform resummation up to $\mathrm{N^3LL}$.

6.2 Theoretical Formalism

The interaction of spin-2 field ($h_{\mu\nu}$) with the SM ones is described through the following effective action,

$$S_{int} = -\frac{1}{2}\int d^4x\; h_{\mu\nu}(x)\left(\hat{k}_I\hat{\mathcal{O}}^{I,\mu\nu}(x)\right)\,, \qquad I \in \{G, Q\}\,. \tag{6.1}$$

Sum over repeated indices is implied in all equations. The interaction action has been split in a way so that $I = G$ contains purely gauge boson sector whereas $I = Q$ contains the fermionic sector and its gauge interactions terms. This decomposition

however is not unique and one can shuffle gauge invariant terms between these two. Here $\hat{k}_I$ are the unrenormalized coupling constants of the spin-2 field to the operators $\hat{\mathcal{O}}^{I,\mu\nu}$. These gauge invariant operators have the following expressions in terms of unrenormalized quarks and gluon fields[1],

$$\hat{\mathcal{O}}^{Q}_{\mu\nu} = \frac{i}{4}\overline{\hat{\psi}}\Big\{\gamma_\mu\overrightarrow{D_\nu} - \overleftarrow{D_\nu}\gamma_\mu\Big\}\hat{\psi} - \frac{i}{2}g_{\mu\nu}\hat{\psi}\gamma^\sigma\overrightarrow{D_\sigma}\hat{\psi} + \Big(\mu \leftrightarrow \nu\Big)\,, \tag{6.2}$$

$$\begin{aligned}\hat{\mathcal{O}}^{G}_{\mu\nu} = {}& \frac{1}{4}g_{\mu\nu}\hat{F}^a_{\rho\sigma}\hat{F}^{a,\rho\sigma} - \hat{F}^a_{\mu\rho}\hat{F}^{a,\rho}_{\nu} - \frac{1}{\hat{\xi}}g_{\mu\nu}\partial^\rho(\hat{A}^a_\rho\partial^\sigma\hat{A}^a_\sigma) - \frac{1}{2\hat{\xi}}g_{\mu\nu}(\partial_\rho\hat{A}^{a,\rho})(\partial_\sigma\hat{A}^{a,\sigma}) \\ & + \Big\{\frac{1}{\hat{\xi}}\hat{A}^a_\mu\partial_\nu(\partial^\rho\hat{A}^a_\rho) + \partial_\mu\overline{\hat{\omega}}(\partial_\nu\hat{\omega}^a - \hat{g}_s f^{abc}\hat{A}^c_\nu\hat{\omega}^b) \\ & - \frac{1}{2}g_{\mu\nu}\partial_\rho\overline{\hat{\omega}}^a(\partial^\rho\hat{\omega}^a - \hat{g}_s f^{abc}\hat{A}_{c,\rho}\hat{\omega}^b) + \mu \leftrightarrow \nu\Big\}\,,\end{aligned} \tag{6.3}$$

where $\overrightarrow{D_\mu} = \overrightarrow{\partial_\mu} - i\hat{g}_s T^a\hat{A}^a_\mu$. $\hat{\omega}$ and $\hat{\xi}$ are the ghost field and gauge fixing parameter respectively. Notice that the sum of these operators are protected against radiative corrections to all orders due to the fact that spin-2 fields couple to the conserved energy momentum tensor of SM fields. However individually they are not conserved and requires additional UV renormalization. These operators are closed under UV renormalization and hence renormalization can be performed [194, 195] through a mixing matrix Z.

The unrenormalized operators $\hat{\mathcal{O}}^{\mu\nu}_I(x)$ can be renormalized in a closed form [194, 195] using renormalization matrix Z_{IJ} as

$$\mathcal{O}_I = Z_{IJ}\;\hat{\mathcal{O}}_J\,. \tag{6.4}$$

We use dimensional regularization in $d = 4-2\epsilon$ dimensions to regulate both UV and IR divergences. In d-dimensions, the bare strong coupling constant can be related to the renormalized one as

$$\hat{a}_s S_d = a_s(\mu_r)Z(a_s(\mu_r))\left(\frac{\mu_r^2}{\mu^2}\right)^{\frac{4-d}{2}}\,, \tag{6.5}$$

where S_d is the spherical factor. Here $Z(a_s(\mu_r))$ is the strong coupling renormaliza-

[1]Throughout this article we use *hat* ($\hat{}$) symbol for bare quantities and without *hat* for renormalized quantities.

tion constant which takes the following form in $d = 4 - 2\epsilon$ dimensions,

$$Z(a_s(\mu_r)) = 1+a_s(\mu_r)\Big\{ -\beta_0\epsilon^{-1}\Big\} + a_s^2(\mu_r)\Big\{\beta_0^2\epsilon^{-2} - \frac{\beta_1}{2}\epsilon^{-1}\Big\} + a_s^3(\mu_r)\Big\{ -\beta_0^3\epsilon^{-3} + \frac{7}{6}\beta_0\beta_1\epsilon^{-2} - \frac{1}{3}\beta_2\epsilon^{-1}\Big\}. \tag{6.6}$$

The UV renormalization constants Z_{IJ} satisfy the following RGE

$$\frac{d}{d\ln\mu_r} Z_{IJ} = \gamma_{IK} Z_{KJ}\,, \tag{6.7}$$

where γ_{IJ} are the UV anomalous dimensions.

The interaction action can be expressed in terms of renormalized quantities as well *i.e.* in terms of renormalized couplings (κ_I) and renormalized operators ($\mathcal{O}_I$)[2] as

$$S_{int} = -\frac{1}{2}\int d^4x\; h_{\mu\nu}(x)\Big(\kappa_I \mathcal{O}_I^{\mu\nu}(x)\Big)\,. \tag{6.8}$$

The unrenormalized coupling constants are then related to the renormalized ones with the transpose of the same renormalization constants Z_{IJ} as

$$\hat{\kappa}_I = Z_{JI}\;\kappa_J\,. \tag{6.9}$$

The solution of UV renormalization constants RGE (Eq.(6.7)), the matrix Z_{IJ}, leads to the following expansion in terms of renormalized strong coupling constant up to the third order,

$$\begin{aligned} Z_{IJ} = \delta_{IJ} + a_s(\mu_r)\Big\{\Big(-\gamma_{IJ}^{(1)}\Big)\epsilon^{-1}\Big\} + a_s(\mu_r)^2\Big\{\Big(\frac{1}{2}\beta_0\gamma_{IJ}^{(1)} + \frac{1}{2}\gamma_{IK}^{(1)}\gamma_{KJ}^{(1)}\Big)\epsilon^{-2} + \Big(-\frac{1}{2}\gamma_{IJ}^{(2)}\Big)\epsilon^{-1}\Big\} \\ + a_s(\mu_r)^3\Big\{\Big(-\frac{1}{3}\beta_0^2\gamma_{IJ}^{(1)} - \frac{1}{2}\beta_0\gamma_{IK}^{(1)}\gamma_{KJ}^{(1)} - \frac{1}{6}\gamma_{IK}^{(1)}\gamma_{KL}^{(1)}\gamma_{LJ}^{(1)}\Big)\epsilon^{-3} + \Big(\frac{1}{3}\beta_1\gamma_{IJ}^{(1)}\frac{1}{3}\beta_0\gamma_{IJ}^{(2)} \\ + \frac{1}{6}\gamma_{IK}^{(1)}\gamma_{KJ}^{(2)} + \frac{1}{3}\gamma_{IK}^{(2)}\gamma_{KJ}^{(1)}\Big)\epsilon^{-2} + \Big(-\frac{1}{3}\gamma_{IJ}^{(3)}\Big)\epsilon^{-1}\Big\}\,. \end{aligned} \tag{6.10}$$

All the relevant anomalous dimensions (γ_{IJ}) are extracted to three loops [174] from the bare quark and gluon form factors and by simply exploiting the universality of

[2]Note that in a pure gauge theory ($n_f = 0$), the operator $\mathcal{O}_G^{\mu\nu}$ is conserved.

the infrared divergences at the same order. Note that one can equivalently perform coupling constant renormalization using Eq.(6.9) instead of operator renormalization in Eq.(6.4) to remove the UV divergences from the form factor.

The DY production cross-section at the LHC takes the following form in terms of partonic coefficient function Δ^I and luminosity $\mathcal{L}$:

$$2S\frac{d\sigma}{dQ^2}(\tau,Q^2) = \sum_{ab=\{q,\bar{q},g\}}\int_0^1 dx_1\int_0^1 dx_2\int_0^1 dz\ \mathcal{L}_{ab}(x_1,x_2,\mu_f^2)\times \sum_I \mathcal{F}_I^{(0)}\Delta_{ab}^I(z,Q^2,\mu_f^2)\delta(\tau-zx_1x_2)\,. \tag{6.11}$$

The luminosity function consists of non-perturbative parton distribution functions. The prefactor $\mathcal{F}_I^{(0)}$ is given for SM and for spin-2 (denoted as GR) channels as follows

$$\mathcal{F}_{SM}^{(0)} = \frac{4\alpha^2}{3Q^2}\Bigg[Q_q^2 - \frac{2Q^2(Q^2-M_Z^2)}{\Big((Q^2-M_Z^2)^2+M_Z^2\Gamma_Z^2\Big)c_w^2s_w^2}Q_q g_e^V g_q^V + \frac{Q^4}{\Big((Q^2-M_Z^2)^2+M_Z^2\Gamma_Z^2\Big)c_w^4s_w^4}\Big((g_e^V)^2+(g_e^A)^2\Big)\Big((g_q^V)^2+(g_q^A)^2\Big)\Bigg]\,. \tag{6.12}$$

$$\mathcal{F}_{GR}^{(0)} = \frac{k_q^2Q^6}{80\pi^2\Lambda^4}|D(Q^2)|^2\,, \tag{6.13}$$

Here α represents the fine structure constant, c_w, s_w are the sine and cosine of the Weinberg angle and M_Z and Γ_Z are the mass and width of the Z boson respectively. The vector and axial coupling of the weak boson is given as

$$g_a^A = -\frac{1}{2}T_a^3\,, \qquad g_a^V = \frac{1}{2}T_a^3 - s_w^2Q_a\,, \tag{6.14}$$

Λ in Eq.(6.13) is the cut-off scale of the spin-2 theory which is of $\mathcal{O}$(TeV) and k_I are introduced for convenience and are defined as $k_I = \sqrt{2}\kappa_I/\Lambda$. The propagator for GR theory with mass M_G is given as

$$D(Q^2) = \frac{1}{(Q^2-M_G^2)+i\ \Gamma_G M_G}\,. \tag{6.15}$$

The analytical results for the partonic coefficient functions are known for some time to the second order for all subprocesses [173]. The partonic coefficients can be decomposed into the following form for the gluon and quark-antiquark initiated processes:

$$\Delta^I_{ab} = \Delta^I_{ab,sv} + \Delta^I_{ab,reg}\,, \qquad ab \in \{gg, q\bar{q}\}\,. \tag{6.16}$$

The first term in the above equation is denoted as the soft-virtual (SV) term which consists of form factor contribution as well as soft gluon radiation. The perturbative expansion of the SV coefficients are given as,

$$\Delta^I_{ab,sv} = \sum_{i=0} a_s^i \mathcal{N}^I_{ab} \Delta^{(i),I}_{ab,sv} \tag{6.17}$$

$\mathcal{N}_I$ are some overall prefactors taken out from the SV coefficient. The $\mathcal{N}_I$ prefactors are given as

$$\begin{aligned} \mathcal{N}^{SM}_{ab} &= \frac{2\pi}{N_c}\,, \\ \mathcal{N}^{GR}_{q\bar{q}} &= \frac{\pi k_q^2}{8N_c}\,, \\ \mathcal{N}^{GR}_{gg} &= \frac{\pi k_g^2}{2(N_c^2-1)}\,. \end{aligned} \tag{6.18}$$

Note that with this normalization in Eq.(6.18), the SV coefficient at LO simply becomes $\delta(1-z)$. The main ingredients to compute the SV coefficients (after the PDF renormalization) are the form factor and universal soft distribution functions. As mentioned earlier, the form factors are available in the literature up to three loops [196].

6.3 Numerical Results

We now turn to the discussion on numerical result up to NNLO+NNLL accuracy in QCD for dilepton production via spin-2 particle at the LHC. The coupling strength of spin-2 particles to bosons is $\kappa_G = \sqrt{2}k_g/\Lambda$ and to fermions is $\kappa_Q = \sqrt{2}k_q/\Lambda$.

Here, Λ, the scale of the theory, is taken to be 3 TeV and we choose $0 < (k_q,\ k_g) < 1$. For this analysis we use `PDF4LHC15` [131] parton distribution functions (PDF) throughout from `LHAPDF` [123] subroutine unless otherwise stated. For the fixed order as well as resummed computation, we convolute NLO(NNLO) level partonic coefficient functions with NLO(NNLO) PDF. The corresponding strong coupling constant $\alpha_s(\mu_r^2)$ is also provided by `LHAPDF` subroutine and for convenience we have defined $a_s(\mu_r^2) = \alpha_s(\mu_r^2)/(4\pi)$. The fine structure constant is taken to be $\alpha_{em} = 1/128$ and the weak mixing angle is $\sin^2\theta_w = 0.22343$. Here we present the results for $n_f = 5$ flavors in the massless limit of quarks. Our default choice for the center of mass energy of the LHC is $\mathrm{E_{CM}} = 13$ TeV. Except for the study of scale variations, we set renormalization (μ_r) and factorization (μ_f) scales equal to the dilepton invariant mass, *i.e.* $\mu_r = \mu_f = Q$.

Before we present the resum result, we discuss some distinctive features of this model that are not observed for the case of universal couplings. For this, in Fig.(6.1) left panel we present the dilepton invariant mass distribution at the resonance $Q = M_G$ for different choices of the model parameters k_q and k_g. For the

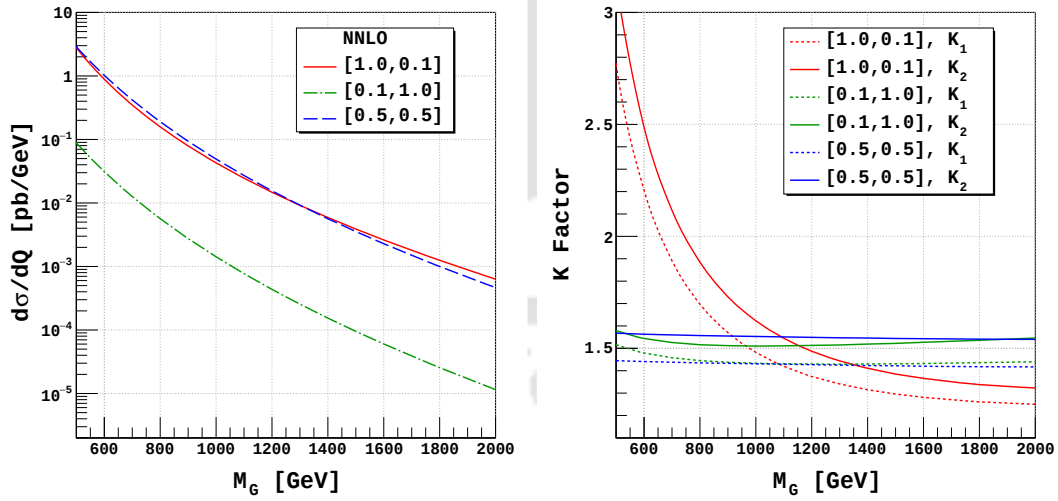

Figure 6.1: Invariant mass distribution of the dilepton for signal for different choice of k_q and k_q at $Q = M_G$ in NNLO QCD (left panel) and the corresponding NLO and NNLO K-factor as defined Eq.(6.19) (right panel).

results presented just in Fig.(6.1), we use NNLO PDF at all orders. We observe that even at the resonance region, the cross section depends on the choice of k_q and k_g,

which is not the case for the RS model where the height of the peak is independent of the corresponding coupling c_0 [116]. This particular nature can be understood from the parton level Born cross sections, Eq.(6.20). In Fig.(6.1) right panel we present the corresponding K-factors (K_1, K_2) defined with respect to LO as,

$$K_n = \frac{d\sigma^{N^n LO}/dQ}{d\sigma^{LO}/dQ}\,. \tag{6.19}$$

Here we observe that for $(k_q, k_g) = (1.0, 0.1)$ at low $Q = M_G$ values, the NLO K-factors K_1 can be as high as 3 while the corresponding K-factors for the universal case are about 1.5 [116]. Because k_q is much larger than k_g, at LO one can expect dominant contributions from Drell-Yan like process while the Higgs-like process is suppressed because of smaller coupling k_g. For the same reason, at NLO the gluon emissions from the underlying born level parton processes is also expected to give smaller contribution. However, at NLO the presence of additional subprocesses like qg with large parton fluxes, give a significant positive contribution comparable to that of $q\bar{q}$ LO as discussed in the introduction. However for $(k_q, k_g) = (0.1, 1.0)$ and $(0.5, 0.5)$, the qg subprocess contribution is very small and comparable to LO $q\bar{q}$ subprocess and is negative. Because of this potentially large and model dependent

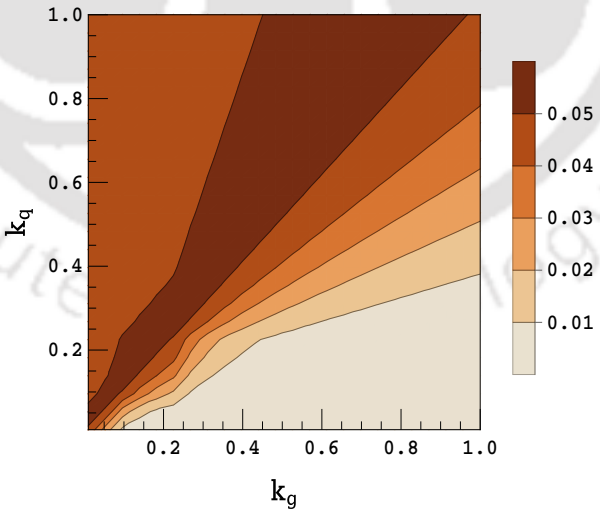

Figure 6.2: The contour plot of couplings k_q and k_g for signal at NNLO with a fixed value of the spin-2 mass $M_G = 1$ TeV. The plot shows the cross-section (in pb) at the resonance $Q = M_G$.

contributions at NLO, it is necessary to include the QCD corrections at second order

and beyond in the perturbation series. We present the NNLO K-factors (K_2) in the right panel of Fig.(6.1) and it can be seen that these second order contributions are smaller than the corresponding NLO ones for different extreme choices of the non-universal couplings and confirms that at NLO all possible dominant contributions are considered giving typical sizeable corrections from NNLO onwards. In this regard, it is convenient to study the higher order QCD corrections in terms of the K-factors R_{nm} defined with respect to NLO. In the rest of the analysis, we present the results in terms of these K-factors R_{nm}.

Next, we present the dependence of model parameters k_q and k_g on the FO cross sections at the resonance for $Q = M_G = 1$ TeV through the contour plot in Fig.(6.2). The cross section is large for larger k_q values and becomes maximum around the universal line ($k_q \sim k_g$). The behaviour can be better understood from the dependence of born level partonic subprocesses on k_q and k_g as,

$$\Delta_{q\bar{q}}^{GR} \propto \frac{k_q^4}{C(Q^2) + [Ak_q^2 + Bk_g^2]^2} \quad , \qquad \Delta_{gg}^{GR} \propto \frac{k_q^2 k_g^2}{C(Q^2) + [Ak_q^2 + Bk_g^2]^2} \, . \tag{6.20}$$

Here the coefficients A and B contain the contributions for the decay of the spin-2 particle to fermions and bosons respectively and $C(Q^2) = (Q^2 - M_G^2)^2$. At resonance where $C(Q^2) = 0$, the cross section will increase with increasing k_q for a fixed k_g and k_g effect is mild here. For any given k_q, the cross sections are maximum when $k_g \lesssim k_q$.

We now discuss the resummed effects for the non-universal couplings. We have performed resummation up to NNLL accuracy and matched them with the fixed order NNLO. In Fig.(6.3), we have shown the dependence of the cross section on k_q and k_g including the resummation effect at NNLL. In the left panel, we present the contour region at the resonance $Q = M_G = 1$ TeV and in the right panel we present the same but at the off-resonance region $Q = 1.5$ TeV. Note that unlike the RS case, here we find non-negligible GR contribution away from the resonance as well. The dependence on the model parameters is found to be the similar as that observed in the FO case Fig.(6.2). However, the maximum cross section region for the resummed case is wider. We have also studied the behaviour of cross-section

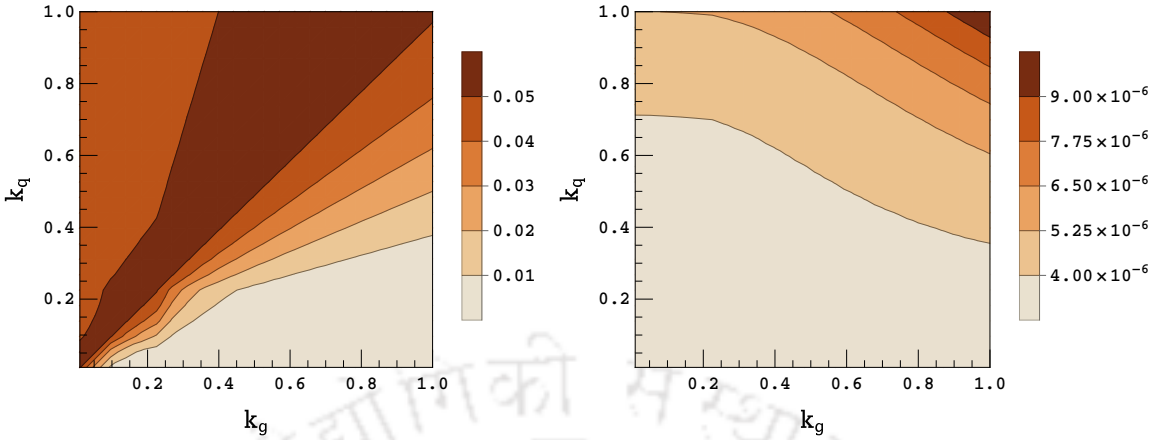

Figure 6.3: The contour plot of couplings k_q and k_g for signal at NNLO+NNLL with a fixed value of the spin-2 mass $M_1 = 1$ TeV. The left plot shows the cross-section (in pb) at the resonance $Q = M_1$, the right plot shows the cross-section (in pb) away from the resonance at $Q = 1.5$ TeV.

by varying the spin-2 mass M_G and either of the couplings while keeping the other coupling fixed. In Fig.(6.4), we present such behaviour at the resonance region $Q = M_G$ to NNLO+NNLL accuracy for different values of M_G and k_q for a given $k_g = 1.0$ in the left panel. We observe that with increasing M_G, for a fixed k_q

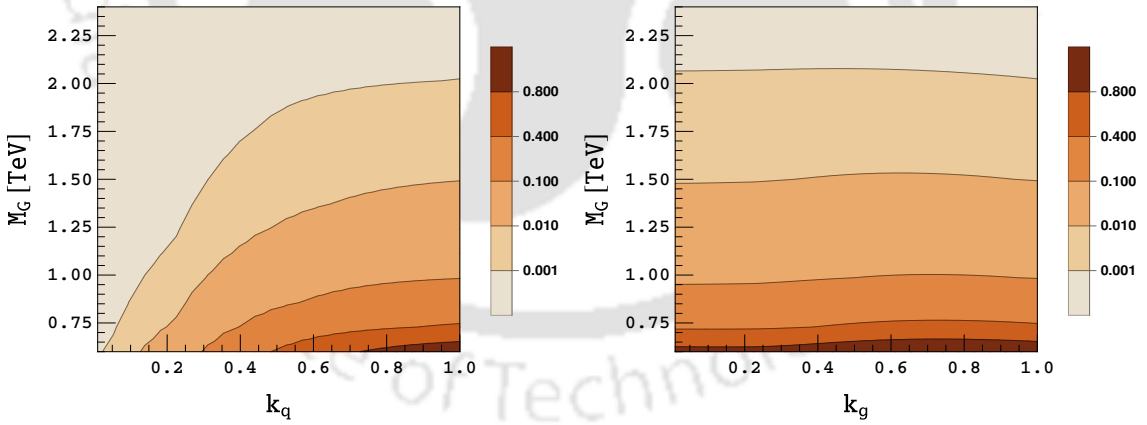

Figure 6.4: The contour plot for mass of the spin-2 particle with coupling k_q and k_g for signal at NNLO+NNLL at $Q = M_G$. The left panel shows the cross section (in pb) for different M_G and k_q region while $k_g = 1.0$ and the right panel shows the cross section for M_G and k_g region with k_q fixed at 1.0.

the cross section is falling due to the decreasing parton fluxes. The cross section is increasing with k_q for a fixed value of M_G as discussed in Eq.(6.20). In the right panel, we present similar results but by varying M_G and k_g for a given value of

$k_q = 1.0$ and we observe the mild effect of k_g on cross section when both M_G and k_q are fixed.

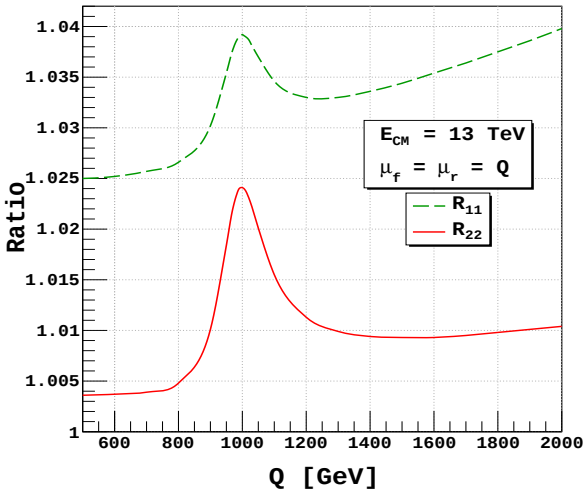

Figure 6.5: Comparison between fixed order results and resummed results. The ratios are defined with respect to NLO as described in the text.

To quantify the resummation effect we define K-factor with respect to NLO as

$$R_{nm} = \frac{d\sigma^{(N^nLO+N^nLL)}/dQ}{d\sigma^{(N^mLO)}/dQ}\,. \tag{6.21}$$

We present in Fig.(6.5), the ratio of resum results to the FO ones as given in Eq.(6.21). We notice that there is around 4% enhancement due to NLL resummation over the NLO FO result at the resonance region while the enhancement due to NNLL resummation is around 2.5% over the NNLO results. In general we notice that in the region $Q > M_G$, the resummation effects keep increasing with Q and are dominant at NLO+NLL level. However at NNLO+NNLL this is almost constant and gives only 1% increment over the NNLO in the region $Q > M_G$.

In Fig.(6.6), we present the invariant mass distribution to NNLO+NNLL accuracy in the left panel and the corresponding K-factors in the right panel for the default choice of model parameters. We observe a significant enhancement in the cross section from lower order to higher order. In Fig.(6.7) we present different contributions coming from SM, pure GR and the signal to the invariant mass

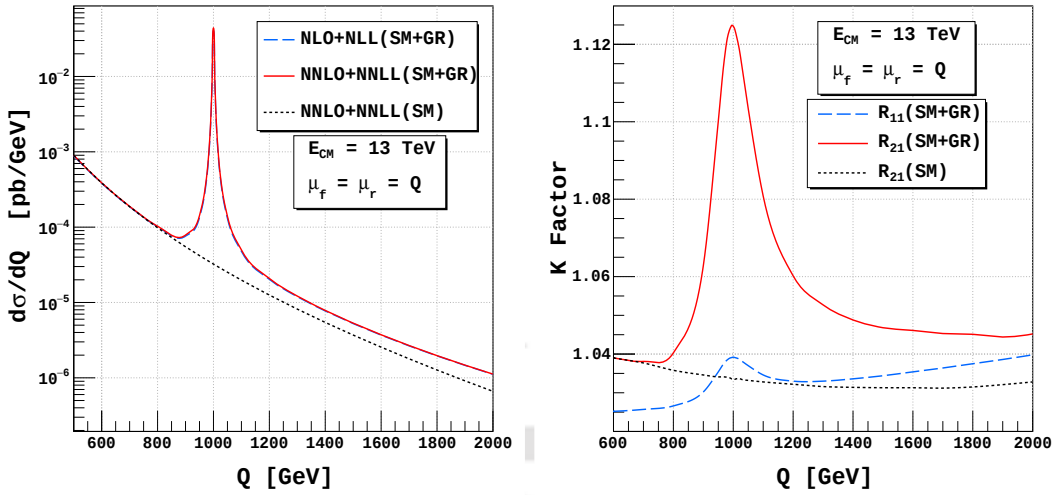

Figure 6.6: Dilepton invariant mass distributions are presented to NNLO+NNLL QCD for signal (left panel) and the corresponding K-factors (right panel).

distributions. We observe that the contribution of gravity to signal is negligible for

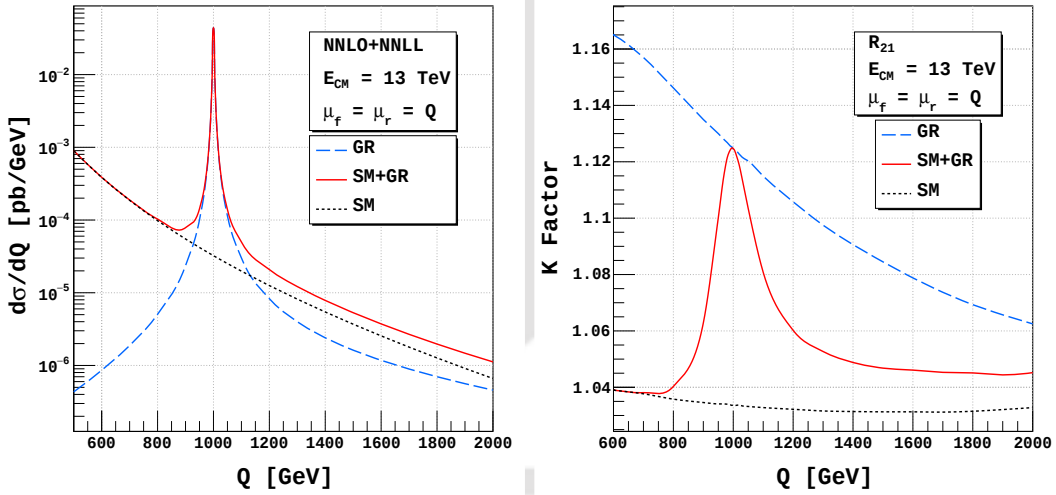

Figure 6.7: Invariant mass distribution of dilepton for the SM, GR model and for the signal (left) and their corresponding K-factors with respect to NLO (right).

$Q < 900$ GeV. However, after the resonance the gravity contribution is also prominent which is in contrast to RS scenario as mentioned earlier. In the right panel we present the corresponding K-factors for the SM, pure gravity and the signal. For low Q values the signal K-factor is equal to that of SM. At the resonance, most of the signal contributions are coming from the gravity, therefore, the signal K-factor is almost equal to that of gravity. In Fig.(6.8), we show the NNLO+NNLL K-

factors for different choices of couplings. It can be seen that the higher cross-section is achieved when $k_g \lesssim k_q$, We note that these K-factors play an essential role in

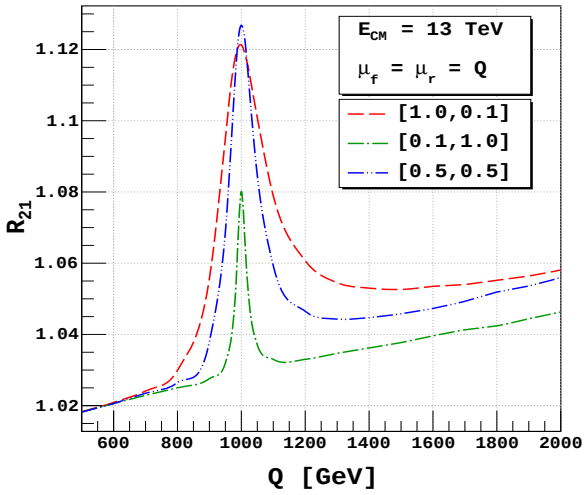

Figure 6.8: K-factor of signal with respect to NLO at NNLO+NNLL level for different choice of k_q and k_g.

the experimental searches. In the searches by CMS and ATLAS collaborations for massive gravitons (with universal couplings of $k_q = k_g = 1.0$) at 13 TeV LHC, it is shown in [1, 3] that the inclusion of NLO K-factors (K_1) have tighten the lower limits at 95% CL on the scale M_s of the large extra dimension (ADD) model and on the mass of the first resonance in the warped extra dimension (RS) model. For example, the lower limit on the scale M_s in the ADD model is changed from 6.8 TeV to 7.2 TeV in ATLAS data analysis of diphoton events, using a K-factor of 1.4. A similar analysis by CMS collaboration using dilepton events has changed the lower limit on the scale M_s from 6.7 TeV to 6.9 TeV when a K-factor of 1.3 is used. Our present analysis involving a generic exotic spin-2 particle estimates even higher order corrections, including resummation effects. These corrections, R_{21} as shown in Fig.(6.8), are found to enhance the cross sections by as large as an additional 10% and reduce the scale uncertainties by a few percent. These improved theory predictions are thus expected to keep stringent bounds on the model parameters, in the present LHC data analysis as well as that in the future collider experiments of even higher center of mass energies.

We also estimate various theoretical uncertainties in our analysis. We first

consider the uncertainties due to the unphysical scales μ_r and μ_f. To quantify these uncertainties, we use the canonical 7-point scale variations by varying μ_r and μ_f simultaneously from $Q/2$ to $2Q$ subject to the constraint that the ratio of unphysical scales should not be than 2 and taking the maximum absolute deviations. We put the following constraints on the variation in order to remove extreme combinations,

$$\left|\ln\frac{\mu_r}{Q}\right| \leq \ln 2, \quad \left|\ln\frac{\mu_f}{Q}\right| \leq \ln 2, \quad \left|\ln\frac{\mu_r}{\mu_f}\right| \leq \ln 2\,. \tag{6.22}$$

In Fig.(6.9), we present these scale uncertainties both in the fixed order results (left panel) as well as in the resummed results (right panel). At NNLO this uncertainty

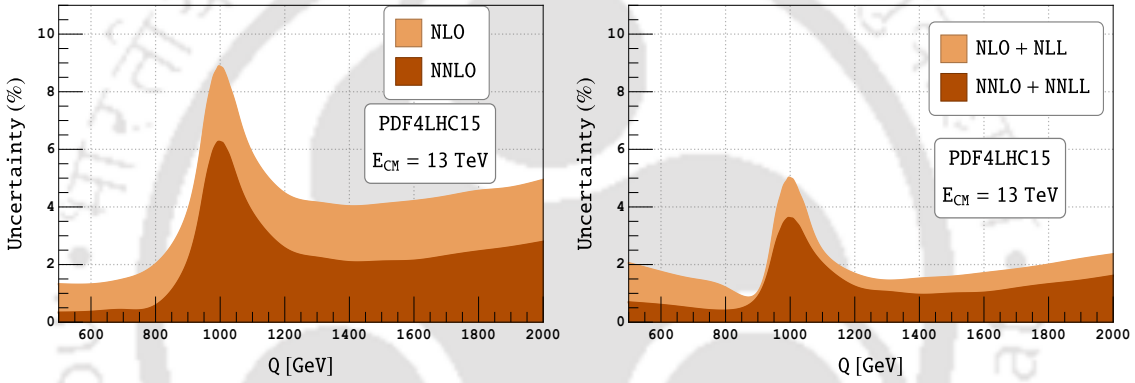

Figure 6.9: The 7-point scale variation in the signal in the range $(\mu_r, \mu_f) \in (1/2, 2)$ is shown up to NNLO and NNLO+NNLL for the dilepton invariant mass distribution.

is estimated to be around $\pm 0.6\%$ for $Q < M_G$, around $\pm 6.3\%$ at the resonance region $Q = M_G = 1$ TeV and is about $\pm 2.0\%$ for $Q > M_G$. However, the corresponding scale uncertainties for the signal at NNLO+NNLL accuracy found to get significantly reduced, respectively, to around $\pm 0.4\%$, $\pm 3.6\%$ and $\pm 1.0\%$. We have also estimated the uncertainties only due to the remormalization scale μ_r by varying it from $Q/2$ to $2Q$ and keeping $\mu_f = Q$ fixed. We observe a significant reduction in the renormalization scale uncertainty from $\pm 1.4\%$ at NNLO to about $\pm 0.5\%$ at NNLO+NNLL accuracy. The corresponding factorization scale uncertainties obtained by varying μ_f from $Q/2$ to $2Q$ and keeping $\mu_r = Q$ fixed are found to get reduced from 5% at NNLO to 2.6% at NNLO+NNLL accuracy at the resonance.

Apart from the unphysical scale uncertainties, we also estimate the uncertainties in the fixed order NNLO results as well as in the resummed NNLO+NNLL

predictions coming from the non-perturbative PDFs. We have estimated the intrinsic PDF uncertainty for the default choice of PDF4LHC15 PDFs using the recommendation in [197], and present our results in Tab.(6.1). We observe that the PDF uncertainty is increasing with invariant mass (Q). However, there is no significant improvement in the PDF uncertainty after inclusion of threshold logarithms. Furthermore, we also compute the cross sections at NNLO+NNLL accuracy for the central set $i = 0$ of different PDF groups namely, MMHT2014nnlo68cl [124], CT14nnlo [129], ABMP16_5_nnlo [178] and NNPDF31_nnlo_as_0118 [130] at resonance $Q = M_G = 1$ TeV and at $Q = 1500$ GeV. The corresponding results are found to be different from those of our default PDF choice by as much as 3%.

$Q(GeV)$	500	1000	1500	2000	2500
NNLO	$8.95 \times 10^{-4} \pm 2.0\%$	$4.28 \times 10^{-2} \pm 2.2\%$	$5.27 \times 10^{-6} \pm 3.4\%$	$1.11 \times 10^{-6} \pm 4.2\%$	$3.37 \times 10^{-7} \pm 5.1\%$
NNLO+NNLL	$8.98 \times 10^{-4} \pm 1.9\%$	$4.39 \times 10^{-2} \pm 2.2\%$	$5.32 \times 10^{-6} \pm 3.3\%$	$1.12 \times 10^{-6} \pm 4.2\%$	$3.41 \times 10^{-7} \pm 5.0\%$

Table 6.1: Intrinsic PDF uncertainties for PDF4LHC15 at 13 TeV LHC

Although the main focus of our phenomenological study is on the threshold resummation, we have also studied the soft plus virtual (SV) corrections at third order in QCD, $\mathrm{N^3LO_{SV}}$. We have computed these third order SV coefficients using the three-loop form factors [196] and exploiting the universality of soft radiations. We finally then give a numerical estimate of these third order corrections by using the running strong coupling constant at 4-loop [35] level. We use the same PDF4LHC15 NNLO set at this order and find that the third order SV result contributes an additional 1% to the NNLO result at the resonance region. The renormalization scale uncertainty reduces to $\pm 0.2\%$ at resonance for a canonical variation[3] within $\mu_r \in \{1/2, 2\}Q$ keeping $\mu_f = Q$ fixed. However for a proper estimation of third order QCD corrections (particularly in the region away from threshold region *viz.* in the lower invariant mass region) one needs to include the regular terms as well as PDF at the third order.

For completeness, we also estimate the size of higher order corrections to NNLO+NNLL for different center of mass energies $\mathrm{E_{CM}}$ of the incoming protons.

[3]Note that it is also possible to estimate theoretical scale uncertainty through a probabilistic description as in [198, 199]. However we refrain from such a study in this article.

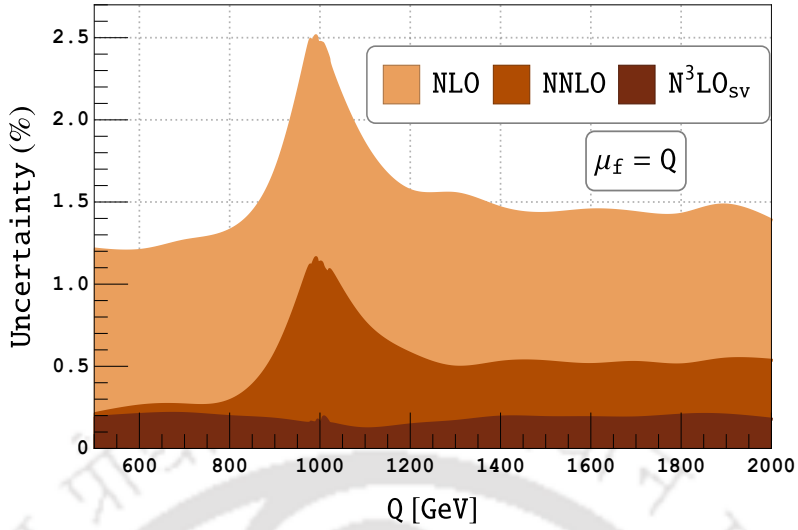

Figure 6.10: The percentage of uncertainty in the signal due to μ_r scale variation around the central scale Q (in the range $\mu_r \in (1/2, 2)Q$) at $\mathrm{N^3LO_{SV}}$ for fixed $\mu_f = Q$.

M_G (TeV) \ E_{CM} (TeV)	7	8	13	14	28
1.0	1.38	1.41	1.67	1.73	3.14
1.5	1.34	1.33	1.40	1.43	2.01
2.0	1.39	1.35	1.33	1.34	1.63
2.5	1.48	1.41	1.31	1.31	1.46

Table 6.2: K-factor (R_{20}) for different collider energies at select resonance masses for $(k_q, k_g) = (1.0, 0.1)$.

M_G (TeV) \ E_{CM} (TeV)	7	8	13	14	28
1.0	1.67	1.63	1.55	1.54	1.55
1.5	1.80	1.73	1.58	1.57	1.50
2.0	1.98	1.87	1.63	1.61	1.50
2.5	2.26	2.05	1.69	1.66	1.51

Table 6.3: K-factor (R_{20}) for different collider energies at select resonance masses for $(k_q, k_g) = (0.1, 1.0)$.

In Tab.(6.2) and Tab.(6.3), we present the mass dependent K-factors R_{20} as defined in Eq.(6.21) for two different choices of couplings $(k_q, k_g) = (1.0, 0.1)$ and $(0.1, 1.0)$ respectively, for $7, 8, 13, 14,$ and 28 TeV hadron colliders. These results show a substantial dependence on the resonance mass as well as on the choice of couplings used. Note that experimental analysis for such models often involves a scaling from LO to take into account the higher order QCD effects at NLO. We stress that in such analysis our mass-dependent K-factors (R_{20}) could be useful to take into account

correctly the QCD effects beyond NLO.

6.4 Conclusion

We have studied a detailed phenomenology for a generic spin-2 particle production at the 13 TeV LHC. We assumed non-universal coupling of the spin-2 particle with the SM fields. This needs additional UV renormalization for individual operators. After performing UV renormalization of the form factors, we have computed the new SV coefficients at the third order. From these coefficients, we were able to extract the process dependent coefficients needed for threshold resummation. Using the universal threshold exponent, which are already available in the literature, as well as the newly computed process dependent coefficients in this article, we find all the ingredients to perform resummation up to NNLL accuracy. We observe a better perturbative convergence after inclusion of these threshold logarithms. Compared to the fixed order, the cross-section increases by 2.5% at the NNLL level at the resonance. We show that inclusion of these threshold logarithms are indeed important in taming the theoretical uncertainties to as small as 3.6% near the resonance. We also discuss the impact of the third order SV coefficients and the corresponding renormalization scale uncertainty. We stress that the K factors in the non-universal case strongly depend on the higher order corrections and a naive scaling from LO will heavily undermine the correct result at NLO(NNLO) level. Our mass-dependent K factors are thus expected to be useful in the search of such spin-2 resonances at the LHC.

Chapter 7

Summary

To understand the dynamics of fundamental particles, not only precise experimental results are required, but also we need very accurate results from the theoretical side to unravel the mystery of nature. The world's most largest and sophisticated collider LHC is now exploring the small distance physics to an unprecedented accuracy. Its high centre of mass energy and high luminosity can provide precise experimental results up to a few TeV. The partonic centre of mass energy of this collider can scan a wide range of kinematic region and hence behaves as a perfect discovery machine. From the theoretical side, precise results can be achieved by taking into account the higher-order perturbative QCD corrections. As SM describes the interaction between the fundamental particles, these precise results from both the theoretical and experimental side will confirm the prediction of this model to unprecedented accuracy and will also help to find the beyond SM signatures through its deviations. Among many processes at the LHC, Drell-Yan is an important process to explore fundamental physics because of its clean final state. This is one of the hadronic processes which is very well understood theoretically and hence is very important to probe BSM signatures. Here, we have studied the precision calculation of the DY process in SM and beyond at the LHC in the context of soft-virtual computation and threshold resummation.

For SM DY production, we have presented dilepton as well as on-shell

Z and $W^{\pm}$ production results up to N^{3}LL accuracy in QCD after matching with N^{3}LO$_{sv}$ results for 13 TeV LHC. We make use of the available three-loop SV results to obtain the process dependent coefficient g_{0i} up to third order in QCD and the universal N-dependent exponent available in the literature up to g_4. We have used all these available necessary ingredients to perform resummation, in particular, the threshold enhanced large-N as well as the N-independent constants. As threshold corrections are important in the high invariant mass region, these results can give significant contributions, say above $Q = 1800$ GeV. However, in the moderate invariant mass region also we find a substantial contribution from the threshold terms. Apart from the `Standard` $\ln N$ exponentiation, we have explored other possibilities of exponentiation namely, `Standard` $\ln \overline{N}$ exponentiation, `Soft` exponentiation and `All` exponentiation. We observed that the resummed results obtained by exponentiating $\ln\bar{N}$ pieces give faster convergence of the perturbation series compared to the conventional case where $\ln N$ terms have been exponentiated. Further, we explored other possibilities of doing resummation where we exponentiate complete soft pieces coming from the universal soft distribution function including $\delta(1-z)$ and notice that the perturbative convergence for the `Soft` case is a bit faster than the `Standard` $\overline{N}$ case. We also presented our results when the complete g_0 coefficients, including the form factor, have been exponentiated (`All` case) and found that the convergence rate of the perturbation series is competing with that of the `Soft` case. Overall, we observe that these different approaches show a systematic behavior of the resummed predictions where the convergence of the perturbation series gets better when more and more N-independent terms are exponentiated. For scale uncertainties up to NNLO+NNLL, `All` has the lowest scale uncertainties for a wide range of Q values. We also note that at N^{3}LL accuracy; however, the missing regular pieces are also important, and so is N^{3}LO PDFs to tame the overall scale uncertainty.

In the absence of any signs of new physics at the LHC, it is high time to explore possible scenarios where we could make a potential discovery of new physics beyond the SM. We have considered the dilepton production at the LHC via spin-2 particles. For this, we consider two scenarios, the ADD model and the RS model. In particular, these models provide a perfect candidate in search of

spin-2 particles either in terms of the deviation from SM background or in terms of heavy resonance in the invariant mass distribution of dilepton. As these particles couple to SM particles universally through energy-momentum tensor, the dilepton can be produced through both $q\bar{q}$ and gg initiated subprocesses. From a precision phenomenology point of view, this process is interesting as it combines both Higgs like and DY like process and one can expect significant QCD correction of this process.

In the RS model, we have studied the complete NNLO QCD corrections for the dilepton production process through graviton propagator and have presented the dilepton invariant mass distribution results up to Q values as high as 3.5 TeV. The underlying born contributions for this process receive both DY-like as well as Higgs-like contributions. Hence, the corresponding QCD corrections for the signal at the resonance region are very significant, while the QCD corrections off the resonance are mostly SM DY-like. This results in K-factors that are strongly dependent on the invariant mass of the dilepton. We have presented these mass-dependent K-factors at NNLO and beyond for 13 TeV LHC. We find that while NLO correction is about 53% of LO, the NNLO correction increases the cross-section by additional 21%. The scale uncertainty in the NNLO result at the resonance region also got significantly reduced to as small as 2% for $Q = M_1 = 1500$ GeV. Further, we have extended our work to include the important SV corrections at the $\mathrm{N^3LO}$ level. We find that the SV contribution at this order for $Q = 1500$ GeV is about 0.7% of LO in magnitude but negative in sign, thus demonstrating very good convergence of the perturbation series. In addition, we also studied the threshold resummation by resuming the threshold logarithms to NNLL accuracy and then matching to the fixed order NNLO ones. We find that these resummed results contribute an additional 7% of LO to the NNLO ones.

In ADD case, we have computed the dilepton production via spin-2 particles beyond NNLO in QCD at hadron colliders. Precisely, we have calculated three-loop SV corrections to the spin-2 production with the help of available three-loop quark and gluon form factors. We have performed a detailed phenomenological study at $\mathrm{N^3LO_{sv}}$ in QCD and presented our numerical results for the dilepton in-

variant mass distribution in the ADD model for 13TeV LHC. The three-loop SV corrections contribute about 2% of LO to the existing NNLO result. The conventional 7-point scale uncertainties of about 8% at NNLO in the high invariant mass region get reduced to about 5% at the three-loop level. Moreover, we have estimated the possible uncertainty in the approximation used to compute the SV corrections at three-loop level and found that the leading and further partial subleading collinear terms contribute by an additional few per cent to the SV results. In addition, we have also performed resummation of large threshold logarithms up to N^3LL accuracy. We have studied the numerical impact of these resummed result after matching them to N^3LO_{sv} fixed order result. While the quantitative enhancement of these resummed results is approximately 2% of LO over the known fixed order NNLO results, the resummed predictions reduce the scale uncertainties significantly to as low as 2%. For completeness, we also estimated the PDF uncertainties in our predictions using the parton densities available at NNLO level from various groups. The uncertainties from these non-perturbative inputs are estimated to be a maximum of about 10% around invariant mass region $Q \sim 1000$ GeV, although they increase further at higher Q values.

Further, we have studied the dilepton production at LHC via spin-2 particles with non-universal couplings. The phenomenology of this model is similar to that in the RS model to some extent. However, here spin-2 particles couple to the SM fermion and gauge bosons with different coupling strength. This non-universal coupling feature makes this model parameters much flexible and less constrained in the LHC searches. The non-universal coupling of this model requires additional UV renormalization for individual operators. After performing UV renormalization of the form factors, we have computed the new SV coefficients in the third order. From these coefficients, we were able to extract the process dependent coefficients needed for threshold resummation. Using the available universal threshold exponent and the newly computed process dependent coefficients in this article, we find all the ingredients required to perform the resummation up to NNLL accuracy. We observe a better perturbative convergence after the inclusion of these threshold logarithms. Compared to the fixed order, the cross-section increases by 2.5% at the NNLL level

at the resonance. We show that the inclusion of these threshold logarithms are vital in taming the theoretical uncertainties to as small as 3.6% near the resonance. We also discuss the impact of the third-order SV coefficients as the corresponding renormalization scale uncertainty. We stress that the K factors in the non-universal case strongly depend on the higher-order corrections and a naive scaling from LO will heavily undermine the correct result at NLO(NNLO) level. Our mass-dependent K factors are thus expected to be helpful in the search of such spin-2 resonances at the LHC.

This thesis presented the most precise theoretical results available so far in the literature for dilepton production in SM, RS, ADD, and generic spin-2 scenarios for 13 TeV LHC. The accurate results for the SM DY process will be helpful for the determination of electroweak parameters more precisely and to probe many BSM scenarios. As the LHC is looking for the signatures of extra dimension scenarios from time to time, our precise results will help in providing a lower bound on the model parameters. For examples, in the search for ADD model, the lower bound on the scale M_s provided by 13 TeV ATLAS data is 8.1 TeV with LO results, and 8.6 TeV with NLO results. Therefore, our mass-dependent K-factor will provide a stringent bound on model parameters for the LHC searches. We can straightforwardly extend our 13 TeV results to other future centre of mass-energies like 27 TeV, 28 TeV and 100 TeV, where this kind of precision calculation will play a vital role. Finally, at this precision level, other corrections like mixed QCD-electroweak corrections are also important. In future, I will devote a significant part of my research work in this direction.

Appendix A

Resummed coefficients for SM DY

Here we collect N-dependent and N-independent coefficients for all different prescriptions for resummation.

A.1 Resummation ingredients for the `Standard` $\overline{N}$ `exponentiation`

For the `Standard` $\overline{N}$ `exponentiation` we present here the $\overline{N}$ independent coefficients g_0 to three loops in Eq.(2.72) below

$$\bar{g}_{01} = \left[\tilde{G}_{11}\left(2\right) + G_{11}\left(2\right) + B_1\left(2\,L_{qr} - 2\,L_{fr}\right) + A_1\left(5\,\zeta_2\right)\right], \tag{A.1}$$

$$\begin{aligned}\bar{g}_{02} = &\left[\tilde{G}_{21}\left(1\right) + \tilde{G}_{12}\left(2\,\beta_0\right) + \tilde{G}_{11}\left(-2\,\beta_0\,L_{qr}\right) + \tilde{G}_{11}^2\left(2\right) + G_{21}\left(1\right)\right.\\ &+ G_{12}\left(2\,\beta_0\right) + G_{11}\left(-2\,\beta_0\,L_{qr}\right) + G_{11}\,\tilde{G}_{11}\left(4\right) + G_{11}^2\left(2\right)\\ &+ f_1\left(5\,\beta_0\,\zeta_2\right) + B_2\left(2\,L_{qr} - 2\,L_{fr}\right) + B_1\left(-\beta_0\,L_{qr}^2 + \beta_0\,L_{fr}^2 + 6\,\beta_0\,\zeta_2\right)\\ &+ B_1\,\tilde{G}_{11}\left(4\,L_{qr} - 4\,L_{fr}\right) + B_1\,G_{11}\left(4\,L_{qr} - 4\,L_{fr}\right) + B_1^2\left(2\,L_{qr}^2\right.\\ &\left.\left.- 4\,L_{fr}\,L_{qr} + 2\,L_{fr}^2\right) + A_2\left(5\,\zeta_2\right) + A_1\left(\frac{8}{3}\,\beta_0\,\zeta_3 - 5\,\beta_0\,\zeta_2\,L_{qr}\right)\right.\end{aligned}$$

$$+ A_1\ \tilde{G}_{11}\ \left(10\ \zeta_2\right) + A_1\ G_{11}\ \left(10\ \zeta_2\right) + A_1\ B_1\ \left(10\ \zeta_2\ L_{qr} - 10\ \zeta_2\ L_{fr}\right)$$
$$+ {A_1}^2\ \left(\frac{25}{2}\ \zeta_2^2\right)\Bigg], \tag{A.2}$$

$$\bar{g}_{03} = \Bigg[\tilde{G}_{31}\ \left(\frac{2}{3}\right) + \tilde{G}_{22}\ \left(\frac{4}{3}\ \beta_0\right) + \tilde{G}_{21}\ \left(-2\ \beta_0\ L_{qr}\right) + \tilde{G}_{13}\ \left(\frac{8}{3}\ \beta_0^2\right) + \tilde{G}_{12}\ \left(\frac{4}{3}\ \beta_1$$
$$- 4\ \beta_0^2\ L_{qr}\right) + \tilde{G}_{11}\ \left(-2\ \beta_1\ L_{qr} + 2\ \beta_0^2\ L_{qr}^2 + 8\ \beta_0^2\ \zeta_2\right) + \tilde{G}_{11}\ \tilde{G}_{21}\ \left(2\right)$$
$$+ \tilde{G}_{11}\ \tilde{G}_{12}\ \left(4\ \beta_0\right) + \tilde{G}_{11}^2\ \left(-4\ \beta_0\ L_{qr}\right) + \tilde{G}_{11}^3\ \left(\frac{4}{3}\right) + G_{31}\ \left(\frac{2}{3}\right)$$
$$+ G_{22}\ \left(\frac{4}{3}\ \beta_0\right) + G_{21}\ \left(-2\ \beta_0\ L_{qr}\right) + G_{21}\ \tilde{G}_{11}\ \left(2\right) + G_{13}\ \left(\frac{8}{3}\ \beta_0^2\right)$$
$$+ G_{12}\ \left(\frac{4}{3}\ \beta_1 - 4\ \beta_0^2\ L_{qr}\right) + G_{12}\ \tilde{G}_{11}\ \left(4\ \beta_0\right) + G_{11}\ \left(-2\ \beta_1\ L_{qr} + 2\ \beta_0^2\ L_{qr}^2\right.$$
$$\left. - 12\ \beta_0^2\ \zeta_2\right) + G_{11}\ \tilde{G}_{21}\ \left(2\right) + G_{11}\ \tilde{G}_{12}\ \left(4\ \beta_0\right) + G_{11}\ \tilde{G}_{11}\ \left(-8\ \beta_0\ L_{qr}\right)$$
$$+ G_{11}\ \tilde{G}_{11}^2\ \left(4\right) + G_{11}\ G_{21}\ \left(2\right) + G_{11}\ G_{12}\ \left(4\ \beta_0\right) + G_{11}^2\ \left(-4\ \beta_0\ L_{qr}\right)$$
$$+ G_{11}^2\ \tilde{G}_{11}\ \left(4\right) + G_{11}^3\ \left(\frac{4}{3}\right) + f_2\ \left(10\ \beta_0\ \zeta_2\right) + f_1\ \left(5\ \beta_1\ \zeta_2 + \frac{16}{3}\ \beta_0^2\ \zeta_3\right.$$
$$\left. - 10\ \beta_0^2\ \zeta_2\ L_{qr}\right) + f_1\ \tilde{G}_{11}\ \left(10\ \beta_0\ \zeta_2\right) + f_1\ G_{11}\ \left(10\ \beta_0\ \zeta_2\right) + B_3\ \left(2\ L_{qr}\right.$$
$$\left. - 2\ L_{fr}\right) + B_2\ \left(-2\ \beta_0\ L_{qr}^2 + 2\ \beta_0\ L_{fr}^2 + 12\ \beta_0\ \zeta_2\right) + B_2\ \tilde{G}_{11}\ \left(4\ L_{qr}\right.$$
$$\left. - 4\ L_{fr}\right) + B_2\ G_{11}\ \left(4\ L_{qr} - 4\ L_{fr}\right) + B_1\ \left(-\beta_1\ L_{qr}^2 + \beta_1\ L_{fr}^2 + 6\ \beta_1\ \zeta_2\right.$$
$$\left. + \frac{2}{3}\ \beta_0^2\ L_{qr}^3 - \frac{2}{3}\ \beta_0^2\ L_{fr}^3 - 12\ \beta_0^2\ \zeta_2\ L_{qr}\right) + B_1\ \tilde{G}_{21}\ \left(2\ L_{qr} - 2\ L_{fr}\right)$$
$$+ B_1\ \tilde{G}_{12}\ \left(4\ \beta_0\ L_{qr} - 4\ \beta_0\ L_{fr}\right) + B_1\ \tilde{G}_{11}\ \left(-6\ \beta_0\ L_{qr}^2 + 4\ \beta_0\ L_{fr}\ L_{qr}\right.$$
$$\left. + 2\ \beta_0\ L_{fr}^2 + 12\ \beta_0\ \zeta_2\right) + B_1\ \tilde{G}_{11}^2\ \left(4\ L_{qr} - 4\ L_{fr}\right) + B_1\ G_{21}\ \left(2\ L_{qr}\right.$$
$$\left. - 2\ L_{fr}\right) + B_1\ G_{12}\ \left(4\ \beta_0\ L_{qr} - 4\ \beta_0\ L_{fr}\right) + B_1\ G_{11}\ \left(-6\ \beta_0\ L_{qr}^2\right.$$
$$\left. + 4\ \beta_0\ L_{fr}\ L_{qr} + 2\ \beta_0\ L_{fr}^2 + 12\ \beta_0\ \zeta_2\right) + B_1\ G_{11}\ \tilde{G}_{11}\ \left(8\ L_{qr} - 8\ L_{fr}\right)$$
$$+ B_1\ G_{11}^2\ \left(4\ L_{qr} - 4\ L_{fr}\right) + B_1\ f_1\ \left(10\ \beta_0\ \zeta_2\ L_{qr} - 10\ \beta_0\ \zeta_2\ L_{fr}\right)$$
$$+ B_1\ B_2\ \left(4\ L_{qr}^2 - 8\ L_{fr}\ L_{qr} + 4\ L_{fr}^2\right) + B_1^2\ \left(-2\ \beta_0\ L_{qr}^3 + 2\ \beta_0\ L_{fr}\ L_{qr}^2\right.$$

$$+ 2\ \beta_0\ L_{fr}^2\ L_{qr} - 2\ \beta_0\ L_{fr}^3 + 12\ \beta_0\ \zeta_2\ L_{qr} - 12\ \beta_0\ \zeta_2\ L_{fr}\Big) + B_1^2\ \tilde{G}_{11}\ \Big(4\ L_{qr}^2$$
$$- 8\ L_{fr}\ L_{qr} + 4\ L_{fr}^2\Big) + B_1^2\ G_{11}\ \Big(4\ L_{qr}^2 - 8\ L_{fr}\ L_{qr} + 4\ L_{fr}^2\Big) + B_1^3\ \Big(\frac{4}{3}\ L_{qr}^3$$
$$- 4\ L_{fr}\ L_{qr}^2 + 4\ L_{fr}^2\ L_{qr} - \frac{4}{3}\ L_{fr}^3\Big) + A_3\ \Big(5\ \zeta_2\Big) + A_2\ \Big(\frac{16}{3}\ \beta_0\ \zeta_3$$
$$- 10\ \beta_0\ \zeta_2\ L_{qr}\Big) + A_2\ \tilde{G}_{11}\ \Big(10\ \zeta_2\Big) + A_2\ G_{11}\ \Big(10\ \zeta_2\Big) + A_2\ B_1\ \Big(10\ \zeta_2\ L_{qr}$$
$$- 10\ \zeta_2\ L_{fr}\Big) + A_1\ \Big(\frac{8}{3}\ \beta_1\ \zeta_3 - 5\ \beta_1\ \zeta_2\ L_{qr} - \frac{16}{3}\ \beta_0^2\ \zeta_3\ L_{qr} + 5\ \beta_0^2\ \zeta_2\ L_{qr}^2$$
$$+ \frac{21}{5}\ \beta_0^2\ \zeta_2^2\Big) + A_1\ \tilde{G}_{21}\ \Big(5\ \zeta_2\Big) + A_1\ \tilde{G}_{12}\ \Big(10\ \beta_0\ \zeta_2\Big) + A_1\ \tilde{G}_{11}\ \Big(\frac{16}{3}\ \beta_0\ \zeta_3$$
$$- 20\ \beta_0\ \zeta_2\ L_{qr}\Big) + A_1\ \tilde{G}_{11}^2\ \Big(10\ \zeta_2\Big) + A_1\ G_{21}\ \Big(5\ \zeta_2\Big) + A_1\ G_{12}\ \Big(10\ \beta_0\ \zeta_2\Big)$$
$$+ A_1\ G_{11}\ \Big(\frac{16}{3}\ \beta_0\ \zeta_3 - 20\ \beta_0\ \zeta_2\ L_{qr}\Big) + A_1\ G_{11}\ \tilde{G}_{11}\ \Big(20\ \zeta_2\Big)$$
$$+ A_1\ G_{11}^2\ \Big(10\ \zeta_2\Big) + A_1\ f_1\ \Big(25\ \beta_0\ \zeta_2^2\Big) + A_1\ B_2\ \Big(10\ \zeta_2\ L_{qr} - 10\ \zeta_2\ L_{fr}\Big)$$
$$+ A_1\ B_1\ \Big(\frac{16}{3}\ \beta_0\ \zeta_3\ L_{qr} - \frac{16}{3}\ \beta_0\ \zeta_3\ L_{fr} - 15\ \beta_0\ \zeta_2\ L_{qr}^2 + 10\ \beta_0\ \zeta_2\ L_{fr}\ L_{qr}$$
$$+ 5\ \beta_0\ \zeta_2\ L_{fr}^2 + 30\ \beta_0\ \zeta_2^2\Big) + A_1\ B_1\ \tilde{G}_{11}\ \Big(20\ \zeta_2\ L_{qr} - 20\ \zeta_2\ L_{fr}\Big)$$
$$+ A_1\ B_1\ G_{11}\ \Big(20\ \zeta_2\ L_{qr} - 20\ \zeta_2\ L_{fr}\Big) + A_1\ B_1^2\ \Big(10\ \zeta_2\ L_{qr}^2 - 20\ \zeta_2\ L_{fr}\ L_{qr}$$
$$+ 10\ \zeta_2\ L_{fr}^2\Big) + A_1\ A_2\ \Big(25\ \zeta_2^2\Big) + {A_1}^2\ \Big(\frac{40}{3}\ \beta_0\ \zeta_2\ \zeta_3 - 25\ \beta_0\ \zeta_2^2\ L_{qr}\Big)$$
$$+ {A_1}^2\ \tilde{G}_{11}\ \Big(25\ \zeta_2^2\Big) + {A_1}^2\ G_{11}\ \Big(25\ \zeta_2^2\Big) + {A_1}^2\ B_1\ \Big(25\ \zeta_2^2\ L_{qr} - 25\ \zeta_2^2\ L_{fr}\Big)$$
$$+ {A_1}^3\ \Big(\frac{125}{6}\ \zeta_2^3\Big)\Big]. \tag{A.3}$$

The resummed exponent is calculated to the N^{3}LL accuracy and collected below (with $\omega = 2\beta_0 a_s \ln \overline{N}$), All the anomalous dimensions A_i are given as

$$g_1 = \Big[\frac{A_1}{\beta_0}\ \Big\{2 - 2\ \ln(1-\omega) + 2\ \ln(1-\omega)\ \omega^{-1}\Big\}\Big], \tag{A.4}$$

$$g_2 = \Big[\frac{D_1}{\beta_0}\ \Big\{\frac{1}{2}\ \ln(1-\omega)\Big\} + \frac{A_2}{\beta_0^2}\ \Big\{-\ln(1-\omega) - \omega\Big\} + \frac{A_1}{\beta_0}\ \Big\{\Big(\ln(1-\omega)$$
$$+ \frac{1}{2}\ \ln(1-\omega)^2 + \omega\Big)\ \Big(\frac{\beta_1}{\beta_0^2}\Big) + \Big(\omega\Big)\ L_{fr} + \Big(\ln(1-\omega)\Big)\ L_{qr}\Big\}\Big], \tag{A.5}$$

$$
\begin{aligned}
g_3 = & \left[\frac{A_3}{\beta_0^2}\left\{-\frac{\omega}{(1-\omega)}+\omega\right\}+\frac{A_2}{\beta_0}\left\{\left(2\,\frac{\omega}{(1-\omega)}\right)L_{qr}+\left(3\,\frac{\omega}{(1-\omega)}+2\,\frac{\ln(1-\omega)}{(1-\omega)}\right.\right.\right.\\
& \left.-\omega\right)\left(\frac{\beta_1}{\beta_0^2}\right)+\left(-2\,\omega\right)L_{fr}\Big\}+A_1\left\{-4\,\zeta_2\,\frac{\omega}{(1-\omega)}+\left(-\frac{\ln(1-\omega)^2}{(1-\omega)}\right.\right.\\
& -\frac{\omega}{(1-\omega)}-2\,\frac{\ln(1-\omega)}{(1-\omega)}+2\,\ln(1-\omega)+\omega\Big)\left(\frac{\beta_1}{\beta_0^2}\right)^2+\left(-\frac{\omega}{(1-\omega)}\right)L_{qr}^2\\
& +\left(-\frac{\omega}{(1-\omega)}-2\,\ln(1-\omega)-\omega\right)\left(\frac{\beta_2}{\beta_0^3}\right)+\left(\left(-2\,\frac{\omega}{(1-\omega)}\right.\right.\\
& \left.\left.-2\,\frac{\ln(1-\omega)}{(1-\omega)}\right)\left(\frac{\beta_1}{\beta_0^2}\right)\right)L_{qr}+\left(\omega\right)L_{fr}^2\Big\}+\frac{D_2}{\beta_0}\left\{\frac{\omega}{(1-\omega)}\right\}+D_1\left\{\left(\right.\right.\\
& \left.\left.-\frac{\omega}{(1-\omega)}\right)L_{qr}+\left(-\frac{\omega}{(1-\omega)}-\frac{\ln(1-\omega)}{(1-\omega)}\right)\left(\frac{\beta_1}{\beta_0^2}\right)\right\}\Big], \qquad \text{(A.6)}\\
g_4 = & \left[\frac{A_4}{\beta_0^2}\left\{\frac{1}{6}\,\frac{\omega(2-\omega)}{(1-\omega)^2}-\frac{1}{3}\,\omega\right\}+\frac{A_3}{\beta_0}\left\{\left(-\frac{1}{2}\,\frac{\omega(2-\omega)}{(1-\omega)^2}\right)L_{qr}+\left(-\frac{5}{12}\,\frac{\omega(2-\omega)}{(1-\omega)^2}\right.\right.\right.\\
& \left.-\frac{1}{2}\,\frac{\ln(1-\omega)}{(1-\omega)^2}+\frac{1}{3}\,\omega\right)\left(\frac{\beta_1}{\beta_0^2}\right)+\left(\omega\right)L_{fr}\Big\}+A_2\left\{2\,\zeta_2\,\frac{\omega(2-\omega)}{(1-\omega)^2}\right.\\
& +\left(\frac{1}{2}\,\frac{\ln(1-\omega)^2}{(1-\omega)^2}-\frac{1}{12}\,\frac{\omega^2}{(1-\omega)^2}+\frac{5}{6}\,\frac{\omega}{(1-\omega)}+\frac{1}{2}\,\frac{\ln(1-\omega)}{(1-\omega)^2}-\frac{1}{3}\,\omega\right)\left(\frac{\beta_1}{\beta_0^2}\right)^2\\
& +\left(\frac{1}{2}\,\frac{\omega(2-\omega)}{(1-\omega)^2}\right)L_{qr}^2+\left(\frac{1}{3}\,\frac{\omega^2}{(1-\omega)^2}-\frac{1}{3}\,\frac{\omega}{(1-\omega)}+\frac{1}{3}\,\omega\right)\left(\frac{\beta_2}{\beta_0^3}\right)+\left(\right.\\
& \left.-\omega\right)L_{fr}^2+\left(\left(\frac{1}{2}\,\frac{\omega(2-\omega)}{(1-\omega)^2}+\frac{\ln(1-\omega)}{(1-\omega)^2}\right)\left(\frac{\beta_1}{\beta_0^2}\right)\right)L_{qr}\Big\}\\
& +\beta_0 A_1\left\{\frac{8}{3}\,\zeta_3\,\frac{\omega(2-\omega)}{(1-\omega)^2}+\left(-\frac{1}{6}\,\frac{\ln(1-\omega)^3}{(1-\omega)^2}+\frac{1}{3}\,\frac{\omega^2}{(1-\omega)^2}-\frac{1}{3}\,\frac{\omega}{(1-\omega)}\right.\right.\\
& \left.\left.+\frac{1}{2}\,\frac{\ln(1-\omega)}{(1-\omega)^2}-\frac{\ln(1-\omega)}{(1-\omega)}+\frac{1}{2}\,\ln(1-\omega)+\frac{1}{3}\,\omega\right)\left(\frac{\beta_1}{\beta_0^2}\right)^3+\left(\right.\right.\\
& \left.\left.-\frac{1}{6}\,\frac{\omega(2-\omega)}{(1-\omega)^2}\right)L_{qr}^3+\left(\frac{1}{12}\,\frac{\omega(2-\omega)}{(1-\omega)^2}+\frac{1}{2}\,\ln(1-\omega)+\frac{1}{3}\,\omega\right)\left(\frac{\beta_3}{\beta_0^4}\right)+\left(\right.\right.\\
& \left.\left.-\frac{5}{12}\,\frac{\omega^2}{(1-\omega)^2}+\frac{1}{6}\,\frac{\omega}{(1-\omega)}-\frac{1}{2}\,\frac{\ln(1-\omega)}{(1-\omega)^2}+\frac{\ln(1-\omega)}{(1-\omega)}-\ln(1-\omega)\right.\right.\\
& \left.\left.-\frac{2}{3}\,\omega\right)\frac{\beta_1\beta_2}{\beta_0^5}+\left(\frac{1}{3}\,\omega\right)L_{fr}^3+\left(-2\,\zeta_2\,\frac{\omega(2-\omega)}{(1-\omega)^2}+\left(-\frac{1}{2}\,\frac{\ln(1-\omega)^2}{(1-\omega)^2}\right.\right.\right.\\
& \left.\left.+\frac{1}{2}\,\frac{\omega^2}{(1-\omega)^2}\right)\left(\frac{\beta_1}{\beta_0^2}\right)^2+\left(-\frac{1}{2}\,\frac{\omega^2}{(1-\omega)^2}\right)\left(\frac{\beta_2}{\beta_0^3}\right)\right)L_{qr}+\left(\right.\\
& \left.-2\,\zeta_2\,\frac{\ln(1-\omega)}{(1-\omega)^2}\right)\left(\frac{\beta_1}{\beta_0^2}\right)+\left(\left(-\frac{1}{2}\,\frac{\ln(1-\omega)}{(1-\omega)^2}\right)\left(\frac{\beta_1}{\beta_0^2}\right)\right)L_{qr}^2+\left(\left(\right.\right.\\
& \left.\left.-\frac{1}{2}\,\omega\right)\left(\frac{\beta_1}{\beta_0^2}\right)\right)L_{fr}^2\Big\}+\frac{D_3}{\beta_0}\left\{-\frac{1}{4}\,\frac{\omega(2-\omega)}{(1-\omega)^2}\right\}+D_2\left\{\left(\frac{1}{4}\,\frac{\omega(2-\omega)}{(1-\omega)^2}\right.\right.
\end{aligned}
$$

$$+\frac{1}{2}\,\frac{\ln(1-\omega)}{(1-\omega)^2}\Big)\,\Big(\frac{\beta_1}{\beta_0^2}\Big)+\Big(\frac{1}{2}\,\frac{\omega(2-\omega)}{(1-\omega)^2}\Big)\,L_{qr}\Big\}+\beta_0 D_1\,\Big\{-\zeta_2\,\frac{\omega(2-\omega)}{(1-\omega)^2}+\Big($$
$$-\frac{1}{4}\,\frac{\ln(1-\omega)^2}{(1-\omega)^2}+\frac{1}{4}\,\frac{\omega^2}{(1-\omega)^2}\Big)\,\Big(\frac{\beta_1}{\beta_0^2}\Big)^2+\Big(-\frac{1}{4}\,\frac{\omega(2-\omega)}{(1-\omega)^2}\Big)\,L_{qr}^2+\Big($$
$$-\frac{1}{4}\,\frac{\omega^2}{(1-\omega)^2}\Big)\,\Big(\frac{\beta_2}{\beta_0^3}\Big)+\Big(\Big(-\frac{1}{2}\,\frac{\ln(1-\omega)}{(1-\omega)^2}\Big)\,\Big(\frac{\beta_1}{\beta_0^2}\Big)\Big)\,L_{qr}\Big\}\Big]. \tag{A.7}$$

All the anomalous dimensions A_i are given as

$$A_1=\mathcal{C}_i\Big\{4\Big\}, \tag{A.8}$$
$$A_2=\mathcal{C}_i\Big\{n_f\Big(-\frac{40}{9}\Big)+C_A\Big(\frac{268}{9}-8\zeta_2\Big)\Big\}, \tag{A.9}$$
$$A_3=\mathcal{C}_i\Big\{{n_f}^2\Big(-\frac{16}{27}\Big)+C_F n_f\Big(-\frac{110}{3}+32\zeta_3\Big)+C_A n_f\Big(-\frac{836}{27}-\frac{112}{3}\zeta_3+\frac{160}{9}\zeta_2\Big)$$
$$+C_A^2\Big(\frac{490}{3}+\frac{88}{3}\zeta_3-\frac{1072}{9}\zeta_2+\frac{176}{5}\zeta_2^2\Big)\Big\}, \tag{A.10}$$
$$A_4=\mathcal{C}_i\Big\{{n_f}^3\Big(-\frac{32}{81}+\frac{64}{27}\zeta_3\Big)+C_F{n_f}^2\Big(\frac{2392}{81}-\frac{640}{9}\zeta_3+\frac{64}{5}\zeta_2^2\Big)+C_F^2 n_f\Big(\frac{572}{9}$$
$$-320\zeta_5+\frac{592}{3}\zeta_3\Big)+C_A{n_f}^2\Big(\frac{923}{81}+\frac{2240}{27}\zeta_3-\frac{608}{81}\zeta_2-\frac{224}{15}\zeta_2^2\Big)+C_A C_F n_f\Big($$
$$-\frac{34066}{81}+160\zeta_5+\frac{3712}{9}\zeta_3+\frac{440}{3}\zeta_2-128\zeta_2\zeta_3-\frac{352}{5}\zeta_2^2\Big)+C_A^2 n_f\Big(-\frac{24137}{81}$$
$$+\frac{2096}{9}\zeta_5-\frac{23104}{27}\zeta_3+\frac{20320}{81}\zeta_2+\frac{448}{3}\zeta_2\zeta_3-\frac{352}{15}\zeta_2^2\Big)+C_A^3\Big(\frac{84278}{81}$$
$$-\frac{3608}{9}\zeta_5+\frac{20944}{27}\zeta_3-16\zeta_3^2-\frac{88400}{81}\zeta_2-\frac{352}{3}\zeta_2\zeta_3+\frac{3608}{5}\zeta_2^2-\frac{20032}{105}\zeta_2^3\Big)\Big\}$$
$$+\frac{d_R^{abcd}d_A^{abcd}}{N_R}\Big(\frac{3520}{3}\zeta_5+\frac{128}{3}\zeta_3-384\zeta_3^2-128\zeta_2-\frac{7936}{35}\zeta_2^3\Big)+n_f\frac{d_R^{abcd}d_F^{abcd}}{N_R}\Big($$
$$-\frac{1280}{3}\zeta_5-\frac{256}{3}\zeta_3+256\zeta_2\Big). \tag{A.11}$$

The coefficients D_i are given as

$$D_1=\mathcal{C}_i\Big\{0\Big\}, \tag{A.12}$$
$$D_2=\mathcal{C}_i\Big\{n_f\Big(\frac{224}{27}-\frac{32}{3}\zeta_2\Big)+C_A\Big(-\frac{1616}{27}+56\zeta_3+\frac{176}{3}\zeta_2\Big)\Big\}, \tag{A.13}$$
$$D_3=\mathcal{C}_i\Big\{{n_f}^2\Big(-\frac{3712}{729}+\frac{320}{27}\zeta_3+\frac{640}{27}\zeta_2\Big)+C_F n_f\Big(\frac{3422}{27}-\frac{608}{9}\zeta_3-32\zeta_2-\frac{64}{5}\zeta_2^2\Big)$$

$$+ C_A n_f \left(\frac{125252}{729} - \frac{2480}{9}\zeta_3 - \frac{29392}{81}\zeta_2 + \frac{736}{15}\zeta_2^2 \right) + C_A^2 \left(- \frac{594058}{729} - 384\zeta_5 + \frac{40144}{27}\zeta_3 + \frac{98224}{81}\zeta_2 - \frac{352}{3}\zeta_2\zeta_3 - \frac{2992}{15}\zeta_2^2 \right) \Bigg\}, \tag{A.14}$$

A.2 Resummation ingredients for the `Standard` N exponentiation

Below we present the resummed exponent for the `Standard` N-exponent

$$g_1 = \left[\tilde{A}_1 \left\{ \lambda^{-1} \left(\ln \lambda^{'} \right) \left(2 \right) + \left(\ln \lambda^{'} \right) \left(-2 \right) + 2 \right\} \right], \tag{A.15}$$

$$g_2 = \left[\tilde{D}_1 \left\{ \left(\ln \lambda^{'} \right) \left(\frac{1}{2} \right) \right\} + \tilde{A}_2 \left\{ \left(\ln \lambda^{'} \right) \left(-1 \right) + \lambda \left(-1 \right) \right\} + \tilde{A}_1 \left\{ \left(\ln \lambda^{'} \right) \left(\tilde{\beta}_1 - 2\,\gamma_E + L_{qr} \right) + \left(\ln \lambda^{'} \right)^2 \left(\frac{1}{2}\,\tilde{\beta}_1 \right) + \lambda \left(\tilde{\beta}_1 + L_{fr} \right) \right\} \right], \tag{A.16}$$

$$\begin{aligned} g_3 = \beta_0 \Bigg[& \tilde{D}_2 \left\{ \frac{\lambda}{\lambda^{'}} \left(-\frac{1}{2} \right) \right\} + \tilde{D}_1 \left\{ \left(\ln \lambda^{'} \right) \left(\frac{1}{\lambda^{'}} \right) \left(\frac{1}{2}\,\tilde{\beta}_1 \right) + \frac{\lambda}{\lambda^{'}} \left(\frac{1}{2}\,\tilde{\beta}_1 - \gamma_E + \frac{1}{2}\,L_{qr} \right) \right\} + \tilde{A}_3 \left\{ \frac{\lambda^2}{(\lambda^{'})^2} \left(\frac{1}{2} \right) \right\} + \tilde{A}_2 \left\{ \frac{\lambda}{\lambda^{'}} \left(-\frac{3}{2}\,\tilde{\beta}_1 + 2\,\gamma_E - L_{qr} \right) \right. \\ & \left. + \left(\ln \lambda^{'} \right) \left(\frac{1}{\lambda^{'}} \right) \left(-\tilde{\beta}_1 \right) + \lambda \left(\frac{1}{2}\,\tilde{\beta}_1 + L_{fr} \right) \right\} + \tilde{A}_1 \left\{ \frac{\lambda}{\lambda^{'}} \left(\frac{1}{2}\,\tilde{\beta}_2 + \frac{1}{2}\,\tilde{\beta}_1^2 - 2\,\gamma_E\,\tilde{\beta}_1 + 2\,\gamma_E^2 + L_{qr}\,\tilde{\beta}_1 - 2\,L_{qr}\,\gamma_E + \frac{1}{2}\,L_{qr}^2 + 2\,\zeta_2 \right) + \left(\ln \lambda^{'} \right) \left(\tilde{\beta}_2 \right. \right. \\ & \left. \left. - 2\,\gamma_E\,\tilde{\beta}_1 + L_{qr}\,\tilde{\beta}_1 \right) + \left(\ln \lambda^{'} \right) \frac{\lambda}{\lambda^{'}} \left(\tilde{\beta}_1^2 - 2\,\gamma_E\,\tilde{\beta}_1 + L_{qr}\,\tilde{\beta}_1 \right) \right. \\ & \left. + \left(\ln \lambda^{'} \right)^2 \left(\frac{1}{\lambda^{'}} \right) \left(\frac{1}{2}\,\tilde{\beta}_1^2 \right) + \lambda \left(\frac{1}{2}\,\tilde{\beta}_2 - \frac{1}{2}\,\tilde{\beta}_1^2 - \frac{1}{2}\,L_{fr}^2 \right) \right\} \Bigg], \end{aligned} \tag{A.17}$$

$$\begin{aligned} g_4 = \beta_0^2 \Bigg[& \tilde{D}_3 \left\{ \frac{\lambda(2-\lambda)}{(\lambda^{'})^2} \left(-\frac{1}{4} \right) \right\} + \tilde{D}_2 \left\{ \frac{\lambda(2-\lambda)}{(\lambda^{'})^2} \left(\frac{1}{4}\,\tilde{\beta}_1 - \gamma_E + \frac{1}{2}\,L_{qr} \right) \right. \\ & \left. + \left(\ln \lambda^{'} \right) \left(\frac{1}{\lambda^{'}} \right)^2 \left(\frac{1}{2}\,\tilde{\beta}_1 \right) \right\} + \tilde{D}_1 \left\{ \frac{\lambda(2-\lambda)}{(\lambda^{'})^2} \left(-\frac{1}{4}\,\tilde{\beta}_2 + \frac{1}{4}\,\tilde{\beta}_1^2 - \gamma_E^2 + L_{qr}\,\gamma_E - \frac{1}{4}\,L_{qr}^2 - \zeta_2 \right) + \frac{\lambda}{\lambda^{'}} \left(\frac{1}{2}\,\tilde{\beta}_2 - \frac{1}{2}\,\tilde{\beta}_1^2 \right) + \left(\ln \lambda^{'} \right) \left(\frac{1}{\lambda^{'}} \right)^2 \left(\gamma_E\,\tilde{\beta}_1 \right. \right. \\ & \left. \left. - \frac{1}{2}\,L_{qr}\,\tilde{\beta}_1 \right) + \left(\ln \lambda^{'} \right)^2 \left(\frac{1}{\lambda^{'}} \right)^2 \left(-\frac{1}{4}\,\tilde{\beta}_1^2 \right) \right\} + \tilde{A}_4 \left\{ \frac{\lambda(2-\lambda)}{(\lambda^{'})^2} \left(\frac{1}{6} \right) + \lambda \left(\right. \right. \end{aligned}$$

$$
\begin{aligned}
&- \frac{1}{3}\Bigg)\Bigg\} + \tilde{A}_3 \left\{\frac{\lambda(2-\lambda)}{(\lambda')^2}\left(-\frac{5}{12}\,\tilde{\beta}_1 + \gamma_E - \frac{1}{2}\,L_{qr}\right) + (\ln\lambda')\left(\frac{1}{\lambda'}\right)^2\Bigg(\right.\\
&\left.- \frac{1}{2}\,\tilde{\beta}_1\right) + \lambda\left(\frac{1}{3}\,\tilde{\beta}_1 + L_{fr}\right)\Bigg\} + \tilde{A}_2\left\{\frac{\lambda(2-\lambda)}{(\lambda')^2}\left(\frac{1}{3}\,\tilde{\beta}_2 - \frac{1}{12}\,\tilde{\beta}_1^2 - \gamma_E\,\tilde{\beta}_1\right.\right.\\
&\left.\left.+ 2\,\gamma_E^2 + \frac{1}{2}\,L_{qr}\,\tilde{\beta}_1 - 2\,L_{qr}\,\gamma_E + \frac{1}{2}\,L_{qr}^2 + 2\,\zeta_2\right) + \frac{\lambda}{\lambda'}\left(-\tilde{\beta}_2 + \tilde{\beta}_1^2\right)\right.\\
&\left.+ (\ln\lambda')\left(\frac{1}{\lambda'}\right)^2\left(\frac{1}{2}\,\tilde{\beta}_1^2 - 2\,\gamma_E\,\tilde{\beta}_1 + L_{qr}\,\tilde{\beta}_1\right) + (\ln\lambda')^2\left(\frac{1}{\lambda'}\right)^2\left(\frac{1}{2}\,\tilde{\beta}_1^2\right)\right.\\
&\left.+ \lambda\left(\frac{1}{3}\,\tilde{\beta}_2 - \frac{1}{3}\,\tilde{\beta}_1^2 - L_{fr}^2\right)\right\} + \tilde{A}_1\left\{\frac{\lambda(2-\lambda)}{(\lambda')^2}\left(\frac{1}{12}\,\tilde{\beta}_3 - \frac{5}{12}\,\tilde{\beta}_1\,\tilde{\beta}_2 + \frac{1}{3}\,\tilde{\beta}_1^3\right.\right.\\
&\left.\left.+ \gamma_E\,\tilde{\beta}_2 - \gamma_E\,\tilde{\beta}_1^2 + \frac{4}{3}\,\gamma_E^3 - \frac{1}{2}\,L_{qr}\,\tilde{\beta}_2 + \frac{1}{2}\,L_{qr}\,\tilde{\beta}_1^2 - 2\,L_{qr}\,\gamma_E^2 + L_{qr}^2\,\gamma_E\right.\right.\\
&\left.\left.- \frac{1}{6}\,L_{qr}^3 + \frac{8}{3}\,\zeta_3 + 4\,\zeta_2\,\gamma_E - 2\,\zeta_2\,L_{qr}\right) + \frac{\lambda}{\lambda'}\left(\tilde{\beta}_1\,\tilde{\beta}_2 - \tilde{\beta}_1^3 - 2\,\gamma_E\,\tilde{\beta}_2\right.\right.\\
&\left.\left.+ 2\,\gamma_E\,\tilde{\beta}_1^2 + L_{qr}\,\tilde{\beta}_2 - L_{qr}\,\tilde{\beta}_1^2\right) + (\ln\lambda')\left(\frac{1}{2}\,\tilde{\beta}_3 - \frac{1}{2}\,\tilde{\beta}_1^3\right)\right.\\
&\left.+ (\ln\lambda')\,\frac{\lambda}{\lambda'}\left(\tilde{\beta}_1\,\tilde{\beta}_2 - \tilde{\beta}_1^3\right) + (\ln\lambda')\left(\frac{1}{\lambda'}\right)^2\left(-\frac{1}{2}\,\tilde{\beta}_1\,\tilde{\beta}_2 + \frac{1}{2}\,\tilde{\beta}_1^3 - 2\,\gamma_E^2\,\tilde{\beta}_1\right.\right.\\
&\left.\left.+ 2\,L_{qr}\,\gamma_E\,\tilde{\beta}_1 - \frac{1}{2}\,L_{qr}^2\,\tilde{\beta}_1 - 2\,\zeta_2\,\tilde{\beta}_1\right) + (\ln\lambda')^2\left(\frac{1}{\lambda'}\right)^2\left(\gamma_E\,\tilde{\beta}_1^2\right.\right.\\
&\left.\left.- \frac{1}{2}\,L_{qr}\,\tilde{\beta}_1^2\right) + (\ln\lambda')^3\left(\frac{1}{\lambda'}\right)^2\left(-\frac{1}{6}\,\tilde{\beta}_1^3\right) + \lambda\left(\frac{1}{3}\,\tilde{\beta}_3 - \frac{2}{3}\,\tilde{\beta}_1\,\tilde{\beta}_2 + \frac{1}{3}\,\tilde{\beta}_1^3\right.\right.\\
&\left.\left.- \frac{1}{2}\,L_{fr}^2\,\tilde{\beta}_1 + \frac{1}{3}\,L_{fr}^3\right)\Bigg\}\Bigg], \qquad \text{(A.18)}
\end{aligned}
$$

with $\lambda' = (1-\lambda)$, where $\lambda = 2a_s\beta_0 \ln N$. $\tilde{A}_i = A_i/{\beta_0}^i$, $\tilde{D}_i = D_i/{\beta_0}^i$, $\tilde{\beta}_i = \beta_i/{\beta_0}^{i+1}$. The constants g_0 are given by

$$
\begin{aligned}
g_{01} = &\Bigg[\tilde{G}_{11}\left(2\right) + G_{11}\left(2\right) + f_1\left(2\,\gamma_E\right) + B_1\left(2\,L_{qr} - 2\,L_{fr}\right) + A_1\left(2\,\gamma_E^2\right.\\
&\left.- 2\,L_{qr}\,\gamma_E + 2\,L_{fr}\,\gamma_E + 5\,\zeta_2\right)\Bigg], \qquad \text{(A.19)}\\
g_{02} = &\Bigg[\tilde{G}_{21}\left(1\right) + \tilde{G}_{12}\left(2\,\beta_0\right) + \tilde{G}_{11}\left(4\,\beta_0\,\gamma_E - 2\,\beta_0\,L_{qr}\right) + \tilde{G}_{11}^2\left(2\right)\\
&+ G_{21}\left(1\right) + G_{12}\left(2\,\beta_0\right) + G_{11}\left(-2\,\beta_0\,L_{qr}\right) + G_{11}\,\tilde{G}_{11}\left(4\right) + G_{11}^2\left(2\right)\\
&+ f_2\left(2\,\gamma_E\right) + f_1\left(2\,\beta_0\,\gamma_E^2 - 2\,\beta_0\,L_{qr}\,\gamma_E + 5\,\beta_0\,\zeta_2\right) + f_1\,\tilde{G}_{11}\left(4\,\gamma_E\right)\\
&+ f_1\,G_{11}\left(4\,\gamma_E\right) + f_1^2\left(2\,\gamma_E^2\right) + B_2\left(2\,L_{qr} - 2\,L_{fr}\right) + B_1\left(-\beta_0\,L_{qr}^2\right.
\end{aligned}
$$

$$+\beta_0\ L_{fr}^2+6\ \beta_0\ \zeta_2\Big)+B_1\ \tilde{G}_{11}\ \Big(4\ L_{qr}-4\ L_{fr}\Big)+B_1\ G_{11}\ \Big(4\ L_{qr}-4\ L_{fr}\Big)$$
$$+B_1\ f_1\ \Big(4\ L_{qr}\ \gamma_E-4\ L_{fr}\ \gamma_E\Big)+B_1^2\ \Big(2\ L_{qr}^2-4\ L_{fr}\ L_{qr}+2\ L_{fr}^2\Big)$$
$$+A_2\ \Big(2\ \gamma_E^2-2\ L_{qr}\ \gamma_E+2\ L_{fr}\ \gamma_E+5\ \zeta_2\Big)+A_1\ \Big(\frac{4}{3}\ \beta_0\ \gamma_E^3-2\ \beta_0\ L_{qr}\ \gamma_E^2$$
$$+\beta_0\ L_{qr}^2\ \gamma_E-\beta_0\ L_{fr}^2\ \gamma_E+\frac{8}{3}\ \beta_0\ \zeta_3+4\ \beta_0\ \zeta_2\ \gamma_E-5\ \beta_0\ \zeta_2\ L_{qr}\Big)$$
$$+A_1\ \tilde{G}_{11}\ \Big(4\ \gamma_E^2-4\ L_{qr}\ \gamma_E+4\ L_{fr}\ \gamma_E+10\ \zeta_2\Big)+A_1\ G_{11}\ \Big(4\ \gamma_E^2$$
$$-4\ L_{qr}\ \gamma_E+4\ L_{fr}\ \gamma_E+10\ \zeta_2\Big)+A_1\ f_1\ \Big(4\ \gamma_E^3-4\ L_{qr}\ \gamma_E^2+4\ L_{fr}\ \gamma_E^2$$
$$+10\ \zeta_2\ \gamma_E\Big)+A_1\ B_1\ \Big(4\ L_{qr}\ \gamma_E^2-4\ L_{qr}^2\ \gamma_E-4\ L_{fr}\ \gamma_E^2+8\ L_{fr}\ L_{qr}\ \gamma_E$$
$$-4\ L_{fr}^2\ \gamma_E+10\ \zeta_2\ L_{qr}-10\ \zeta_2\ L_{fr}\Big)+{A_1}^2\ \Big(2\ \gamma_E^4-4\ L_{qr}\ \gamma_E^3+2\ L_{qr}^2\ \gamma_E^2$$
$$+4\ L_{fr}\ \gamma_E^3-4\ L_{fr}\ L_{qr}\ \gamma_E^2+2\ L_{fr}^2\ \gamma_E^2+10\ \zeta_2\ \gamma_E^2-10\ \zeta_2\ L_{qr}\ \gamma_E$$
$$+10\ \zeta_2\ L_{fr}\ \gamma_E+\frac{25}{2}\ \zeta_2^2\Big)\Big], \tag{A.20}$$

$$g_{03}=\Big[\tilde{G}_{31}\ \Big(\frac{2}{3}\Big)+\tilde{G}_{22}\ \Big(\frac{4}{3}\ \beta_0\Big)+\tilde{G}_{21}\ \Big(4\ \beta_0\ \gamma_E-2\ \beta_0\ L_{qr}\Big)+\tilde{G}_{13}\ \Big(\frac{8}{3}\ \beta_0^2\Big)$$
$$+\tilde{G}_{12}\ \Big(\frac{4}{3}\ \beta_1+8\ \beta_0^2\ \gamma_E-4\ \beta_0^2\ L_{qr}\Big)+\tilde{G}_{11}\ \Big(4\ \beta_1\ \gamma_E-2\ \beta_1\ L_{qr}+8\ \beta_0^2\ \gamma_E^2$$
$$-8\ \beta_0^2\ L_{qr}\ \gamma_E+2\ \beta_0^2\ L_{qr}^2+8\ \beta_0^2\ \zeta_2\Big)+\tilde{G}_{11}\ \tilde{G}_{21}\ \Big(2\Big)+\tilde{G}_{11}\ \tilde{G}_{12}\ \Big(4\ \beta_0\Big)$$
$$+\tilde{G}_{11}^2\ \Big(8\ \beta_0\ \gamma_E-4\ \beta_0\ L_{qr}\Big)+\tilde{G}_{11}^3\ \Big(\frac{4}{3}\Big)+G_{31}\ \Big(\frac{2}{3}\Big)+G_{22}\ \Big(\frac{4}{3}\ \beta_0\Big)$$
$$+G_{21}\ \Big(-2\ \beta_0\ L_{qr}\Big)+G_{21}\ \tilde{G}_{11}\ \Big(2\Big)+G_{13}\ \Big(\frac{8}{3}\ \beta_0^2\Big)+G_{12}\ \Big(\frac{4}{3}\ \beta_1$$
$$-4\ \beta_0^2\ L_{qr}\Big)+G_{12}\ \tilde{G}_{11}\ \Big(4\ \beta_0\Big)+G_{11}\ \Big(-2\ \beta_1\ L_{qr}+2\ \beta_0^2\ L_{qr}^2-12\ \beta_0^2\ \zeta_2\Big)$$
$$+G_{11}\ \tilde{G}_{21}\ \Big(2\Big)+G_{11}\ \tilde{G}_{12}\ \Big(4\ \beta_0\Big)+G_{11}\ \tilde{G}_{11}\ \Big(8\ \beta_0\ \gamma_E-8\ \beta_0\ L_{qr}\Big)$$
$$+G_{11}\ \tilde{G}_{11}^2\ \Big(4\Big)+G_{11}\ G_{21}\ \Big(2\Big)+G_{11}\ G_{12}\ \Big(4\ \beta_0\Big)+G_{11}^2\ \Big(-4\ \beta_0\ L_{qr}\Big)$$
$$+G_{11}^2\ \tilde{G}_{11}\ \Big(4\Big)+G_{11}^3\ \Big(\frac{4}{3}\Big)+f_3\ \Big(2\ \gamma_E\Big)+f_2\ \Big(4\ \beta_0\ \gamma_E^2-4\ \beta_0\ L_{qr}\ \gamma_E$$
$$+10\ \beta_0\ \zeta_2\Big)+f_2\ \tilde{G}_{11}\ \Big(4\ \gamma_E\Big)+f_2\ G_{11}\ \Big(4\ \gamma_E\Big)+f_1\ \Big(2\ \beta_1\ \gamma_E^2$$

$$
\begin{aligned}
&- 2\ \beta_1\ L_{qr}\ \gamma_E + 5\ \beta_1\ \zeta_2 + \frac{8}{3}\ \beta_0^2\ \gamma_E^3 - 4\ \beta_0^2\ L_{qr}\ \gamma_E^2 + 2\ \beta_0^2\ L_{qr}^2\ \gamma_E + \frac{16}{3}\ \beta_0^2\ \zeta_3 \\
&+ 8\ \beta_0^2\ \zeta_2\ \gamma_E - 10\ \beta_0^2\ \zeta_2\ L_{qr}\Big) + f_1\ \tilde{G}_{21}\ \Big(2\ \gamma_E\Big) + f_1\ \tilde{G}_{12}\ \Big(4\ \beta_0\ \gamma_E\Big) \\
&+ f_1\ \tilde{G}_{11}\ \Big(12\ \beta_0\ \gamma_E^2 - 8\ \beta_0\ L_{qr}\ \gamma_E + 10\ \beta_0\ \zeta_2\Big) + f_1\ \tilde{G}_{11}^2\ \Big(4\ \gamma_E\Big) \\
&+ f_1\ G_{21}\ \Big(2\ \gamma_E\Big) + f_1\ G_{12}\ \Big(4\ \beta_0\ \gamma_E\Big) + f_1\ G_{11}\ \Big(4\ \beta_0\ \gamma_E^2 - 8\ \beta_0\ L_{qr}\ \gamma_E \\
&+ 10\ \beta_0\ \zeta_2\Big) + f_1\ G_{11}\ \tilde{G}_{11}\ \Big(8\ \gamma_E\Big) + f_1\ G_{11}^2\ \Big(4\ \gamma_E\Big) + f_1\ f_2\ \Big(4\ \gamma_E^2\Big) \\
&+ f_1^2\ \Big(4\ \beta_0\ \gamma_E^3 - 4\ \beta_0\ L_{qr}\ \gamma_E^2 + 10\ \beta_0\ \zeta_2\ \gamma_E\Big) + f_1^2\ \tilde{G}_{11}\ \Big(4\ \gamma_E^2\Big) \\
&+ f_1^2\ G_{11}\ \Big(4\ \gamma_E^2\Big) + f_1^3\ \Big(\frac{4}{3}\ \gamma_E^3\Big) + B_3\ \Big(2\ L_{qr} - 2\ L_{fr}\Big) + B_2\ \Big(- 2\ \beta_0\ L_{qr}^2 \\
&+ 2\ \beta_0\ L_{fr}^2 + 12\ \beta_0\ \zeta_2\Big) + B_2\ \tilde{G}_{11}\ \Big(4\ L_{qr} - 4\ L_{fr}\Big) + B_2\ G_{11}\ \Big(4\ L_{qr} \\
&- 4\ L_{fr}\Big) + B_2\ f_1\ \Big(4\ L_{qr}\ \gamma_E - 4\ L_{fr}\ \gamma_E\Big) + B_1\ \Big(- \beta_1\ L_{qr}^2 + \beta_1\ L_{fr}^2 \\
&+ 6\ \beta_1\ \zeta_2 + \frac{2}{3}\ \beta_0^2\ L_{qr}^3 - \frac{2}{3}\ \beta_0^2\ L_{fr}^3 - 12\ \beta_0^2\ \zeta_2\ L_{qr}\Big) + B_1\ \tilde{G}_{21}\ \Big(2\ L_{qr} - 2\ L_{fr}\Big) \\
&+ B_1\ \tilde{G}_{12}\ \Big(4\ \beta_0\ L_{qr} - 4\ \beta_0\ L_{fr}\Big) + B_1\ \tilde{G}_{11}\ \Big(8\ \beta_0\ L_{qr}\ \gamma_E - 6\ \beta_0\ L_{qr}^2 \\
&- 8\ \beta_0\ L_{fr}\ \gamma_E + 4\ \beta_0\ L_{fr}\ L_{qr} + 2\ \beta_0\ L_{fr}^2 + 12\ \beta_0\ \zeta_2\Big) + B_1\ \tilde{G}_{11}^2\ \Big(4\ L_{qr} \\
&- 4\ L_{fr}\Big) + B_1\ G_{21}\ \Big(2\ L_{qr} - 2\ L_{fr}\Big) + B_1\ G_{12}\ \Big(4\ \beta_0\ L_{qr} - 4\ \beta_0\ L_{fr}\Big) \\
&+ B_1\ G_{11}\ \Big(- 6\ \beta_0\ L_{qr}^2 + 4\ \beta_0\ L_{fr}\ L_{qr} + 2\ \beta_0\ L_{fr}^2 + 12\ \beta_0\ \zeta_2\Big) \\
&+ B_1\ G_{11}\ \tilde{G}_{11}\ \Big(8\ L_{qr} - 8\ L_{fr}\Big) + B_1\ G_{11}^2\ \Big(4\ L_{qr} - 4\ L_{fr}\Big) \\
&+ B_1\ f_2\ \Big(4\ L_{qr}\ \gamma_E - 4\ L_{fr}\ \gamma_E\Big) + B_1\ f_1\ \Big(4\ \beta_0\ L_{qr}\ \gamma_E^2 - 6\ \beta_0\ L_{qr}^2\ \gamma_E \\
&- 4\ \beta_0\ L_{fr}\ \gamma_E^2 + 4\ \beta_0\ L_{fr}\ L_{qr}\ \gamma_E + 2\ \beta_0\ L_{fr}^2\ \gamma_E + 12\ \beta_0\ \zeta_2\ \gamma_E + 10\ \beta_0\ \zeta_2\ L_{qr} \\
&- 10\ \beta_0\ \zeta_2\ L_{fr}\Big) + B_1\ f_1\ \tilde{G}_{11}\ \Big(8\ L_{qr}\ \gamma_E - 8\ L_{fr}\ \gamma_E\Big) + B_1\ f_1\ G_{11}\ \Big(8\ L_{qr}\ \gamma_E \\
&- 8\ L_{fr}\ \gamma_E\Big) + B_1\ f_1^2\ \Big(4\ L_{qr}\ \gamma_E^2 - 4\ L_{fr}\ \gamma_E^2\Big) + B_1\ B_2\ \Big(4\ L_{qr}^2 - 8\ L_{fr}\ L_{qr} \\
&+ 4\ L_{fr}^2\Big) + B_1^2\ \Big(- 2\ \beta_0\ L_{qr}^3 + 2\ \beta_0\ L_{fr}\ L_{qr}^2 + 2\ \beta_0\ L_{fr}^2\ L_{qr} - 2\ \beta_0\ L_{fr}^3
\end{aligned}
$$

$$+ 12\ \beta_0\ \zeta_2\ L_{qr} - 12\ \beta_0\ \zeta_2\ L_{fr}\Big) + B_1^2\ \tilde{G}_{11}\ \Big(4\ L_{qr}^2 - 8\ L_{fr}\ L_{qr} + 4\ L_{fr}^2\Big)$$
$$+ B_1^2\ G_{11}\ \Big(4\ L_{qr}^2 - 8\ L_{fr}\ L_{qr} + 4\ L_{fr}^2\Big) + B_1^2\ f_1\ \Big(4\ L_{qr}^2\ \gamma_E - 8\ L_{fr}\ L_{qr}\ \gamma_E$$
$$+ 4\ L_{fr}^2\ \gamma_E\Big) + B_1^3\ \Big(\frac{4}{3}\ L_{qr}^3 - 4\ L_{fr}\ L_{qr}^2 + 4\ L_{fr}^2\ L_{qr} - \frac{4}{3}\ L_{fr}^3\Big) + A_3\ \Big(2\ \gamma_E^2$$
$$- 2\ L_{qr}\ \gamma_E + 2\ L_{fr}\ \gamma_E + 5\ \zeta_2\Big) + A_2\ \Big(\frac{8}{3}\ \beta_0\ \gamma_E^3 - 4\ \beta_0\ L_{qr}\ \gamma_E^2 + 2\ \beta_0\ L_{qr}^2\ \gamma_E$$
$$- 2\ \beta_0\ L_{fr}^2\ \gamma_E + \frac{16}{3}\ \beta_0\ \zeta_3 + 8\ \beta_0\ \zeta_2\ \gamma_E - 10\ \beta_0\ \zeta_2\ L_{qr}\Big) + A_2\ \tilde{G}_{11}\ \Big(4\ \gamma_E^2$$
$$- 4\ L_{qr}\ \gamma_E + 4\ L_{fr}\ \gamma_E + 10\ \zeta_2\Big) + A_2\ G_{11}\ \Big(4\ \gamma_E^2 - 4\ L_{qr}\ \gamma_E + 4\ L_{fr}\ \gamma_E$$
$$+ 10\ \zeta_2\Big) + A_2\ f_1\ \Big(4\ \gamma_E^3 - 4\ L_{qr}\ \gamma_E^2 + 4\ L_{fr}\ \gamma_E^2 + 10\ \zeta_2\ \gamma_E\Big)$$
$$+ A_2\ B_1\ \Big(4\ L_{qr}\ \gamma_E^2 - 4\ L_{qr}^2\ \gamma_E - 4\ L_{fr}\ \gamma_E^2 + 8\ L_{fr}\ L_{qr}\ \gamma_E - 4\ L_{fr}^2\ \gamma_E$$
$$+ 10\ \zeta_2\ L_{qr} - 10\ \zeta_2\ L_{fr}\Big) + A_1\ \Big(\frac{4}{3}\ \beta_1\ \gamma_E^3 - 2\ \beta_1\ L_{qr}\ \gamma_E^2 + \beta_1\ L_{qr}^2\ \gamma_E$$
$$- \beta_1\ L_{fr}^2\ \gamma_E + \frac{8}{3}\ \beta_1\ \zeta_3 + 4\ \beta_1\ \zeta_2\ \gamma_E - 5\ \beta_1\ \zeta_2\ L_{qr} + \frac{4}{3}\ \beta_0^2\ \gamma_E^4 - \frac{8}{3}\ \beta_0^2\ L_{qr}\ \gamma_E^3$$
$$+ 2\ \beta_0^2\ L_{qr}^2\ \gamma_E^2 - \frac{2}{3}\ \beta_0^2\ L_{qr}^3\ \gamma_E + \frac{2}{3}\ \beta_0^2\ L_{fr}^3\ \gamma_E + \frac{32}{3}\ \beta_0^2\ \zeta_3\ \gamma_E - \frac{16}{3}\ \beta_0^2\ \zeta_3\ L_{qr}$$
$$+ 8\ \beta_0^2\ \zeta_2\ \gamma_E^2 - 8\ \beta_0^2\ \zeta_2\ L_{qr}\ \gamma_E + 5\ \beta_0^2\ \zeta_2\ L_{qr}^2 + \frac{21}{5}\ \beta_0^2\ \zeta_2^2\Big) + A_1\ \tilde{G}_{21}\ \Big(2\ \gamma_E^2$$
$$- 2\ L_{qr}\ \gamma_E + 2\ L_{fr}\ \gamma_E + 5\ \zeta_2\Big) + A_1\ \tilde{G}_{12}\ \Big(4\ \beta_0\ \gamma_E^2 - 4\ \beta_0\ L_{qr}\ \gamma_E$$
$$+ 4\ \beta_0\ L_{fr}\ \gamma_E + 10\ \beta_0\ \zeta_2\Big) + A_1\ \tilde{G}_{11}\ \Big(\frac{32}{3}\ \beta_0\ \gamma_E^3 - 16\ \beta_0\ L_{qr}\ \gamma_E^2$$
$$+ 6\ \beta_0\ L_{qr}^2\ \gamma_E + 8\ \beta_0\ L_{fr}\ \gamma_E^2 - 4\ \beta_0\ L_{fr}\ L_{qr}\ \gamma_E - 2\ \beta_0\ L_{fr}^2\ \gamma_E + \frac{16}{3}\ \beta_0\ \zeta_3$$
$$+ 28\ \beta_0\ \zeta_2\ \gamma_E - 20\ \beta_0\ \zeta_2\ L_{qr}\Big) + A_1\ \tilde{G}_{11}^2\ \Big(4\ \gamma_E^2 - 4\ L_{qr}\ \gamma_E + 4\ L_{fr}\ \gamma_E$$
$$+ 10\ \zeta_2\Big) + A_1\ G_{21}\ \Big(2\ \gamma_E^2 - 2\ L_{qr}\ \gamma_E + 2\ L_{fr}\ \gamma_E + 5\ \zeta_2\Big)$$
$$+ A_1\ G_{12}\ \Big(4\ \beta_0\ \gamma_E^2 - 4\ \beta_0\ L_{qr}\ \gamma_E + 4\ \beta_0\ L_{fr}\ \gamma_E + 10\ \beta_0\ \zeta_2\Big)$$
$$+ A_1\ G_{11}\ \Big(\frac{8}{3}\ \beta_0\ \gamma_E^3 - 8\ \beta_0\ L_{qr}\ \gamma_E^2 + 6\ \beta_0\ L_{qr}^2\ \gamma_E - 4\ \beta_0\ L_{fr}\ L_{qr}\ \gamma_E$$
$$- 2\ \beta_0\ L_{fr}^2\ \gamma_E + \frac{16}{3}\ \beta_0\ \zeta_3 + 8\ \beta_0\ \zeta_2\ \gamma_E - 20\ \beta_0\ \zeta_2\ L_{qr}\Big) + A_1\ G_{11}\ \tilde{G}_{11}\ \Big(8\ \gamma_E^2$$

$$
\begin{aligned}
&- 8\ L_{qr}\ \gamma_E + 8\ L_{fr}\ \gamma_E + 20\ \zeta_2\Big) + A_1\ G_{11}^2\ \Big(4\ \gamma_E^2 - 4\ L_{qr}\ \gamma_E + 4\ L_{fr}\ \gamma_E \\
&+ 10\ \zeta_2\Big) + A_1\ f_2\ \Big(4\ \gamma_E^3 - 4\ L_{qr}\ \gamma_E^2 + 4\ L_{fr}\ \gamma_E^2 + 10\ \zeta_2\ \gamma_E\Big) \\
&+ A_1\ f_1\ \Big(\frac{20}{3}\ \beta_0\ \gamma_E^4 - 12\ \beta_0\ L_{qr}\ \gamma_E^3 + 6\ \beta_0\ L_{qr}^2\ \gamma_E^2 + 4\ \beta_0\ L_{fr}\ \gamma_E^3 \\
&- 4\ \beta_0\ L_{fr}\ L_{qr}\ \gamma_E^2 - 2\ \beta_0\ L_{fr}^2\ \gamma_E^2 + \frac{16}{3}\ \beta_0\ \zeta_3\ \gamma_E + 28\ \beta_0\ \zeta_2\ \gamma_E^2 \\
&- 30\ \beta_0\ \zeta_2\ L_{qr}\ \gamma_E + 10\ \beta_0\ \zeta_2\ L_{fr}\ \gamma_E + 25\ \beta_0\ \zeta_2^2\Big) + A_1\ f_1\ \tilde{G}_{11}\ \Big(8\ \gamma_E^3 \\
&- 8\ L_{qr}\ \gamma_E^2 + 8\ L_{fr}\ \gamma_E^2 + 20\ \zeta_2\ \gamma_E\Big) + A_1\ f_1\ G_{11}\ \Big(8\ \gamma_E^3 - 8\ L_{qr}\ \gamma_E^2 \\
&+ 8\ L_{fr}\ \gamma_E^2 + 20\ \zeta_2\ \gamma_E\Big) + A_1\ f_1^2\ \Big(4\ \gamma_E^4 - 4\ L_{qr}\ \gamma_E^3 + 4\ L_{fr}\ \gamma_E^3 + 10\ \zeta_2\ \gamma_E^2\Big) \\
&+ A_1\ B_2\ \Big(4\ L_{qr}\ \gamma_E^2 - 4\ L_{qr}^2\ \gamma_E - 4\ L_{fr}\ \gamma_E^2 + 8\ L_{fr}\ L_{qr}\ \gamma_E - 4\ L_{fr}^2\ \gamma_E \\
&+ 10\ \zeta_2\ L_{qr} - 10\ \zeta_2\ L_{fr}\Big) + A_1\ B_1\ \Big(\frac{8}{3}\ \beta_0\ L_{qr}\ \gamma_E^3 - 6\ \beta_0\ L_{qr}^2\ \gamma_E^2 \\
&+ 4\ \beta_0\ L_{qr}^3\ \gamma_E - \frac{8}{3}\ \beta_0\ L_{fr}\ \gamma_E^3 + 4\ \beta_0\ L_{fr}\ L_{qr}\ \gamma_E^2 - 4\ \beta_0\ L_{fr}\ L_{qr}^2\ \gamma_E \\
&+ 2\ \beta_0\ L_{fr}^2\ \gamma_E^2 - 4\ \beta_0\ L_{fr}^2\ L_{qr}\ \gamma_E + 4\ \beta_0\ L_{fr}^3\ \gamma_E + \frac{16}{3}\ \beta_0\ \zeta_3\ L_{qr} \\
&- \frac{16}{3}\ \beta_0\ \zeta_3\ L_{fr} + 12\ \beta_0\ \zeta_2\ \gamma_E^2 - 4\ \beta_0\ \zeta_2\ L_{qr}\ \gamma_E - 15\ \beta_0\ \zeta_2\ L_{qr}^2 \\
&+ 4\ \beta_0\ \zeta_2\ L_{fr}\ \gamma_E + 10\ \beta_0\ \zeta_2\ L_{fr}\ L_{qr} + 5\ \beta_0\ \zeta_2\ L_{fr}^2 + 30\ \beta_0\ \zeta_2^2\Big) \\
&+ A_1\ B_1\ \tilde{G}_{11}\ \Big(8\ L_{qr}\ \gamma_E^2 - 8\ L_{qr}^2\ \gamma_E - 8\ L_{fr}\ \gamma_E^2 + 16\ L_{fr}\ L_{qr}\ \gamma_E - 8\ L_{fr}^2\ \gamma_E \\
&+ 20\ \zeta_2\ L_{qr} - 20\ \zeta_2\ L_{fr}\Big) + A_1\ B_1\ G_{11}\ \Big(8\ L_{qr}\ \gamma_E^2 - 8\ L_{qr}^2\ \gamma_E - 8\ L_{fr}\ \gamma_E^2 \\
&+ 16\ L_{fr}\ L_{qr}\ \gamma_E - 8\ L_{fr}^2\ \gamma_E + 20\ \zeta_2\ L_{qr} - 20\ \zeta_2\ L_{fr}\Big) + A_1\ B_1\ f_1\ \Big(8\ L_{qr}\ \gamma_E^3 \\
&- 8\ L_{qr}^2\ \gamma_E^2 - 8\ L_{fr}\ \gamma_E^3 + 16\ L_{fr}\ L_{qr}\ \gamma_E^2 - 8\ L_{fr}^2\ \gamma_E^2 + 20\ \zeta_2\ L_{qr}\ \gamma_E \\
&- 20\ \zeta_2\ L_{fr}\ \gamma_E\Big) + A_1\ B_1^2\ \Big(4\ L_{qr}^2\ \gamma_E^2 - 4\ L_{qr}^3\ \gamma_E - 8\ L_{fr}\ L_{qr}\ \gamma_E^2 \\
&+ 12\ L_{fr}\ L_{qr}^2\ \gamma_E + 4\ L_{fr}^2\ \gamma_E^2 - 12\ L_{fr}^2\ L_{qr}\ \gamma_E + 4\ L_{fr}^3\ \gamma_E + 10\ \zeta_2\ L_{qr}^2 \\
&- 20\ \zeta_2\ L_{fr}\ L_{qr} + 10\ \zeta_2\ L_{fr}^2\Big) + A_1\ A_2\ \Big(4\ \gamma_E^4 - 8\ L_{qr}\ \gamma_E^3 + 4\ L_{qr}^2\ \gamma_E^2 \\
&+ 8\ L_{fr}\ \gamma_E^3 - 8\ L_{fr}\ L_{qr}\ \gamma_E^2 + 4\ L_{fr}^2\ \gamma_E^2 + 20\ \zeta_2\ \gamma_E^2 - 20\ \zeta_2\ L_{qr}\ \gamma_E
\end{aligned}
$$

$$
\begin{aligned}
&+ 20\ \zeta_2\ L_{fr}\ \gamma_E + 25\ \zeta_2^2\Big) + {A_1}^2\ \Big(\frac{8}{3}\ \beta_0\ \gamma_E^5 - \frac{20}{3}\ \beta_0\ L_{qr}\ \gamma_E^4 + 6\ \beta_0\ L_{qr}^2\ \gamma_E^3 \\
&- 2\ \beta_0\ L_{qr}^3\ \gamma_E^2 + \frac{8}{3}\ \beta_0\ L_{fr}\ \gamma_E^4 - 4\ \beta_0\ L_{fr}\ L_{qr}\ \gamma_E^3 + 2\ \beta_0\ L_{fr}\ L_{qr}^2\ \gamma_E^2 \\
&- 2\ \beta_0\ L_{fr}^2\ \gamma_E^3 + 2\ \beta_0\ L_{fr}^2\ L_{qr}\ \gamma_E^2 - 2\ \beta_0\ L_{fr}^3\ \gamma_E^2 + \frac{16}{3}\ \beta_0\ \zeta_3\ \gamma_E^2 \\
&- \frac{16}{3}\ \beta_0\ \zeta_3\ L_{qr}\ \gamma_E + \frac{16}{3}\ \beta_0\ \zeta_3\ L_{fr}\ \gamma_E + \frac{44}{3}\ \beta_0\ \zeta_2\ \gamma_E^3 - 28\ \beta_0\ \zeta_2\ L_{qr}\ \gamma_E^2 \\
&+ 15\ \beta_0\ \zeta_2\ L_{qr}^2\ \gamma_E + 8\ \beta_0\ \zeta_2\ L_{fr}\ \gamma_E^2 - 10\ \beta_0\ \zeta_2\ L_{fr}\ L_{qr}\ \gamma_E - 5\ \beta_0\ \zeta_2\ L_{fr}^2\ \gamma_E \\
&+ \frac{40}{3}\ \beta_0\ \zeta_2\ \zeta_3 + 20\ \beta_0\ \zeta_2^2\ \gamma_E - 25\ \beta_0\ \zeta_2^2\ L_{qr}\Big) + {A_1}^2\ \tilde{G}_{11}\ \Big(4\ \gamma_E^4 - 8\ L_{qr}\ \gamma_E^3 \\
&+ 4\ L_{qr}^2\ \gamma_E^2 + 8\ L_{fr}\ \gamma_E^3 - 8\ L_{fr}\ L_{qr}\ \gamma_E^2 + 4\ L_{fr}^2\ \gamma_E^2 + 20\ \zeta_2\ \gamma_E^2 - 20\ \zeta_2\ L_{qr}\ \gamma_E \\
&+ 20\ \zeta_2\ L_{fr}\ \gamma_E + 25\ \zeta_2^2\Big) + {A_1}^2\ G_{11}\ \Big(4\ \gamma_E^4 - 8\ L_{qr}\ \gamma_E^3 + 4\ L_{qr}^2\ \gamma_E^2 + 8\ L_{fr}\ \gamma_E^3 \\
&- 8\ L_{fr}\ L_{qr}\ \gamma_E^2 + 4\ L_{fr}^2\ \gamma_E^2 + 20\ \zeta_2\ \gamma_E^2 - 20\ \zeta_2\ L_{qr}\ \gamma_E + 20\ \zeta_2\ L_{fr}\ \gamma_E \\
&+ 25\ \zeta_2^2\Big) + {A_1}^2\ f_1\ \Big(4\ \gamma_E^5 - 8\ L_{qr}\ \gamma_E^4 + 4\ L_{qr}^2\ \gamma_E^3 + 8\ L_{fr}\ \gamma_E^4 - 8\ L_{fr}\ L_{qr}\ \gamma_E^3 \\
&+ 4\ L_{fr}^2\ \gamma_E^3 + 20\ \zeta_2\ \gamma_E^3 - 20\ \zeta_2\ L_{qr}\ \gamma_E^2 + 20\ \zeta_2\ L_{fr}\ \gamma_E^2 + 25\ \zeta_2^2\ \gamma_E\Big) \\
&+ {A_1}^2\ B_1\ \Big(4\ L_{qr}\ \gamma_E^4 - 8\ L_{qr}^2\ \gamma_E^3 + 4\ L_{qr}^3\ \gamma_E^2 - 4\ L_{fr}\ \gamma_E^4 + 16\ L_{fr}\ L_{qr}\ \gamma_E^3 \\
&- 12\ L_{fr}\ L_{qr}^2\ \gamma_E^2 - 8\ L_{fr}^2\ \gamma_E^3 + 12\ L_{fr}^2\ L_{qr}\ \gamma_E^2 - 4\ L_{fr}^3\ \gamma_E^2 + 20\ \zeta_2\ L_{qr}\ \gamma_E^2 \\
&- 20\ \zeta_2\ L_{qr}^2\ \gamma_E - 20\ \zeta_2\ L_{fr}\ \gamma_E^2 + 40\ \zeta_2\ L_{fr}\ L_{qr}\ \gamma_E - 20\ \zeta_2\ L_{fr}^2\ \gamma_E \\
&+ 25\ \zeta_2^2\ L_{qr} - 25\ \zeta_2^2\ L_{fr}\Big) + {A_1}^3\ \Big(\frac{4}{3}\ \gamma_E^6 - 4\ L_{qr}\ \gamma_E^5 + 4\ L_{qr}^2\ \gamma_E^4 - \frac{4}{3}\ L_{qr}^3\ \gamma_E^3 \\
&+ 4\ L_{fr}\ \gamma_E^5 - 8\ L_{fr}\ L_{qr}\ \gamma_E^4 + 4\ L_{fr}\ L_{qr}^2\ \gamma_E^3 + 4\ L_{fr}^2\ \gamma_E^4 - 4\ L_{fr}^2\ L_{qr}\ \gamma_E^3 \\
&+ \frac{4}{3}\ L_{fr}^3\ \gamma_E^3 + 10\ \zeta_2\ \gamma_E^4 - 20\ \zeta_2\ L_{qr}\ \gamma_E^3 + 10\ \zeta_2\ L_{qr}^2\ \gamma_E^2 + 20\ \zeta_2\ L_{fr}\ \gamma_E^3 \\
&- 20\ \zeta_2\ L_{fr}\ L_{qr}\ \gamma_E^2 + 10\ \zeta_2\ L_{fr}^2\ \gamma_E^2 + 25\ \zeta_2^2\ \gamma_E^2 - 25\ \zeta_2^2\ L_{qr}\ \gamma_E + 25\ \zeta_2^2\ L_{fr}\ \gamma_E \\
&+ \frac{125}{6}\ \zeta_2^3\Big)\Big]\,. \qquad \text{(A.21)}
\end{aligned}
$$

A.3 Resummation ingredients for the Soft exponentiation

In the case for Soft exponentiation, all the terms coming from the soft function are exponentiated and hence this means all the contribution to the finite (N-independent) piece from the soft function is also being exponentiated. This renders the g_0 coefficients of the Standard $\overline{N}$ threshold and changes also the resumed exponent. We write these changes below in terms of the Standard $\overline{N}$ threshold exponent and pre-factor,

$$\begin{aligned} g_1^{\rm Soft} &= \bar{g}_1\,, \\ g_2^{\rm Soft} &= \bar{g}_2 + a_s\,\Delta_{g_2}^{\rm Soft}\,, \\ g_3^{\rm Soft} &= \bar{g}_3 + a_s^2\,\Delta_{g_3}^{\rm Soft}\,, \\ g_4^{\rm Soft} &= \bar{g}_4 + a_s^3\,\Delta_{g_4}^{\rm Soft}\,, \end{aligned} \tag{A.22}$$

where the coefficients $\Delta_{g_i}^{\rm Soft}$ are given as,

$$\Delta_{g_1}^{\rm Soft} = \left[\tilde{G}_{11}\left(2\right) + f_1\left(-L_{qr}\right) + A_1\left(\frac{1}{2}\,L_{qr}^2 + 2\,\zeta_2\right)\right], \tag{A.23}$$

$$\begin{aligned} \Delta_{g_2}^{\rm Soft} = \Bigg[&\tilde{G}_{21}\left(1\right) + \tilde{G}_{12}\left(2\,\beta_0\right) + \tilde{G}_{11}\left(-2\,\beta_0\,L_{qr}\right) + f_2\left(-L_{qr}\right) \\ &+ f_1\left(\frac{1}{2}\,\beta_0\,L_{qr}^2 + 2\,\beta_0\,\zeta_2\right) + A_2\left(\frac{1}{2}\,L_{qr}^2 + 2\,\zeta_2\right) + A_1\left(-\frac{1}{6}\,\beta_0\,L_{qr}^3 \right. \\ &\left. + \frac{8}{3}\,\beta_0\,\zeta_3 - 2\,\beta_0\,\zeta_2\,L_{qr}\right)\Bigg], \end{aligned} \tag{A.24}$$

$$\begin{aligned} \Delta_{g_3}^{\rm Soft} = \Bigg[&\tilde{G}_{31}\left(\frac{2}{3}\right) + \tilde{G}_{22}\left(\frac{4}{3}\,\beta_0\right) + \tilde{G}_{21}\left(-2\,\beta_0\,L_{qr}\right) + \tilde{G}_{13}\left(\frac{8}{3}\,\beta_0^2\right) \\ &+ \tilde{G}_{12}\left(\frac{4}{3}\,\beta_1 - 4\,\beta_0^2\,L_{qr}\right) + \tilde{G}_{11}\left(-2\,\beta_1\,L_{qr} + 2\,\beta_0^2\,L_{qr}^2 + 8\,\beta_0^2\,\zeta_2\right) \\ &+ f_3\left(-L_{qr}\right) + f_2\left(\beta_0\,L_{qr}^2 + 4\,\beta_0\,\zeta_2\right) + f_1\left(\frac{1}{2}\,\beta_1\,L_{qr}^2 + 2\,\beta_1\,\zeta_2\right. \\ &\left. - \frac{1}{3}\,\beta_0^2\,L_{qr}^3 + \frac{16}{3}\,\beta_0^2\,\zeta_3 - 4\,\beta_0^2\,\zeta_2\,L_{qr}\right) + A_3\left(\frac{1}{2}\,L_{qr}^2 + 2\,\zeta_2\right) + A_2\left(\right. \\ &\left. - \frac{1}{3}\,\beta_0\,L_{qr}^3 + \frac{16}{3}\,\beta_0\,\zeta_3 - 4\,\beta_0\,\zeta_2\,L_{qr}\right) + A_1\left(-\frac{1}{6}\,\beta_1\,L_{qr}^3 + \frac{8}{3}\,\beta_1\,\zeta_3\right. \end{aligned}$$

$$- 2\ \beta_1\ \zeta_2\ L_{qr} + \frac{1}{12}\ \beta_0^2\ L_{qr}^4 - \frac{16}{3}\ \beta_0^2\ \zeta_3\ L_{qr} + 2\ \beta_0^2\ \zeta_2\ L_{qr}^2 + \frac{36}{5}\ \beta_0^2\ \zeta_2^2\Bigg)\Bigg]. \tag{A.25}$$

The N-independent constants in the case can be put in the following form:

$$\begin{aligned} g_{01}^{\text{Soft}} &= \bar{g}_{01} + a_s\ \Delta_{g01}^{\text{Soft}}, \\ g_{02}^{\text{Soft}} &= \bar{g}_{02} + a_s^2\ \Delta_{g02}^{\text{Soft}}, \\ g_{03}^{\text{Soft}} &= \bar{g}_{03} + a_s^3\ \Delta_{g03}^{\text{Soft}}, \end{aligned} \tag{A.26}$$

where the coefficients $\Delta_{g0i}^{\text{Soft}}$ are given by,

$$\Delta_{g01}^{\text{Soft}} = \Bigg[\tilde{G}_{11}\ \Big(-2\Big) + f_1\ \Big(L_{qr}\Big) + A_1\ \Big(-\frac{1}{2}\ L_{qr}^2 - 2\ \zeta_2\Big)\Bigg], \tag{A.27}$$

$$\begin{aligned} \Delta_{g02}^{\text{Soft}} = \Bigg[&\tilde{G}_{21}\ \Big(-1\Big) + \tilde{G}_{12}\ \Big(-2\ \beta_0\Big) + \tilde{G}_{11}\ \Big(2\ \beta_0\ L_{qr}\Big) + \tilde{G}_{11}^2\ \Big(-2\Big) \\ &+ G_{11}\ \tilde{G}_{11}\ \Big(-4\Big) + f_2\ \Big(L_{qr}\Big) + f_1\ \Big(-\frac{1}{2}\ \beta_0\ L_{qr}^2 - 2\ \beta_0\ \zeta_2\Big) \\ &+ f_1\ G_{11}\ \Big(2\ L_{qr}\Big) + f_1^2\ \Big(\frac{1}{2}\ L_{qr}^2\Big) + B_1\ \tilde{G}_{11}\ \Big(-4\ L_{qr} + 4\ L_{fr}\Big) \\ &+ B_1\ f_1\ \Big(2\ L_{qr}^2 - 2\ L_{fr}\ L_{qr}\Big) + A_2\ \Big(-\frac{1}{2}\ L_{qr}^2 - 2\ \zeta_2\Big) + A_1\ \Big(\frac{1}{6}\ \beta_0\ L_{qr}^3 \\ &- \frac{8}{3}\ \beta_0\ \zeta_3 + 2\ \beta_0\ \zeta_2\ L_{qr}\Big) + A_1\ \tilde{G}_{11}\ \Big(-10\ \zeta_2\Big) + A_1\ G_{11}\ \Big(-L_{qr}^2 - 4\ \zeta_2\Big) \\ &+ A_1\ f_1\ \Big(-\frac{1}{2}\ L_{qr}^3 + 3\ \zeta_2\ L_{qr}\Big) + A_1\ B_1\ \Big(-L_{qr}^3 + L_{fr}\ L_{qr}^2 - 4\ \zeta_2\ L_{qr} \\ &+ 4\ \zeta_2\ L_{fr}\Big) + {A_1}^2\ \Big(\frac{1}{8}\ L_{qr}^4 - \frac{3}{2}\ \zeta_2\ L_{qr}^2 - 8\ \zeta_2^2\Big)\Bigg], \end{aligned} \tag{A.28}$$

$$\begin{aligned} \Delta_{g03}^{\text{Soft}} = \Bigg[&\tilde{G}_{31}\ \Big(-\frac{2}{3}\Big) + \tilde{G}_{22}\ \Big(-\frac{4}{3}\ \beta_0\Big) + \tilde{G}_{21}\ \Big(2\ \beta_0\ L_{qr}\Big) + \tilde{G}_{13}\ \Big(-\frac{8}{3}\ \beta_0^2\Big) \\ &+ \tilde{G}_{12}\ \Big(-\frac{4}{3}\ \beta_1 + 4\ \beta_0^2\ L_{qr}\Big) + \tilde{G}_{11}\ \Big(2\ \beta_1\ L_{qr} - 2\ \beta_0^2\ L_{qr}^2 - 8\ \beta_0^2\ \zeta_2\Big) \\ &+ \tilde{G}_{11}\ \tilde{G}_{21}\ \Big(-2\Big) + \tilde{G}_{11}\ \tilde{G}_{12}\ \Big(-4\ \beta_0\Big) + \tilde{G}_{11}^2\ \Big(4\ \beta_0\ L_{qr}\Big) + \tilde{G}_{11}^3\ \Big(-\frac{4}{3}\Big) \\ &+ G_{21}\ \tilde{G}_{11}\ \Big(-2\Big) + G_{12}\ \tilde{G}_{11}\ \Big(-4\ \beta_0\Big) + G_{11}\ \tilde{G}_{21}\ \Big(-2\Big) + G_{11}\ \tilde{G}_{12}\ \Big(\end{aligned} \tag{A.29}$$

$$
- 4\ \beta_0\Big) + G_{11}\ \tilde{G}_{11}\ \Big(8\ \beta_0\ L_{qr}\Big) + G_{11}\ \tilde{G}_{11}^2\ \Big(-4\Big) + G_{11}^2\ \tilde{G}_{11}\ \Big(-4\Big)
+ f_3\ \Big(L_{qr}\Big) + f_2\ \Big(-\beta_0\ L_{qr}^2 - 4\ \beta_0\ \zeta_2\Big) + f_2\ G_{11}\ \Big(2\ L_{qr}\Big) + f_1\ \Big(
- \frac{1}{2}\ \beta_1\ L_{qr}^2 - 2\ \beta_1\ \zeta_2 + \frac{1}{3}\ \beta_0^2\ L_{qr}^3 - \frac{16}{3}\ \beta_0^2\ \zeta_3 + 4\ \beta_0^2\ \zeta_2\ L_{qr}\Big) + f_1\ \tilde{G}_{11}\ \Big(
- 10\ \beta_0\ \zeta_2\Big) + f_1\ G_{21}\ \Big(L_{qr}\Big) + f_1\ G_{12}\ \Big(2\ \beta_0\ L_{qr}\Big) + f_1\ G_{11}\ \Big(-3\ \beta_0\ L_{qr}^2
- 4\ \beta_0\ \zeta_2\Big) + f_1\ G_{11}^2\ \Big(2\ L_{qr}\Big) + f_1\ f_2\ \Big(L_{qr}^2\Big) + f_1^2\ \Big(-\frac{1}{2}\ \beta_0\ L_{qr}^3
+ 3\ \beta_0\ \zeta_2\ L_{qr}\Big) + f_1^2\ G_{11}\ \Big(L_{qr}^2\Big) + f_1^3\ \Big(\frac{1}{6}\ L_{qr}^3\Big) + B_2\ \tilde{G}_{11}\ \Big(-4\ L_{qr}
+ 4\ L_{fr}\Big) + B_2\ f_1\ \Big(2\ L_{qr}^2 - 2\ L_{fr}\ L_{qr}\Big) + B_1\ \tilde{G}_{21}\ \Big(-2\ L_{qr} + 2\ L_{fr}\Big)
+ B_1\ \tilde{G}_{12}\ \Big(-4\ \beta_0\ L_{qr} + 4\ \beta_0\ L_{fr}\Big) + B_1\ \tilde{G}_{11}\ \Big(6\ \beta_0\ L_{qr}^2 - 4\ \beta_0\ L_{fr}\ L_{qr}
- 2\ \beta_0\ L_{fr}^2 - 12\ \beta_0\ \zeta_2\Big) + B_1\ \tilde{G}_{11}^2\ \Big(-4\ L_{qr} + 4\ L_{fr}\Big) + B_1\ G_{11}\ \tilde{G}_{11}\ \Big(
- 8\ L_{qr} + 8\ L_{fr}\Big) + B_1\ f_2\ \Big(2\ L_{qr}^2 - 2\ L_{fr}\ L_{qr}\Big) + B_1\ f_1\ \Big(-2\ \beta_0\ L_{qr}^3
+ \beta_0\ L_{fr}\ L_{qr}^2 + \beta_0\ L_{fr}^2\ L_{qr} + 2\ \beta_0\ \zeta_2\ L_{qr} + 4\ \beta_0\ \zeta_2\ L_{fr}\Big)
+ B_1\ f_1\ G_{11}\ \Big(4\ L_{qr}^2 - 4\ L_{fr}\ L_{qr}\Big) + B_1\ f_1^2\ \Big(L_{qr}^3 - L_{fr}\ L_{qr}^2\Big) + B_1^2\ \tilde{G}_{11}\ \Big(
- 4\ L_{qr}^2 + 8\ L_{fr}\ L_{qr} - 4\ L_{fr}^2\Big) + B_1^2\ f_1\ \Big(2\ L_{qr}^3 - 4\ L_{fr}\ L_{qr}^2 + 2\ L_{fr}^2\ L_{qr}\Big)
+ A_3\ \Big(-\frac{1}{2}\ L_{qr}^2 - 2\ \zeta_2\Big) + A_2\ \Big(\frac{1}{3}\ \beta_0\ L_{qr}^3 - \frac{16}{3}\ \beta_0\ \zeta_3 + 4\ \beta_0\ \zeta_2\ L_{qr}\Big)
+ A_2\ \tilde{G}_{11}\ \Big(-10\ \zeta_2\Big) + A_2\ G_{11}\ \Big(-L_{qr}^2 - 4\ \zeta_2\Big) + A_2\ f_1\ \Big(-\frac{1}{2}\ L_{qr}^3
+ 3\ \zeta_2\ L_{qr}\Big) + A_2\ B_1\ \Big(-L_{qr}^3 + L_{fr}\ L_{qr}^2 - 4\ \zeta_2\ L_{qr} + 4\ \zeta_2\ L_{fr}\Big)
+ A_1\ \Big(\frac{1}{6}\ \beta_1\ L_{qr}^3 - \frac{8}{3}\ \beta_1\ \zeta_3 + 2\ \beta_1\ \zeta_2\ L_{qr} - \frac{1}{12}\ \beta_0^2\ L_{qr}^4 + \frac{16}{3}\ \beta_0^2\ \zeta_3\ L_{qr}
- 2\ \beta_0^2\ \zeta_2\ L_{qr}^2 - \frac{36}{5}\ \beta_0^2\ \zeta_2^2\Big) + A_1\ \tilde{G}_{21}\ \Big(-5\ \zeta_2\Big) + A_1\ \tilde{G}_{12}\ \Big(-10\ \beta_0\ \zeta_2\Big)
+ A_1\ \tilde{G}_{11}\ \Big(-\frac{16}{3}\ \beta_0\ \zeta_3 + 20\ \beta_0\ \zeta_2\ L_{qr}\Big) + A_1\ \tilde{G}_{11}^2\ \Big(-10\ \zeta_2\Big) + A_1\ G_{21}\ \Big(
- \frac{1}{2}\ L_{qr}^2 - 2\ \zeta_2\Big) + A_1\ G_{12}\ \Big(-\beta_0\ L_{qr}^2 - 4\ \beta_0\ \zeta_2\Big) + A_1\ G_{11}\ \Big(\frac{4}{3}\ \beta_0\ L_{qr}^3
$$

$$
\begin{aligned}
&- \frac{16}{3}\,\beta_0\,\zeta_3 + 8\,\beta_0\,\zeta_2\,L_{qr}\Big) + A_1\,G_{11}\,\tilde{G}_{11}\,\Big(-20\,\zeta_2\Big) + A_1\,G_{11}^2\,\Big(-L_{qr}^2 \\
&- 4\,\zeta_2\Big) + A_1\,f_2\,\Big(-\frac{1}{2}\,L_{qr}^3 + 3\,\zeta_2\,L_{qr}\Big) + A_1\,f_1\,\Big(\frac{5}{12}\,\beta_0\,L_{qr}^4 - 6\,\beta_0\,\zeta_2\,L_{qr}^2 \\
&- 16\,\beta_0\,\zeta_2^2\Big) + A_1\,f_1\,G_{11}\,\Big(-L_{qr}^3 + 6\,\zeta_2\,L_{qr}\Big) + A_1\,f_1^2\,\Big(-\frac{1}{4}\,L_{qr}^4 \\
&+ \frac{3}{2}\,\zeta_2\,L_{qr}^2\Big) + A_1\,B_2\,\Big(-L_{qr}^3 + L_{fr}\,L_{qr}^2 - 4\,\zeta_2\,L_{qr} + 4\,\zeta_2\,L_{fr}\Big) \\
&+ A_1\,B_1\,\Big(\frac{5}{6}\,\beta_0\,L_{qr}^4 - \frac{1}{3}\,\beta_0\,L_{fr}\,L_{qr}^3 - \frac{1}{2}\,\beta_0\,L_{fr}^2\,L_{qr}^2 - \frac{16}{3}\,\beta_0\,\zeta_3\,L_{qr} \\
&+ \frac{16}{3}\,\beta_0\,\zeta_3\,L_{fr} + 3\,\beta_0\,\zeta_2\,L_{qr}^2 - 4\,\beta_0\,\zeta_2\,L_{fr}\,L_{qr} - 2\,\beta_0\,\zeta_2\,L_{fr}^2 - 12\,\beta_0\,\zeta_2^2\Big) \\
&+ A_1\,B_1\,\tilde{G}_{11}\,\Big(-20\,\zeta_2\,L_{qr} + 20\,\zeta_2\,L_{fr}\Big) + A_1\,B_1\,G_{11}\,\Big(-2\,L_{qr}^3 \\
&+ 2\,L_{fr}\,L_{qr}^2 - 8\,\zeta_2\,L_{qr} + 8\,\zeta_2\,L_{fr}\Big) + A_1\,B_1\,f_1\,\Big(-L_{qr}^4 + L_{fr}\,L_{qr}^3 \\
&+ 6\,\zeta_2\,L_{qr}^2 - 6\,\zeta_2\,L_{fr}\,L_{qr}\Big) + A_1\,B_1^2\,\Big(-L_{qr}^4 + 2\,L_{fr}\,L_{qr}^3 - L_{fr}^2\,L_{qr}^2 \\
&- 4\,\zeta_2\,L_{qr}^2 + 8\,\zeta_2\,L_{fr}\,L_{qr} - 4\,\zeta_2\,L_{fr}^2\Big) + A_1\,A_2\,\Big(\frac{1}{4}\,L_{qr}^4 - 3\,\zeta_2\,L_{qr}^2 \\
&- 16\,\zeta_2^2\Big) + {A_1}^2\,\Big(-\frac{1}{12}\,\beta_0\,L_{qr}^5 + 2\,\beta_0\,\zeta_2\,L_{qr}^3 - \frac{40}{3}\,\beta_0\,\zeta_2\,\zeta_3 \\
&+ 16\,\beta_0\,\zeta_2^2\,L_{qr}\Big) + {A_1}^2\,\tilde{G}_{11}\,\Big(-25\,\zeta_2^2\Big) + {A_1}^2\,G_{11}\,\Big(\frac{1}{4}\,L_{qr}^4 - 3\,\zeta_2\,L_{qr}^2 \\
&- 16\,\zeta_2^2\Big) + {A_1}^2\,f_1\,\Big(\frac{1}{8}\,L_{qr}^5 - \frac{3}{2}\,\zeta_2\,L_{qr}^3 + \frac{9}{2}\,\zeta_2^2\,L_{qr}\Big) + {A_1}^2\,B_1\,\Big(\frac{1}{4}\,L_{qr}^5 \\
&- \frac{1}{4}\,L_{fr}\,L_{qr}^4 - 3\,\zeta_2\,L_{qr}^3 + 3\,\zeta_2\,L_{fr}\,L_{qr}^2 - 16\,\zeta_2^2\,L_{qr} + 16\,\zeta_2^2\,L_{fr}\Big) + {A_1}^3\,\Big(\\
&- \frac{1}{48}\,L_{qr}^6 + \frac{3}{8}\,\zeta_2\,L_{qr}^4 - \frac{9}{4}\,\zeta_2^2\,L_{qr}^2 - \frac{49}{3}\,\zeta_2^3\Big)\Big]. \qquad \text{(A.29)}
\end{aligned}
$$

A.4 Resummation ingredients for the `All exponentiation`

In the case for `All exponentiation`, the complete g_0 is being exponentiated along with the large-N pieces. This brings into modification only for the resummed exponent compared to the `Standard` $\overline{N}$ `exponentiation`. We write the resummed

exponent in this case in terms of $\overline{N}$ exponents as,

$$\begin{aligned} g_1^{\rm All} &= \overline{g}_1\,, \\ g_2^{\rm All} &= \overline{g}_2 + a_s\ \Delta_{g_2}^{\rm All}\,, \\ g_3^{\rm All} &= \overline{g}_3 + a_s^2\ \Delta_{g_3}^{\rm All}\,, \\ g_4^{\rm All} &= \overline{g}_4 + a_s^3\ \Delta_{g_4}^{\rm All}\,, \end{aligned} \tag{A.30}$$

where $\Delta_{g_i}^{\rm All}$ terms are found from exponentiating also the complete g_0 prefactor and they are given as,

$$\begin{aligned} \Delta_{g_2}^{\rm All} &= \overline{g}_{01}\,, \\ \Delta_{g_2}^{\rm All} &= \left(-\frac{\overline{g}_{01}^2}{2} + \overline{g}_{02}\right), \\ \Delta_{g_2}^{\rm All} &= \left(\frac{\overline{g}_{01}^3}{3} - \overline{g}_{01}\overline{g}_{02} + \overline{g}_{03}\right), \end{aligned} \tag{A.31}$$

Appendix B

Coefficients of universal gravity

Here we present all process dependent part for universal gravity model like ADD and RS.

B.1 SV coefficients

Here we present the SV coefficient for spin-2 production up to three loops for both quark and gluon initiated channels. The third loop results are new.

$$\Delta_{q\bar{q}}^{(1),G} = \frac{\pi}{8n_c}\Bigg[\delta(1-z)\Bigg\{\Bigg(-20+8\zeta_2+\Big(6\Big)L_{qf}\Bigg)C_F\Bigg\}+\mathcal{D}_1\Bigg\{\Big(16\Big)C_F\Bigg\} + \mathcal{D}_0\Bigg\{\Bigg(\Big(8\Big)L_{qf}\Bigg)C_F\Bigg\}\Bigg] \tag{B.1}$$

$$\begin{aligned}\Delta_{q\bar{q}}^{(2),G} = \frac{\pi}{8n_c}\Bigg[&\delta(1-z)\Bigg\{\Bigg(-\frac{5941}{36}+92\zeta_3+\frac{328}{9}\zeta_2-\frac{12}{5}\zeta_2^2+\Big(79-24\zeta_3\Big)L_{qf} \\ &+\Big(-11\Big)L_{qf}^2\Bigg)C_AC_F+\Bigg(\frac{461}{18}+8\zeta_3-\frac{64}{9}\zeta_2+\Big(-14\Big)L_{qf} \\ &+\Big(2\Big)L_{qf}^2\Bigg)C_Fn_f+\Bigg(\frac{2293}{12}-124\zeta_3-70\zeta_2+\frac{8}{5}\zeta_2^2+\Big(-117+176\zeta_3 \\ &+24\zeta_2\Big)L_{qf}+\Big(18-32\zeta_2\Big)L_{qf}^2\Bigg)C_F^2\Bigg\}+\mathcal{D}_3\Bigg\{\Big(128\Big)C_F^2\Bigg\}+\mathcal{D}_2\Bigg\{\Bigg(\end{aligned}$$

$$
\begin{aligned}
&- \frac{176}{3}\Big)C_AC_F + \Big(\frac{32}{3}\Big)C_Fn_f + \Big(\Big(192\Big)L_{qf}\Big)C_F^2\Big\} + \mathcal{D}_1\Big\{\Big(- 320 - 128\zeta_2 \\
&+ \Big(64\Big)L_{qf}^2 + \Big(96\Big)L_{qf}\Big)C_F^2 + \Big(- \frac{160}{9} + \Big(\frac{32}{3}\Big)L_{qf}\Big)C_Fn_f + \Big(\frac{1072}{9} \\
&- 32\zeta_2 + \Big(- \frac{176}{3}\Big)L_{qf}\Big)C_AC_F\Big\} + \mathcal{D}_0\Big\{\Big(- \frac{1616}{27} + 56\zeta_3 + \frac{176}{3}\zeta_2 + \Big(\\
&- \frac{44}{3}\Big)L_{qf}^2 + \Big(\frac{536}{9} - 16\zeta_2\Big)L_{qf}\Big)C_AC_F + \Big(\frac{224}{27} - \frac{32}{3}\zeta_2 + \Big(- \frac{80}{9}\Big)L_{qf} \\
&+ \Big(\frac{8}{3}\Big)L_{qf}^2\Big)C_Fn_f + \Big(256\zeta_3 + \Big(- 160 - 64\zeta_2\Big)L_{qf} + \Big(48\Big)L_{qf}^2\Big)C_F^2\Big\}\Big]
\end{aligned}
\tag{B.2}
$$

$$
\begin{aligned}
\Delta_{q\bar{q}}^{(3),G} = \frac{\pi}{8n_c}\Big[&\delta(1-z)\Big\{\Big(- \frac{1970041}{972} - \frac{4292}{3}\zeta_5 + \frac{282365}{81}\zeta_3 - \frac{400}{3}\zeta_3^2 + \frac{9685}{27}\zeta_2 \\
&- \frac{1028}{3}\zeta_2\zeta_3 + \frac{5459}{27}\zeta_2^2 + \frac{13264}{315}\zeta_2^3 + \Big(- \frac{971}{3} + 88\zeta_3\Big)L_{qf}^2 + \Big(\frac{242}{9}\Big)L_{qf}^3 \\
&+ \Big(\frac{36310}{27} + 80\zeta_5 - \frac{9176}{9}\zeta_3 - \frac{224}{9}\zeta_2 + \frac{68}{5}\zeta_2^2\Big)L_{qf}\Big)C_A^2C_F + \Big(- \frac{2807}{2} \\
&+ \frac{3344}{3}\zeta_5 + \frac{4300}{3}\zeta_3 + \frac{10336}{3}\zeta_3^2 - \frac{1082}{3}\zeta_2 - 432\zeta_2\zeta_3 + \frac{892}{5}\zeta_2^2 - \frac{184736}{315}\zeta_2^3 \\
&+ \Big(- 342 + 1056\zeta_3 + 640\zeta_2 - \frac{1792}{5}\zeta_2^2\Big)L_{qf}^2 + \Big(36 + \frac{512}{3}\zeta_3 - 192\zeta_2\Big)L_{qf}^3 \\
&+ \Big(\frac{2231}{2} + 5664\zeta_5 - 4128\zeta_3 + 120\zeta_2 - 2752\zeta_2\zeta_3 - \frac{336}{5}\zeta_2^2\Big)L_{qf}\Big)C_F^3 + \Big(\\
&- \frac{697}{3} + \frac{5536}{9}\zeta_5 + \frac{6200}{9}\zeta_3 - \frac{1256}{27}\zeta_2 - \frac{5504}{9}\zeta_2\zeta_3 + \frac{3536}{135}\zeta_2^2 + \Big(- 116 \\
&+ 160\zeta_3 + \frac{640}{9}\zeta_2\Big)L_{qf}^2 + \Big(12 - \frac{64}{3}\zeta_2\Big)L_{qf}^3 + \Big(\frac{3022}{9} - \frac{4432}{9}\zeta_3 - \frac{1936}{27}\zeta_2 \\
&+ \frac{112}{15}\zeta_2^2\Big)L_{qf}\Big)C_F^2n_f + \Big(- \frac{7345}{243} - \frac{2416}{81}\zeta_3 + \frac{1744}{81}\zeta_2 + \frac{128}{27}\zeta_2^2 + \Big(\\
&- \frac{28}{3}\Big)L_{qf}^2 + \Big(\frac{8}{9}\Big)L_{qf}^3 + \Big(\frac{820}{27} + \frac{64}{9}\zeta_3 - \frac{32}{9}\zeta_2\Big)L_{qf}\Big)C_Fn_f{}^2 + \Big(\frac{130871}{243} \\
&+ \frac{136}{3}\zeta_5 - \frac{29488}{81}\zeta_3 - \frac{16348}{81}\zeta_2 + \frac{224}{3}\zeta_2\zeta_3 - \frac{7988}{135}\zeta_2^2 + \Big(- \frac{11732}{27} + \frac{976}{9}\zeta_3 \\
&+ \frac{256}{9}\zeta_2 - \frac{8}{5}\zeta_2^2\Big)L_{qf} + \Big(- \frac{88}{9}\Big)L_{qf}^3 + \Big(114 - 16\zeta_3\Big)L_{qf}^2\Big)C_AC_Fn_f \\
&+ \Big(\frac{328511}{108} - \frac{26824}{9}\zeta_5 - \frac{57388}{9}\zeta_3 + \frac{3280}{3}\zeta_3^2 + \frac{8894}{27}\zeta_2 + \frac{33728}{9}\zeta_2\zeta_3 \\
&- \frac{26288}{135}\zeta_2^2 - \frac{20816}{315}\zeta_2^3 + \Big(- \frac{43727}{18} + 240\zeta_5 + \frac{39688}{9}\zeta_3 + \frac{10696}{27}\zeta_2
\end{aligned}
$$

$$
\begin{aligned}
&- 1120\zeta_2\zeta_3 - \frac{256}{15}\zeta_2^2\Big)L_{qf} + \Big(- 66 + \frac{352}{3}\zeta_2\Big)L_{qf}^3 + \Big(683 - 1024\zeta_3 \\
&- \frac{4288}{9}\zeta_2 + 128\zeta_2^2\Big)L_{qf}^2\Big)C_AC_F^2\Big\} + \mathcal{D}_5\Big\{\Big(512\Big)C_F^3\Big\} + \mathcal{D}_4\Big\{\Big(\\
&- \frac{7040}{9}\Big)C_AC_F^2 + \Big(\frac{1280}{9}\Big)C_F^2n_f + \Big(\Big(1280\Big)L_{qf}\Big)C_F^3\Big\} + \mathcal{D}_3\Big\{\Big(- 2560 \\
&- 3072\zeta_2 + \Big(768\Big)L_{qf} + \Big(1024\Big)L_{qf}^2\Big)C_F^3 + \Big(- \frac{2560}{9} \\
&+ \Big(\frac{2560}{9}\Big)L_{qf}\Big)C_F^2n_f + \Big(- \frac{2816}{27}\Big)C_AC_Fn_f + \Big(\frac{256}{27}\Big)C_F{n_f}^2 \\
&+ \Big(\frac{7744}{27}\Big)C_A^2C_F + \Big(\frac{17152}{9} - 512\zeta_2 + \Big(- \frac{14080}{9}\Big)L_{qf}\Big)C_AC_F^2\Big\} + \mathcal{D}_2\Big\{\Big(\\
&- \frac{28480}{27} + \frac{704}{3}\zeta_2 + \Big(\frac{3872}{9}\Big)L_{qf}\Big)C_A^2C_F + \Big(- \frac{2368}{9} + 1344\zeta_3 + \frac{11264}{3}\zeta_2 \\
&+ \Big(\frac{7520}{3} - 768\zeta_2\Big)L_{qf} + \Big(- 1056\Big)L_{qf}^2\Big)C_AC_F^2 + \Big(- \frac{640}{27} \\
&+ \Big(\frac{128}{9}\Big)L_{qf}\Big){C_Fn_f}^2 + \Big(\frac{160}{9} - \frac{2048}{3}\zeta_2 + \Big(- \frac{1088}{3}\Big)L_{qf} \\
&+ \Big(192\Big)L_{qf}^2\Big)C_F^2n_f + \Big(\frac{9248}{27} - \frac{128}{3}\zeta_2 + \Big(- \frac{1408}{9}\Big)L_{qf}\Big)C_AC_Fn_f \\
&+ \Big(10240\zeta_3 + \Big(- 3840 - 4608\zeta_2\Big)L_{qf} + \Big(256\Big)L_{qf}^3 + \Big(1152\Big)L_{qf}^2\Big)C_F^3\Big\} \\
&+ \mathcal{D}_1\Big\{\Big(- \frac{15068}{3} - 4160\zeta_3 - \frac{14720}{9}\zeta_2 + \frac{3648}{5}\zeta_2^2 + \Big(- \frac{704}{3}\Big)L_{qf}^3 \\
&+ \Big(\frac{3824}{9} - 256\zeta_2\Big)L_{qf}^2 + \Big(\frac{59248}{27} + 512\zeta_3 + \frac{9280}{3}\zeta_2\Big)L_{qf}\Big)C_AC_F^2 + \Big(\\
&- \frac{32816}{81} + 384\zeta_2 + \Big(- \frac{704}{9}\Big)L_{qf}^2 + \Big(\frac{9248}{27} - \frac{128}{3}\zeta_2\Big)L_{qf}\Big)C_AC_Fn_f \\
&+ \Big(\frac{1600}{81} - \frac{256}{9}\zeta_2 + \Big(- \frac{640}{27}\Big)L_{qf} + \Big(\frac{64}{9}\Big)L_{qf}^2\Big){C_Fn_f}^2 + \Big(\frac{1856}{3} + 1280\zeta_3 \\
&+ \frac{2816}{9}\zeta_2 + \Big(- \frac{10240}{27} - \frac{1792}{3}\zeta_2\Big)L_{qf} + \Big(- \frac{416}{9}\Big)L_{qf}^2 \\
&+ \Big(\frac{128}{3}\Big)L_{qf}^3\Big)C_F^2n_f + \Big(\frac{124024}{81} - 704\zeta_3 - \frac{12032}{9}\zeta_2 + \frac{704}{5}\zeta_2^2 + \Big(- \frac{28480}{27} \\
&+ \frac{704}{3}\zeta_2\Big)L_{qf} + \Big(\frac{1936}{9}\Big)L_{qf}^2\Big)C_A^2C_F + \Big(\frac{9172}{3} - 1984\zeta_3 + 4000\zeta_2 \\
&- \frac{14208}{5}\zeta_2^2 + \Big(- 1872 + 11008\zeta_3 - 1152\zeta_2\Big)L_{qf} + \Big(- 992 - 2048\zeta_2\Big)L_{qf}^2 \\
&+ \Big(384\Big)L_{qf}^3\Big)C_F^3\Big\} + \mathcal{D}_0\Big\{\Big(- \frac{594058}{729} - 384\zeta_5 + \frac{40144}{27}\zeta_3 + \frac{98224}{81}\zeta_2
\end{aligned}
$$

$$
\begin{aligned}
&- \frac{352}{3}\zeta_2\zeta_3 - \frac{2992}{15}\zeta_2^2 + \Big(- \frac{7120}{27} + \frac{176}{3}\zeta_2 \Big) L_{qf}^2 + \Big(\frac{968}{27} \Big) L_{qf}^3 + \Big(\frac{62012}{81} \\
&- 352\zeta_3 - \frac{6016}{9}\zeta_2 + \frac{352}{5}\zeta_2^2 \Big) L_{qf} \Big) C_A^2 C_F + \Big(- \frac{1058}{27} - \frac{5728}{9}\zeta_3 + \frac{3104}{27}\zeta_2 \\
&- \frac{1472}{15}\zeta_2^2 + \Big(- \frac{632}{3} - \frac{320}{3}\zeta_2 \Big) L_{qf}^2 + \Big(\frac{3232}{9} + 640\zeta_3 + \frac{832}{9}\zeta_2 \Big) L_{qf} \\
&+ \Big(32 \Big) L_{qf}^3 \Big) C_F^2 n_f + \Big(- \frac{3712}{729} + \frac{320}{27}\zeta_3 + \frac{640}{27}\zeta_2 + \Big(- \frac{160}{27} \Big) L_{qf}^2 \\
&+ \Big(\frac{32}{27} \Big) L_{qf}^3 + \Big(\frac{800}{81} - \frac{128}{9}\zeta_2 \Big) L_{qf} \Big) C_F {n_f}^2 + \Big(\frac{125252}{729} - \frac{2480}{9}\zeta_3 \\
&- \frac{29392}{81}\zeta_2 + \frac{736}{15}\zeta_2^2 + \Big(- \frac{16408}{81} + 192\zeta_2 \Big) L_{qf} + \Big(- \frac{352}{27} \Big) L_{qf}^3 + \Big(\frac{2312}{27} \\
&- \frac{32}{3}\zeta_2 \Big) L_{qf}^2 \Big) C_A C_F n_f + \Big(\frac{32320}{27} + \frac{24224}{9}\zeta_3 - \frac{18752}{27}\zeta_2 - 1472\zeta_2\zeta_3 \\
&+ \frac{1408}{3}\zeta_2^2 + \Big(- \frac{25834}{9} - 1744\zeta_3 - \frac{4192}{9}\zeta_2 + \frac{1824}{5}\zeta_2^2 \Big) L_{qf} + \Big(\frac{3848}{3} \\
&- 192\zeta_3 + \frac{1472}{3}\zeta_2 \Big) L_{qf}^2 + \Big(- 176 \Big) L_{qf}^3 \Big) C_A C_F^2 + \Big(12288\zeta_5 - 5120\zeta_3 \\
&- 6144\zeta_2\zeta_3 + \Big(- 936 + 2432\zeta_3 - 576\zeta_2 \Big) L_{qf}^2 + \Big(144 - 256\zeta_2 \Big) L_{qf}^3 \\
&+ \Big(\frac{4586}{3} + 544\zeta_3 + 2000\zeta_2 - \frac{7104}{5}\zeta_2^2 \Big) L_{qf} \Big) C_F^3 \Big\} \Big] \qquad \text{(B.3)}
\end{aligned}
$$

$$
\begin{aligned}
\Delta_{gg}^{(1),G} = \frac{\pi}{2(n_c^2-1)} \Bigg[& \delta(1-z) \Big\{ \Big(- \frac{203}{9} + 8\zeta_2 + \Big(\frac{22}{3} \Big) L_{qf} \Big) C_A + \Big(\frac{35}{9} + \Big(\\
& - \frac{4}{3} \Big) L_{qf} \Big) n_f \Big\} + \mathcal{D}_1 \Big\{ \Big(16 \Big) C_A \Big\} + \mathcal{D}_0 \Big\{ \Big(\Big(8 \Big) L_{qf} \Big) C_A \Big\} \Bigg] \qquad \text{(B.4)}
\end{aligned}
$$

$$
\begin{aligned}
\Delta_{gg}^{(2),G} = \frac{\pi}{2(n_c^2-1)} \Bigg[& \delta(1-z) \Big\{ \Big(- \frac{2983}{162} + \frac{64}{3}\zeta_3 - \frac{94}{9}\zeta_2 + \Big(- \frac{44}{9} \Big) L_{qf}^2 + \Big(\frac{647}{27} \\
& - \frac{16}{3}\zeta_2 \Big) L_{qf} \Big) C_A n_f + \Big(\frac{1225}{324} + \frac{8}{3}\zeta_2 + \Big(- \frac{70}{27} \Big) L_{qf} + \Big(\frac{4}{9} \Big) L_{qf}^2 \Big) {n_f}^2 + \Big(\frac{61}{3} \\
& - 16\zeta_3 + \Big(- 4 \Big) L_{qf} \Big) C_F n_f + \Big(\frac{7801}{324} - \frac{88}{3}\zeta_3 - \frac{224}{9}\zeta_2 - \frac{4}{5}\zeta_2^2 + \Big(- \frac{1657}{27} \\
& + 152\zeta_3 + \frac{88}{3}\zeta_2 \Big) L_{qf} + \Big(\frac{121}{9} - 32\zeta_2 \Big) L_{qf}^2 \Big) C_A^2 \Big\} + \mathcal{D}_3 \Big\{ \Big(128 \Big) C_A^2 \Big\}
\end{aligned}
$$

$$+\mathcal{D}_2\Big\{\Big(-\frac{176}{3}+\Big(192\Big)L_{qf}\Big)C_A^2+\Big(\frac{32}{3}\Big)C_An_f\Big\}+\mathcal{D}_1\Big\{\Big(-\frac{2176}{9}$$
$$-160\zeta_2+\Big(\frac{176}{3}\Big)L_{qf}+\Big(64\Big)L_{qf}^2\Big)C_A^2+\Big(\frac{400}{9}+\Big(-\frac{32}{3}\Big)L_{qf}\Big)C_An_f\Big\}$$
$$+\mathcal{D}_0\Big\{\Big(-\frac{1616}{27}+312\zeta_3+\frac{176}{3}\zeta_2+\Big(-\frac{1088}{9}-80\zeta_2\Big)L_{qf}$$
$$+\Big(44\Big)L_{qf}^2\Big)C_A^2+\Big(\frac{224}{27}-\frac{32}{3}\zeta_2+\Big(\frac{200}{9}\Big)L_{qf}+\Big(-8\Big)L_{qf}^2\Big)C_An_f\Big\}\Big]\tag{B.5}$$

$$\Delta_{gg}^{(3),G}=\frac{\pi}{2(n_c^2-1)}\Big[\delta(1-z)\Big\{\Big(-\frac{303707}{810}-\frac{28636}{9}\zeta_5-\frac{186194}{135}\zeta_3+\frac{13216}{3}\zeta_3^2$$
$$+\frac{923}{3}\zeta_2+\frac{8944}{3}\zeta_2\zeta_3+\frac{29416}{135}\zeta_2^2-\frac{64096}{105}\zeta_2^3+\Big(-\frac{1319}{9}+5984\zeta_5$$
$$-\frac{3496}{3}\zeta_3+\frac{15232}{27}\zeta_2-3872\zeta_2\zeta_3-\frac{396}{5}\zeta_2^2\Big)L_{qf}+\Big(\frac{110}{3}+\frac{968}{3}\zeta_3+\frac{736}{3}\zeta_2$$
$$-\frac{1152}{5}\zeta_2^2\Big)L_{qf}^2+\Big(\frac{512}{3}\zeta_3-\frac{352}{3}\zeta_2\Big)L_{qf}^3\Big)C_A^3+\Big(-\frac{241}{9}+160\zeta_5-\frac{296}{3}\zeta_3$$
$$+\Big(2\Big)L_{qf}\Big)C_F^2n_f+\Big(-\frac{2617}{162}+8\zeta_3+24\zeta_2+\Big(-\frac{16}{3}\Big)L_{qf}$$
$$+\Big(\frac{4}{3}\Big)L_{qf}^2\Big)C_F{n_f}^2+\Big(-\frac{1487}{135}-\frac{448}{45}\zeta_3+\frac{1019}{27}\zeta_2+\frac{304}{45}\zeta_2^2+\Big(-\frac{41}{9}\Big)L_{qf}$$
$$+\Big(\frac{4}{3}\Big)L_{qf}^2\Big)C_A{n_f}^2+\Big(\frac{55546}{405}+\frac{2752}{9}\zeta_5+\frac{55229}{135}\zeta_3-\frac{5369}{27}\zeta_2-\frac{1508}{3}\zeta_2\zeta_3$$
$$-\frac{10393}{135}\zeta_2^2+\Big(-14-\frac{176}{3}\zeta_3-\frac{160}{3}\zeta_2\Big)L_{qf}^2+\Big(\frac{523}{9}+\frac{760}{3}\zeta_3-\frac{2368}{27}\zeta_2$$
$$+\frac{72}{5}\zeta_2^2\Big)L_{qf}+\Big(\frac{64}{3}\zeta_2\Big)L_{qf}^3\Big)C_A^2n_f+\Big(\frac{65866}{405}+80\zeta_5-\frac{5552}{45}\zeta_3-\frac{520}{9}\zeta_2$$
$$-\frac{128}{3}\zeta_2\zeta_3-\frac{32}{45}\zeta_2^2+\Big(-\frac{22}{3}\Big)L_{qf}^2+\Big(\frac{55}{3}-16\zeta_2\Big)L_{qf}\Big)C_AC_Fn_f\Big\}$$
$$+\mathcal{D}_5\Big\{\Big(512\Big)C_A^3\Big\}+\mathcal{D}_4\Big\{\Big(-\frac{7040}{9}+\Big(1280\Big)L_{qf}\Big)C_A^3+\Big(\frac{1280}{9}\Big)C_A^2n_f\Big\}$$
$$+\mathcal{D}_3\Big\{\Big(-\frac{18752}{27}-3584\zeta_2+\Big(-\frac{5632}{9}\Big)L_{qf}+\Big(1024\Big)L_{qf}^2\Big)C_A^3$$
$$+\Big(\frac{256}{27}\Big)C_A{n_f}^2+\Big(\frac{2944}{27}+\Big(\frac{1024}{9}\Big)L_{qf}\Big)C_A^2n_f\Big\}+\mathcal{D}_2\Big\{\Big(-1168$$
$$+11584\zeta_3+\frac{11968}{3}\zeta_2+\Big(-1472-5376\zeta_2\Big)L_{qf}+\Big(256\Big)L_{qf}^3$$
$$+\Big(352\Big)L_{qf}^2\Big)C_A^3+\Big(\frac{160}{9}\Big)C_A{n_f}^2+\Big(\frac{656}{9}-\frac{2176}{3}\zeta_2+\Big(-64\Big)L_{qf}^2$$

$$+\Big(320\Big)L_{qf}\Big)C_A^2n_f+\Big(32\Big)C_AC_Fn_f\Big\}+\mathcal{D}_1\Big\{\Big(-\frac{6932}{9}-\frac{20416}{3}\zeta_3$$
$$+\frac{17120}{9}\zeta_2-\frac{9856}{5}\zeta_2^2+\Big(-\frac{21536}{27}+11520\zeta_3+\frac{5632}{3}\zeta_2\Big)L_{qf}+\Big(-\frac{1472}{3}$$
$$-2304\zeta_2\Big)L_{qf}^2+\Big(\frac{704}{3}\Big)L_{qf}^3\Big)C_A^3+\Big(\frac{100}{9}+\frac{128}{9}\zeta_2\Big)C_A{n_f}^2+\Big(\frac{1480}{9}$$
$$+\frac{4096}{3}\zeta_3-\frac{4288}{9}\zeta_2+\Big(-\frac{128}{3}\Big)L_{qf}^3+\Big(\frac{2720}{27}-\frac{1024}{3}\zeta_2\Big)L_{qf}$$
$$+\Big(\frac{320}{3}\Big)L_{qf}^2\Big)C_A^2n_f+\Big(\frac{536}{3}-128\zeta_3+\Big(-32\Big)L_{qf}\Big)C_AC_Fn_f\Big\}+\mathcal{D}_0\Big\{\Big($$
$$-\frac{180844}{729}+\frac{3320}{9}\zeta_3+\frac{3200}{81}\zeta_2-\frac{544}{15}\zeta_2^2+\Big(-\frac{352}{27}\Big)L_{qf}^3+\Big(\frac{140}{9}$$
$$+32\zeta_2\Big)L_{qf}^2+\Big(\frac{18052}{81}+\frac{800}{3}\zeta_3-\frac{1184}{3}\zeta_2\Big)L_{qf}\Big)C_A^2n_f+\Big(\frac{19808}{729}+\frac{320}{27}\zeta_3$$
$$-\frac{160}{9}\zeta_2+\Big(-\frac{446}{81}+\frac{64}{3}\zeta_2\Big)L_{qf}+\Big(-\frac{40}{9}\Big)L_{qf}^2+\Big(\frac{32}{27}\Big)L_{qf}^3\Big)C_A{n_f}^2$$
$$+\Big(\frac{3422}{27}-\frac{608}{9}\zeta_3-32\zeta_2-\frac{64}{5}\zeta_2^2+\Big(\frac{268}{3}-64\zeta_3\Big)L_{qf}$$
$$+\Big(-24\Big)L_{qf}^2\Big)C_AC_Fn_f+\Big(\frac{390086}{729}+11904\zeta_5-\frac{46952}{27}\zeta_3+\frac{29824}{81}\zeta_2$$
$$-\frac{23200}{3}\zeta_2\zeta_3+\frac{4048}{15}\zeta_2^2+\Big(-\frac{66746}{81}-\frac{3344}{3}\zeta_3+\frac{4144}{3}\zeta_2-\frac{4928}{5}\zeta_2^2\Big)L_{qf}$$
$$+\Big(\frac{116}{9}+2240\zeta_3-176\zeta_2\Big)L_{qf}^2+\Big(\frac{968}{27}-256\zeta_2\Big)L_{qf}^3\Big)C_A^3\Big\}\Big] \tag{B.6}$$

B.2 Process dependent resum coefficients

Here we present the process-dependent coefficients used for N^{3}LL resummation for spin-2 production for both the quark and gluon initiated channels.

$$g_{01}^{q\bar{q}}=C_F\Big\{-20+16\zeta_2+\Big(-6\Big)L_{fr}+\Big(6\Big)L_{qr}\Big\}, \tag{B.7}$$
$$g_{02}^{q\bar{q}}=C_Fn_f\Big\{\frac{461}{18}+\frac{8}{9}\zeta_3-16\zeta_2+\Big(-14+\frac{16}{3}\zeta_2\Big)L_{qr}+\Big(\frac{2}{3}+\frac{16}{3}\zeta_2\Big)L_{fr}$$
$$+\Big(-2\Big)L_{fr}^2+\Big(2\Big)L_{qr}^2\Big\}+C_F^2\Big\{\frac{2293}{12}-124\zeta_3-230\zeta_2+\frac{552}{5}\zeta_2^2+\Big(-117$$
$$+48\zeta_3+72\zeta_2\Big)L_{qr}+\Big(117-48\zeta_3-72\zeta_2\Big)L_{fr}+\Big(-36\Big)L_{qr}L_{fr}+\Big(18\Big)L_{fr}^2$$

$$+\left(18\right)L_{qr}^{2}\Big\}+C_{A}C_{F}\Big\{-\frac{5941}{36}+\frac{1180}{9}\zeta_{3}+96\zeta_{2}-\frac{92}{5}\zeta_{2}^{2}+\Big(-\frac{17}{3}+24\zeta_{3}$$
$$-\frac{88}{3}\zeta_{2}\Big)L_{fr}+\Big(79-24\zeta_{3}-\frac{88}{3}\zeta_{2}\Big)L_{qr}+\Big(-11\Big)L_{qr}^{2}+\Big(11\Big)L_{fr}^{2}\Big\},\qquad\text{(B.8)}$$

$$g_{03}^{q\bar{q}}=C_{F}{n_{f}}^{2}\Big\{-\frac{7345}{243}-\frac{1136}{81}\zeta_{3}+\frac{848}{27}\zeta_{2}+\frac{448}{135}\zeta_{2}^{2}+\Big(-\frac{28}{3}+\frac{32}{9}\zeta_{2}\Big)L_{qr}^{2}+\Big($$
$$-\frac{8}{9}\Big)L_{fr}^{3}+\Big(\frac{4}{9}+\frac{32}{9}\zeta_{2}\Big)L_{fr}^{2}+\Big(\frac{8}{9}\Big)L_{qr}^{3}+\Big(\frac{34}{9}+\frac{32}{9}\zeta_{3}-\frac{160}{27}\zeta_{2}\Big)L_{fr}+\Big(\frac{820}{27}$$
$$-\frac{64}{27}\zeta_{3}-\frac{416}{27}\zeta_{2}\Big)L_{qr}\Big\}+C_{F}^{2}n_{f}\Big\{-\frac{697}{3}-\frac{608}{9}\zeta_{5}+\frac{18280}{27}\zeta_{3}+\frac{7096}{27}\zeta_{2}$$
$$-\frac{256}{3}\zeta_{2}\zeta_{3}-\frac{27184}{135}\zeta_{2}^{2}+\Big(-121+\frac{256}{3}\zeta_{3}-\frac{40}{3}\zeta_{2}+\frac{272}{5}\zeta_{2}^{2}\Big)L_{fr}+\Big(-116$$
$$+32\zeta_{3}+48\zeta_{2}\Big)L_{qr}^{2}+\Big(28-32\zeta_{3}-48\zeta_{2}\Big)L_{fr}^{2}+\Big(\frac{3022}{9}-\frac{752}{3}\zeta_{3}-\frac{784}{3}\zeta_{2}$$
$$+\frac{464}{5}\zeta_{2}^{2}\Big)L_{qr}+\Big(-12\Big)L_{qr}L_{fr}^{2}+\Big(-12\Big)L_{qr}^{2}L_{fr}+\Big(12\Big)L_{fr}^{3}+\Big(12\Big)L_{qr}^{3}$$
$$+\Big(88\Big)L_{qr}L_{fr}\Big\}+C_{F}^{3}\Big\{-\frac{2807}{2}+\frac{3344}{3}\zeta_{5}+\frac{4300}{3}\zeta_{3}+32\zeta_{3}^{2}+1168\zeta_{2}$$
$$-1424\zeta_{2}\zeta_{3}-\frac{6388}{5}\zeta_{2}^{2}+\frac{169504}{315}\zeta_{2}^{3}+\Big(-\frac{2231}{2}+480\zeta_{5}+1568\zeta_{3}+816\zeta_{2}$$
$$-704\zeta_{2}\zeta_{3}-\frac{1968}{5}\zeta_{2}^{2}\Big)L_{fr}+\Big(-342+288\zeta_{3}+144\zeta_{2}\Big)L_{fr}^{2}+\Big(-342+288\zeta_{3}$$
$$+144\zeta_{2}\Big)L_{qr}^{2}+\Big(684-576\zeta_{3}-288\zeta_{2}\Big)L_{qr}L_{fr}+\Big(\frac{2231}{2}-480\zeta_{5}-1568\zeta_{3}$$
$$-816\zeta_{2}+704\zeta_{2}\zeta_{3}+\frac{1968}{5}\zeta_{2}^{2}\Big)L_{qr}+\Big(-108\Big)L_{qr}^{2}L_{fr}+\Big(-36\Big)L_{fr}^{3}$$
$$+\Big(36\Big)L_{qr}^{3}+\Big(108\Big)L_{qr}L_{fr}^{2}\Big\}+C_{A}C_{F}n_{f}\Big\{\frac{130871}{243}+\frac{136}{3}\zeta_{5}-\frac{47984}{81}\zeta_{3}$$
$$-\frac{32756}{81}\zeta_{2}+\frac{928}{9}\zeta_{2}\zeta_{3}-\frac{1076}{135}\zeta_{2}^{2}+\Big(-\frac{11732}{27}+\frac{5744}{27}\zeta_{3}+\frac{5392}{27}\zeta_{2}$$
$$-\frac{344}{15}\zeta_{2}^{2}\Big)L_{qr}+\Big(-40-\frac{400}{9}\zeta_{3}+\frac{2672}{27}\zeta_{2}-\frac{8}{5}\zeta_{2}^{2}\Big)L_{fr}+\Big(-\frac{146}{9}+16\zeta_{3}$$
$$-\frac{352}{9}\zeta_{2}\Big)L_{fr}^{2}+\Big(-\frac{88}{9}\Big)L_{qr}^{3}+\Big(\frac{88}{9}\Big)L_{fr}^{3}+\Big(114-16\zeta_{3}-\frac{352}{9}\zeta_{2}\Big)L_{qr}^{2}\Big\}$$
$$+C_{A}C_{F}^{2}\Big\{\frac{328511}{108}+\frac{6968}{9}\zeta_{5}-\frac{167428}{27}\zeta_{3}+\frac{592}{3}\zeta_{3}^{2}-\frac{58912}{27}\zeta_{2}+\frac{6880}{3}\zeta_{2}\zeta_{3}$$
$$+\frac{42128}{27}\zeta_{2}^{2}-\frac{123632}{315}\zeta_{2}^{3}+\Big(-\frac{43727}{18}+240\zeta_{5}+\frac{8216}{3}\zeta_{3}+\frac{4480}{3}\zeta_{2}-352\zeta_{2}\zeta_{3}$$
$$-\frac{2912}{5}\zeta_{2}^{2}\Big)L_{qr}+\Big(-508+288\zeta_{3}\Big)L_{qr}L_{fr}+\Big(-175+32\zeta_{3}+264\zeta_{2}\Big)L_{fr}^{2}$$

$$+\Big(683-320\zeta_3-264\zeta_2\Big)L_{qr}^2+\Big(1028-240\zeta_5-\frac{5488}{3}\zeta_3+\frac{580}{3}\zeta_2+352\zeta_2\zeta_3$$
$$-\frac{1136}{5}\zeta_2^2\Big)L_{fr}+\Big(-66\Big)L_{fr}^3+\Big(-66\Big)L_{qr}^3+\Big(66\Big)L_{qr}L_{fr}^2+\Big(66\Big)L_{qr}^2L_{fr}\Big\}$$
$$+C_A^2C_F\Big\{-\frac{1970041}{972}-\frac{4292}{3}\zeta_5+\frac{339325}{81}\zeta_3-\frac{400}{3}\zeta_3^2+\frac{91067}{81}\zeta_2-\frac{7660}{9}\zeta_2\zeta_3$$
$$-\frac{10673}{135}\zeta_2^2+\frac{7088}{63}\zeta_2^3+\Big(-\frac{971}{3}+88\zeta_3+\frac{968}{9}\zeta_2\Big)L_{qr}^2+\Big(-\frac{242}{9}\Big)L_{fr}^3$$
$$+\Big(\frac{242}{9}\Big)L_{qr}^3+\Big(\frac{493}{9}-88\zeta_3+\frac{968}{9}\zeta_2\Big)L_{fr}^2+\Big(\frac{1657}{18}-80\zeta_5+\frac{3104}{9}\zeta_3$$
$$-\frac{8992}{27}\zeta_2+4\zeta_2^2\Big)L_{fr}+\Big(\frac{36310}{27}+80\zeta_5-\frac{35272}{27}\zeta_3-\frac{14912}{27}\zeta_2$$
$$+\frac{1964}{15}\zeta_2^2\Big)L_{qr}\Big\}, \tag{B.9}$$

$$g_{01}^{gg}=n_f\Big\{\frac{35}{9}+\Big(-\frac{4}{3}\Big)L_{qr}+\Big(\frac{4}{3}\Big)L_{fr}\Big\}+C_A\Big\{-\frac{203}{9}+16\zeta_2+\Big(-\frac{22}{3}\Big)L_{fr}$$
$$+\Big(\frac{22}{3}\Big)L_{qr}\Big\}, \tag{B.10}$$
$$g_{02}^{gg}={n_f}^2\Big\{\frac{1225}{324}+\frac{8}{3}\zeta_2+\Big(-\frac{70}{27}\Big)L_{qr}+\Big(-\frac{16}{9}\Big)L_{qr}L_{fr}+\Big(\frac{4}{9}\Big)L_{qr}^2+\Big(\frac{4}{3}\Big)L_{fr}^2$$
$$+\Big(\frac{140}{27}\Big)L_{fr}\Big\}+C_F{n_f}\Big\{\frac{61}{3}-16\zeta_3+\Big(-4\Big)L_{qr}+\Big(4\Big)L_{fr}\Big\}+C_A{n_f}\Big\{$$
$$-\frac{2983}{162}+\frac{128}{9}\zeta_3+\frac{106}{9}\zeta_2+\Big(-\frac{1438}{27}+\frac{64}{3}\zeta_2\Big)L_{fr}+\Big(-\frac{44}{3}\Big)L_{fr}^2+\Big($$
$$-\frac{44}{9}\Big)L_{qr}^2+\Big(\frac{176}{9}\Big)L_{qr}L_{fr}+\Big(\frac{647}{27}-\frac{32}{3}\zeta_2\Big)L_{qr}\Big\}+C_A^2\Big\{\frac{7801}{324}+\frac{88}{9}\zeta_3$$
$$-\frac{1312}{9}\zeta_2+92\zeta_2^2+\Big(-\frac{1657}{27}+24\zeta_3+\frac{176}{3}\zeta_2\Big)L_{qr}+\Big(-\frac{484}{9}\Big)L_{qr}L_{fr}$$
$$+\Big(\frac{121}{9}\Big)L_{qr}^2+\Big(\frac{121}{3}\Big)L_{fr}^2+\Big(\frac{3890}{27}-24\zeta_3-\frac{352}{3}\zeta_2\Big)L_{fr}\Big\}, \tag{B.11}$$
$$g_{03}^{gg}={n_f}^3\Big\{\Big(-\frac{280}{81}\Big)L_{qr}L_{fr}+\Big(-\frac{16}{9}\Big)L_{qr}L_{fr}^2+\Big(\frac{16}{27}\Big)L_{qr}^2L_{fr}+\Big(\frac{32}{27}\Big)L_{fr}^3$$
$$+\Big(\frac{1225}{243}+\frac{32}{9}\zeta_2\Big)L_{fr}+\Big(\frac{140}{27}\Big)L_{fr}^2\Big\}+C_F{n_f}^2\Big\{-\frac{2617}{162}+8\zeta_3+24\zeta_2+\Big($$
$$-\frac{32}{3}\Big)L_{qr}L_{fr}+\Big(-\frac{16}{3}\Big)L_{qr}+\Big(\frac{4}{3}\Big)L_{qr}^2+\Big(\frac{28}{3}\Big)L_{fr}^2+\Big(\frac{362}{9}-\frac{64}{3}\zeta_3\Big)L_{fr}\Big\}$$

$$
+ C_F^2 n_f \Bigg\{ - \frac{241}{9} + 160\zeta_5 - \frac{296}{3}\zeta_3 + \Big(- 2 \Big) L_{fr} + \Big(2 \Big) L_{qr} \Bigg\} + C_A {n_f}^2 \Bigg\{
$$

$$
- \frac{1487}{135} - \frac{2944}{135}\zeta_3 + \frac{1169}{27}\zeta_2 + \frac{80}{3}\zeta_2^2 + \Big(- \frac{668}{9} + \frac{64}{3}\zeta_2 \Big) L_{fr}^2 + \Big(- \frac{1877}{54}
$$

$$
+ \frac{512}{27}\zeta_3 - \frac{104}{27}\zeta_2 \Big) L_{fr} + \Big(- \frac{176}{9} \Big) L_{fr}^3 + \Big(- \frac{88}{9} \Big) L_{qr}^2 L_{fr} + \Big(- \frac{41}{9} \Big) L_{qr}
$$

$$
+ \Big(\frac{4}{3} \Big) L_{qr}^2 + \Big(\frac{88}{3} \Big) L_{qr} L_{fr}^2 + \Big(\frac{1184}{27} - \frac{128}{9}\zeta_2 \Big) L_{qr} L_{fr} \Bigg\} + C_A C_F n_f \Bigg\{ \frac{65866}{405}
$$

$$
+ 80\zeta_5 - \frac{6512}{45}\zeta_3 + \frac{284}{9}\zeta_2 - \frac{320}{3}\zeta_2\zeta_3 - \frac{32}{45}\zeta_2^2 + \Big(- \frac{1913}{9} + \frac{352}{3}\zeta_3 + 64\zeta_2 \Big) L_{fr}
$$

$$
+ \Big(- \frac{154}{3} \Big) L_{fr}^2 + \Big(- \frac{22}{3} \Big) L_{qr}^2 + \Big(\frac{55}{3} - 32\zeta_2 \Big) L_{qr} + \Big(\frac{176}{3} \Big) L_{qr} L_{fr} \Bigg\}
$$

$$
+ C_A^2 n_f \Bigg\{ \frac{55546}{405} - \frac{3392}{9}\zeta_5 + \frac{16223}{45}\zeta_3 - \frac{3149}{27}\zeta_2 + \frac{284}{3}\zeta_2\zeta_3 - \frac{22681}{135}\zeta_2^2 + \Big(
$$

$$
- 190 + 64\zeta_3 + \frac{1408}{9}\zeta_2 \Big) L_{qr} L_{fr} + \Big(- \frac{484}{3} \Big) L_{qr} L_{fr}^2 + \Big(- 14 - 16\zeta_3 \Big) L_{qr}^2
$$

$$
+ \Big(- \frac{829}{81} - \frac{3544}{27}\zeta_3 - \frac{5132}{27}\zeta_2 + \frac{376}{3}\zeta_2^2 \Big) L_{fr} + \Big(\frac{484}{9} \Big) L_{qr}^2 L_{fr} + \Big(\frac{523}{9}
$$

$$
+ 40\zeta_3 - \frac{112}{3}\zeta_2 - \frac{8}{3}\zeta_2^2 \Big) L_{qr} + \Big(\frac{968}{9} \Big) L_{fr}^3 + \Big(\frac{3299}{9} - 48\zeta_3 - \frac{704}{3}\zeta_2 \Big) L_{fr}^2 \Bigg\}
$$

$$
+ C_A^3 \Bigg\{ - \frac{303707}{810} + \frac{5156}{9}\zeta_5 - \frac{81074}{135}\zeta_3 + 96\zeta_3^2 - \frac{697}{9}\zeta_2 + 48\zeta_2\zeta_3 + \frac{6248}{27}\zeta_2^2
$$

$$
+ \frac{3872}{15}\zeta_2^3 + \Big(- \frac{17105}{27} + 264\zeta_3 + \frac{1936}{3}\zeta_2 \Big) L_{fr}^2 + \Big(- \frac{5324}{27} \Big) L_{fr}^3 + \Big(- \frac{1319}{9}
$$

$$
- 160\zeta_5 - 184\zeta_3 + \frac{496}{3}\zeta_2 + 352\zeta_2\zeta_3 + \frac{44}{3}\zeta_2^2 \Big) L_{qr} + \Big(- \frac{2662}{27} \Big) L_{qr}^2 L_{fr} + \Big(\frac{110}{3}
$$

$$
+ 88\zeta_3 \Big) L_{qr}^2 + \Big(\frac{109651}{486} + 160\zeta_5 + \frac{3032}{27}\zeta_3 + \frac{19504}{27}\zeta_2 - 352\zeta_2\zeta_3
$$

$$
- \frac{2068}{3}\zeta_2^2 \Big) L_{fr} + \Big(\frac{23782}{81} - 352\zeta_3 - \frac{3872}{9}\zeta_2 \Big) L_{qr} L_{fr} + \Big(\frac{2662}{9} \Big) L_{qr} L_{fr}^2 \Bigg\}. \tag{B.12}
$$

Appendix C

Coefficients of non-universal gravity

C.1 Soft-virtual coefficients

$$\Delta_{q\bar{q}}^{(3),G} = \delta(1-z)\Bigg\{\Bigg(-\frac{6131417}{1458}+\frac{3344}{3}\zeta_5+\frac{188276}{81}\zeta_3+\frac{10336}{3}\zeta_3^2+\frac{8122}{9}\zeta_2 - 432\zeta_2\zeta_3+\frac{4156}{45}\zeta_2^2-\frac{184736}{315}\zeta_2^3+\Bigg(-\frac{49402}{27}+\frac{5984}{3}\zeta_3+\frac{10112}{9}\zeta_2 - \frac{1792}{5}\zeta_2^2\Bigg)L_{qf}^2+\Bigg(\frac{19652}{81}+\frac{512}{3}\zeta_3-\frac{1088}{3}\zeta_2\Bigg)L_{qf}^3+\Bigg(\frac{760175}{162}+5664\zeta_5 - \frac{54304}{9}\zeta_3-\frac{26584}{27}\zeta_2-2752\zeta_2\zeta_3-\frac{176}{3}\zeta_2^2\Bigg)L_{qf}\Bigg)C_F^3+\Bigg(-\frac{31255393}{8748} - \frac{2852}{3}\zeta_5+\frac{84131}{27}\zeta_3-\frac{400}{3}\zeta_3^2+\frac{39781}{27}\zeta_2-\frac{820}{3}\zeta_2\zeta_3+\frac{20323}{135}\zeta_2^2+\frac{13264}{315}\zeta_2^3 + \Bigg(-\frac{15055}{27}+88\zeta_3\Bigg)L_{qf}^2+\Bigg(\frac{4114}{81}\Bigg)L_{qf}^3+\Bigg(\frac{561610}{243}+80\zeta_5-\frac{8792}{9}\zeta_3 - \frac{11056}{27}\zeta_2+\frac{68}{5}\zeta_2^2\Bigg)L_{qf}\Bigg)C_A^2C_F+\Bigg(-\frac{2467183}{2187}+\frac{5536}{9}\zeta_5+\frac{38488}{81}\zeta_3 + \frac{66184}{81}\zeta_2-\frac{5504}{9}\zeta_2\zeta_3-\frac{21808}{135}\zeta_2^2+\Bigg(-\frac{40028}{81}+160\zeta_3+\frac{896}{9}\zeta_2\Bigg)L_{qf}^2 + \Bigg(\frac{4972}{81}-\frac{64}{3}\zeta_2\Bigg)L_{qf}^3+\Bigg(\frac{109118}{81}-\frac{3280}{9}\zeta_3-\frac{13328}{27}\zeta_2 + \frac{112}{15}\zeta_2^2\Bigg)L_{qf}\Bigg)C_F^2n_f+\Bigg(-\frac{61807}{729}-\frac{2416}{81}\zeta_3+\frac{10384}{81}\zeta_2+\frac{128}{27}\zeta_2^2+\Bigg($$

$$
\begin{aligned}
&- \frac{244}{9}\Big)L_{qf}^2 + \Big(\frac{88}{27}\Big)L_{qf}^3 + \Big(\frac{6556}{81} + \frac{64}{9}\zeta_3 - \frac{416}{9}\zeta_2\Big)L_{qf}\Big){C_F{n_f}^2} \\
&+ \Big(\frac{2446783}{2187} + \frac{136}{3}\zeta_5 - \frac{6320}{27}\zeta_3 - \frac{8540}{9}\zeta_2 + \frac{224}{3}\zeta_2\zeta_3 - \frac{1060}{27}\zeta_2^2 + \Big(\\
&- \frac{213536}{243} + \frac{208}{9}\zeta_3 + \frac{2608}{9}\zeta_2 - \frac{8}{5}\zeta_2^2\Big)L_{qf} + \Big(- \frac{2024}{81}\Big)L_{qf}^3 + \Big(\frac{20014}{81} \\
&- 16\zeta_3\Big)L_{qf}^2\Big)C_AC_F{n_f} + \Big(\frac{65475811}{8748} - \frac{30664}{9}\zeta_5 - \frac{178948}{27}\zeta_3 + \frac{3280}{3}\zeta_3^2 \\
&- \frac{201062}{81}\zeta_2 + \frac{32960}{9}\zeta_2\zeta_3 + \frac{40576}{135}\zeta_2^2 - \frac{20816}{315}\zeta_2^3 + \Big(- \frac{3309509}{486} + 240\zeta_5 \\
&+ \frac{44584}{9}\zeta_3 + \frac{46808}{27}\zeta_2 - 1120\zeta_2\zeta_3 - \frac{448}{15}\zeta_2^2\Big)L_{qf} + \Big(- \frac{6358}{27} + \frac{352}{3}\zeta_2\Big)L_{qf}^3 \\
&+ \Big(\frac{57157}{27} - 1152\zeta_3 - \frac{1664}{3}\zeta_2 + 128\zeta_2^2\Big)L_{qf}^2\Big)C_AC_F^2 + \Big(\Big(- \frac{10514857}{2187} \\
&+ \frac{1280}{3}\zeta_5 + \frac{6784}{27}\zeta_3 + \frac{19088}{9}\zeta_2 + \frac{256}{3}\zeta_2\zeta_3 - \frac{22288}{45}\zeta_2^2 + \Big(- \frac{131140}{81} \\
&+ 128\zeta_3 + \frac{704}{9}\zeta_2\Big)L_{qf}^2 + \Big(\frac{1760}{9}\Big)L_{qf}^3 + \Big(\frac{1178048}{243} - 544\zeta_3 - \frac{10480}{9}\zeta_2 \\
&+ \frac{64}{5}\zeta_2^2\Big)L_{qf}\Big)C_AC_F^2 + \Big(- \frac{1268944}{2187} - \frac{10528}{81}\zeta_3 + \frac{60512}{81}\zeta_2 - \frac{896}{45}\zeta_2^2 + \Big(\\
&- \frac{10780}{81}\Big)L_{qf}^2 + \Big(\frac{1232}{81}\Big)L_{qf}^3 + \Big(\frac{107948}{243} + \frac{256}{3}\zeta_3 - \frac{784}{3}\zeta_2\Big)L_{qf}\Big)C_AC_F{n_f} \\
&+ \Big(\frac{39772}{729} - \frac{320}{3}\zeta_2 + \Big(- \frac{4096}{81} + \frac{128}{3}\zeta_2\Big)L_{qf} + \Big(- \frac{64}{27}\Big)L_{qf}^3 \\
&+ \Big(\frac{160}{9}\Big)L_{qf}^2\Big){C_F{n_f}^2} + \Big(\frac{2196934}{2187} + \frac{17312}{81}\zeta_3 - \frac{53440}{81}\zeta_2 + \frac{2816}{15}\zeta_2^2 + \Big(\\
&- \frac{280736}{243} - 128\zeta_3 + \frac{9856}{27}\zeta_2\Big)L_{qf} + \Big(- \frac{4768}{81}\Big)L_{qf}^3 + \Big(\frac{35560}{81} \\
&- \frac{256}{9}\zeta_2\Big)L_{qf}^2\Big)C_F^2{n_f} + \Big(\frac{3381256}{2187} - 480\zeta_5 + \frac{29972}{81}\zeta_3 - \frac{3344}{3}\zeta_2 - \frac{208}{3}\zeta_2\zeta_3 \\
&+ \frac{2324}{45}\zeta_2^2 + \Big(- \frac{234820}{243} - \frac{128}{3}\zeta_3 + \frac{10384}{27}\zeta_2\Big)L_{qf} + \Big(- \frac{1936}{81}\Big)L_{qf}^3 \\
&+ \Big(\frac{6316}{27}\Big)L_{qf}^2\Big)C_A^2C_F + \Big(\frac{263089}{81} - \frac{72176}{81}\zeta_3 - \frac{22984}{81}\zeta_2 - \frac{11488}{45}\zeta_2^2 + \Big(\\
&- \frac{1041604}{243} + \frac{17152}{9}\zeta_3 + \frac{25216}{27}\zeta_2 - \frac{128}{15}\zeta_2^2\Big)L_{qf} + \Big(- \frac{21728}{81} \\
&+ \frac{512}{3}\zeta_2\Big)L_{qf}^3 + \Big(\frac{150136}{81} - \frac{2816}{3}\zeta_3 - \frac{4864}{9}\zeta_2\Big)L_{qf}^2\Big)C_F^3\Big)r_q + \Big(\Big(\\
&- \frac{325244}{729} - \frac{79328}{81}\zeta_2 + \frac{1024}{3}\zeta_2^2 + \Big(- \frac{29632}{81} + \frac{512}{9}\zeta_2\Big)L_{qf}^2 + \Big(\frac{1664}{27}\Big)L_{qf}^3
\end{aligned}
$$

$$
+\left(\frac{172408}{243}+\frac{512}{3}\zeta_2\right)L_{qf}\Big)C_F^3+\Big(-\frac{79288}{729}-\frac{5504}{27}\zeta_2+\Big(-\frac{4928}{81}\Big)L_{qf}^2
+\left(\frac{256}{27}\right)L_{qf}^3+\left(\frac{34976}{243}+\frac{512}{9}\zeta_2\right)L_{qf}\Big)C_F^2n_f+\Big(\frac{266084}{729}+\frac{55952}{81}\zeta_2+\Big(
-\frac{113608}{243}-\frac{4672}{27}\zeta_2\Big)L_{qf}+\Big(-\frac{704}{27}\Big)L_{qf}^3+\left(\frac{14992}{81}\right)L_{qf}^2\Big)C_AC_F^2\Big)r_q^2\Big\}
+\mathcal{D}_5\Big\{\Big(512\Big)C_F^3\Big\}+\mathcal{D}_4\Big\{\Big(-\frac{7040}{9}\Big)C_AC_F^2+\left(\frac{1280}{9}\right)C_F^2n_f
+\Big(\Big(1280\Big)L_{qf}\Big)C_F^3\Big\}+\mathcal{D}_3\Big\{\Big(-\frac{31744}{9}-3072\zeta_2+\left(\frac{4352}{3}\right)L_{qf}
+\left(1024\right)L_{qf}^2\Big)C_F^3+\Big(-\frac{2560}{9}+\left(\frac{2560}{9}\right)L_{qf}\Big)C_F^2n_f+\Big(
-\frac{2816}{27}\Big)C_AC_Fn_f+\left(\frac{256}{27}\right)C_F{n_f}^2+\left(\frac{7744}{27}\right)C_A^2C_F+\Big(\frac{17152}{9}-512\zeta_2
+\Big(-\frac{14080}{9}\Big)L_{qf}\Big)C_AC_F^2+\Big(\Big(\frac{8704}{9}+\Big(-\frac{2048}{3}\Big)L_{qf}\Big)C_F^3\Big)r_q\Big\}
+\mathcal{D}_2\Big\{\Big(-\frac{28480}{27}+\frac{704}{3}\zeta_2+\left(\frac{3872}{9}\right)L_{qf}\Big)C_A^2C_F+\Big(-\frac{1696}{27}-\frac{2048}{3}\zeta_2
+\Big(-\frac{2752}{9}\Big)L_{qf}+\left(192\right)L_{qf}^2\Big)C_F^2n_f+\Big(-\frac{640}{27}+\left(\frac{128}{9}\right)L_{qf}\Big)C_F{n_f}^2
+\left(\frac{4864}{27}+1344\zeta_3+\frac{11264}{3}\zeta_2+\left(\frac{19744}{9}-768\zeta_2\right)L_{qf}\right.
+\Big(-1056\Big)L_{qf}^2\Big)C_AC_F^2+\Big(\frac{9248}{27}-\frac{128}{3}\zeta_2+\Big(-\frac{1408}{9}\Big)L_{qf}\Big)C_AC_Fn_f
+\left(10240\zeta_3+\Big(-\frac{15872}{3}-4608\zeta_2\Big)L_{qf}+\left(256\right)L_{qf}^3+\left(2176\right)L_{qf}^2\right)C_F^3
+\Big(\Big(-\frac{11968}{27}+\left(\frac{2816}{9}\right)L_{qf}\Big)C_AC_F^2+\left(\frac{2176}{27}+\Big(-\frac{512}{9}\Big)L_{qf}\right)C_F^2n_f
+\Big(\Big(\frac{4352}{3}\Big)L_{qf}+\Big(-1024\Big)L_{qf}^2\Big)C_F^3\Big)r_q\Big\}+\mathcal{D}_1\Big\{\Big(-\frac{604948}{81}-4160\zeta_3
-\frac{1664}{3}\zeta_2+\frac{3648}{5}\zeta_2^2+\Big(-\frac{704}{3}\Big)L_{qf}^3+\Big(-\frac{400}{9}-256\zeta_2\Big)L_{qf}^2+\Big(\frac{37456}{9}
+512\zeta_3+\frac{8768}{3}\zeta_2\Big)L_{qf}\Big)C_AC_F^2+\Big(-\frac{32816}{81}+384\zeta_2+\Big(-\frac{704}{9}\Big)L_{qf}^2
+\Big(\frac{9248}{27}-\frac{128}{3}\zeta_2\Big)L_{qf}\Big)C_AC_Fn_f+\Big(\frac{1600}{81}-\frac{256}{9}\zeta_2+\Big(-\frac{640}{27}\Big)L_{qf}
+\left(\frac{64}{9}\right)L_{qf}^2\Big)C_F{n_f}^2+\Big(\frac{32768}{27}+1280\zeta_3-\frac{256}{9}\zeta_2+\Big(-\frac{7552}{9}
-\frac{1792}{3}\zeta_2\Big)L_{qf}+\left(\frac{128}{3}\right)L_{qf}^3+\left(\frac{608}{9}\right)L_{qf}^2\Big)C_F^2n_f+\Big(\frac{124024}{81}-704\zeta_3
$$

$$
- \frac{12032}{9}\zeta_2 + \frac{704}{5}\zeta_2^2 + \left(- \frac{28480}{27} + \frac{704}{3}\zeta_2 \right) L_{qf} + \left(\frac{1936}{9} \right) L_{qf}^2 \Big) C_A^2 C_F
$$

$$
+ \left(\frac{172372}{27} - 1984\zeta_3 + \frac{42656}{9}\zeta_2 - \frac{14208}{5}\zeta_2^2 + \left(- \frac{137200}{27} + 11008\zeta_3 \right.\right.
$$

$$
\left. - \frac{5504}{3}\zeta_2 \right) L_{qf} + \left(- 736 - 2048\zeta_2 \right) L_{qf}^2 + \left(\frac{2176}{3} \right) L_{qf}^3 \Big) C_F^3 + \Big(\Big(\Big.
$$

$$
- \frac{287968}{81} - \frac{12800}{9}\zeta_2 + \left(- \frac{3328}{9} \right) L_{qf}^2 + \left(- \frac{1024}{3} \right) L_{qf}^3 + \left(\frac{95360}{27} \right.
$$

$$
\left. + \frac{2048}{3}\zeta_2 \right) L_{qf} \Big) C_F^3 + \left(- \frac{16064}{27} + \frac{1024}{3}\zeta_2 + \left(- \frac{1024}{9} \right) L_{qf}^2 \right.
$$

$$
+ \left(\frac{12416}{27} \right) L_{qf} \Big) C_F^2 n_f + \left(\frac{198112}{81} - \frac{9728}{9}\zeta_2 + \left(- \frac{53120}{27} + \frac{512}{3}\zeta_2 \right) L_{qf} \right.
$$

$$
+ \left(\frac{1408}{3} \right) L_{qf}^2 \Big) C_A C_F^2 \Big) r_q + \Big(\Big(\left(\frac{18496}{81} + \frac{2048}{3}\zeta_2 + \left(- \frac{8704}{27} \right) L_{qf} \right.
$$

$$
\left. + \left(\frac{1024}{9} \right) L_{qf}^2 \right) C_F^3 \Big) r_q^2 \Big\} + \mathcal{D}_0 \Big\{ \Big(- \frac{594058}{729} - 384\zeta_5 + \frac{40144}{27}\zeta_3
$$

$$
+ \frac{98224}{81}\zeta_2 - \frac{352}{3}\zeta_2\zeta_3 - \frac{2992}{15}\zeta_2^2 + \left(- \frac{7120}{27} + \frac{176}{3}\zeta_2 \right) L_{qf}^2 + \left(\frac{968}{27} \right) L_{qf}^3
$$

$$
+ \left(\frac{62012}{81} - 352\zeta_3 - \frac{6016}{9}\zeta_2 + \frac{352}{5}\zeta_2^2 \right) L_{qf} \Big) C_A^2 C_F + \Big(- \frac{24754}{243} - \frac{5728}{9}\zeta_3
$$

$$
+ \frac{1760}{9}\zeta_2 - \frac{1472}{15}\zeta_2^2 + \left(- \frac{3784}{9} - \frac{320}{3}\zeta_2 \right) L_{qf}^2 + \left(\frac{224}{3} \right) L_{qf}^3 + \left(\frac{56768}{81} \right.
$$

$$
\left. + 640\zeta_3 - \frac{1216}{9}\zeta_2 \right) L_{qf} \Big) C_F^2 n_f + \Big(- \frac{3712}{729} + \frac{320}{27}\zeta_3 + \frac{640}{27}\zeta_2 + \Big(
$$

$$
- \frac{160}{27} \Big) L_{qf}^2 + \left(\frac{32}{27} \right) L_{qf}^3 + \left(\frac{800}{81} - \frac{128}{9}\zeta_2 \right) L_{qf} \Big) C_F {n_f}^2 + \left(\frac{125252}{729} \right.
$$

$$
- \frac{2480}{9}\zeta_3 - \frac{29392}{81}\zeta_2 + \frac{736}{15}\zeta_2^2 + \left(- \frac{16408}{81} + 192\zeta_2 \right) L_{qf} + \left(- \frac{352}{27} \right) L_{qf}^3
$$

$$
+ \left(\frac{2312}{27} - \frac{32}{3}\zeta_2 \right) L_{qf}^2 \Big) C_A C_F n_f + \left(\frac{400768}{243} + \frac{20416}{9}\zeta_3 - \frac{10240}{9}\zeta_2 \right.
$$

$$
- 1472\zeta_2\zeta_3 + \frac{1408}{3}\zeta_2^2 + \left(- \frac{357418}{81} - \frac{4336}{3}\zeta_3 + \frac{3488}{9}\zeta_2 + \frac{1824}{5}\zeta_2^2 \right) L_{qf}
$$

$$
+ \left(- \frac{2992}{9} \right) L_{qf}^3 + \left(\frac{19400}{9} - 192\zeta_3 + \frac{1216}{3}\zeta_2 \right) L_{qf}^2 \Big) C_A C_F^2 + \Big(12288\zeta_5
$$

$$
- \frac{63488}{9}\zeta_3 - 6144\zeta_2\zeta_3 + \left(- \frac{68600}{27} + 2432\zeta_3 - \frac{2752}{3}\zeta_2 \right) L_{qf}^2 + \left(\frac{4624}{9} \right.
$$

$$
\left. - 256\zeta_2 \right) L_{qf}^3 + \left(\frac{86186}{27} + \frac{5728}{3}\zeta_3 + \frac{21328}{9}\zeta_2 - \frac{7104}{5}\zeta_2^2 \right) L_{qf} \Big) C_F^3 + \Big(\Big(\Big.
$$

$$
- \frac{109888}{243} + \frac{3808}{9}\zeta_3 + \frac{11968}{27}\zeta_2 + \left(- \frac{7856}{9} + \frac{256}{3}\zeta_2 \right) L_{qf}^2 + \left(\frac{1408}{9} \right) L_{qf}^3
$$

$$+\left(\frac{124912}{81}-\frac{896}{3}\zeta_3-\frac{2560}{3}\zeta_2\right)L_{qf}\Bigg)C_AC_F^2+\Bigg(\frac{15232}{243}-\frac{2176}{27}\zeta_2+\Bigg(-\frac{27680}{81}+\frac{2048}{9}\zeta_2\Bigg)L_{qf}+\Bigg(-\frac{128}{3}\Bigg)L_{qf}^3+\left(\frac{1888}{9}\right)L_{qf}^2\Bigg)C_F^2n_f+\Bigg(\frac{17408}{9}\zeta_3+\Bigg(-\frac{143984}{81}-\frac{4096}{3}\zeta_3-\frac{6400}{9}\zeta_2\Bigg)L_{qf}+\Bigg(-\frac{1280}{3}\Bigg)L_{qf}^3+\left(\frac{47680}{27}+\frac{1024}{3}\zeta_2\right)L_{qf}^2\Bigg)C_F^3\Bigg)r_q+\Bigg(\Bigg(\Bigg(-\frac{4352}{27}\Bigg)L_{qf}^2+\left(\frac{512}{9}\right)L_{qf}^3+\left(\frac{9248}{81}+\frac{1024}{3}\zeta_2\right)L_{qf}\Bigg)C_F^3\Bigg)r_q^2\Bigg\}. \tag{C.1}$$

$$\Delta_{gg}^{(3),G}=\delta(1-z)\Bigg\{\Bigg(-\frac{303707}{810}-\frac{28636}{9}\zeta_5-\frac{186194}{135}\zeta_3+\frac{13216}{3}\zeta_3^2+\frac{923}{3}\zeta_2+\frac{8944}{3}\zeta_2\zeta_3+\frac{29416}{135}\zeta_2^2-\frac{64096}{105}\zeta_2^3+\Bigg(-\frac{1319}{9}+5984\zeta_5-\frac{3496}{3}\zeta_3+\frac{15232}{27}\zeta_2-3872\zeta_2\zeta_3-\frac{396}{5}\zeta_2^2\Bigg)L_{qf}+\Bigg(\frac{110}{3}+\frac{968}{3}\zeta_3+\frac{736}{3}\zeta_2-\frac{1152}{5}\zeta_2^2\Bigg)L_{qf}^2+\left(\frac{512}{3}\zeta_3-\frac{352}{3}\zeta_2\right)L_{qf}^3\Bigg)C_A^3+\Bigg(-\frac{442583}{4374}-\frac{1136}{81}\zeta_3+\frac{8396}{81}\zeta_2-\frac{208}{15}\zeta_2^2+\Bigg(-\frac{320}{27}+\frac{32}{9}\zeta_2\Bigg)L_{qf}^2+\left(\frac{88}{81}\right)L_{qf}^3+\Bigg(\frac{13291}{243}+\frac{64}{9}\zeta_3-\frac{1024}{27}\zeta_2\Bigg)L_{qf}\Bigg){C_An_f}^2+\Bigg(-\frac{46372}{729}-\frac{128}{81}\zeta_3+\frac{5504}{81}\zeta_2+\Bigg(-\frac{688}{81}\Bigg)L_{qf}^2+\left(\frac{64}{81}\right)L_{qf}^3+\left(\frac{8776}{243}-\frac{512}{27}\zeta_2\right)L_{qf}\Bigg){C_Fn_f}^2+\Bigg(-\frac{62429}{3645}-\frac{10592}{405}\zeta_3+\frac{6016}{81}\zeta_2+\frac{64}{15}\zeta_2^2+\Bigg(-\frac{752}{81}\Bigg)L_{qf}^2+\left(\frac{128}{81}\right)L_{qf}^3+\Bigg(\frac{3932}{243}+\frac{64}{3}\zeta_3-\frac{1024}{27}\zeta_2\Bigg)L_{qf}\Bigg)C_F^2n_f+\Bigg(\frac{5410051}{21870}+\frac{5032}{9}\zeta_5+\frac{177278}{405}\zeta_3-\frac{20276}{81}\zeta_2-\frac{1840}{3}\zeta_2\zeta_3+\frac{964}{27}\zeta_2^2+\Bigg(-\frac{1046}{27}+144\zeta_3+\frac{272}{3}\zeta_2\Bigg)L_{qf}^2+\Bigg(\frac{484}{81}-\frac{64}{3}\zeta_2\Bigg)L_{qf}^3+\left(\frac{9029}{243}-\frac{3824}{9}\zeta_3-\frac{2704}{27}\zeta_2+\frac{40}{3}\zeta_2^2\right)L_{qf}\Bigg)C_A^2n_f+\Bigg(\frac{1056967}{3645}-\frac{5296}{45}\zeta_3-\frac{4868}{27}\zeta_2+64\zeta_2\zeta_3-112\zeta_2^2+\Bigg(-\frac{2722}{81}+\frac{128}{9}\zeta_2\Bigg)L_{qf}^2+\Bigg(-\frac{5075}{243}+\frac{80}{3}\zeta_3-\frac{544}{27}\zeta_2\Bigg)L_{qf}+\left(\frac{176}{27}\right)L_{qf}^3\Bigg)C_AC_Fn_f$$

$$
+\Bigg(\Bigg(-\frac{464173}{3645}+80\zeta_5-\frac{256}{45}\zeta_3+\frac{3308}{27}\zeta_2-\frac{320}{3}\zeta_2\zeta_3+\frac{5008}{45}\zeta_2^2+\Bigg(
-\frac{176}{27}\Bigg)L_{qf}^3+\Bigg(\frac{2128}{81}-\frac{128}{9}\zeta_2\Bigg)L_{qf}^2+\Bigg(\frac{9530}{243}-\frac{80}{3}\zeta_3
+\frac{112}{27}\zeta_2\Bigg)L_{qf}\Bigg)C_AC_Fn_f+\Bigg(-\frac{2410567}{21870}-\frac{760}{3}\zeta_5-\frac{11591}{405}\zeta_3+\frac{4169}{81}\zeta_2
+\frac{332}{3}\zeta_2\zeta_3-\frac{5071}{45}\zeta_2^2+\Bigg(-\frac{484}{81}+\frac{128}{3}\zeta_2\Bigg)L_{qf}^3+\Bigg(\frac{5092}{243}+\frac{6104}{9}\zeta_3+\frac{112}{9}\zeta_2
+\frac{16}{15}\zeta_2^2\Bigg)L_{qf}+\Bigg(\frac{668}{27}-\frac{608}{3}\zeta_3-144\zeta_2\Bigg)L_{qf}^2\Bigg)C_A^2n_f+\Bigg(-\frac{35176}{3645}+160\zeta_5
-\frac{29368}{405}\zeta_3-\frac{6016}{81}\zeta_2-\frac{64}{15}\zeta_2^2+\Bigg(-\frac{3446}{243}-\frac{64}{3}\zeta_3+\frac{1024}{27}\zeta_2\Bigg)L_{qf}+\Bigg(
-\frac{128}{81}\Bigg)L_{qf}^3+\Bigg(\frac{752}{81}\Bigg)L_{qf}^2\Bigg)C_F^2n_f+\Bigg(\frac{16087}{486}+\frac{3296}{81}\zeta_3-\frac{4216}{81}\zeta_2+\Bigg(
-\frac{11186}{243}-\frac{32}{3}\zeta_3+\frac{128}{9}\zeta_2\Bigg)L_{qf}+\Bigg(-\frac{160}{81}\Bigg)L_{qf}^3+\Bigg(\frac{1340}{81}\Bigg)L_{qf}^2\Bigg)C_F{n_f}^2
+\Bigg(\frac{1404698}{10935}-\frac{10952}{405}\zeta_3-\frac{2104}{27}\zeta_2-\frac{32}{45}\zeta_2^2+\Bigg(-\frac{23468}{243}+\frac{32}{9}\zeta_3
+\frac{1348}{27}\zeta_2\Bigg)L_{qf}+\Bigg(-\frac{220}{81}\Bigg)L_{qf}^3+\Bigg(\frac{2125}{81}-\frac{64}{9}\zeta_2\Bigg)L_{qf}^2\Bigg)C_A{n_f}^2\Bigg)r_g+\Bigg(\Bigg(
-\frac{55825}{1458}+\frac{280}{9}\zeta_3+\frac{973}{81}\zeta_2+\frac{64}{3}\zeta_2^2+\Bigg(-\frac{1057}{81}+\frac{32}{9}\zeta_2\Bigg)L_{qf}^2+\Bigg(\frac{44}{27}\Bigg)L_{qf}^3
+\Bigg(\frac{9070}{243}-\frac{32}{3}\zeta_3-12\zeta_2\Bigg)L_{qf}\Bigg)C_A{n_f}^2+\Bigg(\frac{10465}{729}-\frac{280}{9}\zeta_3+\frac{656}{81}\zeta_2+\Bigg(
-\frac{544}{81}\Bigg)L_{qf}^2+\Bigg(\frac{32}{27}\Bigg)L_{qf}^3+\Bigg(\frac{1114}{243}+\frac{32}{3}\zeta_3+\frac{128}{27}\zeta_2\Bigg)L_{qf}\Bigg)C_F{n_f}^2\Bigg)r_g^2\Bigg\}
+\mathcal{D}_5\Bigg\{\Bigg(512\Bigg)C_A^3\Bigg\}+\mathcal{D}_4\Bigg\{\Bigg(-\frac{7040}{9}+\Bigg(1280\Bigg)L_{qf}\Bigg)C_A^3+\Bigg(\frac{1280}{9}\Bigg)C_A^2n_f\Bigg\}
+\mathcal{D}_3\Bigg\{\Bigg(-\frac{18752}{27}-3584\zeta_2+\Bigg(-\frac{5632}{9}\Bigg)L_{qf}+\Bigg(1024\Bigg)L_{qf}^2\Bigg)C_A^3+\Bigg(
-\frac{10496}{27}+\Bigg(\frac{2560}{9}\Bigg)L_{qf}\Bigg)C_A^2n_f+\Bigg(\frac{256}{27}\Bigg)C_A{n_f}^2+\Bigg(\Bigg(\frac{4480}{9}+\Bigg(
-\frac{512}{3}\Bigg)L_{qf}\Bigg)C_A^2n_f\Bigg)r_g\Bigg\}+\mathcal{D}_2\Bigg\{\Bigg(-1168+11584\zeta_3+\frac{11968}{3}\zeta_2+\Bigg(-1472
-5376\zeta_2\Bigg)L_{qf}+\Bigg(256\Bigg)L_{qf}^3+\Bigg(352\Bigg)L_{qf}^2\Bigg)C_A^3+\Bigg(-\frac{640}{27}
+\Bigg(\frac{128}{9}\Bigg)L_{qf}\Bigg)C_A{n_f}^2+\Bigg(\frac{8128}{27}-\frac{2176}{3}\zeta_2+\Bigg(-\frac{4544}{9}\Bigg)L_{qf}
+\Bigg(192\Bigg)L_{qf}^2\Bigg)C_A^2n_f+\Bigg(\Bigg(-\frac{6160}{27}+\Bigg(\frac{7424}{9}\Bigg)L_{qf}+\Bigg(-256\Bigg)L_{qf}^2\Bigg)C_A^2n_f
$$

$$+\left(\frac{1120}{27}+\left(-\frac{128}{9}\right)L_{qf}\right)C_A{n_f}^2\Big)r_g+\left(32\right)C_AC_Fn_f\Big\}+\mathcal{D}_1\Big\{\Big(-\frac{6932}{9}$$
$$-\frac{20416}{3}\zeta_3+\frac{17120}{9}\zeta_2-\frac{9856}{5}\zeta_2^2+\left(-\frac{21536}{27}+11520\zeta_3+\frac{5632}{3}\zeta_2\right)L_{qf}$$
$$+\left(-\frac{1472}{3}-2304\zeta_2\right)L_{qf}^2+\left(\frac{704}{3}\right)L_{qf}^3\Big)C_A^3+\Big(\frac{1600}{81}-\frac{256}{9}\zeta_2+\Big($$
$$-\frac{640}{27}\Big)L_{qf}+\left(\frac{64}{9}\right)L_{qf}^2\Big)C_A{n_f}^2+\Big(\frac{4904}{81}+128\zeta_3-\frac{2048}{9}\zeta_2+\Big($$
$$-\frac{992}{9}\Big)L_{qf}+\left(\frac{256}{9}\right)L_{qf}^2\Big)C_AC_Fn_f+\Big(\frac{58160}{81}+\frac{3328}{3}\zeta_3+\frac{3200}{9}\zeta_2+\Big($$
$$-\frac{4864}{27}-\frac{1664}{3}\zeta_2\Big)L_{qf}+\left(-\frac{928}{9}\right)L_{qf}^2+\left(\frac{128}{3}\right)L_{qf}^3\Big)C_A^2n_f+\Big(\Big($$
$$-\frac{44840}{81}+256\zeta_3-832\zeta_2+\left(-\frac{256}{3}\right)L_{qf}^3+\left(\frac{1888}{9}\right)L_{qf}^2+\Big(\frac{2528}{9}$$
$$+\frac{640}{3}\zeta_2\Big)L_{qf}\Big)C_A^2n_f+\Big(-\frac{5600}{81}+\Big(-\frac{128}{9}\Big)L_{qf}^2+\left(\frac{1760}{27}\right)L_{qf}\Big)C_A{n_f}^2$$
$$+\left(\frac{9568}{81}-256\zeta_3+\frac{2048}{9}\zeta_2+\left(-\frac{256}{9}\right)L_{qf}^2+\left(\frac{704}{9}\right)L_{qf}\right)C_AC_Fn_f\Big)r_g$$
$$+\Big(\Big(\frac{4900}{81}+\frac{128}{3}\zeta_2+\left(-\frac{1120}{27}\right)L_{qf}+\left(\frac{64}{9}\right)L_{qf}^2\Big)C_A{n_f}^2\Big)r_g^2\Big\}+\mathcal{D}_0\Big\{\Big($$
$$-\frac{11164}{729}-\frac{7600}{9}\zeta_3-\frac{15280}{81}\zeta_2-\frac{544}{15}\zeta_2^2+\left(-\frac{4912}{27}-\frac{224}{3}\zeta_2\right)L_{qf}^2$$
$$+\left(\frac{704}{27}\right)L_{qf}^3+\left(\frac{11336}{27}+\frac{1664}{3}\zeta_3+\frac{896}{9}\zeta_2\right)L_{qf}\Big)C_A^2n_f+\Big(-\frac{3712}{729}$$
$$+\frac{320}{27}\zeta_3+\frac{640}{27}\zeta_2+\left(-\frac{160}{27}\right)L_{qf}^2+\left(\frac{32}{27}\right)L_{qf}^3+\Big(\frac{800}{81}$$
$$-\frac{128}{9}\zeta_2\Big)L_{qf}\Big)C_A{n_f}^2+\Big(\frac{3422}{27}-\frac{608}{9}\zeta_3-32\zeta_2-\frac{64}{5}\zeta_2^2+\left(-\frac{568}{9}\right)L_{qf}^2$$
$$+\left(\frac{128}{9}\right)L_{qf}^3+\left(\frac{2452}{81}+64\zeta_3-\frac{1024}{9}\zeta_2\right)L_{qf}\Big)C_AC_Fn_f+\Big(\frac{390086}{729}$$
$$+11904\zeta_5-\frac{46952}{27}\zeta_3+\frac{29824}{81}\zeta_2-\frac{23200}{3}\zeta_2\zeta_3+\frac{4048}{15}\zeta_2^2+\Big(-\frac{66746}{81}$$
$$-\frac{3344}{3}\zeta_3+\frac{4144}{3}\zeta_2-\frac{4928}{5}\zeta_2^2\Big)L_{qf}+\Big(\frac{116}{9}+2240\zeta_3-176\zeta_2\Big)L_{qf}^2$$
$$+\left(\frac{968}{27}-256\zeta_2\right)L_{qf}^3\Big)C_A^3+\Big(\Big(-\frac{56560}{243}+\frac{3640}{3}\zeta_3+\frac{6160}{27}\zeta_2+\Big($$
$$-\frac{15956}{81}-288\zeta_3-\frac{4448}{9}\zeta_2\Big)L_{qf}+\left(-\frac{352}{9}\right)L_{qf}^3+\Big(\frac{5332}{27}$$
$$+\frac{320}{3}\zeta_2\Big)L_{qf}^2\Big)C_A^2n_f+\Big(\frac{7840}{243}-\frac{1120}{27}\zeta_2+\Big(-\frac{1232}{27}+\frac{128}{9}\zeta_2\Big)L_{qf}+\Big($$

$$- \frac{32}{9}\Big)L_{qf}^3 + \Big(\frac{200}{9}\Big)L_{qf}^2\Big)C_A{n_f}^2 + \Big(\Big(- \frac{128}{9}\Big)L_{qf}^3 + \Big(\frac{352}{9}\Big)L_{qf}^2 + \Big(\frac{4784}{81} - 128\zeta_3 + \frac{1024}{9}\zeta_2\Big)L_{qf}\Big)C_AC_Fn_f\Big)r_g + \Big(\Big(\Big(- \frac{560}{27}\Big)L_{qf}^2 + \Big(\frac{32}{9}\Big)L_{qf}^3 + \Big(\frac{2450}{81} + \frac{64}{3}\zeta_2\Big)L_{qf}\Big)C_A{n_f}^2\Big)r_g^2\Big\}. \tag{C.2}$$

$$g_{01}^{gg} = r_g\Big\{\Big(\frac{35}{9} + \Big(- \frac{4}{3}\Big)L_{qr}\Big)n_f\Big\} + \Big\{\Big(- \frac{203}{9} + 16\zeta_2 + \Big(- \frac{22}{3}\Big)L_{fr} + \Big(\frac{22}{3}\Big)L_{qr}\Big)C_A + \Big(\Big(\frac{4}{3}\Big)L_{fr}\Big)n_f\Big\}, \tag{C.3}$$

$$g_{02}^{gg} = r_g\Big\{\Big(- \frac{10295}{162} + 16\zeta_3 + \frac{442}{9}\zeta_2 + \Big(- \frac{770}{27}\Big)L_{fr} + \Big(- \frac{22}{3}\Big)L_{qr}^2 + \Big(\frac{88}{9}\Big)L_{qr}L_{fr} + \Big(\frac{1127}{27} - \frac{64}{3}\zeta_2\Big)L_{qr}\Big)C_An_f + \Big(\frac{598}{81} - 16\zeta_3 + \frac{128}{9}\zeta_2 + \Big(- \frac{16}{9}\Big)L_{qr}^2 + \Big(\frac{44}{9}\Big)L_{qr}\Big)C_Fn_f + \Big(\Big(- \frac{16}{9}\Big)L_{qr}L_{fr} + \Big(\frac{140}{27}\Big)L_{fr}\Big){n_f}^2\Big\} + r_g^2\Big\{\Big(\frac{1225}{324} + \frac{8}{3}\zeta_2 + \Big(- \frac{70}{27}\Big)L_{qr} + \Big(\frac{4}{9}\Big)L_{qr}^2\Big){n_f}^2\Big\} + \Big\{\Big(\frac{1049}{81} - \frac{128}{9}\zeta_2 + \Big(- \frac{80}{9}\Big)L_{qr} + \Big(\frac{16}{9}\Big)L_{qr}^2 + \Big(4\Big)L_{fr}\Big)C_Fn_f + \Big(\frac{7801}{324} + \frac{88}{9}\zeta_3 - \frac{1312}{9}\zeta_2 + 92\zeta_2^2 + \Big(- \frac{1657}{27} + 24\zeta_3 + \frac{176}{3}\zeta_2\Big)L_{qr} + \Big(- \frac{484}{9}\Big)L_{qr}L_{fr} + \Big(\frac{121}{9}\Big)L_{qr}^2 + \Big(\frac{121}{3}\Big)L_{fr}^2 + \Big(\frac{3890}{27} - 24\zeta_3 - \frac{352}{3}\zeta_2\Big)L_{fr}\Big)C_A^2 + \Big(\frac{3656}{81} - \frac{16}{9}\zeta_3 - \frac{112}{3}\zeta_2 + \Big(- \frac{668}{27} + \frac{64}{3}\zeta_2\Big)L_{fr} + \Big(- \frac{160}{9} + \frac{32}{3}\zeta_2\Big)L_{qr} + \Big(- \frac{44}{3}\Big)L_{fr}^2 + \Big(\frac{22}{9}\Big)L_{qr}^2 + \Big(\frac{88}{9}\Big)L_{qr}L_{fr}\Big)C_An_f + \Big(\Big(\frac{4}{3}\Big)L_{fr}^2\Big){n_f}^2\Big\}, \tag{C.4}$$

$$g_{03}^{gg} = r_g\Big\{\Big(- \frac{464173}{3645} + 80\zeta_5 - \frac{256}{45}\zeta_3 + \frac{14708}{81}\zeta_2 - \frac{704}{3}\zeta_2\zeta_3 + \frac{3376}{15}\zeta_2^2 + \Big(- \frac{13156}{243} + \frac{352}{3}\zeta_3 - \frac{2816}{27}\zeta_2\Big)L_{fr} + \Big(- \frac{968}{27}\Big)L_{qr}L_{fr} + \Big(- \frac{176}{27}\Big)L_{qr}^3 + \Big(\frac{352}{27}\Big)L_{qr}^2L_{fr} + \Big(\frac{2128}{81} - \frac{256}{9}\zeta_2\Big)L_{qr}^2 + \Big(\frac{9530}{243} - \frac{80}{3}\zeta_3 + \frac{1168}{27}\zeta_2\Big)L_{qr}\Big)C_AC_Fn_f + \Big(- \frac{2410567}{21870} - \frac{760}{3}\zeta_5 + \frac{50009}{405}\zeta_3 - \frac{18251}{81}\zeta_2 + \frac{716}{3}\zeta_2\zeta_3 + \frac{6449}{45}\zeta_2^2 + \Big(- \frac{22490}{81}$$

$$+ 32\zeta_3 + \frac{1408}{9}\zeta_2\Big)L_{qr}L_{fr} + \Big(-\frac{484}{9}\Big)L_{qr}L_{fr}^2 + \Big(-\frac{484}{81}\Big)L_{qr}^3 + \Big(\frac{5092}{243}$$
$$+ \frac{3464}{27}\zeta_3 + \frac{1376}{9}\zeta_2 - \frac{368}{3}\zeta_2^2\Big)L_{qr} + \Big(\frac{668}{27} - 32\zeta_3 - \frac{352}{9}\zeta_2\Big)L_{qr}^2$$
$$+ \Big(\frac{484}{9}\Big)L_{qr}^2L_{fr} + \Big(\frac{4235}{27}\Big)L_{fr}^2 + \Big(\frac{93085}{243} - \frac{632}{3}\zeta_3 - \frac{9724}{27}\zeta_2\Big)L_{fr}\Big)C_A^2n_f$$
$$+ \Big(-\frac{35176}{3645} + 160\zeta_5 - \frac{29368}{405}\zeta_3 - \frac{6016}{81}\zeta_2 - \frac{64}{15}\zeta_2^2 + \Big(-\frac{3446}{243} - \frac{64}{3}\zeta_3$$
$$+ \frac{1024}{27}\zeta_2\Big)L_{qr} + \Big(-\frac{128}{81}\Big)L_{qr}^3 + \Big(\frac{752}{81}\Big)L_{qr}^2\Big)C_F^2n_f + \Big(\frac{16087}{486} + \frac{3296}{81}\zeta_3$$
$$- \frac{4216}{81}\zeta_2 + \Big(-\frac{11186}{243} - \frac{32}{3}\zeta_3 + \frac{128}{9}\zeta_2\Big)L_{qr} + \Big(-\frac{64}{27}\Big)L_{qr}^2L_{fr} + \Big($$
$$-\frac{160}{81}\Big)L_{qr}^3 + \Big(\frac{32}{27}\Big)L_{qr}L_{fr} + \Big(\frac{1340}{81}\Big)L_{qr}^2 + \Big(\frac{6172}{243} - \frac{64}{3}\zeta_3$$
$$+ \frac{512}{27}\zeta_2\Big)L_{fr}\Big)C_F{n_f}^2 + \Big(\frac{1404698}{10935} - \frac{7384}{135}\zeta_3 - \frac{9112}{81}\zeta_2 - \frac{32}{45}\zeta_2^2 + \Big(-\frac{23468}{243}$$
$$+ \frac{352}{27}\zeta_3 + \frac{2228}{27}\zeta_2\Big)L_{qr} + \Big(-\frac{15550}{243} + \frac{64}{3}\zeta_3 + \frac{1768}{27}\zeta_2\Big)L_{fr} + \Big(-\frac{1540}{27}\Big)L_{fr}^2$$
$$+ \Big(-\frac{88}{9}\Big)L_{qr}^2L_{fr} + \Big(-\frac{220}{81}\Big)L_{qr}^3 + \Big(\frac{176}{9}\Big)L_{qr}L_{fr}^2 + \Big(\frac{2125}{81} - \frac{128}{9}\zeta_2\Big)L_{qr}^2$$
$$+ \Big(\frac{3932}{81} - \frac{256}{9}\zeta_2\Big)L_{qr}L_{fr}\Big)C_A{n_f}^2 + \Big(\Big(-\frac{16}{9}\Big)L_{qr}L_{fr}^2 + \Big(\frac{140}{27}\Big)L_{fr}^2\Big){n_f}^3\Big\}$$
$$+ r_g^2\Big\{\Big(-\frac{55825}{1458} + \frac{280}{9}\zeta_3 + \frac{1141}{27}\zeta_2 + \frac{128}{3}\zeta_2^2 + \Big(-\frac{13475}{486} - \frac{176}{9}\zeta_2\Big)L_{fr} + \Big($$
$$-\frac{1057}{81} + \frac{64}{9}\zeta_2\Big)L_{qr}^2 + \Big(-\frac{88}{27}\Big)L_{qr}^2L_{fr} + \Big(\frac{44}{27}\Big)L_{qr}^3 + \Big(\frac{1540}{81}\Big)L_{qr}L_{fr}$$
$$+ \Big(\frac{9070}{243} - \frac{32}{3}\zeta_3 - \frac{884}{27}\zeta_2\Big)L_{qr}\Big)C_A{n_f}^2 + \Big(\frac{10465}{729} - \frac{280}{9}\zeta_3 + \frac{656}{81}\zeta_2 + \Big($$
$$-\frac{544}{81}\Big)L_{qr}^2 + \Big(\frac{32}{27}\Big)L_{qr}^3 + \Big(\frac{1114}{243} + \frac{32}{3}\zeta_3 + \frac{128}{27}\zeta_2\Big)L_{qr}\Big)C_F{n_f}^2 + \Big(\Big($$
$$-\frac{280}{81}\Big)L_{qr}L_{fr} + \Big(\frac{16}{27}\Big)L_{qr}^2L_{fr} + \Big(\frac{1225}{243} + \frac{32}{9}\zeta_2\Big)L_{fr}\Big){n_f}^3\Big\} + \Big\{\Big(-\frac{303707}{810}$$
$$+ \frac{5156}{9}\zeta_5 - \frac{81074}{135}\zeta_3 + 96\zeta_3^2 - \frac{697}{9}\zeta_2 + 48\zeta_2\zeta_3 + \frac{6248}{27}\zeta_2^2 + \frac{3872}{15}\zeta_2^3 + \Big($$
$$-\frac{17105}{27} + 264\zeta_3 + \frac{1936}{3}\zeta_2\Big)L_{fr}^2 + \Big(-\frac{5324}{27}\Big)L_{fr}^3 + \Big(-\frac{1319}{9} - 160\zeta_5$$
$$- 184\zeta_3 + \frac{496}{3}\zeta_2 + 352\zeta_2\zeta_3 + \frac{44}{3}\zeta_2^2\Big)L_{qr} + \Big(-\frac{2662}{27}\Big)L_{qr}^2L_{fr} + \Big(\frac{110}{3}$$
$$+ 88\zeta_3\Big)L_{qr}^2 + \Big(\frac{109651}{486} + 160\zeta_5 + \frac{3032}{27}\zeta_3 + \frac{19504}{27}\zeta_2 - 352\zeta_2\zeta_3$$

$$
\begin{aligned}
&- \frac{2068}{3}\zeta_2^2\Big)L_{fr} + \Big(\frac{23782}{81} - 352\zeta_3 - \frac{3872}{9}\zeta_2\Big)L_{qr}L_{fr} + \Big(\frac{2662}{9}\Big)L_{qr}L_{fr}^2\Big)C_A^3 \\
&+ \Big(- \frac{442583}{4374} + \frac{16}{9}\zeta_3 + \frac{9196}{81}\zeta_2 - \frac{688}{45}\zeta_2^2 + \Big(- \frac{640}{27} + \frac{128}{9}\zeta_2\Big)L_{qr}L_{fr} + \Big(\\
&- \frac{176}{9}\Big)L_{fr}^3 + \Big(- \frac{464}{27} + \frac{64}{3}\zeta_2\Big)L_{fr}^2 + \Big(- \frac{320}{27} + \frac{64}{9}\zeta_2\Big)L_{qr}^2 + \Big(\frac{88}{81}\Big)L_{qr}^3 \\
&+ \Big(\frac{88}{27}\Big)L_{qr}^2L_{fr} + \Big(\frac{88}{9}\Big)L_{qr}L_{fr}^2 + \Big(\frac{13291}{243} - \frac{64}{27}\zeta_3 - \frac{448}{9}\zeta_2\Big)L_{qr} + \Big(\frac{13841}{243} \\
&- \frac{64}{27}\zeta_3 - \frac{448}{9}\zeta_2\Big)L_{fr}\Big)C_A{n_f}^2 + \Big(- \frac{46372}{729} - \frac{128}{81}\zeta_3 + \frac{5504}{81}\zeta_2 + \Big(\\
&- \frac{320}{27}\Big)L_{qr}L_{fr} + \Big(- \frac{688}{81}\Big)L_{qr}^2 + \Big(\frac{64}{81}\Big)L_{qr}^3 + \Big(\frac{64}{27}\Big)L_{qr}^2L_{fr} + \Big(\frac{28}{3}\Big)L_{fr}^2 \\
&+ \Big(\frac{3602}{243} - \frac{512}{27}\zeta_2\Big)L_{fr} + \Big(\frac{8776}{243} - \frac{512}{27}\zeta_2\Big)L_{qr}\Big)C_F{n_f}^2 + \Big(- \frac{62429}{3645} \\
&- \frac{10592}{405}\zeta_3 + \frac{6016}{81}\zeta_2 + \frac{64}{15}\zeta_2^2 + \Big(- \frac{752}{81}\Big)L_{qr}^2 + \Big(\frac{128}{81}\Big)L_{qr}^3 + \Big(\frac{3932}{243} + \frac{64}{3}\zeta_3 \\
&- \frac{1024}{27}\zeta_2\Big)L_{qr} + \Big(- 2\Big)L_{fr}\Big)C_F^2n_f + \Big(\frac{5410051}{21870} - \frac{1112}{9}\zeta_5 + \frac{95998}{405}\zeta_3 \\
&+ \frac{8804}{81}\zeta_2 - 144\zeta_2\zeta_3 - \frac{42028}{135}\zeta_2^2 + \Big(- \frac{95572}{243} + \frac{2144}{27}\zeta_3 + \frac{4592}{27}\zeta_2 \\
&+ \frac{376}{3}\zeta_2^2\Big)L_{fr} + \Big(- \frac{968}{9}\Big)L_{qr}L_{fr}^2 + \Big(- \frac{1046}{27} + 16\zeta_3 + \frac{352}{9}\zeta_2\Big)L_{qr}^2 \\
&+ \Big(\frac{484}{81}\Big)L_{qr}^3 + \Big(\frac{9029}{243} - \frac{2384}{27}\zeta_3 - \frac{1712}{9}\zeta_2 + 120\zeta_2^2\Big)L_{qr} + \Big(\frac{7100}{81} \\
&+ 32\zeta_3\Big)L_{qr}L_{fr} + \Big(\frac{968}{9}\Big)L_{fr}^3 + \Big(\frac{5662}{27} - 48\zeta_3 - \frac{704}{3}\zeta_2\Big)L_{fr}^2\Big)C_A^2n_f \\
&+ \Big(\frac{1056967}{3645} - \frac{6256}{45}\zeta_3 - \frac{12152}{81}\zeta_2 + 128\zeta_2\zeta_3 - \frac{2032}{9}\zeta_2^2 + \Big(- \frac{38495}{243} \\
&+ \frac{4544}{27}\zeta_2\Big)L_{fr} + \Big(- \frac{154}{3}\Big)L_{fr}^2 + \Big(- \frac{2722}{81} + \frac{256}{9}\zeta_2\Big)L_{qr}^2 + \Big(- \frac{5075}{243} \\
&+ \frac{80}{3}\zeta_3 - \frac{2032}{27}\zeta_2\Big)L_{qr} + \Big(- \frac{352}{27}\Big)L_{qr}^2L_{fr} + \Big(\frac{176}{27}\Big)L_{qr}^3 \\
&+ \Big(\frac{2552}{27}\Big)L_{qr}L_{fr}\Big)C_AC_Fn_f + \Big(\Big(\frac{32}{27}\Big)L_{fr}^3\Big){n_f}^3\Big\}. \qquad \text{(C.5)}
\end{aligned}
$$

C.2 Resum coefficients

$$g_{01}^{gg} = r_g\Bigg\{\Bigg(\frac{35}{9}+\Bigg(-\frac{4}{3}\Bigg)L_{qr}\Bigg)n_f\Bigg\}+\Bigg\{\Bigg(-\frac{203}{9}+16\zeta_2+\Bigg(-\frac{22}{3}\Bigg)L_{fr} + \Bigg(\frac{22}{3}\Bigg)L_{qr}\Bigg)C_A+\Bigg(\Bigg(\frac{4}{3}\Bigg)L_{fr}\Bigg)n_f\Bigg\}, \tag{C.6}$$

$$\begin{aligned} g_{02}^{gg} = r_g\Bigg\{&\Bigg(-\frac{10295}{162}+16\zeta_3+\frac{442}{9}\zeta_2+\Bigg(-\frac{770}{27}\Bigg)L_{fr}+\Bigg(-\frac{22}{3}\Bigg)L_{qr}^2 \\ &+\Bigg(\frac{88}{9}\Bigg)L_{qr}L_{fr}+\Bigg(\frac{1127}{27}-\frac{64}{3}\zeta_2\Bigg)L_{qr}\Bigg)C_An_f+\Bigg(\frac{598}{81}-16\zeta_3+\frac{128}{9}\zeta_2+\Bigg(\\ &-\frac{16}{9}\Bigg)L_{qr}^2+\Bigg(\frac{44}{9}\Bigg)L_{qr}\Bigg)C_Fn_f+\Bigg(\Bigg(-\frac{16}{9}\Bigg)L_{qr}L_{fr}+\Bigg(\frac{140}{27}\Bigg)L_{fr}\Bigg){n_f}^2\Bigg\} \\ &+r_g^2\Bigg\{\Bigg(\frac{1225}{324}+\frac{8}{3}\zeta_2+\Bigg(-\frac{70}{27}\Bigg)L_{qr}+\Bigg(\frac{4}{9}\Bigg)L_{qr}^2\Bigg){n_f}^2\Bigg\}+\Bigg\{\Bigg(\frac{1049}{81}-\frac{128}{9}\zeta_2+\Bigg(\\ &-\frac{80}{9}\Bigg)L_{qr}+\Bigg(\frac{16}{9}\Bigg)L_{qr}^2+\Bigg(4\Bigg)L_{fr}\Bigg)C_Fn_f+\Bigg(\frac{7801}{324}+\frac{88}{9}\zeta_3-\frac{1312}{9}\zeta_2+92\zeta_2^2 \\ &+\Bigg(-\frac{1657}{27}+24\zeta_3+\frac{176}{3}\zeta_2\Bigg)L_{qr}+\Bigg(-\frac{484}{9}\Bigg)L_{qr}L_{fr}+\Bigg(\frac{121}{9}\Bigg)L_{qr}^2 \\ &+\Bigg(\frac{121}{3}\Bigg)L_{fr}^2+\Bigg(\frac{3890}{27}-24\zeta_3-\frac{352}{3}\zeta_2\Bigg)L_{fr}\Bigg)C_A^2+\Bigg(\frac{3656}{81}-\frac{16}{9}\zeta_3-\frac{112}{3}\zeta_2 \\ &+\Bigg(-\frac{668}{27}+\frac{64}{3}\zeta_2\Bigg)L_{fr}+\Bigg(-\frac{160}{9}+\frac{32}{3}\zeta_2\Bigg)L_{qr}+\Bigg(-\frac{44}{3}\Bigg)L_{fr}^2+\Bigg(\frac{22}{9}\Bigg)L_{qr}^2 \\ &+\Bigg(\frac{88}{9}\Bigg)L_{qr}L_{fr}\Bigg)C_An_f+\Bigg(\Bigg(\frac{4}{3}\Bigg)L_{fr}^2\Bigg){n_f}^2\Bigg\}, \end{aligned} \tag{C.7}$$

$$\begin{aligned} g_{03}^{gg} = r_g\Bigg\{&\Bigg(-\frac{464173}{3645}+80\zeta_5-\frac{256}{45}\zeta_3+\frac{14708}{81}\zeta_2-\frac{704}{3}\zeta_2\zeta_3+\frac{3376}{15}\zeta_2^2+\Bigg(-\frac{13156}{243} \\ &+\frac{352}{3}\zeta_3-\frac{2816}{27}\zeta_2\Bigg)L_{fr}+\Bigg(-\frac{968}{27}\Bigg)L_{qr}L_{fr}+\Bigg(-\frac{176}{27}\Bigg)L_{qr}^3+\Bigg(\frac{352}{27}\Bigg)L_{qr}^2L_{fr} \\ &+\Bigg(\frac{2128}{81}-\frac{256}{9}\zeta_2\Bigg)L_{qr}^2+\Bigg(\frac{9530}{243}-\frac{80}{3}\zeta_3+\frac{1168}{27}\zeta_2\Bigg)L_{qr}\Bigg)C_AC_Fn_f+\Bigg(\\ &-\frac{2410567}{21870}-\frac{760}{3}\zeta_5+\frac{50009}{405}\zeta_3-\frac{18251}{81}\zeta_2+\frac{716}{3}\zeta_2\zeta_3+\frac{6449}{45}\zeta_2^2+\Bigg(-\frac{22490}{81} \\ &+32\zeta_3+\frac{1408}{9}\zeta_2\Bigg)L_{qr}L_{fr}+\Bigg(-\frac{484}{9}\Bigg)L_{qr}L_{fr}^2+\Bigg(-\frac{484}{81}\Bigg)L_{qr}^3+\Bigg(\frac{5092}{243} \\ &+\frac{3464}{27}\zeta_3+\frac{1376}{9}\zeta_2-\frac{368}{3}\zeta_2^2\Bigg)L_{qr}+\Bigg(\frac{668}{27}-32\zeta_3-\frac{352}{9}\zeta_2\Bigg)L_{qr}^2 \\ &+\Bigg(\frac{484}{9}\Bigg)L_{qr}^2L_{fr}+\Bigg(\frac{4235}{27}\Bigg)L_{fr}^2+\Bigg(\frac{93085}{243}-\frac{632}{3}\zeta_3-\frac{9724}{27}\zeta_2\Bigg)L_{fr}\Bigg)C_A^2n_f \end{aligned}$$

$$+\left(-\frac{35176}{3645}+160\zeta_5-\frac{29368}{405}\zeta_3-\frac{6016}{81}\zeta_2-\frac{64}{15}\zeta_2^2+\left(-\frac{3446}{243}-\frac{64}{3}\zeta_3\right.\right.$$
$$\left.\left.+\frac{1024}{27}\zeta_2\right)L_{qr}+\left(-\frac{128}{81}\right)L_{qr}^3+\left(\frac{752}{81}\right)L_{qr}^2\right)C_F^2n_f+\left(\frac{16087}{486}+\frac{3296}{81}\zeta_3\right.$$
$$\left.-\frac{4216}{81}\zeta_2+\left(-\frac{11186}{243}-\frac{32}{3}\zeta_3+\frac{128}{9}\zeta_2\right)L_{qr}+\left(-\frac{64}{27}\right)L_{qr}^2L_{fr}+\right.$$
$$\left.-\frac{160}{81}\right)L_{qr}^3+\left(\frac{32}{27}\right)L_{qr}L_{fr}+\left(\frac{1340}{81}\right)L_{qr}^2+\left(\frac{6172}{243}-\frac{64}{3}\zeta_3\right.$$
$$\left.+\frac{512}{27}\zeta_2\right)L_{fr}\Big)C_F{n_f}^2+\left(\frac{1404698}{10935}-\frac{7384}{135}\zeta_3-\frac{9112}{81}\zeta_2-\frac{32}{45}\zeta_2^2+\left(-\frac{23468}{243}\right.\right.$$
$$\left.\left.+\frac{352}{27}\zeta_3+\frac{2228}{27}\zeta_2\right)L_{qr}+\left(-\frac{15550}{243}+\frac{64}{3}\zeta_3+\frac{1768}{27}\zeta_2\right)L_{fr}+\left(-\frac{1540}{27}\right)L_{fr}^2\right.$$
$$\left.+\left(-\frac{88}{9}\right)L_{qr}^2L_{fr}+\left(-\frac{220}{81}\right)L_{qr}^3+\left(\frac{176}{9}\right)L_{qr}L_{fr}^2+\left(\frac{2125}{81}-\frac{128}{9}\zeta_2\right)L_{qr}^2\right.$$
$$\left.+\left(\frac{3932}{81}-\frac{256}{9}\zeta_2\right)L_{qr}L_{fr}\right)C_A{n_f}^2+\left(\left(-\frac{16}{9}\right)L_{qr}L_{fr}^2+\left(\frac{140}{27}\right)L_{fr}^2\right){n_f}^3\Big\}$$
$$+r_g^2\Big\{\left(-\frac{55825}{1458}+\frac{280}{9}\zeta_3+\frac{1141}{27}\zeta_2+\frac{128}{3}\zeta_2^2+\left(-\frac{13475}{486}-\frac{176}{9}\zeta_2\right)L_{fr}+\right.$$
$$\left.-\frac{1057}{81}+\frac{64}{9}\zeta_2\right)L_{qr}^2+\left(-\frac{88}{27}\right)L_{qr}^2L_{fr}+\left(\frac{44}{27}\right)L_{qr}^3+\left(\frac{1540}{81}\right)L_{qr}L_{fr}$$
$$+\left(\frac{9070}{243}-\frac{32}{3}\zeta_3-\frac{884}{27}\zeta_2\right)L_{qr}\Big)C_A{n_f}^2+\left(\frac{10465}{729}-\frac{280}{9}\zeta_3+\frac{656}{81}\zeta_2+\left(\right.\right.$$
$$\left.\left.-\frac{544}{81}\right)L_{qr}^2+\left(\frac{32}{27}\right)L_{qr}^3+\left(\frac{1114}{243}+\frac{32}{3}\zeta_3+\frac{128}{27}\zeta_2\right)L_{qr}\right)C_F{n_f}^2+\left(\left(\right.\right.$$
$$\left.\left.-\frac{280}{81}\right)L_{qr}L_{fr}+\left(\frac{16}{27}\right)L_{qr}^2L_{fr}+\left(\frac{1225}{243}+\frac{32}{9}\zeta_2\right)L_{fr}\right){n_f}^3\Big\}+\Big\{\Big(-\frac{303707}{810}$$
$$+\frac{5156}{9}\zeta_5-\frac{81074}{135}\zeta_3+96\zeta_3^2-\frac{697}{9}\zeta_2+48\zeta_2\zeta_3+\frac{6248}{27}\zeta_2^2+\frac{3872}{15}\zeta_2^3+\left(\right.$$
$$\left.-\frac{17105}{27}+264\zeta_3+\frac{1936}{3}\zeta_2\right)L_{fr}^2+\left(-\frac{5324}{27}\right)L_{fr}^3+\left(-\frac{1319}{9}-160\zeta_5\right.$$
$$\left.-184\zeta_3+\frac{496}{3}\zeta_2+352\zeta_2\zeta_3+\frac{44}{3}\zeta_2^2\right)L_{qr}+\left(-\frac{2662}{27}\right)L_{qr}^2L_{fr}+\left(\frac{110}{3}\right.$$
$$\left.+88\zeta_3\right)L_{qr}^2+\left(\frac{109651}{486}+160\zeta_5+\frac{3032}{27}\zeta_3+\frac{19504}{27}\zeta_2-352\zeta_2\zeta_3\right.$$
$$\left.-\frac{2068}{3}\zeta_2^2\right)L_{fr}+\left(\frac{23782}{81}-352\zeta_3-\frac{3872}{9}\zeta_2\right)L_{qr}L_{fr}+\left(\frac{2662}{9}\right)L_{qr}L_{fr}^2\Big)C_A^3$$
$$+\left(-\frac{442583}{4374}+\frac{16}{9}\zeta_3+\frac{9196}{81}\zeta_2-\frac{688}{45}\zeta_2^2+\left(-\frac{640}{27}+\frac{128}{9}\zeta_2\right)L_{qr}L_{fr}+\left(\right.\right.$$
$$\left.\left.-\frac{176}{9}\right)L_{fr}^3+\left(-\frac{464}{27}+\frac{64}{3}\zeta_2\right)L_{fr}^2+\left(-\frac{320}{27}+\frac{64}{9}\zeta_2\right)L_{qr}^2+\left(\frac{88}{81}\right)L_{qr}^3\right.$$

$$+\left(\frac{88}{27}\right)L_{qr}^2L_{fr}+\left(\frac{88}{9}\right)L_{qr}L_{fr}^2+\left(\frac{13291}{243}-\frac{64}{27}\zeta_3-\frac{448}{9}\zeta_2\right)L_{qr}+\left(\frac{13841}{243}-\frac{64}{27}\zeta_3-\frac{448}{9}\zeta_2\right)L_{fr}\Bigg)C_A{n_f}^2+\Bigg(-\frac{46372}{729}-\frac{128}{81}\zeta_3+\frac{5504}{81}\zeta_2+\Bigg(-\frac{320}{27}\Bigg)L_{qr}L_{fr}+\Bigg(-\frac{688}{81}\Bigg)L_{qr}^2+\left(\frac{64}{81}\right)L_{qr}^3+\left(\frac{64}{27}\right)L_{qr}^2L_{fr}+\left(\frac{28}{3}\right)L_{fr}^2+\left(\frac{3602}{243}-\frac{512}{27}\zeta_2\right)L_{fr}+\left(\frac{8776}{243}-\frac{512}{27}\zeta_2\right)L_{qr}\Bigg)C_F{n_f}^2+\Bigg(-\frac{62429}{3645}-\frac{10592}{405}\zeta_3+\frac{6016}{81}\zeta_2+\frac{64}{15}\zeta_2^2+\Bigg(-\frac{752}{81}\Bigg)L_{qr}^2+\left(\frac{128}{81}\right)L_{qr}^3+\left(\frac{3932}{243}+\frac{64}{3}\zeta_3-\frac{1024}{27}\zeta_2\right)L_{qr}+\Bigg(-2\Bigg)L_{fr}\Bigg)C_F^2n_f+\left(\frac{5410051}{21870}-\frac{1112}{9}\zeta_5+\frac{95998}{405}\zeta_3+\frac{8804}{81}\zeta_2-144\zeta_2\zeta_3-\frac{42028}{135}\zeta_2^2+\Bigg(-\frac{95572}{243}+\frac{2144}{27}\zeta_3+\frac{4592}{27}\zeta_2+\frac{376}{3}\zeta_2^2\Bigg)L_{fr}+\Bigg(-\frac{968}{9}\Bigg)L_{qr}L_{fr}^2+\Bigg(-\frac{1046}{27}+16\zeta_3+\frac{352}{9}\zeta_2\Bigg)L_{qr}^2+\left(\frac{484}{81}\right)L_{qr}^3+\left(\frac{9029}{243}-\frac{2384}{27}\zeta_3-\frac{1712}{9}\zeta_2+120\zeta_2^2\right)L_{qr}+\left(\frac{7100}{81}+32\zeta_3\right)L_{qr}L_{fr}+\left(\frac{968}{9}\right)L_{fr}^3+\left(\frac{5662}{27}-48\zeta_3-\frac{704}{3}\zeta_2\right)L_{fr}^2\Bigg)C_A^2n_f+\Bigg(\frac{1056967}{3645}-\frac{6256}{45}\zeta_3-\frac{12152}{81}\zeta_2+128\zeta_2\zeta_3-\frac{2032}{9}\zeta_2^2+\Bigg(-\frac{38495}{243}+\frac{4544}{27}\zeta_2\Bigg)L_{fr}+\Bigg(-\frac{154}{3}\Bigg)L_{fr}^2+\Bigg(-\frac{2722}{81}+\frac{256}{9}\zeta_2\Bigg)L_{qr}^2+\Bigg(-\frac{5075}{243}+\frac{80}{3}\zeta_3-\frac{2032}{27}\zeta_2\Bigg)L_{qr}+\Bigg(-\frac{352}{27}\Bigg)L_{qr}^2L_{fr}+\left(\frac{176}{27}\right)L_{qr}^3+\left(\frac{2552}{27}\right)L_{qr}L_{fr}\Bigg)C_AC_Fn_f+\left(\left(\frac{32}{27}\right)L_{fr}^3\right){n_f}^3\Bigg\}. \tag{C.8}$$

$$g_{01}^{q\bar{q}}=r_q\Bigg\{\left(\frac{68}{9}+\Bigg(-\frac{16}{3}\Bigg)L_{qr}\right)C_F\Bigg\}+\Bigg\{\Bigg(-\frac{248}{9}+16\zeta_2+\left(\frac{34}{3}\right)L_{qr}+\Bigg(-6\Bigg)L_{fr}\Bigg)C_F\Bigg\}, \tag{C.9}$$

$$g_{02}^{q\bar{q}}=r_q\Bigg\{\Bigg(-\frac{17998}{81}+\frac{832}{9}\zeta_2+\Bigg(-\frac{160}{3}\Bigg)L_{qr}^2+\Bigg(-\frac{136}{3}\Bigg)L_{fr}+\left(\frac{5960}{27}-\frac{256}{3}\zeta_2\right)L_{qr}+\left(32\right)L_{qr}L_{fr}\Bigg)C_F^2+\Bigg(-\frac{2332}{81}+\frac{64}{3}\zeta_2+\Bigg(-\frac{32}{9}\Bigg)L_{qr}^2$$

$$+\left(\frac{160}{9}\right)L_{qr}\Big)C_F n_f+\left(\frac{7826}{81}-\frac{472}{9}\zeta_2+\left(-\frac{500}{9}\right)L_{qr}+\left(\frac{88}{9}\right)L_{qr}^2\Big)C_A C_F\Big\}$$
$$+r_q^2\Big\{\left(\frac{1156}{81}+\frac{128}{3}\zeta_2+\left(-\frac{544}{27}\right)L_{qr}+\left(\frac{64}{9}\right)L_{qr}^2\Big)C_F^2\Big\}+\Big\{\Big(-\frac{84773}{324}$$
$$+\frac{1180}{9}\zeta_3+\frac{1336}{9}\zeta_2-\frac{92}{5}\zeta_2^2+\left(-\frac{187}{9}\right)L_{qr}^2+\left(-\frac{17}{3}+24\zeta_3-\frac{88}{3}\zeta_2\right)L_{fr}$$
$$+\left(\frac{1211}{9}-24\zeta_3-\frac{88}{3}\zeta_2\right)L_{qr}+\left(11\right)L_{fr}^2\Big)C_A C_F+\Big(\frac{8813}{162}+\frac{8}{9}\zeta_3-\frac{112}{3}\zeta_2$$
$$+\left(-\frac{286}{9}+\frac{16}{3}\zeta_2\right)L_{qr}+\left(\frac{2}{3}+\frac{16}{3}\zeta_2\right)L_{fr}+\left(\frac{50}{9}\right)L_{qr}^2+\left(-2\right)L_{fr}^2\Big)C_F n_f$$
$$+\Big(\frac{43093}{108}-124\zeta_3-\frac{3286}{9}\zeta_2+\frac{552}{5}\zeta_2^2+\left(-\frac{8575}{27}+48\zeta_3+\frac{472}{3}\zeta_2\right)L_{qr}$$
$$+\left(\frac{578}{9}\right)L_{qr}^2+\left(\frac{487}{3}-48\zeta_3-72\zeta_2\right)L_{fr}+\left(-68\right)L_{qr}L_{fr}$$
$$+\left(18\right)L_{fr}^2\Big)C_F^2\Big\}\,, \tag{C.10}$$

$$g_{03}^{q\bar{q}}=r_q\Big\{\Big(-\frac{10514857}{2187}+\frac{1280}{3}\zeta_5+\frac{44288}{81}\zeta_3+\frac{270848}{81}\zeta_2+\frac{256}{3}\zeta_2\zeta_3-\frac{15536}{15}\zeta_2^2+\Big($$
$$-\frac{131140}{81}+128\zeta_3+\frac{2816}{9}\zeta_2\Big)L_{qr}^2+\Big(-\frac{16808}{27}+\frac{544}{3}\zeta_3+\frac{2512}{27}\zeta_2\Big)L_{fr}+\Big($$
$$-\frac{176}{3}\Big)L_{qr}L_{fr}^2+\Big(-\frac{176}{3}\Big)L_{qr}^2L_{fr}+\Big(\frac{748}{9}\Big)L_{fr}^2+\Big(\frac{1760}{9}\Big)L_{qr}^3+\Big(\frac{3272}{9}$$
$$-128\zeta_3+\frac{1408}{9}\zeta_2\Big)L_{qr}L_{fr}+\Big(\frac{1178048}{243}-\frac{20320}{27}\zeta_3-\frac{58000}{27}\zeta_2$$
$$+\frac{1472}{15}\zeta_2^2\Big)L_{qr}\Big)C_A C_F^2+\Big(-\frac{1268944}{2187}-\frac{10528}{81}\zeta_3+\frac{60512}{81}\zeta_2-\frac{896}{45}\zeta_2^2+\Big($$
$$-\frac{10780}{81}\Big)L_{qr}^2+\Big(\frac{1232}{81}\Big)L_{qr}^3+\Big(\frac{107948}{243}+\frac{256}{3}\zeta_3-\frac{784}{3}\zeta_2\Big)L_{qr}\Big)C_A C_F n_f$$
$$+\Big(\frac{39772}{729}-\frac{320}{3}\zeta_2+\Big(-\frac{4096}{81}+\frac{128}{3}\zeta_2\Big)L_{qr}+\Big(-\frac{64}{27}\Big)L_{qr}^3$$
$$+\Big(\frac{160}{9}\Big)L_{qr}^2\Big)C_F {n_f}^2+\Big(\frac{2196934}{2187}+160\zeta_3-\frac{77536}{81}\zeta_2+\frac{1792}{5}\zeta_2^2+\Big($$
$$-\frac{280736}{243}-\frac{2432}{27}\zeta_3+\frac{16064}{27}\zeta_2\Big)L_{qr}+\Big(-\frac{992}{9}-\frac{256}{9}\zeta_2\Big)L_{qr}L_{fr}+\Big($$
$$-\frac{4768}{81}\Big)L_{qr}^3+\Big(-\frac{136}{9}\Big)L_{fr}^2+\Big(\frac{32}{3}\Big)L_{qr}L_{fr}^2+\Big(\frac{64}{3}\Big)L_{qr}^2L_{fr}+\Big(\frac{1600}{9}$$
$$-\frac{2368}{27}\zeta_2\Big)L_{fr}+\Big(\frac{35560}{81}-\frac{256}{3}\zeta_2\Big)L_{qr}^2\Big)C_F^2 n_f+\Big(\frac{3381256}{2187}-480\zeta_5$$
$$+\frac{29972}{81}\zeta_3-\frac{3344}{3}\zeta_2-\frac{208}{3}\zeta_2\zeta_3+\frac{2324}{45}\zeta_2^2+\Big(-\frac{234820}{243}-\frac{128}{3}\zeta_3$$

$$+\frac{10384}{27}\zeta_2\Big)L_{qr}+\Big(-\frac{1936}{81}\Big)L_{qr}^3+\Big(\frac{6316}{27}\Big)L_{qr}^2\Big)C_A^2C_F+\Big(\frac{263089}{81}$$
$$-\frac{72176}{81}\zeta_3-\frac{6184}{3}\zeta_2+\frac{1696}{5}\zeta_2^2+\Big(-\frac{1041604}{243}+\frac{2816}{3}\zeta_3+\frac{72896}{27}\zeta_2$$
$$-\frac{2944}{5}\zeta_2^2\Big)L_{qr}+\Big(-\frac{11776}{9}+256\zeta_3+384\zeta_2\Big)L_{qr}L_{fr}+\Big(-\frac{21728}{81}\Big)L_{qr}^3$$
$$+\Big(\frac{35384}{27}-\frac{1088}{3}\zeta_3-\frac{1120}{3}\zeta_2\Big)L_{fr}+\Big(\frac{150136}{81}-256\zeta_3-\frac{2176}{3}\zeta_2\Big)L_{qr}^2$$
$$+\Big(-96\Big)L_{qr}L_{fr}^2+\Big(136\Big)L_{fr}^2+\Big(320\Big)L_{qr}^2L_{fr}\Big)C_F^3\Big\}+r_q^2\Big\{\Big(-\frac{325244}{729}$$
$$-\frac{23360}{27}\zeta_2+\frac{2048}{3}\zeta_2^2+\Big(-\frac{29632}{81}+\frac{1024}{9}\zeta_2\Big)L_{qr}^2+\Big(-\frac{2312}{27}-256\zeta_2\Big)L_{fr}$$
$$+\Big(-\frac{128}{3}\Big)L_{qr}^2L_{fr}+\Big(\frac{1664}{27}\Big)L_{qr}^3+\Big(\frac{1088}{9}\Big)L_{qr}L_{fr}+\Big(\frac{172408}{243}$$
$$+\frac{256}{27}\zeta_2\Big)L_{qr}\Big)C_F^3+\Big(-\frac{79288}{729}-\frac{5504}{27}\zeta_2+\Big(-\frac{4928}{81}\Big)L_{qr}^2+\Big(\frac{256}{27}\Big)L_{qr}^3$$
$$+\Big(\frac{34976}{243}+\frac{512}{9}\zeta_2\Big)L_{qr}\Big)C_F^2n_f+\Big(\frac{266084}{729}+\frac{55952}{81}\zeta_2+\Big(-\frac{113608}{243}$$
$$-\frac{4672}{27}\zeta_2\Big)L_{qr}+\Big(-\frac{704}{27}\Big)L_{qr}^3+\Big(\frac{14992}{81}\Big)L_{qr}^2\Big)C_AC_F^2\Big\}+\Big\{\Big(-\frac{6131417}{1458}$$
$$+\frac{3344}{3}\zeta_5+\frac{188276}{81}\zeta_3+32\zeta_3^2+\frac{110552}{27}\zeta_2-1424\zeta_2\zeta_3-\frac{34492}{15}\zeta_2^2+\frac{169504}{315}\zeta_2^3$$
$$+\Big(-\frac{42127}{18}+480\zeta_5+\frac{5792}{3}\zeta_3+\frac{4336}{3}\zeta_2-704\zeta_2\zeta_3-\frac{1968}{5}\zeta_2^2\Big)L_{fr}+\Big($$
$$-\frac{49402}{27}+544\zeta_3+\frac{6800}{9}\zeta_2\Big)L_{qr}^2+\Big(-478+288\zeta_3+144\zeta_2\Big)L_{fr}^2+\Big($$
$$-\frac{1156}{3}\Big)L_{qr}^2L_{fr}+\Big(\frac{19652}{81}\Big)L_{qr}^3+\Big(\frac{16844}{9}-832\zeta_3-672\zeta_2\Big)L_{qr}L_{fr}$$
$$+\Big(\frac{760175}{162}-480\zeta_5-\frac{7520}{3}\zeta_3-\frac{10576}{3}\zeta_2+704\zeta_2\zeta_3+\frac{4912}{5}\zeta_2^2\Big)L_{qr}$$
$$+\Big(-36\Big)L_{fr}^3+\Big(204\Big)L_{qr}L_{fr}^2\Big)C_F^3+\Big(-\frac{31255393}{8748}-\frac{2852}{3}\zeta_5+\frac{309353}{81}\zeta_3$$
$$-\frac{400}{3}\zeta_3^2+\frac{181355}{81}\zeta_2-\frac{7036}{9}\zeta_2\zeta_3-\frac{3529}{27}\zeta_2^2+\frac{7088}{63}\zeta_2^3+\Big(-\frac{15055}{27}+88\zeta_3$$
$$+\frac{968}{9}\zeta_2\Big)L_{qr}^2+\Big(-\frac{242}{9}\Big)L_{fr}^3+\Big(\frac{4114}{81}\Big)L_{qr}^3+\Big(\frac{493}{9}-88\zeta_3+\frac{968}{9}\zeta_2\Big)L_{fr}^2$$
$$+\Big(\frac{1657}{18}-80\zeta_5+\frac{3104}{9}\zeta_3-\frac{8992}{27}\zeta_2+4\zeta_2^2\Big)L_{fr}+\Big(\frac{561610}{243}+80\zeta_5$$
$$-\frac{34120}{27}\zeta_3-\frac{8432}{9}\zeta_2+\frac{1964}{15}\zeta_2^2\Big)L_{qr}\Big)C_A^2C_F+\Big(-\frac{2467183}{2187}-\frac{608}{9}\zeta_5$$

$$+\frac{13960}{27}\zeta_3+\frac{115336}{81}\zeta_2-\frac{256}{3}\zeta_2\zeta_3-\frac{75568}{135}\zeta_2^2+\Bigg(-\frac{40028}{81}+32\zeta_3$$
$$+\frac{400}{3}\zeta_2\Bigg)L_{qr}^2+\Bigg(-\frac{2689}{9}+\frac{256}{3}\zeta_3+\frac{2008}{27}\zeta_2+\frac{272}{5}\zeta_2^2\Bigg)L_{fr}+\Bigg($$
$$-\frac{100}{3}\Bigg)L_{qr}^2L_{fr}+\Bigg(-\frac{68}{3}\Bigg)L_{qr}L_{fr}^2+\Bigg(\frac{388}{9}-32\zeta_3-48\zeta_2\Bigg)L_{fr}^2+\Bigg(\frac{4972}{81}\Bigg)L_{qr}^3$$
$$+\Bigg(\frac{1784}{9}+\frac{256}{9}\zeta_2\Bigg)L_{qr}L_{fr}+\Bigg(\frac{109118}{81}-\frac{4336}{27}\zeta_3-\frac{24656}{27}\zeta_2+\frac{464}{5}\zeta_2^2\Bigg)L_{qr}$$
$$+\Bigg(12\Bigg)L_{fr}^3\Bigg)C_F^2n_f+\Bigg(-\frac{61807}{729}-\frac{1136}{81}\zeta_3+\frac{3728}{27}\zeta_2+\frac{448}{135}\zeta_2^2+\Bigg(-\frac{244}{9}$$
$$+\frac{32}{9}\zeta_2\Bigg)L_{qr}^2+\Bigg(-\frac{8}{9}\Bigg)L_{fr}^3+\Bigg(\frac{4}{9}+\frac{32}{9}\zeta_2\Bigg)L_{fr}^2+\Bigg(\frac{88}{27}\Bigg)L_{qr}^3+\Bigg(\frac{34}{9}+\frac{32}{9}\zeta_3$$
$$-\frac{160}{27}\zeta_2\Bigg)L_{fr}+\Bigg(\frac{6556}{81}-\frac{64}{27}\zeta_3-\frac{1568}{27}\zeta_2\Bigg)L_{qr}\Bigg)C_F{n_f}^2+\Bigg(\frac{2446783}{2187}+\frac{136}{3}\zeta_5$$
$$-\frac{37456}{81}\zeta_3-\frac{93268}{81}\zeta_2+\frac{928}{9}\zeta_2\zeta_3+\frac{1612}{135}\zeta_2^2+\Bigg(-\frac{213536}{243}+\frac{3440}{27}\zeta_3$$
$$+\frac{12448}{27}\zeta_2-\frac{344}{15}\zeta_2^2\Bigg)L_{qr}+\Bigg(-40-\frac{400}{9}\zeta_3+\frac{2672}{27}\zeta_2-\frac{8}{5}\zeta_2^2\Bigg)L_{fr}+\Bigg($$
$$-\frac{2024}{81}\Bigg)L_{qr}^3+\Bigg(-\frac{146}{9}+16\zeta_3-\frac{352}{9}\zeta_2\Bigg)L_{fr}^2+\Bigg(\frac{88}{9}\Bigg)L_{fr}^3+\Bigg(\frac{20014}{81}-16\zeta_3$$
$$-\frac{352}{9}\zeta_2\Bigg)L_{qr}^2\Bigg)C_AC_Fn_f+\Bigg(\frac{65475811}{8748}+\frac{3128}{9}\zeta_5-\frac{546572}{81}\zeta_3+\frac{592}{3}\zeta_3^2$$
$$-\frac{503536}{81}\zeta_2+2208\zeta_2\zeta_3+\frac{350464}{135}\zeta_2^2-\frac{123632}{315}\zeta_2^3+\Bigg(-\frac{3309509}{486}+240\zeta_5$$
$$+\frac{94264}{27}\zeta_3+\frac{102992}{27}\zeta_2-352\zeta_2\zeta_3-\frac{10208}{15}\zeta_2^2\Bigg)L_{qr}+\Bigg(-\frac{7844}{9}+416\zeta_3$$
$$-\frac{1408}{9}\zeta_2\Bigg)L_{qr}L_{fr}+\Bigg(-\frac{2323}{9}+32\zeta_3+264\zeta_2\Bigg)L_{fr}^2+\Bigg(-\frac{6358}{27}\Bigg)L_{qr}^3$$
$$+\Bigg(\frac{374}{3}\Bigg)L_{qr}L_{fr}^2+\Bigg(\frac{374}{3}\Bigg)L_{qr}^2L_{fr}+\Bigg(\frac{44564}{27}-240\zeta_5-\frac{6032}{3}\zeta_3+\frac{2708}{27}\zeta_2$$
$$+352\zeta_2\zeta_3-\frac{1136}{5}\zeta_2^2\Bigg)L_{fr}+\Bigg(\frac{57157}{27}-448\zeta_3-\frac{5192}{9}\zeta_2\Bigg)L_{qr}^2$$
$$+\Bigg(-66\Bigg)L_{fr}^3\Bigg)C_AC_F^2\Bigg\}. \tag{C.11}$$

Appendix D

Feynman rules for extra dimension

$$
\begin{aligned}
B_{\mu\nu,\rho\sigma}(k) = &\left(\eta_{\mu\rho} - \frac{k_\mu k_\rho}{{M_n}^2}\right)\left(\eta_{\nu\sigma} - \frac{k_\nu k_\sigma}{{M_n}^2}\right) \\
&+\left(\eta_{\mu\sigma} - \frac{k_\mu k_\sigma}{{M_n}^2}\right)\left(\eta_{\nu\rho} - \frac{k_\nu k_\rho}{{M_n}^2}\right) \\
&-\frac{2}{3}\left(\eta_{\mu\nu} - \frac{k_\mu k_\nu}{{M_n}^2}\right)\left(\eta_{\rho\sigma} - \frac{k_\rho k_\sigma}{{M_n}^2}\right)
\end{aligned} \tag{D.1}
$$

$$
C_{\mu\nu,\rho\sigma} = \eta_{\mu\rho}\eta_{\nu\sigma} + \eta_{\mu\sigma}\eta_{\nu\rho} - \eta_{\mu\nu}\eta_{\rho\sigma} \tag{D.2}
$$

$$
D_{\mu\nu,\rho\sigma}(k_1,k_2) = \eta_{\mu\nu}k_{1\sigma}k_{2\rho} - [\eta_{\mu\sigma}k_{1\nu}k_{2\rho} + \eta_{\mu\rho}k_{1\nu}k_{2\sigma} - \eta_{\rho\sigma}k_{1\mu}k_{2\nu} + (\mu \leftrightarrow \nu)], \tag{D.3}
$$

$$
\begin{aligned}
E_{\mu\nu,\rho\sigma}(k_1,k_2) = &\eta_{\mu\nu}(k_{1\sigma}k_{1\rho} + k_{2\sigma}k_{2\rho} + k_{2\sigma}k_{1\rho}) \\
&-[\eta_{\nu\sigma}k_{1\mu}k_{1\rho} + \eta_{\mu\rho}k_{2\mu}k_{2\sigma} + (\mu \leftrightarrow \nu)]
\end{aligned} \tag{D.4}
$$

Bibliography

[1] ATLAS collaboration, *Search for new phenomena in high-mass diphoton final states using 37 fb^{-1} of proton–proton collisions collected at $\sqrt{s} = 13$ TeV with the ATLAS detector*, *Phys. Lett.* **B775** (2017) 105 [1707.04147].

[2] T. Han, J. D. Lykken and R.-J. Zhang, *On Kaluza-Klein states from large extra dimensions*, *Phys. Rev.* **D59** (1999) 105006 [hep-ph/9811350].

[3] CMS collaboration, *Search for contact interactions and large extra dimensions in the dilepton mass spectra from proton-proton collisions at $\sqrt{s} = 13$ TeV*, *JHEP* **04** (2019) 114 [1812.10443].

[4] CMS collaboration, *Search for narrow resonances in dilepton mass spectra in proton-proton collisions at $\sqrt{s} = 13$ TeV and combination with 8 TeV data*, *Phys. Lett.* **B768** (2017) 57 [1609.05391].

[5] S. Weinberg, *A Model of Leptons*, *Phys. Rev. Lett.* **19** (1967) 1264.

[6] J. Goldstone, A. Salam and S. Weinberg, *Broken Symmetries*, *Phys. Rev.* **127** (1962) 965.

[7] S. L. Glashow and S. Weinberg, *Breaking chiral symmetry*, *Phys. Rev. Lett.* **20** (1968) 224.

[8] P. W. Higgs, *Spontaneous Symmetry Breakdown without Massless Bosons*, *Phys. Rev.* **145** (1966) 1156.

[9] P. W. Higgs, *Broken Symmetries and the Masses of Gauge Bosons*, *Phys. Rev. Lett.* **13** (1964) 508.

[10] P. W. Higgs, *Broken symmetries, massless particles and gauge fields*, *Phys. Lett.* **12** (1964) 132.

[11] CMS collaboration, *Combined results of searches for the standard model Higgs boson in pp collisions at $\sqrt{s} = 7$ TeV*, *Phys. Lett. B* **710** (2012) 26 [1202.1488].

[12] ATLAS collaboration, *Combined search for the Standard Model Higgs boson using up to 4.9 fb^{-1} of pp collision data at $\sqrt{s} = 7$ TeV with the ATLAS detector at the LHC*, *Phys. Lett. B* **710** (2012) 49 [1202.1408].

[13] T. Kaluza, *Zum Unitätsproblem der Physik*, *Sitzungsber. Preuss. Akad. Wiss. Berlin (Math. Phys.)* **1921** (1921) 966 [1803.08616].

[14] A. B. Lahanas, *Light Singlet, Gauge Hierarchy and Supergravity*, *Phys. Lett. B* **124** (1983) 341.

[15] N. Arkani-Hamed, S. Dimopoulos and G. R. Dvali, *The Hierarchy problem and new dimensions at a millimeter*, *Phys. Lett.* **B429** (1998) 263 [hep-ph/9803315].

[16] L. Randall and R. Sundrum, *A Large mass hierarchy from a small extra dimension*, *Phys. Rev. Lett.* **83** (1999) 3370 [hep-ph/9905221].

[17] Planck collaboration, *Planck 2018 results. VI. Cosmological parameters*, *Astron. Astrophys.* **641** (2020) A6 [1807.06209].

[18] C. Csaki, *TASI lectures on extra dimensions and branes*, in *Theoretical Advanced Study Institute in Elementary Particle Physics (TASI 2002): Particle Physics and Cosmology: The Quest for Physics Beyond the Standard Model(s)*, 4, 2004, hep-ph/0404096.

[19] C. Csaki, J. Hubisz and P. Meade, *TASI lectures on electroweak symmetry breaking from extra dimensions*, in *Theoretical Advanced Study Institute in Elementary Particle Physics: Physics in $D \geqq 4$*, 10, 2005, hep-ph/0510275.

[20] SLD collaboration, *An improved measurement of the left-right Z^0 cross-section asymmetry*, *Phys. Rev. Lett.* **78** (1997) 2075 [hep-ex/9611011].

[21] S. Cotsakis and I. Klaoudatou, *Future singularities of isotropic cosmologies*, *J. Geom. Phys.* **55** (2005) 306 [gr-qc/0409022].

[22] R. Maartens, *Brane world gravity*, *Living Rev. Rel.* **7** (2004) 7 [gr-qc/0312059].

[23] M. Alishahiha, E. Silverstein and D. Tong, *DBI in the sky*, *Phys. Rev. D* **70** (2004) 123505 [hep-th/0404084].

[24] G. F. Giudice, R. Rattazzi and J. D. Wells, *Quantum gravity and extra dimensions at high-energy colliders*, *Nucl. Phys. B* **544** (1999) 3 [hep-ph/9811291].

[25] ATLAS collaboration, *Search for contact interactions and large extra dimensions in dilepton events from pp collisions at $\sqrt{s} = 7$ TeV with the ATLAS detector*, *Phys. Rev. D* **87** (2013) 015010 [1211.1150].

[26] CMS collaboration, *Search for large extra dimensions in dimuon and dielectron events in pp collisions at $\sqrt{s} = 7$ TeV*, *Phys. Lett. B* **711** (2012) 15 [1202.3827].

[27] ATLAS collaboration, *Search for contact interactions and large extra dimensions in the dilepton channel using proton-proton collisions at $\sqrt{s} = 8$ TeV with the ATLAS detector*, *Eur. Phys. J. C* **74** (2014) 3134 [1407.2410].

[28] CMS collaboration, *Search for physics beyond the standard model in dilepton mass spectra in proton-proton collisions at $\sqrt{s} = 8$ TeV*, *JHEP* **04** (2015) 025

[1412.6302].

[29] D. J. Gross and F. Wilczek, *Ultraviolet Behavior of Nonabelian Gauge Theories*, *Phys. Rev. Lett.* **30** (1973) 1343.

[30] H. D. Politzer, *Reliable Perturbative Results for Strong Interactions*, *Phys. Rev. Lett.* **30** (1973) 1346.

[31] W. E. Caswell, *Asymptotic Behavior of Nonabelian Gauge Theories to Two Loop Order*, *Phys. Rev. Lett.* **33** (1974) 244.

[32] D. R. T. Jones, *Two Loop Diagrams in Yang-Mills Theory*, *Nucl. Phys. B* **75** (1974) 531.

[33] O. V. Tarasov, A. A. Vladimirov and A. Y. Zharkov, *The Gell-Mann-Low Function of QCD in the Three Loop Approximation*, *Phys. Lett. B* **93** (1980) 429.

[34] S. A. Larin and J. A. M. Vermaseren, *The Three loop QCD Beta function and anomalous dimensions*, *Phys. Lett. B* **303** (1993) 334 [hep-ph/9302208].

[35] T. van Ritbergen, J. A. M. Vermaseren and S. A. Larin, *The Four loop beta function in quantum chromodynamics*, *Phys. Lett. B* **400** (1997) 379 [hep-ph/9701390].

[36] M. Czakon, *The Four-loop QCD beta-function and anomalous dimensions*, *Nucl. Phys. B* **710** (2005) 485 [hep-ph/0411261].

[37] F. Herzog, B. Ruijl, T. Ueda, J. A. M. Vermaseren and A. Vogt, *The five-loop beta function of Yang-Mills theory with fermions*, *JHEP* **02** (2017) 090 [1701.01404].

[38] G. Altarelli and G. Parisi, *Asymptotic Freedom in Parton Language*, *Nucl. Phys. B* **126** (1977) 298.

[39] S. D. Badger and E. W. N. Glover, *Two loop splitting functions in QCD*, *JHEP* **07** (2004) 040 [hep-ph/0405236].

[40] S. Moch, J. A. M. Vermaseren and A. Vogt, *The Three loop splitting functions in QCD: The Nonsinglet case*, *Nucl. Phys. B* **688** (2004) 101 [hep-ph/0403192].

[41] A. Vogt, S. Moch and J. A. M. Vermaseren, *The Three-loop splitting functions in QCD: The Singlet case*, *Nucl. Phys. B* **691** (2004) 129 [hep-ph/0404111].

[42] M. Bonvini and S. Marzani, *Four-loop splitting functions at small x*, *JHEP* **06** (2018) 145 [1805.06460].

[43] J. M. Henn, G. P. Korchemsky and B. Mistlberger, *The full four-loop cusp anomalous dimension in $\mathcal{N} = 4$ super Yang-Mills and QCD*, *JHEP* **04** (2020) 018 [1911.10174].

[44] V. Ravindran, *On Sudakov and soft resummations in QCD*, *Nucl. Phys.* **B746** (2006) 58 [hep-ph/0512249].

[45] V. Ravindran, *Higher-order threshold effects to inclusive processes in QCD*, *Nucl.*

Phys. **B752** (2006) 173 [hep-ph/0603041].

[46] K. G. Chetyrkin, B. A. Kniehl and M. Steinhauser, *Decoupling relations to O (alpha-s**3) and their connection to low-energy theorems*, *Nucl. Phys. B* **510** (1998) 61 [hep-ph/9708255].

[47] J. C. Collins and D. E. Soper, *Back-To-Back Jets in QCD*, *Nucl. Phys. B* **193** (1981) 381.

[48] L. Magnea and G. F. Sterman, *Analytic continuation of the Sudakov form-factor in QCD*, *Phys. Rev. D* **42** (1990) 4222.

[49] L. J. Dixon, L. Magnea and G. F. Sterman, *Universal structure of subleading infrared poles in gauge theory amplitudes*, *JHEP* **08** (2008) 022 [0805.3515].

[50] V. V. Sudakov, *Vertex parts at very high-energies in quantum electrodynamics*, *Sov. Phys. JETP* **3** (1956) 65.

[51] A. H. Mueller, *On the Asymptotic Behavior of the Sudakov Form-factor*, *Phys. Rev.* **D20** (1979) 2037.

[52] J. C. Collins, *Algorithm to Compute Corrections to the Sudakov Form-factor*, *Phys. Rev.* **D22** (1980) 1478.

[53] A. Sen, *Asymptotic Behavior of the Sudakov Form-Factor in QCD*, *Phys. Rev.* **D24** (1981) 3281.

[54] J. Henn, A. V. Smirnov, V. A. Smirnov, M. Steinhauser and R. N. Lee, *Four-loop photon quark form factor and cusp anomalous dimension in the large-N_c limit of QCD*, *JHEP* **03** (2017) 139 [1612.04389].

[55] S. Moch, B. Ruijl, T. Ueda, J. A. M. Vermaseren and A. Vogt, *Four-Loop Non-Singlet Splitting Functions in the Planar Limit and Beyond*, *JHEP* **10** (2017) 041 [1707.08315].

[56] A. Grozin, *Four-loop cusp anomalous dimension in QED*, *JHEP* **06** (2018) 073 [1805.05050].

[57] J. M. Henn, T. Peraro, M. Stahlhofen and P. Wasser, *Matter dependence of the four-loop cusp anomalous dimension*, *Phys. Rev. Lett.* **122** (2019) 201602 [1901.03693].

[58] J. Davies, A. Vogt, B. Ruijl, T. Ueda and J. A. M. Vermaseren, *Large-n_f contributions to the four-loop splitting functions in QCD*, *Nucl. Phys.* **B915** (2017) 335 [1610.07477].

[59] R. N. Lee, A. V. Smirnov, V. A. Smirnov and M. Steinhauser, *The n_f^2 contributions to fermionic four-loop form factors*, *Phys. Rev.* **D96** (2017) 014008 [1705.06862].

[60] J. A. Gracey, *Anomalous dimension of nonsinglet Wilson operators at O (1 / N(f)) in deep inelastic scattering*, *Phys. Lett.* **B322** (1994) 141 [hep-ph/9401214].

[61] M. Beneke and V. M. Braun, *Power corrections and renormalons in Drell-Yan production*, *Nucl. Phys.* **B454** (1995) 253 [hep-ph/9506452].

[62] S. Moch, B. Ruijl, T. Ueda, J. A. M. Vermaseren and A. Vogt, *On quartic colour factors in splitting functions and the gluon cusp anomalous dimension*, *Phys. Lett.* **B782** (2018) 627 [1805.09638].

[63] R. Brüser, A. Grozin, J. M. Henn and M. Stahlhofen, *Matter dependence of the four-loop QCD cusp anomalous dimension: from small angles to all angles*, *JHEP* **05** (2019) 186 [1902.05076].

[64] R. N. Lee, A. V. Smirnov, V. A. Smirnov and M. Steinhauser, *Four-loop quark form factor with quartic fundamental colour factor*, *JHEP* **02** (2019) 172 [1901.02898].

[65] A. von Manteuffel, E. Panzer and R. M. Schabinger, *Analytic four-loop anomalous dimensions in massless QCD from form factors*, 2002.04617.

[66] S. Catani and L. Trentadue, *Resummation of the QCD Perturbative Series for Hard Processes*, *Nucl. Phys.* **B327** (1989) 323.

[67] G. F. Sterman, *Partons, factorization and resummation, TASI 95*, in *Theoretical Advanced Study Institute in Elementary Particle Physics (TASI 95): QCD and Beyond*, pp. 327–408, 6, 1995, hep-ph/9606312.

[68] S. Catani, M. L. Mangano, P. Nason and L. Trentadue, *The Resummation of soft gluons in hadronic collisions*, *Nucl. Phys.* **B478** (1996) 273 [hep-ph/9604351].

[69] E. Laenen, *Resummation for observables at TeV colliders*, *Pramana* **63** (2004) 1225.

[70] S. Moch, J. A. M. Vermaseren and A. Vogt, *Higher-order corrections in threshold resummation*, *Nucl. Phys. B* **726** (2005) 317 [hep-ph/0506288].

[71] G. Luisoni and S. Marzani, *QCD resummation for hadronic final states*, *J. Phys. G* **42** (2015) 103101 [1505.04084].

[72] M. Bonvini, S. Forte, M. Ghezzi and G. Ridolfi, *Threshold Resummation in SCET vs. Perturbative QCD: An Analytic Comparison*, *Nucl. Phys. B* **861** (2012) 337 [1201.6364].

[73] L. Rottoli, *Threshold resummation in SCET vs. direct QCD: a systematic comparison*, other thesis, 5, 2014.

[74] G. Sterman and M. Zeng, *Quantifying Comparisons of Threshold Resummations*, *JHEP* **05** (2014) 132 [1312.5397].

[75] T. Becher, A. Broggio and A. Ferroglia, *Introduction to Soft-Collinear Effective Theory*, vol. 896. Springer, 2015, 10.1007/978-3-319-14848-9, [1410.1892].

[76] E. Remiddi and J. A. M. Vermaseren, *Harmonic polylogarithms*, *Int. J. Mod. Phys. A* **15** (2000) 725 [hep-ph/9905237].

[77] M. Bonvini, *Resummation of soft and hard gluon radiation in perturbative QCD*, Ph.D. thesis, Genoa U., 2012. 1212.0480.

[78] S. Catani, D. de Florian, M. Grazzini and P. Nason, *Soft gluon resummation for Higgs boson production at hadron colliders*, *JHEP* **07** (2003) 028 [hep-ph/0306211].

[79] G. Das, S.-O. Moch and A. Vogt, *Soft corrections to inclusive deep-inelastic scattering at four loops and beyond*, *JHEP* **03** (2020) 116 [1912.12920].

[80] M. Bonvini and S. Marzani, *Resummed Higgs cross section at N^3LL*, *JHEP* **09** (2014) 007 [1405.3654].

[81] M. Bonvini, S. Marzani, C. Muselli and L. Rottoli, *On the Higgs cross section at N^3LO+N^3LL and its uncertainty*, *JHEP* **08** (2016) 105 [1603.08000].

[82] T. O. Eynck, E. Laenen and L. Magnea, *Exponentiation of the Drell-Yan cross-section near partonic threshold in the DIS and MS-bar schemes*, *JHEP* **06** (2003) 057 [hep-ph/0305179].

[83] D. Graudenz, M. Hampel, A. Vogt and C. Berger, *The Mellin transform technique for the extraction of the gluon density*, *Z. Phys. C* **70** (1996) 77 [hep-ph/9506333].

[84] A. Vogt, *Efficient evolution of unpolarized and polarized parton distributions with QCD-PEGASUS*, *Comput. Phys. Commun.* **170** (2005) 65 [hep-ph/0408244].

[85] M. Bonvini, S. Forte and G. Ridolfi, *Soft gluon resummation of Drell-Yan rapidity distributions: Theory and phenomenology*, *Nucl. Phys. B* **847** (2011) 93 [1009.5691].

[86] S. Forte, G. Ridolfi, J. Rojo and M. Ubiali, *Borel resummation of soft gluon radiation and higher twists*, *Phys. Lett. B* **635** (2006) 313 [hep-ph/0601048].

[87] R. Abbate, S. Forte and G. Ridolfi, *A New prescription for soft gluon resummation*, *Phys. Lett. B* **657** (2007) 55 [0707.2452].

[88] R. Hamberg, W. L. van Neerven and T. Matsuura, *A complete calculation of the order $\alpha - s^2$ correction to the Drell-Yan K factor*, *Nucl. Phys.* **B359** (1991) 343.

[89] T. Matsuura, R. Hamberg and W. L. van Neerven, *The Contribution of the Gluon-gluon Subprocess to the Drell-Yan K Factor*, *Nucl. Phys.* **B345** (1990) 331.

[90] R. V. Harlander and W. B. Kilgore, *Next-to-next-to-leading order Higgs production at hadron colliders*, *Phys. Rev. Lett.* **88** (2002) 201801 [hep-ph/0201206].

[91] C. Duhr, F. Dulat and B. Mistlberger, *The Drell-Yan cross section to third order in the strong coupling constant*, 2001.07717.

[92] C. Anastasiou, C. Duhr, F. Dulat, E. Furlan, T. Gehrmann, F. Herzog et al., *Higgs boson gluon fusion production at threshold in N^3LO QCD*, *Phys. Lett.* **B737** (2014) 325 [1403.4616].

[93] S. Moch and A. Vogt, *Higher-order soft corrections to lepton pair and Higgs boson production*, *Phys. Lett.* **B631** (2005) 48 [hep-ph/0508265].

[94] E. Laenen and L. Magnea, *Threshold resummation for electroweak annihilation from DIS data*, *Phys. Lett.* **B632** (2006) 270 [hep-ph/0508284].

[95] A. Idilbi, X.-d. Ji, J.-P. Ma and F. Yuan, *Threshold resummation for Higgs production in effective field theory*, *Phys. Rev.* **D73** (2006) 077501 [hep-ph/0509294].

[96] Y. Li, A. von Manteuffel, R. M. Schabinger and H. X. Zhu, *Soft-virtual corrections to Higgs production at N^3LO*, *Phys. Rev.* **D91** (2015) 036008 [1412.2771].

[97] M. C. Kumar, M. K. Mandal and V. Ravindran, *Associated production of Higgs boson with vector boson at threshold N^3LO in QCD*, *JHEP* **03** (2015) 037 [1412.3357].

[98] K. Melnikov and M. Schulze, *NLO QCD corrections to top quark pair production and decay at hadron colliders*, *JHEP* **08** (2009) 049 [0907.3090].

[99] M. L. Czakon et al., *Top quark pair production at complete NLO accuracy with NNLO+NNLL' corrections in QCD*, *Chin. Phys. C* **44** (2020) 083104 [1901.08281].

[100] M. Czakon, D. Heymes, A. Mitov, D. Pagani, I. Tsinikos and M. Zaro, *Top-pair production at the LHC through NNLO QCD and NLO EW*, *JHEP* **10** (2017) 186 [1705.04105].

[101] M. Czakon and A. Mitov, *NNLO corrections to top-pair production at hadron colliders: the all-fermionic scattering channels*, *JHEP* **12** (2012) 054 [1207.0236].

[102] T. Ahmed, N. Rana and V. Ravindran, *Higgs boson production through $b\bar{b}$ annihilation at threshold in N^3LO QCD*, *JHEP* **10** (2014) 139 [1408.0787].

[103] T. Ahmed, M. C. Kumar, P. Mathews, N. Rana and V. Ravindran, *Pseudo-scalar Higgs boson production at threshold N^3 LO and N^3 LL QCD*, *Eur. Phys. J.* **C76** (2016) 355 [1510.02235].

[104] T. Gehrmann, E. W. N. Glover, T. Huber, N. Ikizlerli and C. Studerus, *Calculation of the quark and gluon form factors to three loops in QCD*, *JHEP* **06** (2010) 094 [1004.3653].

[105] V. Ravindran, J. Smith and W. L. van Neerven, *QCD threshold corrections to di-lepton and Higgs rapidity distributions beyond N^2 LO*, *Nucl. Phys.* **B767** (2007) 100 [hep-ph/0608308].

[106] T. Ahmed, M. Mahakhud, N. Rana and V. Ravindran, *Drell-Yan Production at Threshold to Third Order in QCD*, *Phys. Rev. Lett.* **113** (2014) 112002

[1404.0366].

[107] Y. Li, A. von Manteuffel, R. M. Schabinger and H. X. Zhu, *N^3LO Higgs boson and Drell-Yan production at threshold: The one-loop two-emission contribution*, *Phys. Rev.* **D90** (2014) 053006 [1404.5839].

[108] S. Catani, L. Cieri, D. de Florian, G. Ferrera and M. Grazzini, *Threshold resummation at N^3LL accuracy and soft-virtual cross sections at N^3LO*, *Nucl. Phys.* **B888** (2014) 75 [1405.4827].

[109] T. Ahmed, G. Das, M. C. Kumar, N. Rana and V. Ravindran, *RG improved Higgs boson production to N^3LO in QCD*, 1505.07422.

[110] A. H. Ajjath, A. Chakraborty, G. Das, P. Mukherjee and V. Ravindran, *Resummed prediction for Higgs boson production through $b\bar{b}$ annihilation at N^3LL*, *JHEP* **11** (2019) 006 [1905.03771].

[111] A. Idilbi, X.-d. Ji and F. Yuan, *Resummation of threshold logarithms in effective field theory for DIS, Drell-Yan and Higgs production*, *Nucl. Phys.* **B753** (2006) 42 [hep-ph/0605068].

[112] T. Ahmed, M. Bonvini, M. C. Kumar, P. Mathews, N. Rana, V. Ravindran et al., *Pseudo-scalar Higgs boson production at N^3 LO_A $+N^3$ LL'*, *Eur. Phys. J.* **C76** (2016) 663 [1606.00837].

[113] T. Schmidt and M. Spira, *Higgs Boson Production via Gluon Fusion: Soft-Gluon Resummation including Mass Effects*, *Phys. Rev.* **D93** (2016) 014022 [1509.00195].

[114] D. de Florian and J. Zurita, *Soft-gluon resummation for pseudoscalar Higgs boson production at hadron colliders*, *Phys. Lett.* **B659** (2008) 813 [0711.1916].

[115] G. Das, M. C. Kumar and K. Samanta, *Resummed inclusive cross-section in ADD model at N^3LL+NNLO*, 1912.13039.

[116] G. Das, M. Kumar and K. Samanta, *Resummed inclusive cross-section in Randall-Sundrum model at NNLO+NNLL*, 2004.03938.

[117] D. Westmark and J. F. Owens, *Enhanced threshold resummation formalism for lepton pair production and its effects in the determination of parton distribution functions*, *Phys. Rev.* **D95** (2017) 056024 [1701.06716].

[118] P. Banerjee, G. Das, P. K. Dhani and V. Ravindran, *Threshold resummation of the rapidity distribution for Higgs production at NNLO+NNLL*, *Phys. Rev.* **D97** (2018) 054024 [1708.05706].

[119] P. Banerjee, G. Das, P. K. Dhani and V. Ravindran, *Threshold resummation of the rapidity distribution for Drell-Yan production at NNLO+NNLL*, *Phys. Rev.* **D98** (2018) 054018 [1805.01186].

[120] G. Lustermans, J. K. L. Michel and F. J. Tackmann, *Generalized Threshold*

Factorization with Full Collinear Dynamics, 1908.00985.

[121] R. V. Harlander, H. Mantler and M. Wiesemann, *Transverse momentum resummation for Higgs production via gluon fusion in the MSSM*, *JHEP* **11** (2014) 116 [1409.0531].

[122] G. Bozzi, S. Catani, D. de Florian and M. Grazzini, *Transverse-momentum resummation and the spectrum of the Higgs boson at the LHC*, *Nucl. Phys. B* **737** (2006) 73 [hep-ph/0508068].

[123] A. Buckley, J. Ferrando, S. Lloyd, K. Nordström, B. Page, M. Rüfenacht et al., *LHAPDF6: parton density access in the LHC precision era*, *Eur. Phys. J.* **C75** (2015) 132 [1412.7420].

[124] L. A. Harland-Lang, A. D. Martin, P. Motylinski and R. S. Thorne, *Parton distributions in the LHC era: MMHT 2014 PDFs*, *Eur. Phys. J.* **C75** (2015) 204 [1412.3989].

[125] S. Catani, D. de Florian and M. Grazzini, *Direct Higgs production and jet veto at the Tevatron and the LHC in NNLO QCD*, *JHEP* **01** (2002) 015 [hep-ph/0111164].

[126] S. Catani, D. de Florian and M. Grazzini, *Higgs production in hadron collisions: Soft and virtual QCD corrections at NNLO*, *JHEP* **05** (2001) 025 [hep-ph/0102227].

[127] C. Anastasiou, C. Duhr, F. Dulat, E. Furlan, T. Gehrmann, F. Herzog et al., *High precision determination of the gluon fusion Higgs boson cross-section at the LHC*, *JHEP* **05** (2016) 058 [1602.00695].

[128] S. Alekhin, J. Bluemlein, S.-O. Moch and R. Placakyte, *The new ABMP16 PDF*, *PoS* **DIS2016** (2016) 016 [1609.03327].

[129] S. Dulat, T.-J. Hou, J. Gao, M. Guzzi, J. Huston, P. Nadolsky et al., *New parton distribution functions from a global analysis of quantum chromodynamics*, *Phys. Rev.* **D93** (2016) 033006 [1506.07443].

[130] NNPDF collaboration, *Parton distributions from high-precision collider data*, *Eur. Phys. J.* **C77** (2017) 663 [1706.00428].

[131] J. Butterworth et al., *PDF4LHC recommendations for LHC Run II*, *J. Phys.* **G43** (2016) 023001 [1510.03865].

[132] C. Duhr, F. Dulat and B. Mistlberger, *Charged current Drell-Yan production at N^3LO*, *JHEP* **11** (2020) 143 [2007.13313].

[133] R. V. Harlander and W. B. Kilgore, *Production of a pseudoscalar Higgs boson at hadron colliders at next-to-next-to leading order*, *JHEP* **10** (2002) 017

[hep-ph/0208096].

[134] C. Anastasiou and K. Melnikov, *Higgs boson production at hadron colliders in NNLO QCD*, *Nucl. Phys.* **B646** (2002) 220 [hep-ph/0207004].

[135] C. Anastasiou and K. Melnikov, *Pseudoscalar Higgs boson production at hadron colliders in NNLO QCD*, *Phys. Rev.* **D67** (2003) 037501 [hep-ph/0208115].

[136] V. Ravindran, J. Smith and W. L. van Neerven, *NNLO corrections to the total cross-section for Higgs boson production in hadron hadron collisions*, *Nucl. Phys.* **B665** (2003) 325 [hep-ph/0302135].

[137] R. V. Harlander and W. B. Kilgore, *Higgs boson production in bottom quark fusion at next-to-next-to leading order*, *Phys. Rev.* **D68** (2003) 013001 [hep-ph/0304035].

[138] C. Anastasiou, C. Duhr, F. Dulat, F. Herzog and B. Mistlberger, *Higgs Boson Gluon-Fusion Production in QCD at Three Loops*, *Phys. Rev. Lett.* **114** (2015) 212001 [1503.06056].

[139] B. Mistlberger, *Higgs boson production at hadron colliders at N^3LO in QCD*, *JHEP* **05** (2018) 028 [1802.00833].

[140] C. Duhr, F. Dulat and B. Mistlberger, *Higgs production in bottom-quark fusion to third order in the strong coupling*, 1904.09990.

[141] C. Anastasiou, K. Melnikov and F. Petriello, *Higgs boson production at hadron colliders: Differential cross sections through next-to-next-to-leading order*, *Phys. Rev. Lett.* **93** (2004) 262002 [hep-ph/0409088].

[142] C. Anastasiou, F. Herzog and A. Lazopoulos, *The fully differential decay rate of a Higgs boson to bottom-quarks at NNLO in QCD*, *JHEP* **03** (2012) 035 [1110.2368].

[143] S. Bühler, F. Herzog, A. Lazopoulos and R. Müller, *The fully differential hadronic production of a Higgs boson via bottom quark fusion at NNLO*, *JHEP* **07** (2012) 115 [1204.4415].

[144] F. Dulat, B. Mistlberger and A. Pelloni, *Precision predictions at N^3LO for the Higgs boson rapidity distribution at the LHC*, *Phys. Rev.* **D99** (2019) 034004 [1810.09462].

[145] L. Cieri, X. Chen, T. Gehrmann, E. W. N. Glover and A. Huss, *Higgs boson production at the LHC using the q_T subtraction formalism at N^3LO QCD*, *JHEP* **02** (2019) 096 [1807.11501].

[146] C. Anastasiou, L. J. Dixon, K. Melnikov and F. Petriello, *Dilepton rapidity distribution in the Drell-Yan process at NNLO in QCD*, *Phys. Rev. Lett.* **91** (2003) 182002 [hep-ph/0306192].

[147] C. Anastasiou, L. J. Dixon, K. Melnikov and F. Petriello, *High precision QCD at hadron colliders: Electroweak gauge boson rapidity distributions at NNLO*, *Phys.*

Rev. **D69** (2004) 094008 [hep-ph/0312266].

[148] S. Catani, L. Cieri, G. Ferrera, D. de Florian and M. Grazzini, *Vector boson production at hadron colliders: a fully exclusive QCD calculation at NNLO*, *Phys. Rev. Lett.* **103** (2009) 082001 [0903.2120].

[149] K. Melnikov and F. Petriello, *Electroweak gauge boson production at hadron colliders through O(alpha(s)**2)*, *Phys. Rev.* **D74** (2006) 114017 [hep-ph/0609070].

[150] R. Gavin, Y. Li, F. Petriello and S. Quackenbush, *W Physics at the LHC with FEWZ 2.1*, *Comput. Phys. Commun.* **184** (2013) 208 [1201.5896].

[151] P. Mathews, V. Ravindran, K. Sridhar and W. L. van Neerven, *Next-to-leading order QCD corrections to the Drell-Yan cross section in models of TeV-scale gravity*, *Nucl. Phys.* **B713** (2005) 333 [hep-ph/0411018].

[152] M. C. Kumar, P. Mathews, V. Ravindran and A. Tripathi, *Unparticle physics in diphoton production at the CERN LHC*, *Phys. Rev.* **D77** (2008) 055013 [0709.2478].

[153] M. C. Kumar, P. Mathews, V. Ravindran and A. Tripathi, *Unparticles in diphoton production to NLO in QCD at the LHC*, *Phys. Rev.* **D79** (2009) 075012 [0804.4054].

[154] M. C. Kumar, P. Mathews, V. Ravindran and A. Tripathi, *Diphoton signals in theories with large extra dimensions to NLO QCD at hadron colliders*, *Phys. Lett.* **B672** (2009) 45 [0811.1670].

[155] M. C. Kumar, P. Mathews, V. Ravindran and A. Tripathi, *Direct photon pair production at the LHC to order α_s in TeV scale gravity models*, *Nucl. Phys.* **B818** (2009) 28 [0902.4894].

[156] N. Agarwal, V. Ravindran, V. K. Tiwari and A. Tripathi, *Z boson pair production at the LHC to O(alpha(s)) in TeV scale gravity models*, *Nucl. Phys.* **B830** (2010) 248 [0909.2651].

[157] N. Agarwal, V. Ravindran, V. K. Tiwari and A. Tripathi, *W^+W^- production in Large extra dimension model at next-to-leading order in QCD at the LHC*, *Phys. Rev.* **D82** (2010) 036001 [1003.5450].

[158] M. C. Kumar, P. Mathews, A. A. Pankov, N. Paver, V. Ravindran and A. V. Tsytrinov, *Spin-analysis of s-channel diphoton resonances at the LHC*, *Phys. Rev.* **D84** (2011) 115008 [1108.3764].

[159] N. Agarwal, V. Ravindran, V. K. Tiwari and A. Tripathi, *Next-to-leading order QCD corrections to the Z boson pair production at the LHC in Randall Sundrum*

model, *Phys. Lett.* **B686** (2010) 244 [0910.1551].

[160] N. Agarwal, V. Ravindran, V. K. Tiwari and A. Tripathi, *Next-to-leading order QCD corrections to W^+W^- production at the LHC in Randall Sundrum model*, *Phys. Lett.* **B690** (2010) 390 [1003.5445].

[161] P. Mathews, V. Ravindran and K. Sridhar, *NLO-QCD corrections to dilepton production in the Randall-Sundrum model*, *JHEP* **10** (2005) 031 [hep-ph/0506158].

[162] R. Frederix, M. K. Mandal, P. Mathews, V. Ravindran, S. Seth, P. Torrielli et al., *Diphoton production in the ADD model to NLO+parton shower accuracy at the LHC*, *JHEP* **12** (2012) 102 [1209.6527].

[163] R. Frederix, M. K. Mandal, P. Mathews, V. Ravindran and S. Seth, *Drell-Yan, ZZ, W^+W^- production in SM & ADD model to NLO+PS accuracy at the LHC*, *Eur. Phys. J.* **C74** (2014) 2745 [1307.7013].

[164] G. Das, P. Mathews, V. Ravindran and S. Seth, *RS resonance in di-final state production at the LHC to NLO+PS accuracy*, *JHEP* **10** (2014) 188 [1408.3970].

[165] M. C. Kumar, P. Mathews, V. Ravindran and S. Seth, *Vector boson production in association with KK modes of the ADD model to NLO in QCD at LHC*, *J. Phys.* **G38** (2011) 055001 [1004.5519].

[166] M. C. Kumar, P. Mathews, V. Ravindran and S. Seth, *Neutral triple electroweak gauge boson production in the large extra-dimension model at the LHC*, *Phys. Rev.* **D85** (2012) 094507 [1111.7063].

[167] G. Das and P. Mathews, *Neutral Triple Vector Boson Production in Randall-Sundrum Model at the LHC*, *Phys. Rev.* **D92** (2015) 094034 [1507.08857].

[168] G. Das, C. Degrande, V. Hirschi, F. Maltoni and H.-S. Shao, *NLO predictions for the production of a spin-two particle at the LHC*, *Phys. Lett.* **B770** (2017) 507 [1605.09359].

[169] A. Alloul, N. D. Christensen, C. Degrande, C. Duhr and B. Fuks, *FeynRules 2.0 - A complete toolbox for tree-level phenomenology*, *Comput. Phys. Commun.* **185** (2014) 2250 [1310.1921].

[170] J. Alwall, R. Frederix, S. Frixione, V. Hirschi, F. Maltoni, O. Mattelaer et al., *The automated computation of tree-level and next-to-leading order differential cross sections, and their matching to parton shower simulations*, *JHEP* **07** (2014) 079 [1405.0301].

[171] D. de Florian, M. Mahakhud, P. Mathews, J. Mazzitelli and V. Ravindran, *Next-to-Next-to-Leading Order QCD Corrections in Models of TeV-Scale Gravity*, *JHEP* **04** (2014) 028 [1312.7173].

[172] D. de Florian, M. Mahakhud, P. Mathews, J. Mazzitelli and V. Ravindran, *Quark and gluon spin-2 form factors to two-loops in QCD*, *JHEP* **02** (2014) 035 [1312.6528].

[173] T. Ahmed, P. Banerjee, P. K. Dhani, M. C. Kumar, P. Mathews, N. Rana et al., *NNLO QCD corrections to the Drell–Yan cross section in models of TeV-scale gravity*, *Eur. Phys. J.* **C77** (2017) 22 [1606.08454].

[174] P. Banerjee, P. K. Dhani, M. C. Kumar, P. Mathews and V. Ravindran, *NNLO QCD corrections to production of a spin-2 particle with nonuniversal couplings in the Drell-Yan process*, *Phys. Rev.* **D97** (2018) 094028 [1710.04184].

[175] T. Ahmed, G. Das, P. Mathews, N. Rana and V. Ravindran, *Spin-2 Form Factors at Three Loop in QCD*, *JHEP* **12** (2015) 084 [1508.05043].

[176] M. A. Ebert, J. K. L. Michel and F. J. Tackmann, *Resummation Improved Rapidity Spectrum for Gluon Fusion Higgs Production*, *JHEP* **05** (2017) 088 [1702.00794].

[177] A. A. H., G. Das, M. C. Kumar, P. Mukherjee, V. Ravindran and K. Samanta, *Resummed Drell-Yan cross-section at N^3LL*, 2001.11377.

[178] S. Alekhin, J. Blumlein and S. Moch, *The ABM parton distributions tuned to LHC data*, *Phys. Rev.* **D89** (2014) 054028 [1310.3059].

[179] D. de Florian, J. Mazzitelli, S. Moch and A. Vogt, *Approximate N^3LO Higgs-boson production cross section using physical-kernel constraints*, *JHEP* **10** (2014) 176 [1408.6277].

[180] G. Das, S. Moch and A. Vogt, *Approximate four-loop QCD corrections to the Higgs-boson production cross section*, 2004.00563.

[181] G. F. Sterman, *Summation of Large Corrections to Short Distance Hadronic Cross-Sections*, *Nucl. Phys.* **B281** (1987) 310.

[182] S. Catani and L. Trentadue, *Comment on QCD exponentiation at large x*, *Nucl. Phys.* **B353** (1991) 183.

[183] W. Bizon, P. F. Monni, E. Re, L. Rottoli and P. Torrielli, *Momentum-space resummation for transverse observables and the Higgs $p_\perp$ at N^3LL+NNLO*, *JHEP* **02** (2018) 108 [1705.09127].

[184] X. Chen, T. Gehrmann, E. N. Glover, A. Huss, Y. Li, D. Neill et al., *Precise QCD Description of the Higgs Boson Transverse Momentum Spectrum*, *Phys. Lett. B* **788** (2019) 425 [1805.00736].

[185] W. Bizoń, X. Chen, A. Gehrmann-De Ridder, T. Gehrmann, N. Glover, A. Huss et al., *Fiducial distributions in Higgs and Drell-Yan production at N^3LL+NNLO*, *JHEP* **12** (2018) 132 [1805.05916].

[186] M. A. Ebert and F. J. Tackmann, *Resummation of Transverse Momentum*

Distributions in Distribution Space, *JHEP* **02** (2017) 110 [1611.08610].

[187] N. Agarwal, P. Banerjee, G. Das, P. K. Dhani, A. Mukhopadhyay, V. Ravindran et al., *Resummed transverse momentum distribution of pseudo-scalar Higgs boson at NNLO$_A$+NNLL*, *JHEP* **12** (2018) 105 [1805.12553].

[188] G. Bozzi, S. Catani, G. Ferrera, D. de Florian and M. Grazzini, *Production of Drell-Yan lepton pairs in hadron collisions: Transverse-momentum resummation at next-to-next-to-leading logarithmic accuracy*, *Phys. Lett. B* **696** (2011) 207 [1007.2351].

[189] W. Bizon, A. Gehrmann-De Ridder, T. Gehrmann, N. Glover, A. Huss, P. F. Monni et al., *The transverse momentum spectrum of weak gauge bosons at N ^{3} LL + NNLO*, *Eur. Phys. J. C* **79** (2019) 868 [1905.05171].

[190] CMS collaboration, *Search for physics beyond the standard model in high-mass diphoton events from proton-proton collisions at $\sqrt{s} = 13$ TeV*, *Phys. Rev. D* **98** (2018) 092001 [1809.00327].

[191] P. Artoisenet et al., *A framework for Higgs characterisation*, *JHEP* **11** (2013) 043 [1306.6464].

[192] T. Becher, M. Neubert and B. D. Pecjak, *Factorization and Momentum-Space Resummation in Deep-Inelastic Scattering*, *JHEP* **01** (2007) 076 [hep-ph/0607228].

[193] T. Ahmed, A. Ajjath, G. Das, P. Mukherjee, V. Ravindran and S. Tiwari, *Soft-virtual correction and threshold resummation for n-colorless particles to fourth order in QCD: Part I*, 2010.02979.

[194] S. D. Joglekar and B. W. Lee, *General Theory of Renormalization of Gauge Invariant Operators*, *Annals Phys.* **97** (1976) 160.

[195] M. Henneaux, *Remarks on the renormalization of gauge invariant operators in Yang-Mills theory*, *Phys. Lett. B* **313** (1993) 35 [hep-th/9306101].

[196] T. Ahmed, P. Banerjee, P. K. Dhani, P. Mathews, N. Rana and V. Ravindran, *Three loop form factors of a massive spin-2 particle with nonuniversal coupling*, *Phys. Rev. D* **95** (2017) 034035 [1612.00024].

[197] M. Botje et al., *The PDF4LHC Working Group Interim Recommendations*, 1101.0538.

[198] M. Cacciari and N. Houdeau, *Meaningful characterisation of perturbative theoretical uncertainties*, *JHEP* **09** (2011) 039 [1105.5152].

[199] M. Bonvini, *Probabilistic definition of the perturbative theoretical uncertainty from missing higher orders*, *Eur. Phys. J. C* **80** (2020) 989 [2006.16293].